

*Final Report on*  
**Cloud-Seeding Feasibility and Preliminary  
Program Design for Southwest Montana**



prepared for  
**Montana Department of Natural Resources and Conservation (DNRC)**

by  
**National Science Foundation National Center for Atmospheric Research  
Research Applications Laboratory**

P.O. Box 3000  
Boulder, CO 80307



**Investigators:**

Sarah Tessendorf, Maria Frediani, Michelle Harrold, Kyoko Ikeda, Meghan Stell-Stewart,  
Courtney Weeks, Jamie Wolff, and Lulin Xue

2 May 2025

This report was prepared by the NSF NCAR/RAL in consultation with Montana DNRC  
through funding provided by the 68th Montana Legislature

# Table of Contents

<b>Executive Summary</b>	<b>2</b>
<b>1. Introduction</b>	<b>10</b>
<b>2. Background</b>	<b>10</b>
2.1. Cloud-Seeding History	10
2.2. Cloud Seeding in the Western U.S. and Canada	12
2.3. Cloud Seeding in Montana	13
<b>3. Data</b>	<b>16</b>
3.1. Observations	16
3.2. Model Dataset	17
<b>4. Feasibility Study for Big Hole Basin</b>	<b>19</b>
4.1. Methodology	19
4.2. Characteristics of Precipitation	21
4.3. Ground-based Seeding Feasibility	33
4.4. Airborne Seeding Feasibility	67
4.5. Combined Airborne and Ground Seeding Feasibility	89
4.6. Fraction of Seedable Precipitation	104
4.7. Summary of Climatology Analysis	104
<b>5. Design for Big Hole Basin Seeding Program</b>	<b>106</b>
5.1. WRF-WxMod Background	106
5.2. WRF-WxMod Configuration	107
5.3. Case Study Selection	109
5.4. Ground-Based Seeding Design Simulations	109
5.5. Airborne Seeding Design Simulations	131
5.6. Summary of Case Study Simulation	144
5.7. Cost-Benefit Analysis	149
<b>6. Overall Summary and Recommendations</b>	<b>154</b>
<b>List of Acronyms</b>	<b>160</b>
<b>References</b>	<b>162</b>
<b>Appendix A: Investigating Sensitivities to Simulated Precipitation</b>	<b>166</b>
<b>Appendix B: Case 2 (14 December 2019)</b>	<b>169</b>

# Executive Summary

Many states in the western U.S. actively conduct cloud seeding operations with the goal of enhancing snowfall. States and agencies throughout the West are increasingly concerned with water supply as droughts and other impacts of climate change affect the region. The State of Montana contracted with the National Science Foundation National Center for Atmospheric Research (NSF NCAR) to conduct a feasibility study to assess the potential for cloud seeding to augment snowpack and subsequent streamflow in the Big Hole Basin of southwestern Montana. There are three main goals of this study: 1) Assess the potential for cloud seeding to augment snowpack and subsequent streamflow in mountain ranges surrounding the Big Hole Basin in southwestern Montana, 2) Complete a preliminary program design and a preliminary cost-benefit analysis based upon the weather/climate analysis, and 3) Support public engagement activities for the feasibility study and implementation of subsequent pilot project.

To address the primary goal, a detailed analysis to understand the cloud and precipitation characteristics in mountainous regions of southwestern Montana was conducted in both current and future climate scenarios, to serve as a basis for designing a program that would optimally target this region. The features of this study are based upon work conducted previously by NSF NCAR for the states of Idaho and Wyoming. Novel components of this study include the use of:

- An unprecedented, 40-year high-resolution (4-km) Weather Research and Forecasting (WRF) model simulation (hereafter, CONUS404) that provides detailed three-dimensional information about the atmospheric conditions relevant to cloud seeding, and
- WRF-WxMod<sup>®</sup>, a state-of-the-art numerical model developed at NSF NCAR that can simulate the physics of cloud seeding with silver iodide, to test and optimize potential cloud-seeding program design options. The WRF-WxMod model provides a three-dimensional simulation of the impact of cloud seeding on precipitation and can be configured to test any potential (or existing) cloud-seeding program design.

This report summarizes the results of the assessment of cloud-seeding potential, as well as the preliminary design that was developed and tested. A fact sheet was also developed, and public meetings were held to present the concepts of cloud seeding and preliminary results of this study to various audiences and stakeholders in the Big Hole Basin and surrounding areas. The meetings included substantial time for addressing questions and concerns as well.

## **Cloud-seeding potential**

The potential for cloud seeding was assessed by conducting a climatological analysis of historical data. The historical precipitation data from SNOTEL snow gauge observations, as well as from the CONUS404 simulation, showed that the greatest wintertime precipitation (>800 mm) falls in the Beaverhead Mountains on the western divide of the Big Hole Basin ([Fig. 1](#)). The Anaconda Range in the north is also a focal point for winter precipitation (>700 mm), while the Pioneer Mountains, in the center of the basin, typically accumulate much less precipitation during the winter (400-600 mm on average). Including the valleys, the entire basin average is 355 mm of precipitation accumulation during the wintertime months.

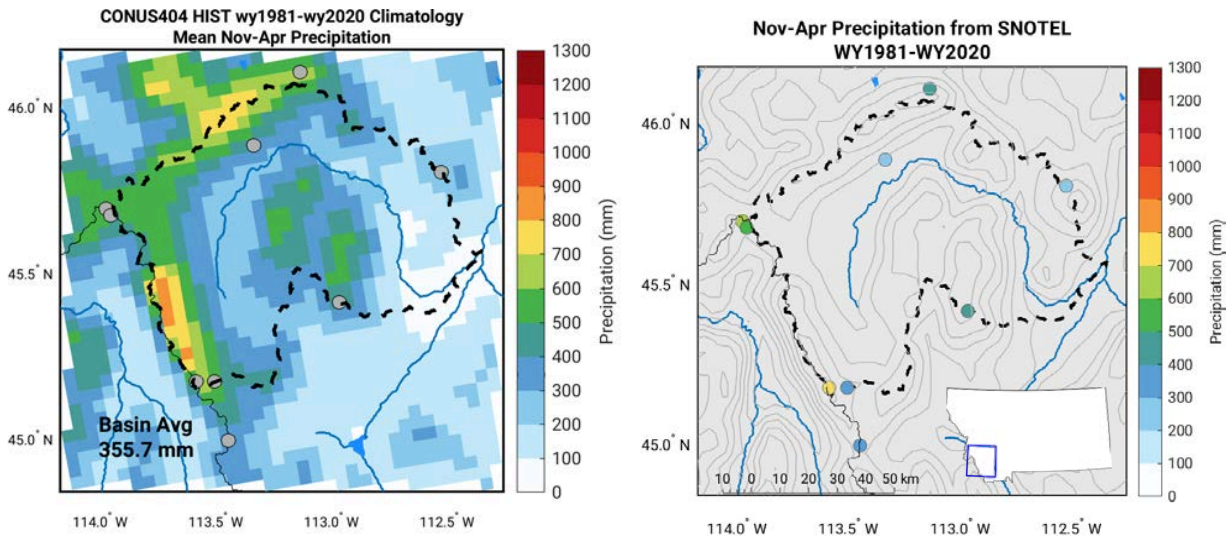


**Figure 1.** 40-year average wintertime (Nov-Apr) precipitation accumulation (1981-2020) from the CONUS404 simulation (left) and SNOTEL gauge data (right). The Big Hole Basin is indicated by the black dashed outline. Inset map in lower right shows the Big Hole Basin study region within the State of Montana for reference.

Given the lack of observations beyond precipitation data from SNOTEL gauges, the rest of the climatological analysis was conducted using the CONUS404 simulation to assess the frequency of opportunities for cloud seeding. Especially of interest, in order to characterize and quantify potential seeding opportunities, is the presence of supercooled liquid water (SLW) at appropriate temperatures for silver iodide (AgI) to nucleate ice, hereafter referred to as seedable SLW. The key areas that have enhanced frequency of seedable SLW are the same regions where the greatest wintertime precipitation falls (Fig. 2). The ground-seeding layer (0-1 km above ground level) has greater overall frequencies of seedable SLW than the airborne seeding layer (3.5-4.5 km above mean sea level), though the locations of seedable conditions are largely the same between the two layers. The less frequent seedable SLW in the airborne layer is in part due to the SLW being more common closer to the ground in these regions than at the aircraft flight altitude.

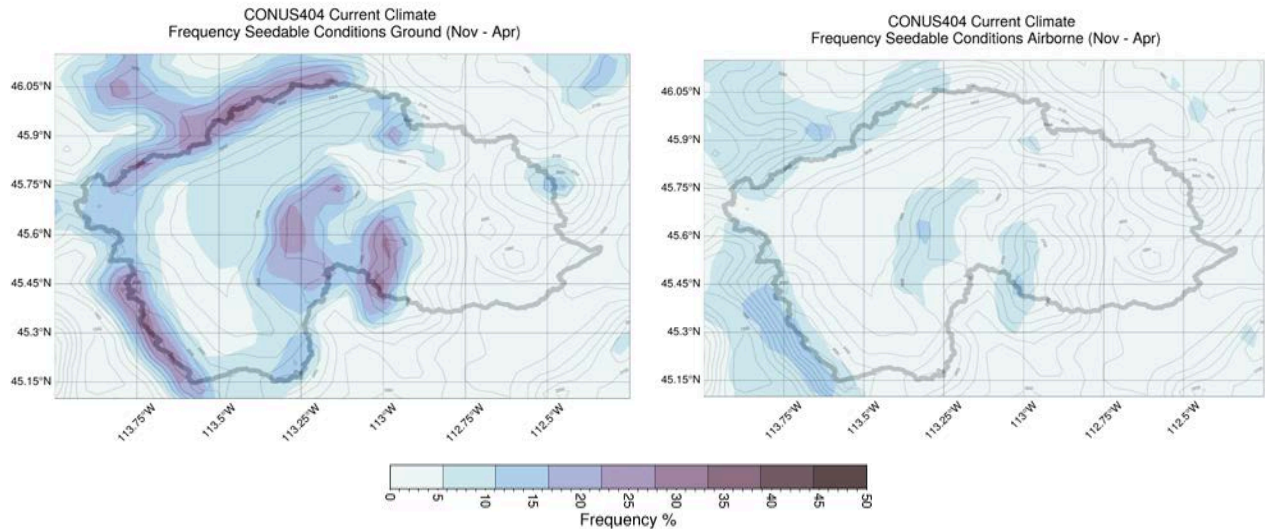


**Figure 2.** 40-year average frequency of seedable SLW (the baseline of cloud-seeding opportunities) in the Big Hole Basin (indicated by gray line) in the ground-seeding layer (left) and airborne seeding layer (right) for Nov-Apr. Seedable SLW is based upon SLW occurring at appropriate temperatures for AgI seeding.

When considering additional factors that are important for ground-based seeding to be effectively dispersed over the targeted mountain barrier, namely wind direction, wind speed, and stability of the atmosphere, some of the regions with the greatest frequency of seedable SLW in the ground-based layer are reduced due to the limited wind direction sector and/or potential for flow blocking that would inhibit the AgI released to reach the targeted clouds over the Big Hole Basin. The northern Beaverhead Mountains had minimal reduction in seeding opportunities due to dispersion criteria though and showed just over 20% of the wintertime period being amenable for ground-based seeding. The Anaconda Range also showed a similar frequency of opportunities. The aircraft layer analysis showed most regions had between 10-12% of the winter having seedable SLW. Airborne seeding is less impacted by wind direction limitations or flow blocking since the aircraft can release the AgI directly in the cloud, and these opportunities are not reduced by other atmospheric conditions like they are for ground-based seeding. However, it is important to note that aircraft have limited flight time, so a single aircraft may not be able to fully target all of the available opportunities. The ability of ground-based seeding to effectively disperse and impact the targeted clouds compared to airborne seeding was evaluated with WRF-WxMod modeling simulations as part of the preliminary design testing.

From the climatology analysis, ground-based seeding in the northern Beaverhead Mountains has the most potential, even more so than aircraft seeding based upon the overall frequency of seeding opportunities. Analysis of a future climate simulation that represents a warming climate indicates that SLW in the region will generally increase, while temperatures generally warm. Therefore, airborne seeding opportunities will increase; however, with warming temperatures especially near the surface, ground-based seeding opportunities may decrease.

### **Preliminary program design**

Based upon the climatological analysis, preliminary designs for both airborne and ground-based cloud seeding programs were developed and tested with WRF-WxMod (Fig. 3). These designs included 10 groups of hypothetical ground-based generators and various aircraft flight tracks. The design options were tested using multiple case studies that represent various common weather patterns in the region (based upon the climatological analysis). Each ground-based seeding case study was simulated to test all hypothetical ground-based generator groups combined as well as each group individually. The model simulations were carried out on Montana Technical University’s high performance computing (HPC) Oredigger cluster and NSF NCAR’s Derecho supercomputer.

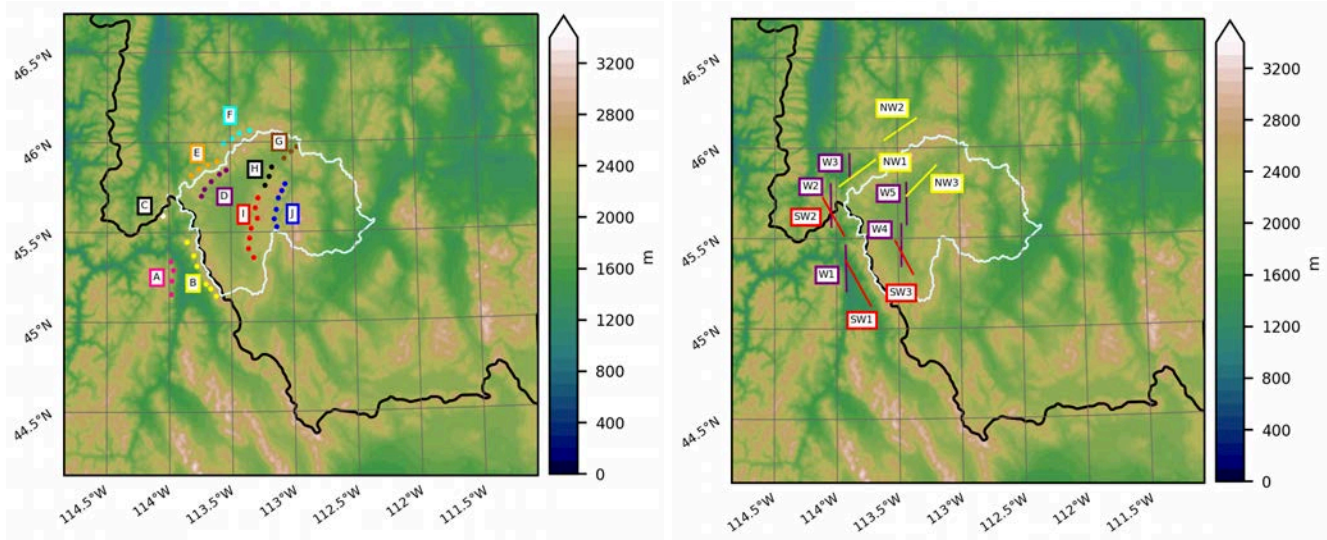


**Figure 3.** Preliminary designs showing hypothetical ground-based generator locations (left) and aircraft tracks (right) that were being tested with WRF-WxMod simulations.

The simulated seeding effects from hypothetical ground generator groups placed along the westward side of Big Hole Basin (A, B, C, D, E, and F) were shown to be more favorable for achieving simulated precipitation enhancements targeting the Big Hole than hypothetical generator groups farther east. *The simulations for these groups indicate the effects are highly dependent on the wind direction and location of SLW.* For example, Group F is located at the northernmost side of the Big Hole, and so its potential to impact the Big Hole decreases when wind directions are not predominantly from the north or northwest (Fig. 4). Groups A and C were the top performing generator groups for targeting the Big Hole and beyond, although their effects for targeting the Big Hole may be diminished in wind directions with a predominantly northerly component (yet they could impact regions south of the Big Hole in those situations). Even though the eastern generator groups (G, H, I, and J) showed more modest simulated seeding effects in some of the cases, the location of these groups leads to simulated seeding effects downwind beyond the catchment of the Big Hole, so they may be effective overall, but less so for immediately targeting the Big Hole Basin.

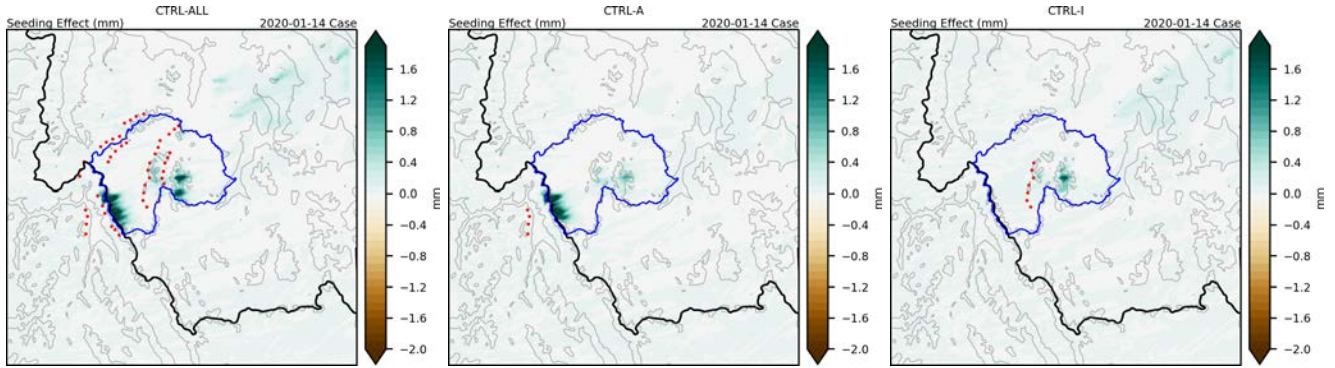


**Figure 4.** Simulated seeding effect (mm of simulated precipitation change from seeding simulation minus the control simulation) from all hypothetical generator groups (A-J) combined (left), and examples of Group A individually (middle) and Group I individually (right) for a case study on 14 Jan 2020 (Case 3). Green hues indicate an increase in simulated precipitation and brown hues indicate a decrease in simulated precipitation.

The airborne seeding simulation experiments evaluated seeding flight tracks at different orientations (favoring directions perpendicular to the predominant wind of each case; Fig. 5), of varying lengths, locations, and altitudes (3750 and 4250 m). The results showed greater simulated seeding effects from lower altitude tracks (3750 m) in all cases. This is an indication that the SLW was generally at a lower altitude for the cases simulated in this region, which was also reflected in the climatology analysis that indicated SLW was most frequently at lower altitudes. In general, simulations of airborne seeding indicated that it can be highly effective for precipitation enhancement in the region, perhaps more so than for ground-based seeding, given the flight tracks can be versatile to accommodate the SLW and wind conditions for each case.

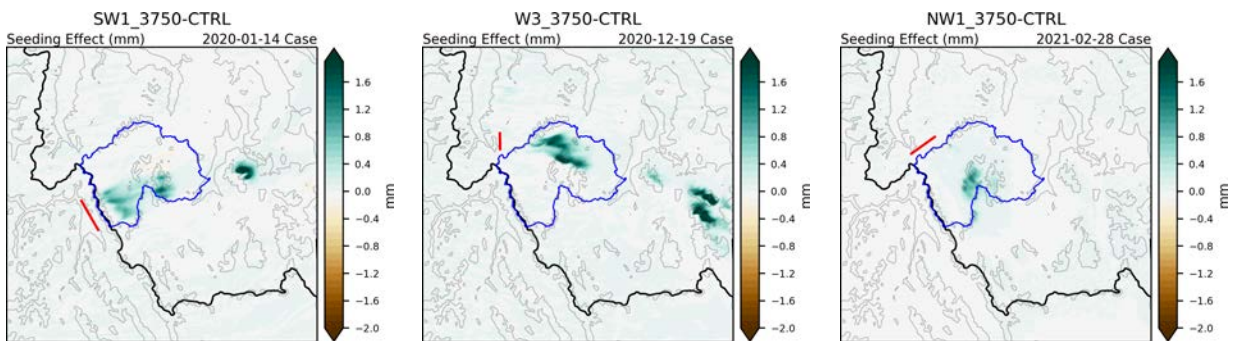


**Figure 5.** Simulated seeding effect (mm of simulated precipitation change from seeding simulation minus the control simulation) from three hypothetical flight tracks (from left to right: SW1, W3, and NW1) at 3750 m for the case studies on 14 Jan 2020 (Case 3; left), 19 Dec 2020 (Case 4; middle), and 28 Dec 2021 (Case 5; right). Green hues indicate an increase in simulated precipitation and brown hues indicate a decrease in simulated precipitation.

In summary, the climatological analysis suggests that ground seeding, at least in some mountain ranges surrounding the Big Hole (namely the Beaverheads), may have more potential than airborne seeding due a greater frequency of seeding opportunities in the lowest layer of the atmosphere than at higher altitudes.

However, some mountain ranges may be constrained by wind direction to target the Big Hole and/or flow blocking thereby limiting the potential for ground-based seeding, and making it occur less frequently than airborne seeding. Airborne seeding simulations have shown that airborne seeding is effective in a variety of cases in the region. Airborne seeding generally has greater operational costs than ground seeding, depending on the type and number of ground-based generators. Yet, the versatility and more consistent climatology of airborne seeding opportunities (without potential flow blocking limitations of ground seeding) and the effectiveness of airborne seeding in the WRF-WxMod simulations led to similar cost-benefit estimates for ground and airborne seeding (~\$10-\$60/acre foot) in this region. This indicates that while ground-based seeding may cost less overall, the amount of water potentially produced by ground-based seeding may also be less. A program including both ground-based and airborne operations would maximize targeting capability—especially since conditions rarely occur at both heights simultaneously—resulting in a small cost increase per acre-feet (AF) relative to the less-expensive ground-based program alone, but with a non-trivial potential increase in water produced.

There may be opportunities to partner on cloud seeding this region with Idaho given they have shown interest in targeting the Lemhi River Basin. If an aircraft or ground generators could be shared between the two programs, then a seeding program in the region could be even more cost effective.

### **Program design and pilot study recommendations**

The following recommendations are made based upon the results of this cloud seeding feasibility and design study. These recommendations can be used to develop a pilot cloud-seeding program in the region.

- Based upon the overall SLW and wind direction frequencies, the Beaverhead Mountains should be a primary focus for seeding, which presents opportunities to share a seeding program with Idaho.
  - Hypothetical ground generators in Groups A-C should be explored ([Fig. 6](#)), with Group A in particular being most relevant to Idaho interests.
  - Airborne seeding should also be considered, in conjunction with ground seeding for this region as it has versatility to target multiple wind directions and locations in the region and has been shown to be effective. A combined ground and airborne seeding program may provide the most overall opportunities for seeding given the climatology of seeding opportunities for ground and airborne tended to not occur simultaneously.
    - Flight tracks should be focused in the western portion of the region to most effectively target the Big Hole Basin, given flight tracks farther east (in the middle of the Big Hole) tended to have more simulated precipitation enhancement downwind of the Big Hole ([Fig. 6](#)).

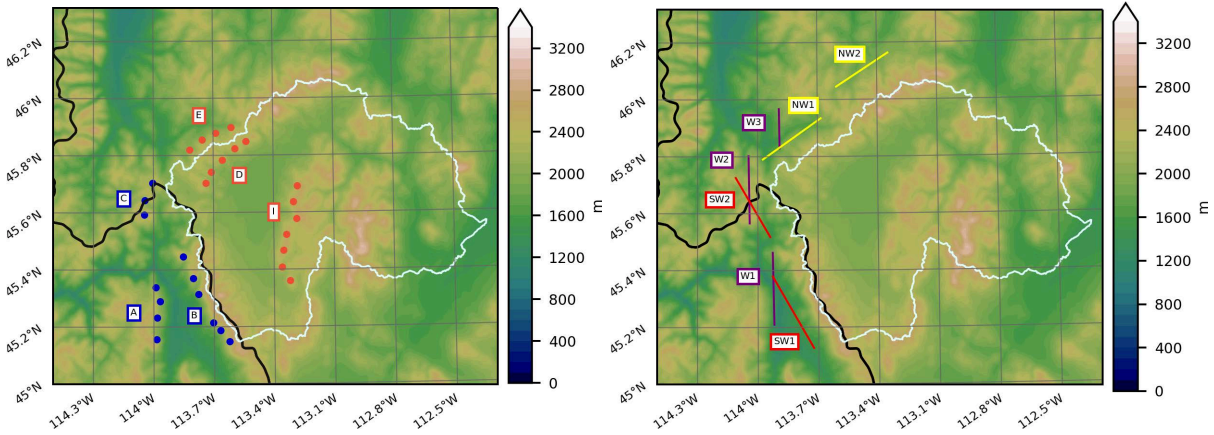


**Figure 6.** Recommended generator groups (left) and recommended airborne cloud-seeding flight tracks (right); western flight tracks are in purple, southwestern flight tracks are in red, and northwestern flight tracks are in yellow.

- While less frequent and strongly dependent on the occurrence of northwesterly winds, the Anaconda Range could be a secondary target, utilizing ground generators Groups D-E (Fig. 6). However, airborne seeding could target these wind conditions and may be more advantageous than ground seeding in this region.
- The Pioneer Mountains should also be a secondary target; however, they can be targeted by upwind seeding facilities (e.g., Groups A-E generator sites or airborne seeding). A section of possible generators in Group I may also be considered to target this area and may be more feasible and cost effective as manual generator sites, though manual generator release rates were not explicitly tested in this study (Fig. 6).
- Ground-based seeding should focus on the November through February months for the most favorable flow and greatest amount of SLW.
- Opportunities to share infrastructure for a cloud seeding program with Idaho should be explored to further boost the cost-benefit by reducing the State of Montana’s cost of operations.

It should also be noted that these recommendations are focused on targeting the Big Hole Basin, however the results of this study also indicate that there is the potential for cloud seeding to enhance precipitation in other regions of Montana surrounding the Big Hole. Therefore, even if some of the generator groups or aircraft flight tracks were not recommended for the Big Hole, they may have potential for use to target the surrounding regions.

Based upon these results and recommendations, for a cloud-seeding pilot program, we recommend an initial focus on the Beaverhead Mountains and siting 8-12 generators in the primary generator groups A-C (Fig. 6). We recommend a pilot study that would include three winter seasons of seeding, to capture year-to-year variability in seeding opportunities and storm conditions, along with an evaluation component after each year of seeding, so the total project period would roughly span four years. Besides the greatest opportunities for seeding in the Beaverhead Mountains region, there is also an opportunity to partner with the State of Idaho, which could lead to cost sharing and reduced overall program costs for a pilot program. However, a shared infrastructure study to determine how to design a combined program

that benefits both states would be a valuable next step before beginning a pilot project shared with Idaho. Aircraft-based seeding could also be deployed in this region for a pilot study and would be most cost efficient if shared with the State of Idaho as well. A low cost addition to the pilot study could include 2-4 manual generators sited on the western slopes of the Pioneer Mountains (Group I, Fig. 6), however this aspect would not be amenable to cost sharing with Idaho.

Besides the cloud-seeding facilities (i.e. ground generators and/or seeding aircraft), a pilot program would also need to include forecasters who determine when to seed and who operate the program. Additional instrumentation would be helpful for a pilot study, to help aid forecasters in determining when to seed, as well as to provide data for an evaluation of the pilot program. Recommended instrumentation includes high-resolution precipitation gauges, a measure of the SLW in the clouds from icing rate sensors or a microwave radiometer, and weather balloon launches to assess cloud temperatures, winds, and atmospheric stability. Numerical weather prediction models would also be helpful for forecasting seeding events.

To complete the pilot study, an evaluation would be recommended that includes analysis of any observational data collected, as well as a numerical model-based evaluation study of all seeded events to estimate the impact of seeding on precipitation and/or streamflow. A best practice is for the evaluation to be conducted independent from the entity operating the cloud-seeding program. Numerical modeling tools like WRF-WxMod and WRF-Hydro are valuable for program evaluation. Statistical analyses are another option for program evaluation, however such approaches are not conclusive when sample sizes are small and therefore often require 10+ years to build a statistically-robust sample of cases. In contrast, a numerical modeling evaluation can be conducted on a storm-by-storm or year-by-year basis, and can be constrained by observations collected during the pilot program.

# 1. Introduction

The primary goal of this study is to assess the potential for cloud seeding to augment snowpack and subsequent streamflow in mountain ranges surrounding the Big Hole Basin in southwestern Montana. To address this goal, a detailed analysis to understand the cloud and precipitation characteristics in these mountainous regions of southwestern Montana was conducted in both the current climate and a future climate scenario, to serve as a basis for designing a program that would optimally target this region.

The features of this study are based upon work conducted by the National Science Foundation's National Center for Atmospheric Research (NSF NCAR) for the Idaho Water Resource Board (IDWR), Wyoming Water Development Commission (WWDC), and Bureau of Reclamation (BOR). Novel components of this study include the use of a 40-year high-resolution (4-km) Weather Research and Forecasting (WRF) model simulation (hereafter, CONUS404) to provide detailed three-dimensional information about the climatology of atmospheric conditions relevant to cloud seeding, as well as the use of WRF-WxMod<sup>®</sup> (Xue et al. 2013a,b), a state-of-the-art numerical model developed at NSF NCAR that can simulate the physics of cloud seeding with silver iodide, to test and optimize potential cloud-seeding program design options. The WRF-WxMod model provides a three-dimensional simulation of the impact of cloud seeding on precipitation and can be configured to test any potential (or existing) cloud-seeding program design.

There are three main goals of this study: 1) Assess the potential for cloud seeding to augment snowpack and subsequent streamflow in the mountain ranges surrounding the Big Hole Basin in southwestern Montana, 2) Complete a preliminary program design and a preliminary cost-benefit analysis based upon the weather/climate analysis, and 3) Support public engagement activities for the feasibility study and implementation of a subsequent pilot project.

Results and findings are detailed in the remainder of this report.

## 2. Background

Background information related to the history of cloud seeding, existing cloud-seeding programs in the western U.S. and Canada, and a historical review of cloud-seeding efforts in the state of Montana are provided in the following sections.

### 2.1. Cloud-Seeding History

In 1938, the modification of clouds containing supercooled liquid water (SLW) with artificial ice nucleating particles was introduced to the atmospheric science community (Findeisen 1938). About a decade later, researchers became interested in precipitation modification in supercooled clouds once the use of silver iodide (AgI) and dry ice nucleation began to be more commonly known (e.g., Schaefer 1946; Vonnegut 1947; Kraus and Squires 1947; Langmuir 1948; Coons et al. 1948; and Bergeron 1949). Modification of supercooled clouds using artificial ice nucleating particles such as AgI is known as glaciogenic seeding. With glaciogenic seeding, cloud ice is formed and grows at the expense of the supercooled water in the cloud.

In the late 1940's, researchers determined that wintertime orographic clouds may be ideal for seeding due to the frequency of supercooled water present in these clouds. One of the first scientists to create a model for cloud seeding in orographic clouds was Ludlum in 1955. Ludlum's (1955) model proposed that seeding orographic clouds would enhance snowfall. This original seeding model is based on the release of AgI from ground-based generators or airborne flares near the mountain range being targeted for increased precipitation. The AgI is then dispersed over a region by wind. Within the cloud, AgI acts as an effective ice nucleating particle (INP) when temperatures are colder than  $-6^{\circ}\text{C}$ . In the presence of SLW droplets within the cloud, the nucleated AgI particle quickly allows ice crystals to grow. Ice crystals grow through a process of vapor deposition, which then may turn to riming or aggregation to eventually grow into a precipitation-sized ice crystal that can fall as snow.

While the basic premise of Ludlum's orographic seeding model still holds for modern day seeding, over the decades since it has been found that the microphysical precipitation processes in winter clouds are much more complex leading to refinements and clarifications of the original conceptual model. Precipitation in winter orographic storms generally develops when ice crystals form on natural INP (typically certain dust particles) and grow through deposition (water vapor forming ice directly, the process that builds the smallest snow crystals), riming (the collection of unfrozen cloud droplets by ice crystals), and/or aggregation (the entanglement of ice crystals with each other to form snowflakes). Measurements suggest that until temperatures cool to less than  $-12^{\circ}\text{C}$ , most orographic clouds do not contain much ice (e.g., Geresdi et al. 2005). Natural INP are scarce at such relatively warm subfreezing temperatures (Hoose and Möhler 2012). In general, at these temperatures, the precipitation process is inefficient due to the lack of natural INP active at warmer cloud temperatures during many storms.

Furthermore, the weak updrafts in orographic clouds, composed mostly of very small droplets of similar sizes, limit the activity of the ice multiplication processes that create cloud ice without additional INP (e.g., Hallett and Mossepe 1974). As a result, many shallow clouds, in particular winter orographic clouds, may largely lack ice crystals and therefore have inefficient precipitation processes. Supercooled cloud droplets are able to persist for long periods in such orographic clouds, instead of being depleted by vapor diffusion, riming, and/or aggregation, due to the absence of ice crystals. This process is well documented by the measurement of sustained SLW in orographic clouds taken by aircraft and ground-based instruments such as radiometers (e.g., Rauber and Grant 1986; Huggins 1995). On the other hand, and in contrast to natural INP, artificial INP such as AgI will nucleate ice crystals at temperatures as warm as  $-5^{\circ}\text{C}$ , ultimately enabling the creation of ice crystals in clouds warmer than  $-12^{\circ}\text{C}$  by "seeding" them with an AgI aerosol (DeMott et al. 1995).

Recent advances in computer modeling have led to new breakthroughs in the science of cloud seeding over the past 10-15 years. The development of WRF-WxMod was one major breakthrough. In addition, modern day field programs, such as the Wyoming Weather Modification Pilot Project (WWMPP; Breed et al. 2014), the AgI Seeding Cloud Impact Investigation (ASCII; Geerts et al. 2013), and the Seeded and Natural Orographic Wintertime clouds: the Idaho Experiment (SNOWIE; Tessendorf et al. 2019), provided a renewed focus on quantifying the impacts of cloud seeding and led to some breakthroughs in observed impacts of seeding. Of note, SNOWIE, conducted in 2017, collected unprecedented measurements from seeded clouds, using a variety of technologies (Tessendorf et al. 2019, French et al

2018, Friedrich et al. 2020). Findings include the unambiguous evidence that cloud seeding resulted in precipitation, as observed via radar. Specifically, a zig-zag pattern of precipitation was observed mimicking the dispersion pattern of AgI released by a seeding aircraft. These and other SNOWIE data are being used to better understand the physical response of seeded clouds and improve the cloud-seeding modeling capability. Together, these observational and modeling advances set the stage for new opportunities to address the research, program design, and evaluation of cloud seeding. Recent advances in modeling and observations of seeding impacts provide new opportunities to understand the impacts of cloud seeding and to more efficiently design and operate cloud-seeding programs.

## 2.2. Cloud Seeding in the Western U.S. and Canada

Cold-season and warm-season cloud seeding is actively being conducted in many parts of Western North America. Agencies throughout the West are becoming increasingly concerned with water supply as the effects of climate change manifest themselves. Glaciogenic cloud seeding has been shown to increase wintertime precipitation in mountainous areas (e.g., Rauber et al. 2019), and the field has been undergoing rapid research, design, and operational implementation (e.g., Rasmussen et al. 2018, Tessendorf et al. 2019, Xue et al. 2022, Mazzetti et al. 2023).

The state of Utah first began cloud-seeding efforts in the early 1950s, and operations have been continuously in place since 1973. Funding has traditionally come from the state, local entities, and lower basin states, and the cloud-seeding program employs the use of ground-based (manual and remote) and airborne operations; water generated from cloud seeding has been estimated to be between \$5-10 per acre-foot (AF) for the additional water [Utah Division of Water Resources (UDWR) [webpage](#)<sup>1</sup>]. In 2023, the state received a one-time funding increment of \$12 million and an annual budget of \$5 million to direct toward cloud-seeding research and operations, and collaborative efforts with neighboring western states are being pursued (UDWR [webpage](#)<sup>2</sup>).

In the state of Idaho, authoritative powers with respect to weather modification fall to the Idaho Water Resources Board (IWRB) director, whose responsibility it is to formulate and implement the state water plan, finance water projects, and operate programs that support sustainable management of Idaho's water resources (IWRB [webpage](#)<sup>3</sup>). Idaho currently has no permitting requirements in place, but in April 2021, the IWRB began requiring cloud-seeding project operators to provide reports and documentation with respect to cloud-seeding activities (IWRB [webpage](#)<sup>4</sup>). Idaho allows for a county commission to hold elections to establish a weather modification district, and the established districts can levy taxes; water districts may authorize weather modification projects; the state water resources board and private entities may fund their own projects. Weather modification efforts are primarily funded by local districts, private entities [e.g., Idaho Power Company (IPC)]. Idaho has a robust portfolio of cloud-seeding projects and programs, including activities currently taking place in the Wood River, Boise, and Upper Snake River Basins (Collaborative Cloud Seeding Program, a statewide program that has partnerships with Idaho

---

<sup>1</sup> Available at: <https://water.utah.gov/cloudseeding/> [Accessed 10/28/2024]

<sup>2</sup> Available at: <https://water.utah.gov/utah-holds-its-first-cloud-seeding-symposium/> [Accessed 10/28/2024]

<sup>3</sup> Available at: <https://idwr.idaho.gov/iwrub/> [Accessed 10/31/2024]

<sup>4</sup> Available at: <https://idwr.idaho.gov/iwrub/programs/cloud-seeding-program/documents-and-reports/> [Accessed 10/31/2024]

Water Resource Board-State of Idaho, IPC, and local water users), Payette Basin (IPC), Upper Snake River Basin (High Country Resource Conservation and Development Projects), and areas on the southern portion of Idaho through the Northern Utah Program (IDWR [webpage](#)<sup>5</sup>). Idaho is also actively pursuing multiple feasibility studies in the Lemhi River Basin and Bear River Basin regions.

The state of Wyoming has been investing in weather modification research and operations for several decades. Wyoming Statute § 9-1-905<sup>6</sup> indicates, “The state of Wyoming claims its sovereign right to the use for its residents and best interests of the moisture contained in the cloud and atmosphere within its sovereign state boundaries.” In addition, the Wyoming Statute § 9-1-907<sup>6</sup> states that the Wyoming state engineer holds power for issuing permits for weather modification activities, where applicants must pay a fee, not to exceed \$100. Overall, the Wyoming Water Development Office (WWDO) oversees conducting water and related resource planning and the operation of projects. From 2004 - 2016, significant research was directed toward feasibility studies over the Wind River, Medicine Bow, Sierra Madres, Salt River, and Wyoming Mountain Ranges. Based on outcomes from feasibility studies, design studies over the Medicine Bow, Sierra Madre, Laramie, and Bighorn Mountain Ranges occurred from 2015 - 2017. Ground-based operational seeding has been occurring over the Wind River Mountain Range from 2014 - present, and aerial operational seeding has occurred over the Medicine Bow, Sierra Madre, and Laramie Mountain Ranges from 2018 - present. Generally, ~37% of funding comes from the state of Wyoming, with the remaining ~63% coming from other partners including some from Lower Basin States (e.g., Southern Nevada Water Authority, Central Arizona Water Conservancy District, Colorado River Board of California, Jackson County Water Conservancy District, and other Wyoming state-based entities).

In Colorado, the Weather Modification Act of 1972 requires the executive director of the Department of Natural Resources to create rules with respect to weather modification (Colorado Department of Natural Resources 2012). Colorado requires a permit for weather modification operations, and fees include the permit fee (\$100) and commercial operations pay an additional fee (2% of base contract). In addition, there is a need for proof of financial responsibility, a public hearing must be conducted, and a legal notice must be published in affected counties; notification to key entities [National Weather Service (NWS), Colorado Avalanche Information Center (CAIC), Colorado Climate Center, and county emergency managers] is also necessary. Cloud-seeding activity also may be suspended when there are areas of high snowpack in conjunction with high avalanche hazard levels [Colorado Water Conservation Board (CWCB) Weather Modification Program [webpage](#)<sup>7</sup>]. As of this report, Colorado currently has 8 permitted weather modification programs using both ground generators and airborne seeding (as per CWCB [webpage](#)<sup>7</sup>).

### 2.3. Cloud Seeding in Montana

While operational cloud seeding is not currently occurring within Montana, there is past history that has supported cold-season and warm-season cloud-seeding efforts. In 1967, the 40th Legislature in Montana passed the Atmospheric Weather Modification Act, which was administered by the Department of Natural

---

<sup>5</sup> Available at: <https://idwr.idaho.gov/iwrp/programs/cloud-seeding-program/current-projects-and-programs/> [Accessed 10/2024]

<sup>6</sup> Available at: <https://wyoleg.gov/statutes/compress/title09.pdf> [Accessed 10/31/2024]

<sup>7</sup> Available at: <https://cwcb.colorado.gov/focus-areas/supply/weather-modification-program> [Access 10/2024]

Resources and Conservation (DNRC) and paved the way for weather modification efforts in Montana. Throughout the 1970s, Montana participated in the High Plains Cooperative Research Program (HIPLEX), a weather modification program operating near Miles City, MT that was sponsored by the Bureau of Reclamation. The program was aimed at better understanding clouds and precipitation and their associated environments as it relates to weather modification in the US high plain states (Carr Jr. 1981). During this program, a randomized field experiment was set up in Montana, with a main goal of testing the link between dry ice seeding and rainfall from cloud base (Dennis 1983). Within the 1970s-1980s, North Dakota operated a summer-time cloud-seeding program along 7 counties that border Montana; North Dakota appealed to Montana that in order to account for the time delta between cloud seeding and rain production, North Dakota needed to begin cloud seeding in Montana air space. During this time Montana did grant North Dakota a weather modification license and permit.

A randomized cloud-seeding experiment took place during the winters of 1969-1972 over the Bridger Range in southwestern Montana near Bozeman, MT (see Super and Heimbach 1983). In this experiment, cloud seeding was carried out via ground-based generators on the westward slope of the north-south oriented Main Ridge (see [Figure 2.1](#)). According to the Bridger Bowl Weather Modification Project Summary of Activities (provided by MT DNRC) focusing on the 1986-1987 winter season showed that from 12 November 1986 - 23 February 1987, there were 59 days where cloud-seeding operations took place [generators ran for 384.8 hours, and 22.6 lbs of silver iodide (AgI) were released]. Overall, the Bridger Range area experienced a drier than normal winter; however, estimates show Bridger Bowl and surrounding stations had snowpack enhanced by about 15-25%. Super and Heimbach (1983) used statistical analysis in combination with upwind and crosswind precipitation gauges to show increased precipitation at the target as well as occasionally downwind of the target. A key finding of the study was that precipitation increases were heavily dependent on the temperature profiles, with Main Ridge having temperatures  $\leq -9^{\circ}\text{C}$  as a critical indicator for positive seeding impacts. It is noted that the results from the Super and Heimbach 1983 study are considered strongly suggestive, but due to the full experimental design, they can not be considered scientifically conclusive. Super (1986) further demonstrated that ground-based AgI cloud seeding was highly effective at increasing precipitation in several particular cases but had minimal-to-no effect most of the time.

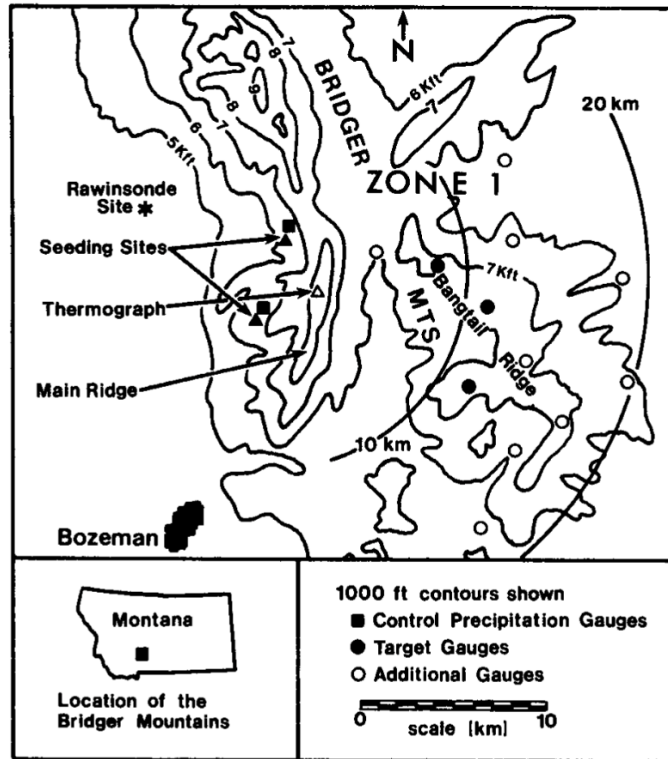


FIG. 1. Bridger Range experimental area.

*Figure 2.1. Experimental area over the Bridger Range [from Fig. 1 in Super (1986)].*

In 1993, the 53rd Legislature revised prior legislation that pertained to the weather modification licensing and permitting process [Senate Bill (SB) 72]. This was in response from citizens in Eastern Montana who believed North Dakota was potentially “stealing” precipitation from Montana during their cloud-seeding activities. SB72 required applicants to demonstrate proof of financial responsibility, and the Montana DNRC was required to provide an Environmental Impact Statement. It is worth noting that since the passage of SB72, Montana has not granted a weather modification permit due to the more stringent legislation. There are exemptions with respect to the licensing and permitting process, including 1) research, development, and experiments conducted by qualified agencies and organizations, 2) emergency activities for protection against fire, frost, sleet, and/or fog, and 3) normal activities engaged in as long as the purpose is not to induce, increase, decrease, or prevent hail and/or precipitation. The Montana DNRC application review process includes 1) preparing a report and an Environmental Impact Statement, 2) conducting any additional analysis, 3) conducting at least 1 public meeting in the area of proposed operation, 3) publishing a Notice of Intention, and 4) holding a public hearing. All costs necessary for the DNRC to conduct the review process must be paid by the applicant.

A decade later, in 2003, the 58th Legislature attempted to revise the licensing and permitting process by 1) limiting weather modification operations to the cool season (Nov. 1 - March 15), 2) removing permitting requirements, and 3) removing requirements for an Environmental Impact Statement. House Bill (HB) 644 passed in the House; however, it was tabled in the Senate Committee on Agriculture, Livestock, and Irrigation and did not move forward. A severe drought in 2017 sparked new interest in the

pursuit of cloud seeding in Montana, and a group of ag producers and legislators sought to renew discussions to remove the obstacles created by SB72. While this effort gathered momentum during the 66<sup>th</sup> legislative session in 2019, action on cloud seeding was limited to the passage of House Joint Resolution 40. The resolution directed the Legislative Services Division to undertake a study to review current practices, reports and regulatory measures in other states and the Canadian provinces with the intent of proposing changes in Montana's laws that would encourage the use of this technology. The delivery of this report in September of 2020 laid the foundation for the introduction of SB29 in early 2021 for the 67<sup>th</sup> legislative session. SB29 offered a comprehensive overhaul of Montana's weather modification statute to enable the more practicable and economically feasible implementation of cloud seeding. Though controversial, the bill was supported through the Senate Natural Resources committee and passed the full Senate on 3<sup>rd</sup> reading by a vote of 26-24. The road to passage was more difficult in the House. The committee initially tabled the bill then revived and passed it on vote of 9-6. The bill died on 2<sup>nd</sup> reading on the house floor by a vote of 35-65 after concerns emerged about the long-term impacts of cloud seeding as a geo-engineering strategy.

Not to be deterred, another effort to change the law was considered in 2023 for the 68<sup>th</sup> legislative session. On advice of DNRC staff, this effort was modified from a change in the weather modification statute to a request for an appropriation to complete a feasibility study and pilot project. \$300,000 was appropriated in the final days of the 68<sup>th</sup> legislative session. This amount was later reduced to \$250,000.

In general, states that support cloud-seeding initiatives surrounding Montana have less restrictive laws and policies with respect to weather modification.

## 3. Data

The data used for this study included both observational data sources and model simulation output. The bulk of the analyses were based upon high-resolution model simulation output, given the types of observational data needed to conduct this analysis largely do not exist or are very limited spatially and/or temporally.

### 3.1. Observations

Public data sources include the Snow Telemetry snow gauge network (SNOTEL) operated by the U.S. Department of Agriculture Natural Resource Conservation Service (NRCS) for precipitation and snowpack measurements. Meteorological data are also available through the National Oceanic and Atmospheric Administration (NOAA).

Data from 9 SNOTEL sites were available for the analysis across the Big Hole Basin ([Figure 3.1](#)). SNOTEL observations provide a long-term record of precipitation from gauges that weigh precipitation and collect snow water content data via pressure-sensing snow pillows located at numerous sites throughout the Western U.S. These sites are owned and operated by the NRCS and are typically located at elevations between 1,800 and 2,700 m above mean sea level (MSL). Historical and real-time data are available from the NRCS web site (<http://www.wcc.nrcs.usda.gov/snow/>) and have been widely used for climatological studies. Several studies also describe known measurement deficiencies (e.g., Serreze et al.

1999; Serreze et al. 2001; and Johnson and Marks 2004) such as an undercatch of snowfall due to wind (Serreze et al. 2001; Yang et al. 1998; Rasmussen et al. 2012). The SNOTEL gauges are placed in a forest clearing where the wind speed is typically  $2 \text{ m s}^{-1}$  or less, and an undercatch of 10–15% is expected. The SNOTEL data resolution is 0.1 inch (2.5 mm), making it difficult to study precipitation characteristics or verify model data on a sub-daily basis. However, these data are suitable for use over monthly or longer periods.

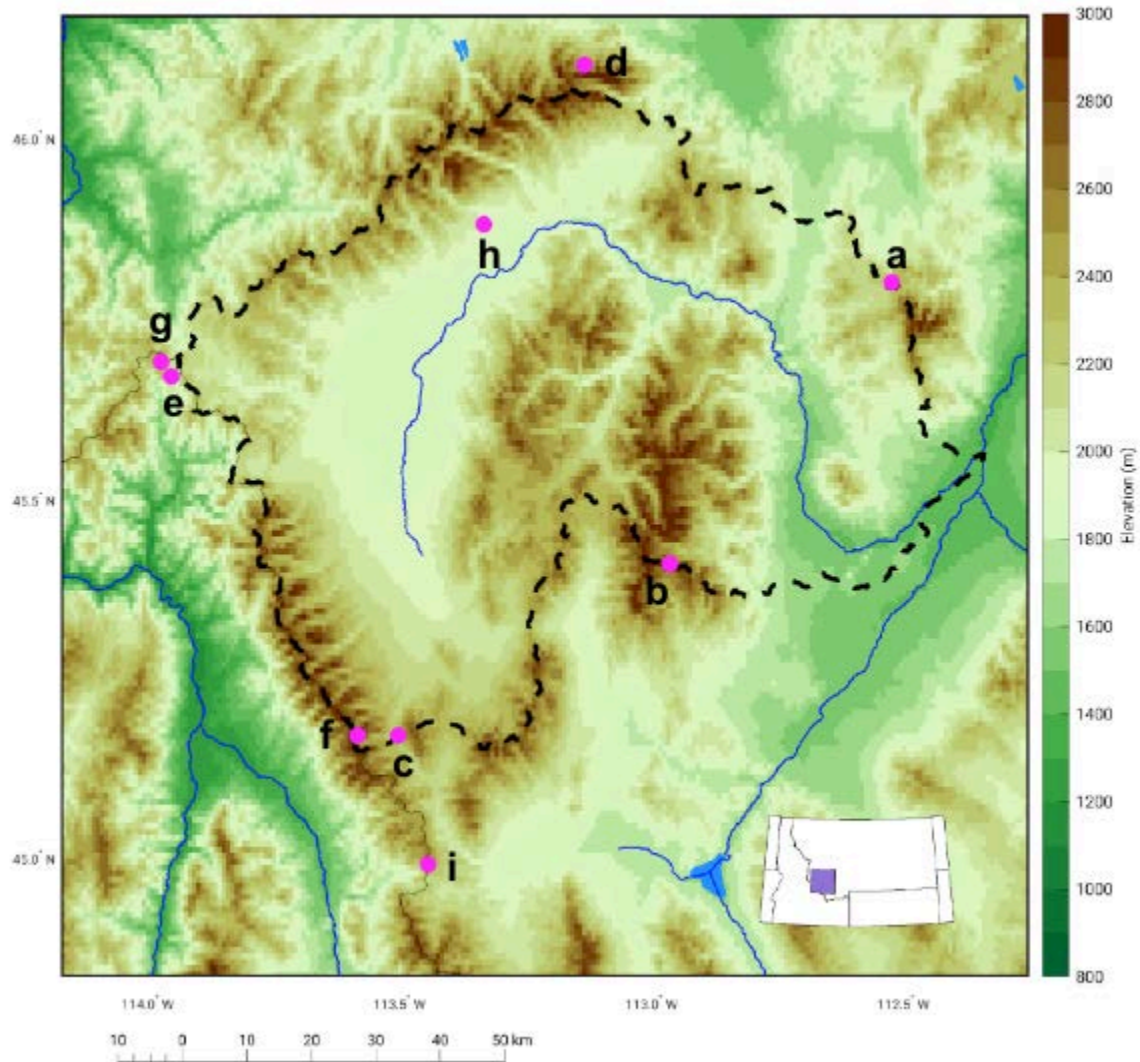


**Figure 3.1.** Terrain map of the study region with the Big Hole Basin outlined with the black dash line and the SNOTEL locations shown by the magenta dots (see [Table 4.1](#) for SNOTEL site name). Inset map shows the location of the study region in the context of the State of Montana.

### 3.2. Model Dataset

Weather Research and Forecasting (WRF) model (Skamarock et al. 2008) data from an updated and expanded 40-year, 4-km CONUS simulation (hereafter, CONUS404) was used in this study. The technical specifications for the CONUS404 simulation are described in Rasmussen et al. (2023). The simulation spans a time period of 1 October 1979 to 30 September 2021, where the first year is discarded to allow for

spin up. Three sets of files were produced at different temporal resolutions, with those used for this study including the hourly full files with all model simulation outputs. [Figure 3.2](#) shows the CONUS404 model simulation domain and [Table 3.1](#) lists the key physical parameterizations used.

A second simulation was also conducted to create a pseudo-global warming (PGW) climate sensitivity experiment. This dataset, called the CONUS404 PGW atmospheric forcing dataset (Xue et al. 2024), is a 42-year simulation covering water years 1980 – 2021 and representing how the weather in those years would have behaved under a future climate scenario.

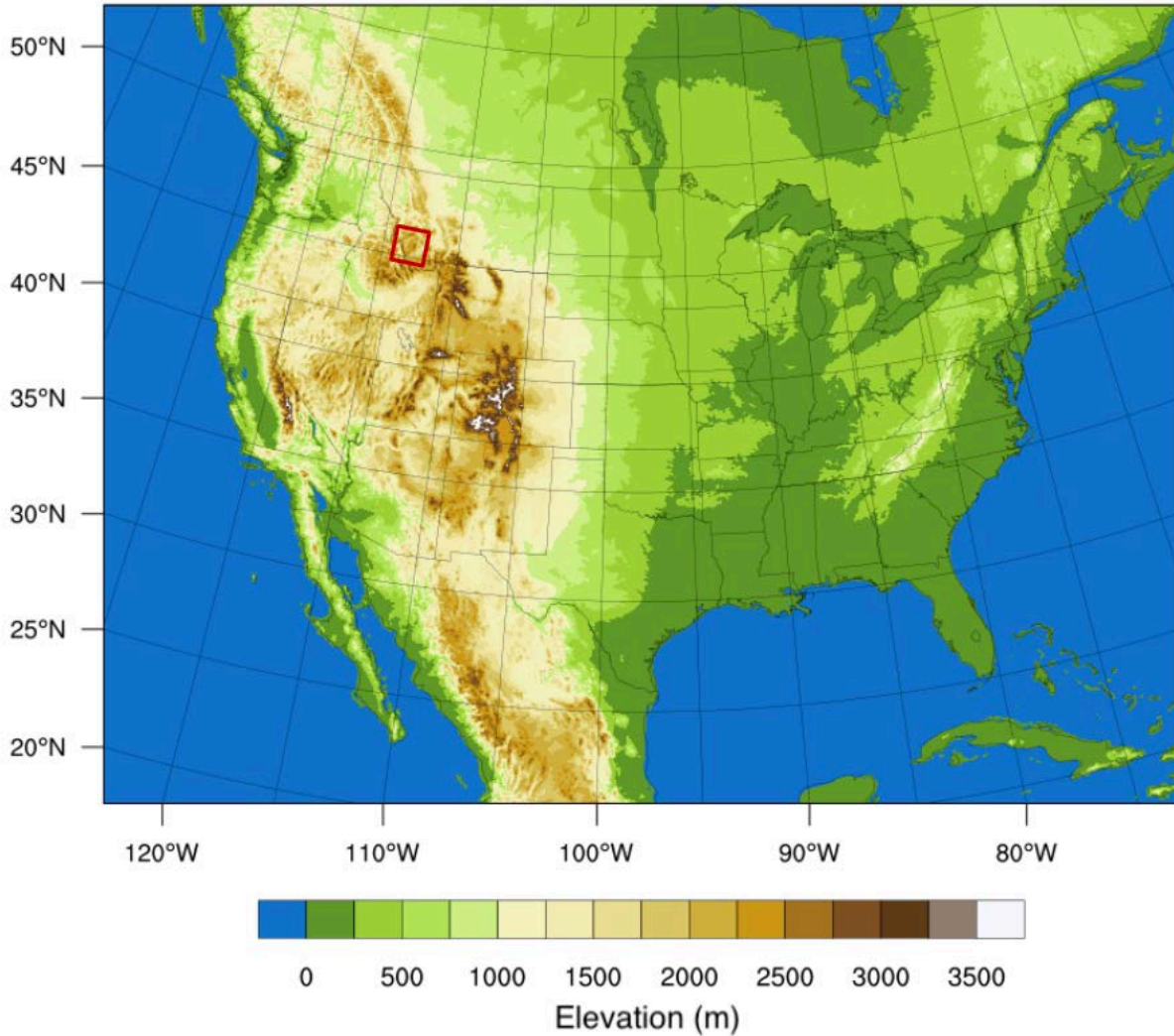


**Figure 3.2:** CONUS404 model domain showing topographical elevation (m). The red box indicates where the climatological analysis was conducted, as reference.

**Table 3.1:** WRF model physics options used in the CONUS404 setup.

NWP physics	CONUS404 Parameterization schemes
-------------	-----------------------------------

Land surface	Noah-MP (multi-physics) Land Surface Model [Niu et al. (2011)]
Microphysics	Thompson scheme [Thompson et al. (2008)]
Planetary boundary layer (PBL)	Yonsei University PBL [Hong et al. (2006)]
Longwave and shortwave radiation	RRTMG [Iacono et al. (2008)]

## 4. Feasibility Study for Big Hole Basin

### 4.1. Methodology

DeMott (1997) indicates that AgI can activate as warm as  $-5^{\circ}\text{C}$ , with activation rates increasing rapidly by  $-6^{\circ}\text{C}$ ; thus, we prescribe a seedable temperature range as being between  $-6^{\circ}\text{C}$  and  $-18^{\circ}\text{C}$ , where temperatures colder than this typically have an abundance of naturally produced ice crystals. In addition to temperature, the other key criterion for cloud seeding is the presence of SLW, which suggests that natural precipitation processes are inefficient and could be augmented by seeding. Therefore, we also utilize a liquid water content (LWC) threshold of 0.01 g/kg (combined with the above temperature threshold) to indicate presence of “seedable SLW”.

Stability and wind estimates may also be necessary to determine how effectively AgI may be transported into a suitable cloud, depending on the method of delivery (ground-based generators or aircraft). Aircraft can target suitable clouds more directly, by burning AgI flares directly inside a targeted cloud. For ground-based seeding to be effective, stability and winds must be conducive to air flowing over the targeted mountain.

To determine the seeding potential of the project areas, analysis was conducted within two layers of the atmosphere. The ground-based layer was defined based upon the depth of the atmosphere within which we assume AgI can be mixed and transported, which is generally within the boundary layer (estimated as 0–1 km above ground level [AGL]). The airborne layer was defined at an altitude that an aircraft can safely fly in cloud (3.5–4.5 km MSL). These results are summarized in [Section 4.3](#) for ground-based and [Section 4.4](#) for airborne opportunities.

First, the 1-hourly CONUS404 model simulation output was used to map the frequency and variability of seedable conditions across the target domain. These statistics were produced for each month and season starting November 1980 and ending April 2021.

In addition to the mapping analysis, two additional methods were employed over the target domain. These included single site analysis of 700-hPa conditions (e.g., winds), and area-based analysis of seeding conditions averaged over areas of the target region for both ground-based and airborne seeding.

The single site analysis was performed by analyzing 700-hPa conditions at individual selected grid points nearest to the 9 SNOTEL locations in and around the Big Hole region denoted by the asterisks in [Figure 4.1](#). The modeled 700-hPa wind conditions at those single grid points were assessed independently as well

as whenever precipitation or SLW was present, thereby representing seedable conditions. For the purposes of model evaluation of precipitation characteristics, modeled precipitation was derived from the inverse distance weighted mean of the four nearest grid points; for the purpose of presence of precipitation for thresholding when characterizing seedable opportunities, the nearest grid point to each SNOTEL site was used.

Targetable regions along each mountain range were defined for the area-based analysis (hatches shown in [Figure 4.1](#)). For this area-based analysis, areal-averaged values for each seedable criterion were produced at every model simulation output time over the grid points shown in [Figure 4.1](#), and used to investigate the seasonal (Nov–Apr) and monthly frequencies of seedable conditions within each region. Following the area-based analysis and initial results of typical wind conditions, theoretical generator locations were proposed; wind and stability conditions at these hypothetical generator sites were then used to evaluate flow for ground-based seeding opportunities.

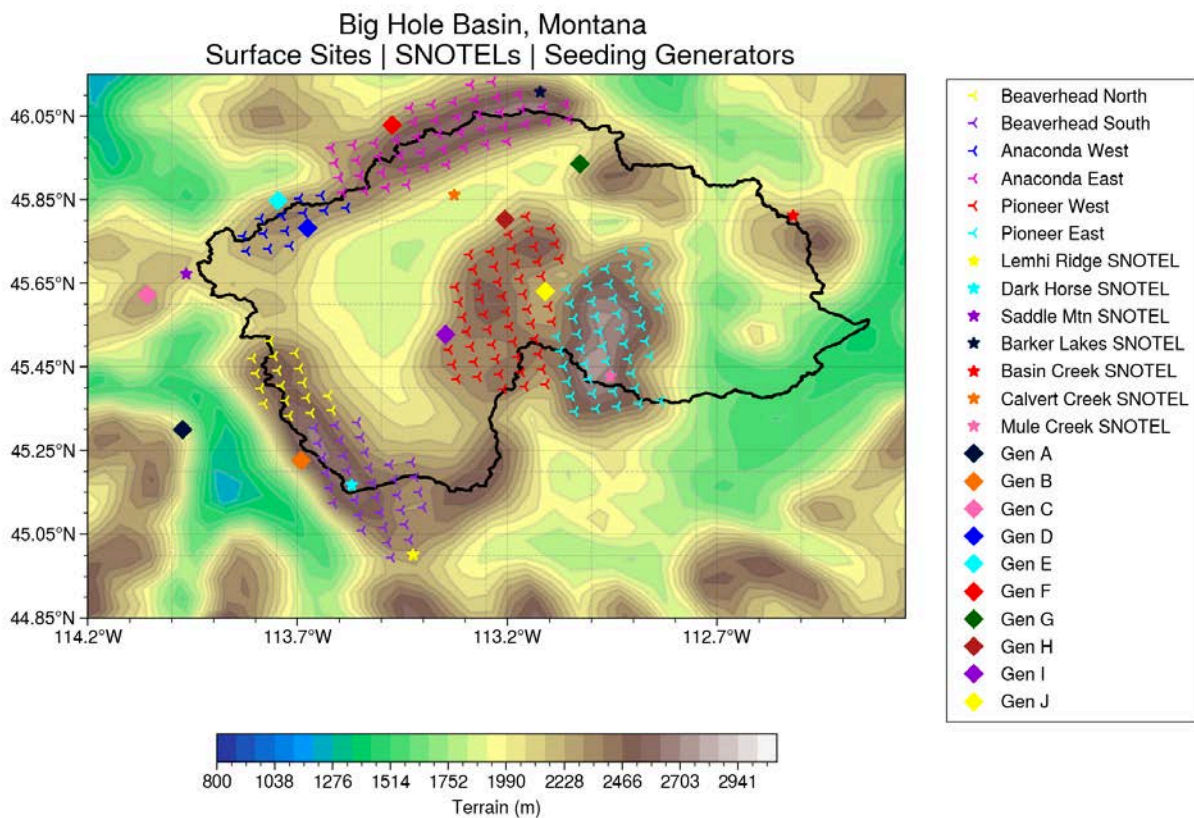


**Figure 4.1.** Target regions (hatches), single site analysis points (diamonds), and precipitation sites (asterisks) used for assessment of CONUS404 simulation output for seedable opportunity frequencies.

For all types of analysis (spatial mapping, single site, and area-based), seeding opportunities were assessed using CONUS404 Current Climate (CC) and PGW. Results are used to provide recommendations under current climate conditions, and the comparison between the PGW and CC simulations provides recommendations for possible future programs.

## 4.2. Characteristics of Precipitation

A description of the precipitation regimes specifically for the Big Hole region follows, along with comparisons between the modeled precipitation and the SNOTEL observations.

### 4.2.1. SNOTEL Precipitation Observations

A total of 9 operational SNOTEL sites are located within the Big Hole Basin area. The locations of these sites are shown above, in [Figure 4.1](#). The elevations and the date at which each site began recording are summarized for each site in [Table 4.1](#). [Figure 4.2](#) shows the mean annual observed precipitation by month for the 40-year period from 1 October 1981 to 30 September 2021. Precipitation across the domain is characterized by local maxima in December and May, with spring experiencing the greatest precipitation. As a whole, the basin sees the least amount of precipitation in the summer months, with a substantial decrease from June into July.

**Table 4.1.** A list of the SNOTEL sites around the Big Hole Basin area, along with their elevation and earliest observation date.

Station label	SNOTEL site	Elevation (m)	Start Year
a	Basin Creek	2188.5	1976
b	Mule Creek	2529.8	1977
c	Bloody Dick	2316.5	1976
d	Barker Lakes	2514.6	1977
e	Moose Creek	1889.8	1979
f	Dark Horse	2726.4	1977
g	Saddle Mountain	2420.1	1967
h	Calvert Creek	1959.9	1974
i	Lemhi Ridge	2468.9	1971

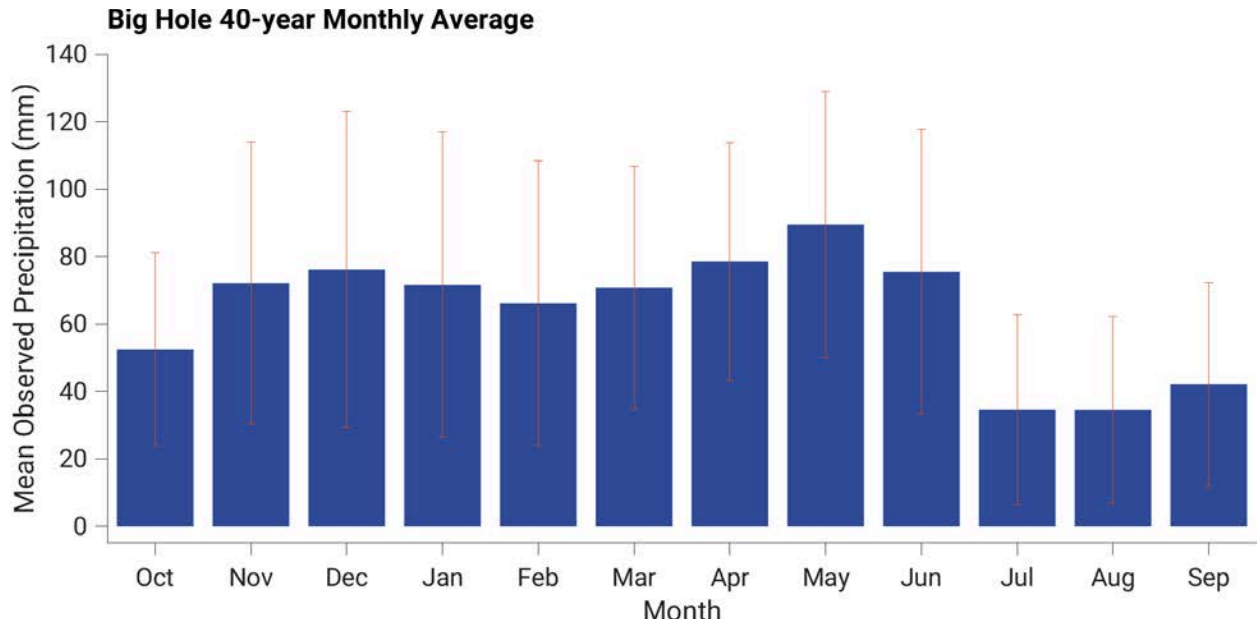
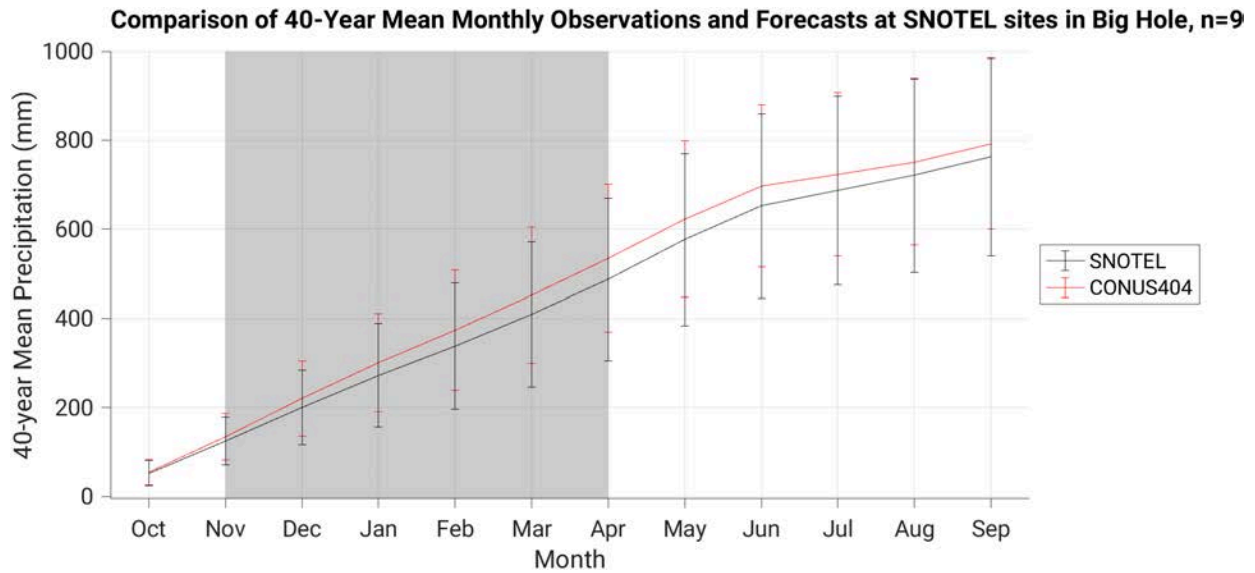


**Figure 4.2.** 40-year monthly average precipitation observed at 9 SNOTEL sites across the Big Hole basin area. Blue bars show the average monthly total precipitation at the SNOTEL sites across the 40-year record. Red whiskers show the standard deviation for each month's average total.

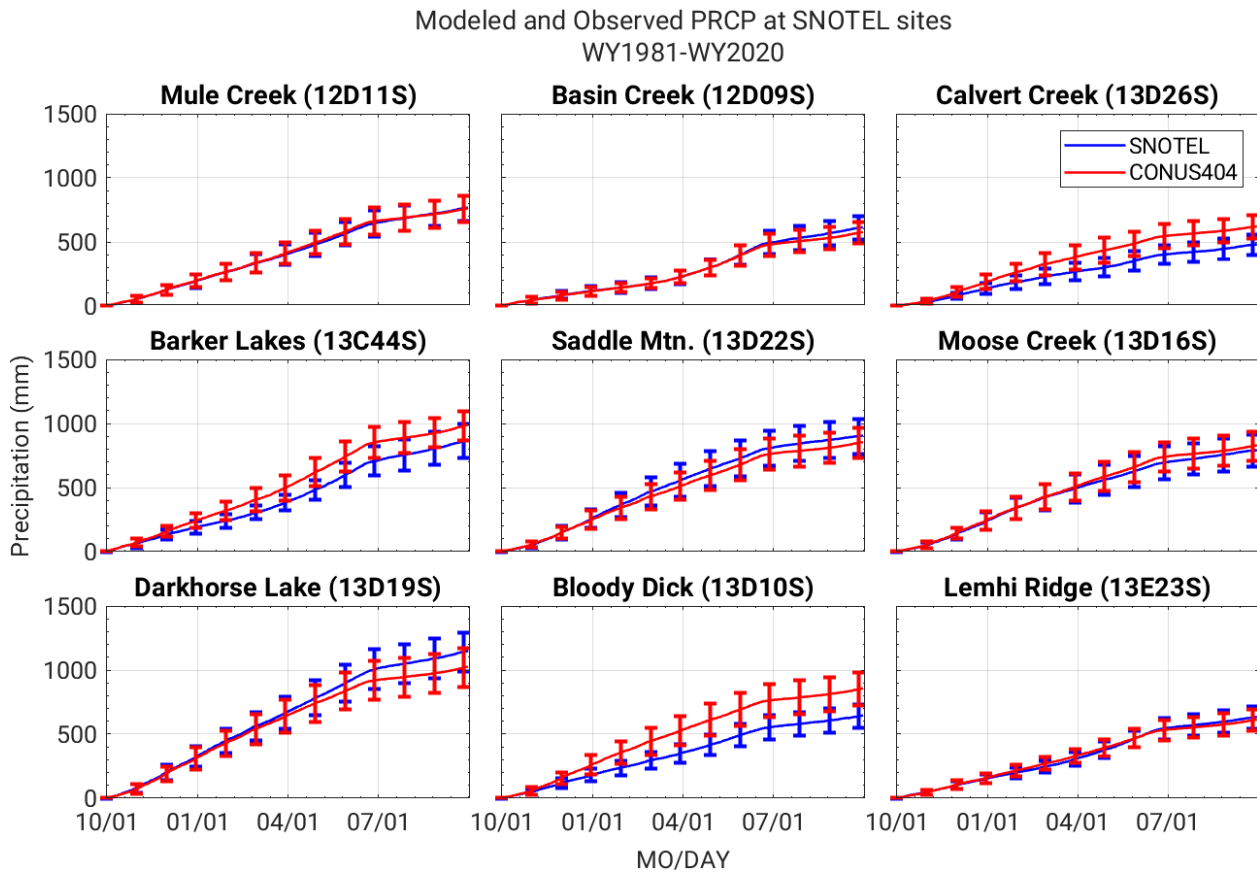
#### 4.2.2. CONUS404 Current Climate vs SNOTEL

To establish a basis for using the model simulation data for this study, the data were compared to measurements from 9 SNOTEL sites across the Big Hole region ([Table 4.1](#)). The model simulation data at the SNOTEL sites were obtained by taking the inverse-distance weighted average of the four data points closest to each SNOTEL site. The domain-wide comparison shown in [Figure 4.3](#) illustrates an overall slight overprediction throughout the water year, with error at a maximum in April at just under 50 mm (9.8% error) and compensating slightly through the summer, with an end of year error just under 30 mm (3.7% error). The comparison by site showed that CONUS404 produced near matches of precipitation accumulation to the SNOTEL observations at most sites; however, a few sites did not compare well ([Figure 4.4](#)). Three sites where the model overpredicted precipitation amounts steadily throughout the water year were at Barker Lakes, Bloody Dick, and Calvert Creek. The overall percent bias at these sites was positive (indicating the overprediction) and >10% ([Table 4.2](#)). One site where the model performed well during the winter, but then underrepresented precipitation in the summer months, was Darkhorse Lake. The percent bias at this site was also >10% ([Table 4.2](#)), but the bias was driven by the summertime precipitation error. The spatial pattern of winter time (Nov–Apr) precipitation accumulation is shown in [Figure 4.5](#), and shows the greatest precipitation (>800 mm) falls in the Beaverhead Mountains on the west and southern portion of the study region. The nearby Darkhorse Lake SNOTEL recorded 708 mm on average during the winter months ([Table 4.2](#)). The next greatest precipitation accumulations are in the Anaconda Range in the north (>700 mm). The Barker Lakes and Calvert Creek SNOTEL sites nearby are not likely representative of the maximum snowfall in this region, as they are on the periphery and/or at lower elevations. The Barker Lakes SNOTEL recorded 425 mm on average during the winter months ([Table 4.2](#)). The Pioneer Mountains, in the center of the domain, typically showed 400–600 mm of

precipitation accumulation during the winter on average. Mule Creek, situated south-centrally in the Eastern Pioneer Mountains, recorded 431 mm on average ([Table 4.2](#)).



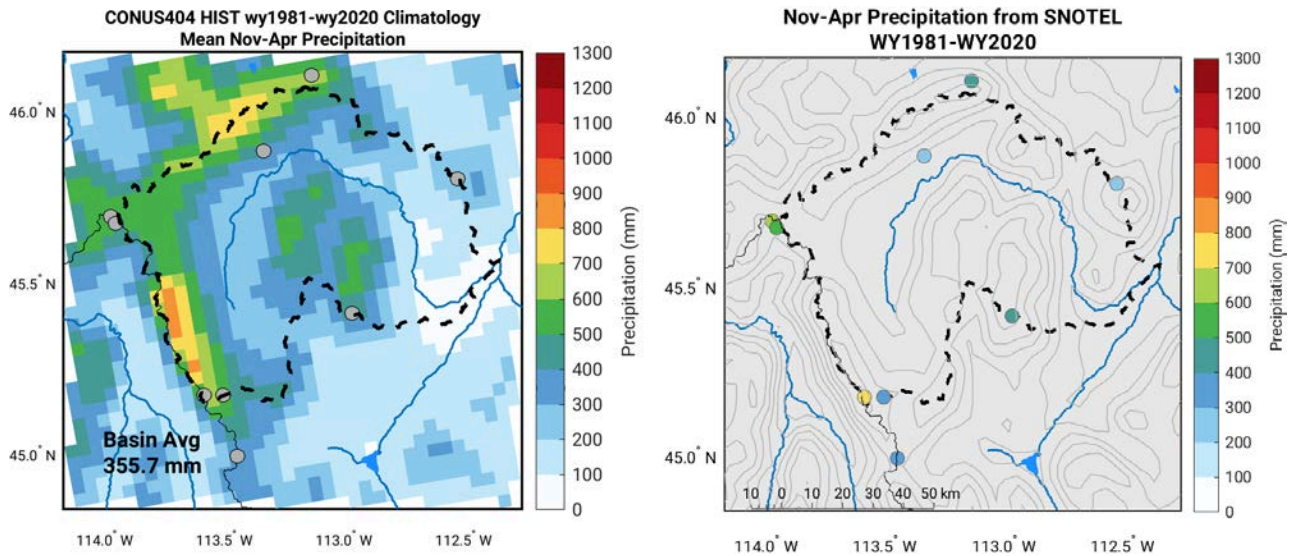
**Figure 4.3.** Comparison of the 40-year mean monthly observations and model simulations across the 9 SNOTEL sites in the Big Hole region.



**Figure 4.4.** Comparison of 40-year average (1981–2020) precipitation accumulation over the water year at each of the 9 SNOTEL sites as listed in [Table 4.1](#) in the Big Hole region from CONUS404 (red) and SNOTEL (blue).

**Table 4.2.** WRF CONUS404 simulation (WRF) vs SNOTEL observations (OBS) 40-year average precipitation statistics at each SNOTEL site.

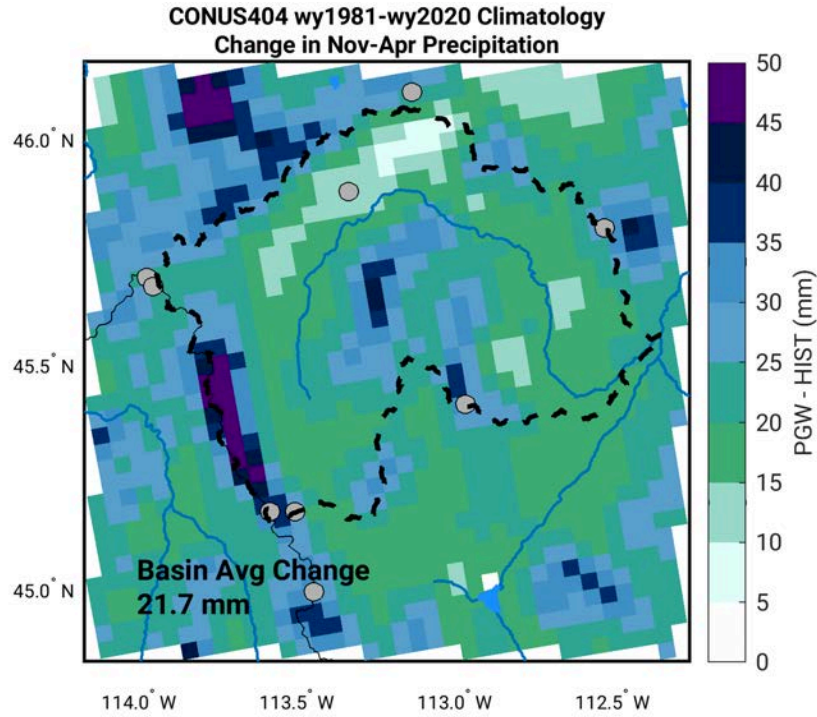
SITE NAME	Annual Total (mm)		Bias		Winter Total (mm)		Bias	
	WRF	OBS	(mm)	%	WRF	OBS	(mm)	%
Basin Creek	576.7	615.3	-38.6	-6.3	260.0	260.5	-0.5	-0.2
Calvert Creek	620.4	481.9	138.5	28.7	396.9	271.5	125.4	46.2
Saddle Mtn.	854.4	906.5	-52.1	-5.7	541.8	600.7	-59.9	-9.8
Mule Creek	761.6	768.5	-6.9	-0.9	443.6	431.6	12.0	2.8
Darkhorse Lake	1026.1	1151.3	-125.1	-10.9	671.4	708.5	-37.1	-5.2
Lemhi Ridge	614.8	636.4	-21.6	-3.4	352.5	334.6	17.9	5.3
Barker Lakes	988.6	868.7	119.9	13.8	555.8	425.9	129.9	30.5
Moose Creek	828.7	792.5	36.2	4.6	534.3	514.4	19.9	3.9
Bloody Dick	857.1	646.7	210.4	32.5	554.4	371.8	182.6	49.1



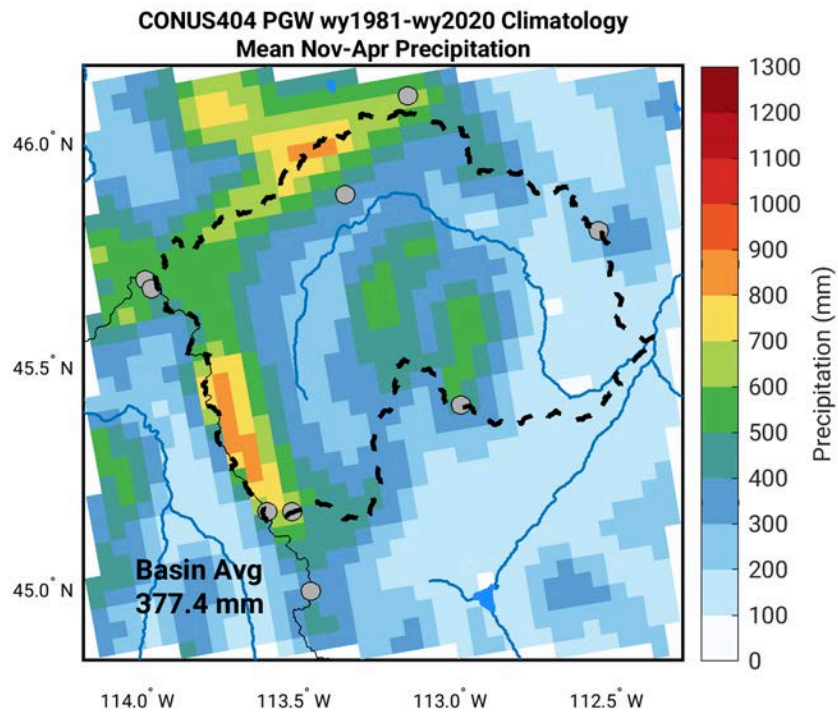
**Figure 4.5.** Map of 40-year average (1981-2020) Nov-Apr precipitation totals from (left) CONUS404 simulation and (right) SNOTEL data.

#### 4.2.3. CONUS404 Current Climate vs Future Climate

A summary of precipitation characteristics from PGW simulations and their relation to the CC results are provided to help determine if there will be anticipated future changes in precipitation in the Big Hole region due to a changing climate. [Figure 4.6](#) shows the difference in wintertime precipitation totals (PGW-CC), and the results from each simulation separately are shown in [Figure 4.5](#) (current climate, above) and [Figure 4.7](#) (PGW, below). The difference field illustrates a uniformly positive change across the domain, with some peaks showing differences near 50 mm. The average increase across the basin is 21.7 mm. Examination of the spatial patterns across both simulations indicates that the greatest changes are not necessarily in the regions with the greatest precipitation (e.g., the large increase in the West Pioneer Mountains and several mountain peaks outside the basin boundary). However, the overall spatial distribution of wintertime precipitation is very similar between both simulations.

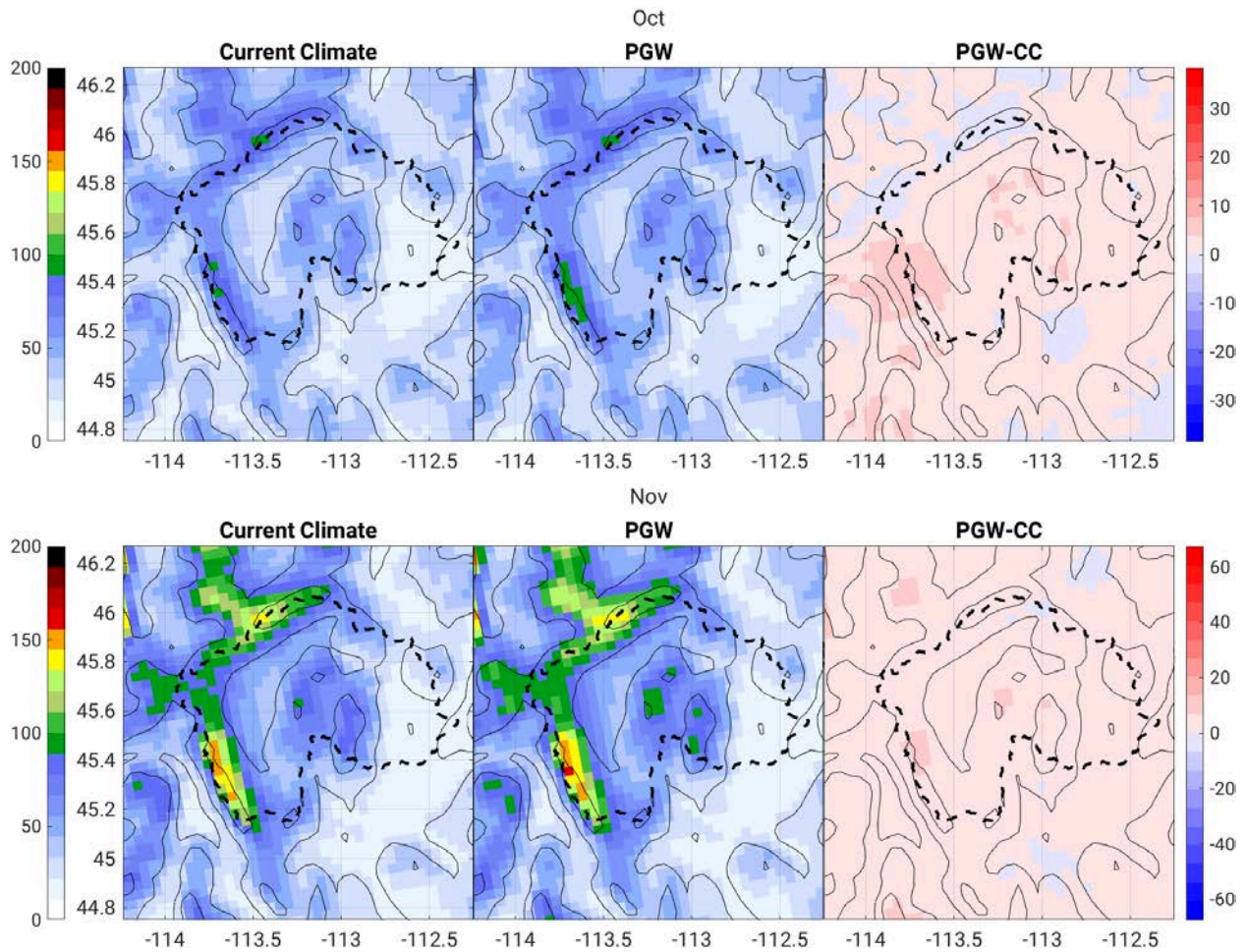


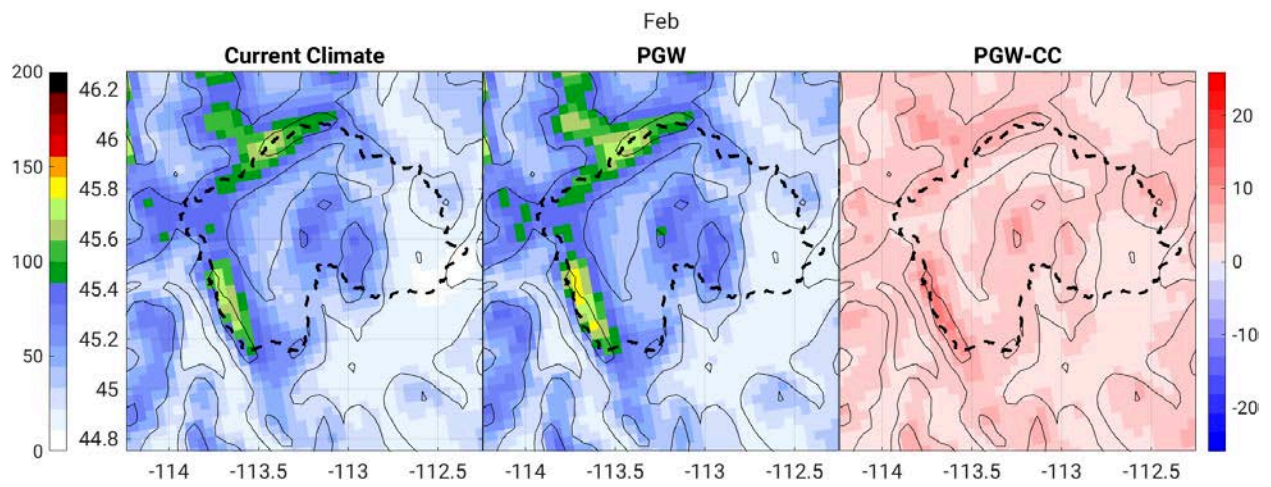
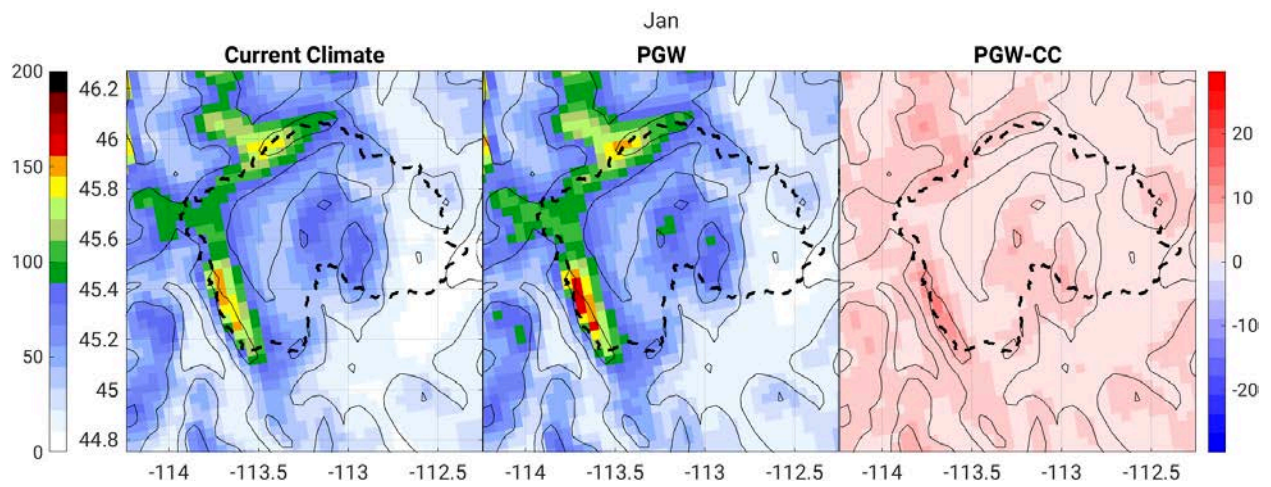
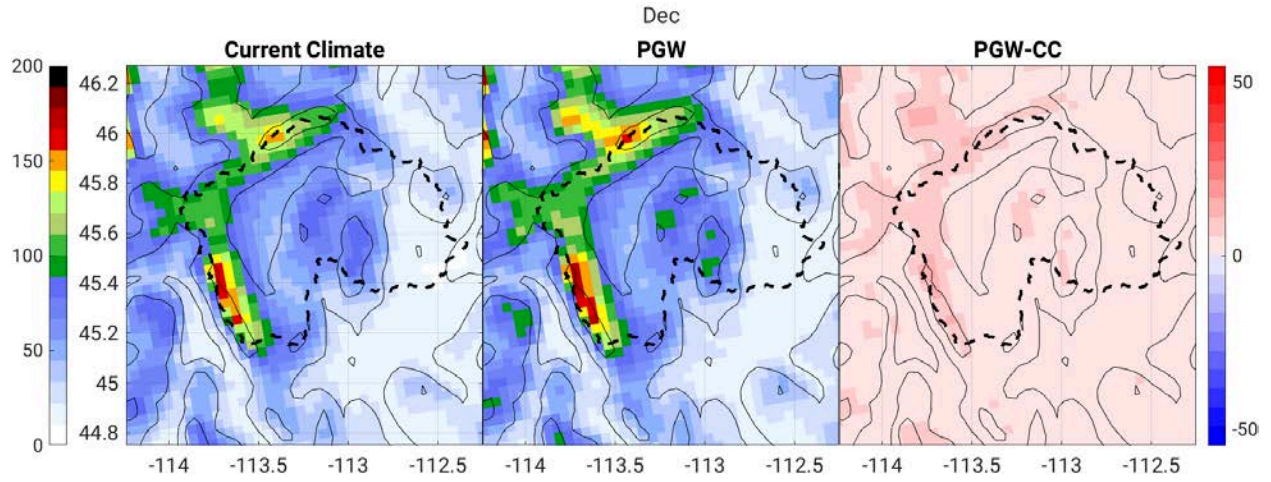
**Figure 4.6.** Difference (PGW-CC) in mean November to April precipitation totals between the CONUS404 current climate (HIST in figure) and PGW simulations. All values in the region are positive.

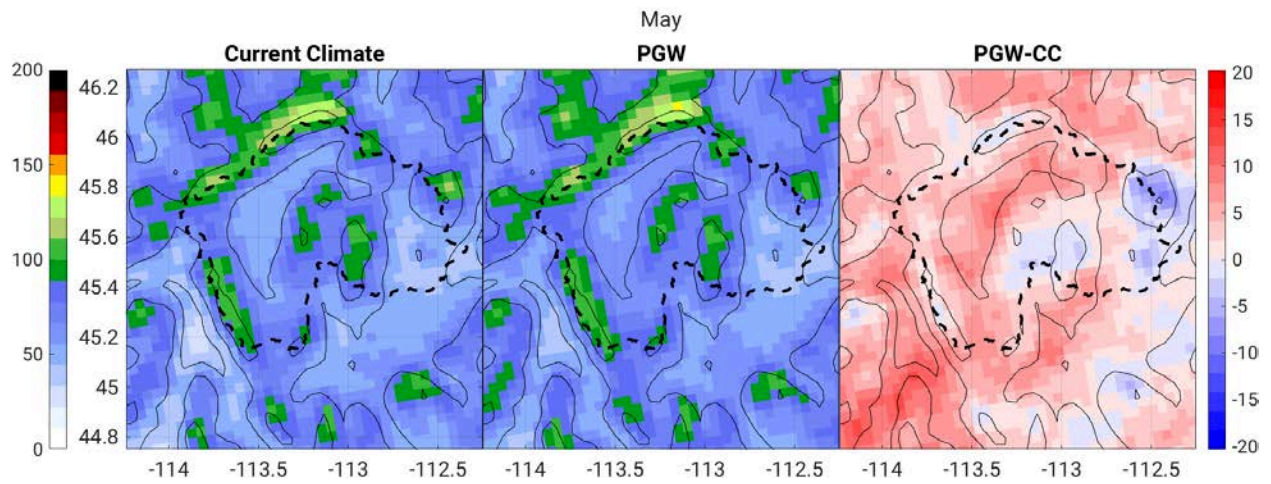
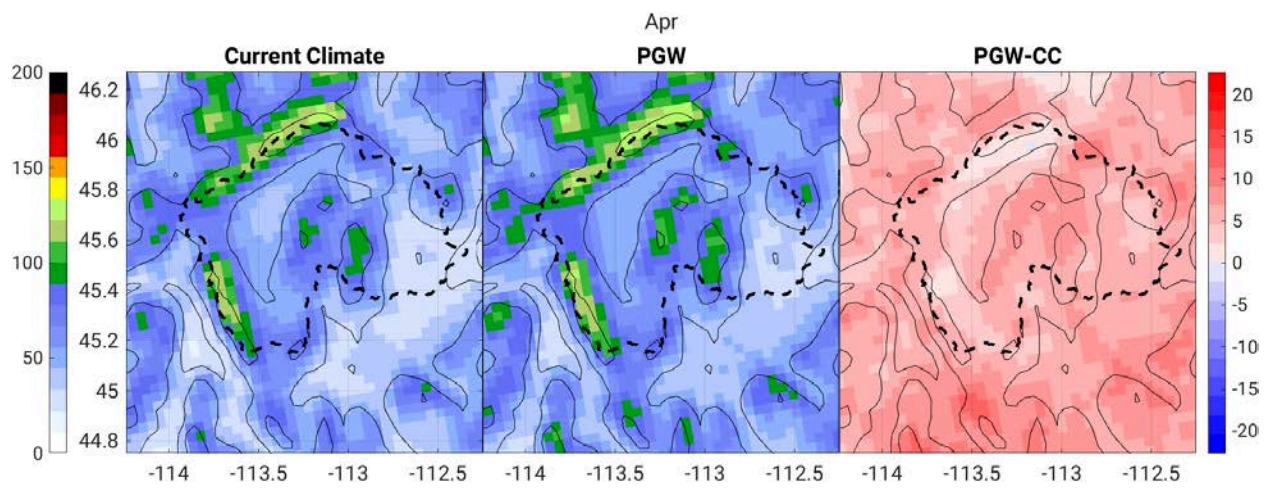
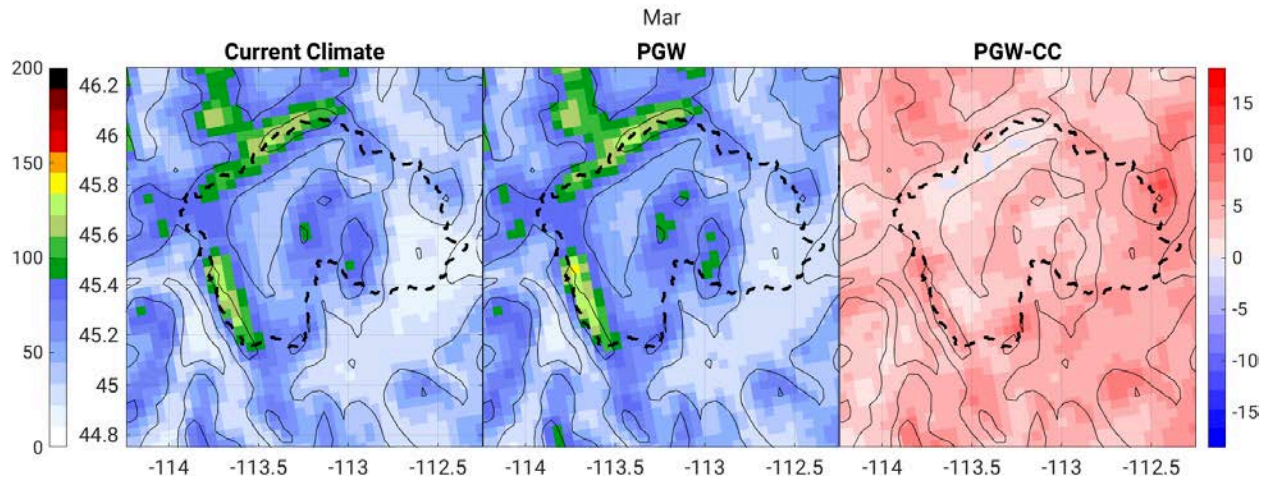


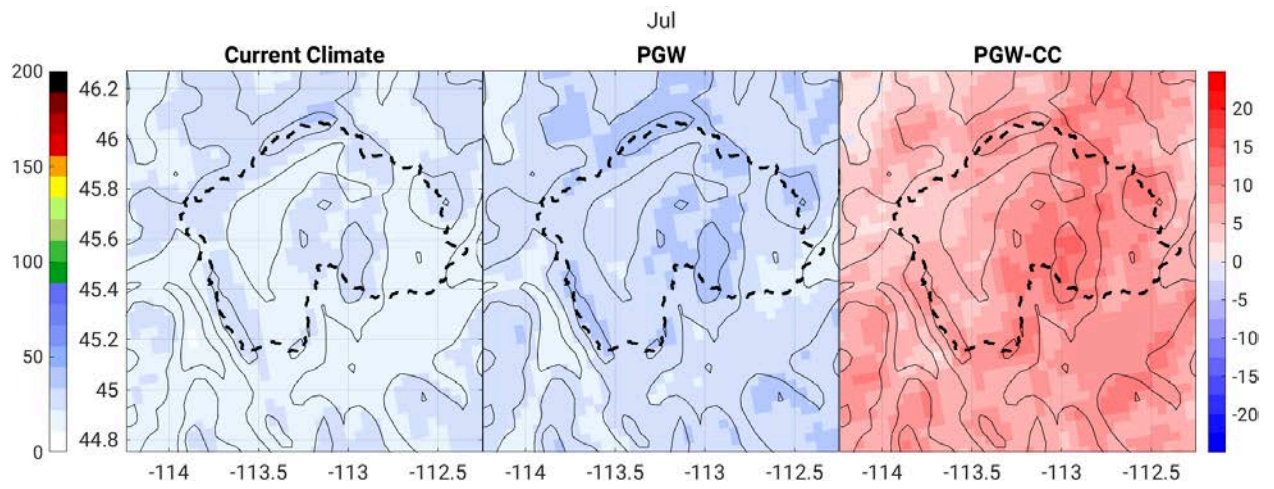
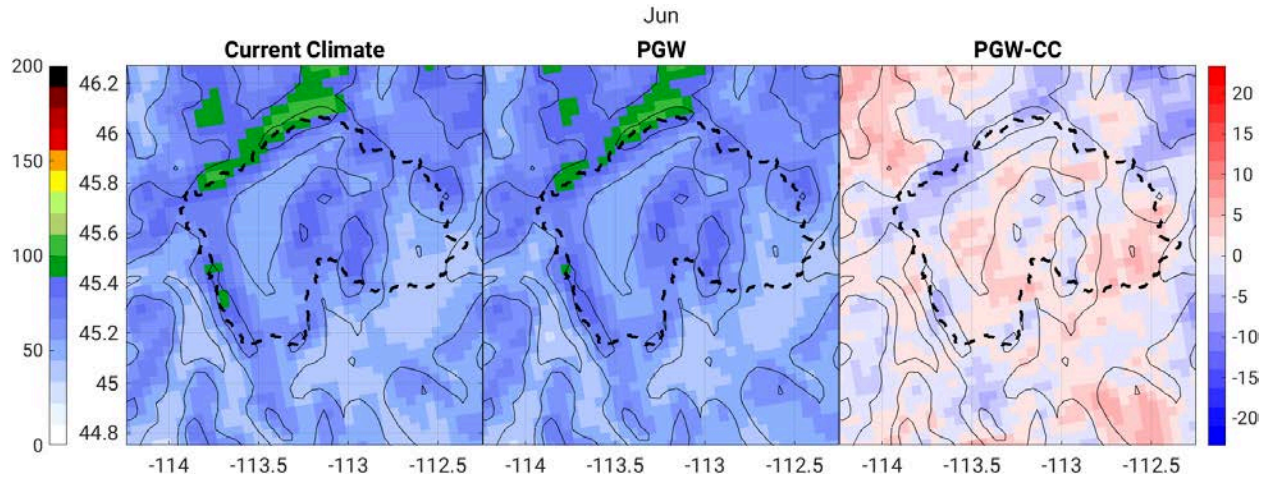
**Figure 4.7.** 40-year mean November to April precipitation totals for the CONUS404 PGW simulation.

Average monthly precipitation totals for both current climate and PGW, as well as the difference between the two (PGW-CC), are shown in [Figure 4.8](#). In both simulations, precipitation peaks in December and January for the Beaverhead Mountains and Anaconda Range, with a later peak in April/May for the Pioneer mountains. The change in spatial precipitation patterns from current climate to PGW varies across individual months. While there are increases in precipitation domain wide in December, January, and February, consistent with the positive change in total winter precipitation shown in [Figure 4.6](#), there is a small decrease in the Anacondas in spring, a decrease in precipitation over the Pioneers in May, and a decrease in precipitation at high elevation in summer.









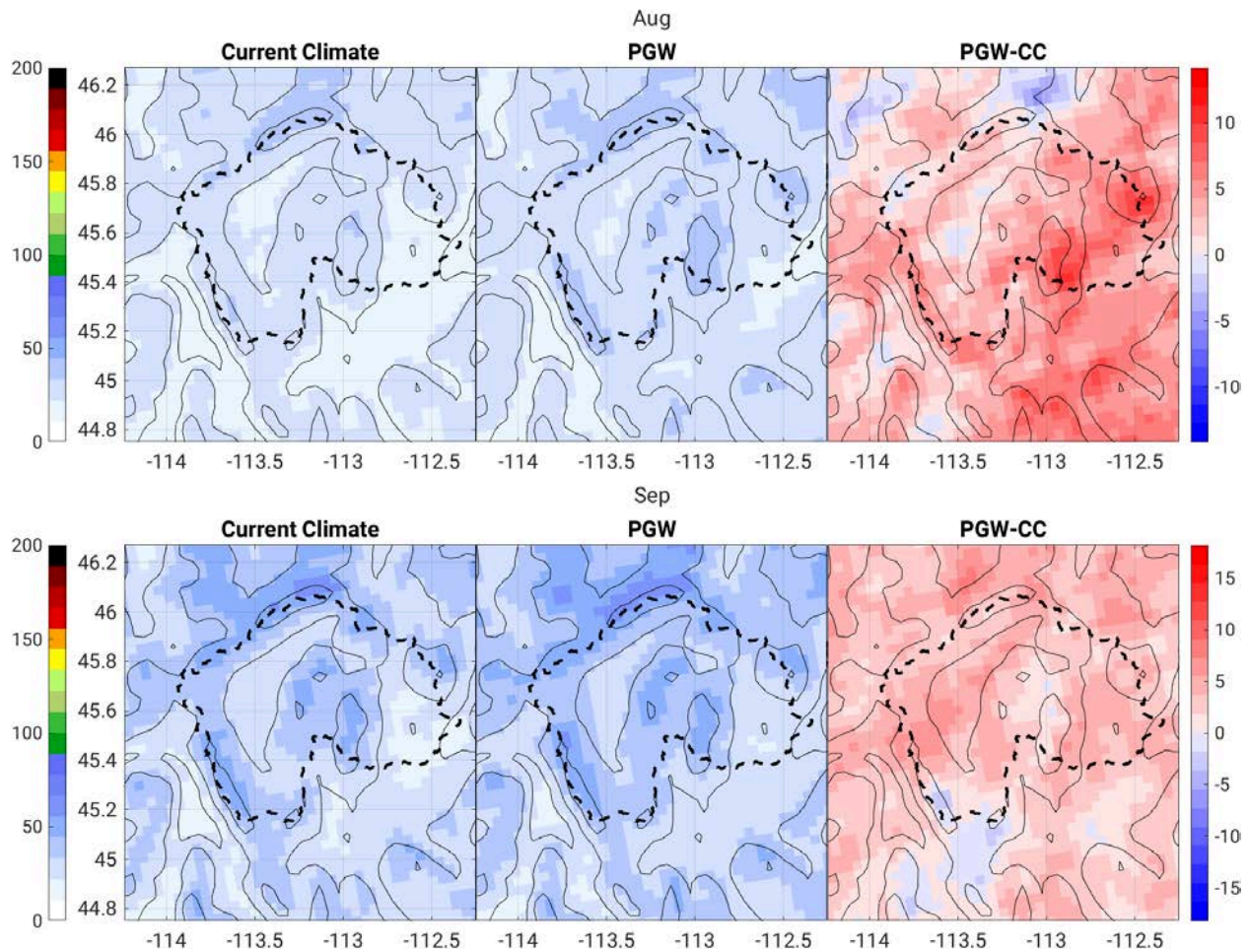


**Figure 4.8.** 40-year average monthly precipitation totals for the CONUS404 current climate (left), PGW (middle), and the difference between the two (PGW-CC, right).

The basin-wide fraction of precipitation falling as snow is shown in [Figure 4.9](#), split by elevations greater than 2000 m (red) and less than 2000 m (blue). At high elevations, nearly all of the precipitation is snow in December through March, with only a small decrease in this fraction in November and April. While the majority of precipitation in October and May is snow, there is a substantial shift towards rain, suggesting that restricting seeding operations to the proposed November-April season would be most effective. The basin-wide average fraction of precipitation falling as snow is reduced at both elevation groups when considering PGW, indicating that while precipitation largely increases in the PGW simulation, less of it is simulated as snow.

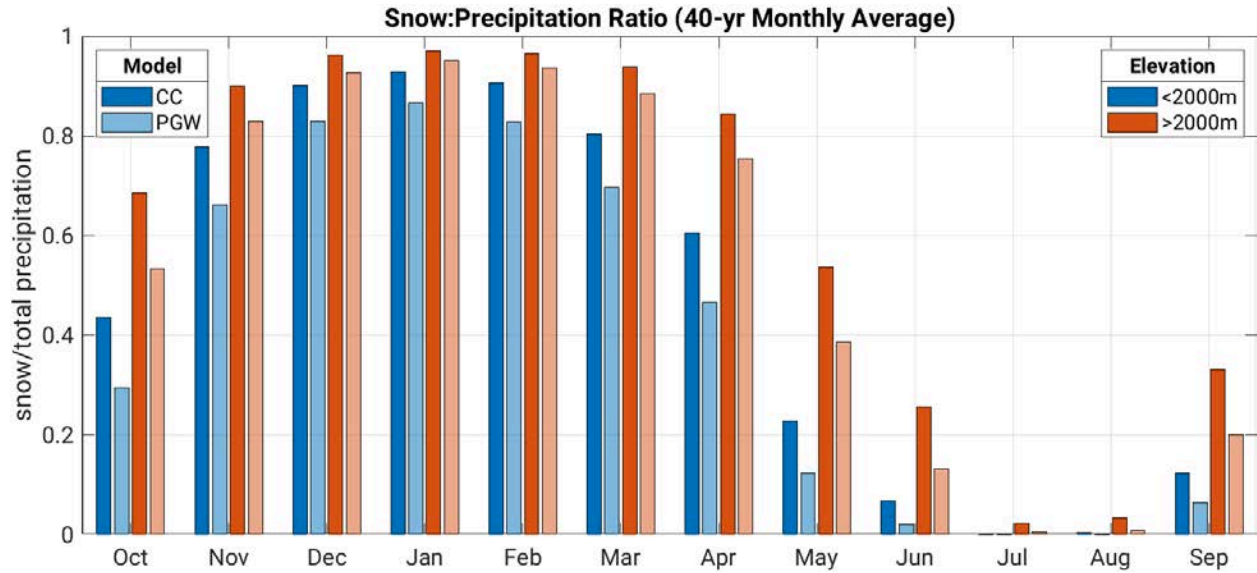


**Figure 4.9.** 40-year average fraction of precipitation falling as snow, by month. Red (blue) bars indicate data from grid points with elevations greater (less) than 2000 m. Darker bars represent current climate, and lighter bars represent PGW.

The spatial distribution of the 40-year average November to April ratio of snow to total precipitation is shown in [Figure 4.10](#). Nearly all current climate precipitation in this period falls as snow in the Pioneer Mountains and Anaconda Range, with a slightly smaller ratio in the Beaverhead Mountains. A large fraction of precipitation in the lower elevations on the western side of the basin is snow in this period as well. However, in PGW, this fraction is reduced domain-wide, with the largest reductions in the low elevations on the eastern side of the Big Hole basin and in the Lemhi basin to the southwest. The northernmost portion of the Anaconda Range and eastern Pioneer Mountains show the smallest reductions in fraction of precipitation falling as snow.

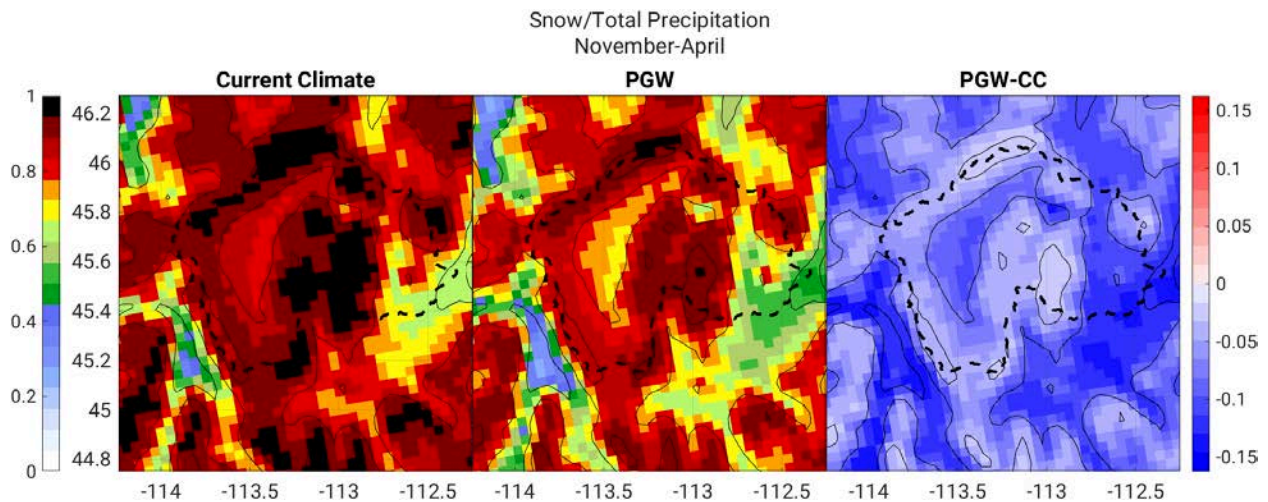


**Figure 4.10.** Spatial distribution of the 40-year average November-April fraction of precipitation falling as snow for current climate (left), PGW (middle), and the difference between the two (PGW-CC; right).

The interannual variability of the November to April fraction of precipitation falling as snow is shown in [Figure 4.11](#). At higher elevations, this fraction is relatively consistent, while the lower elevation fraction is far more variable. The gap between current climate and PGW is highly variable at both high and low elevation, ranging from nearly no change to as great as a 10% reduction at high elevation and over 15% reduction at low elevations.

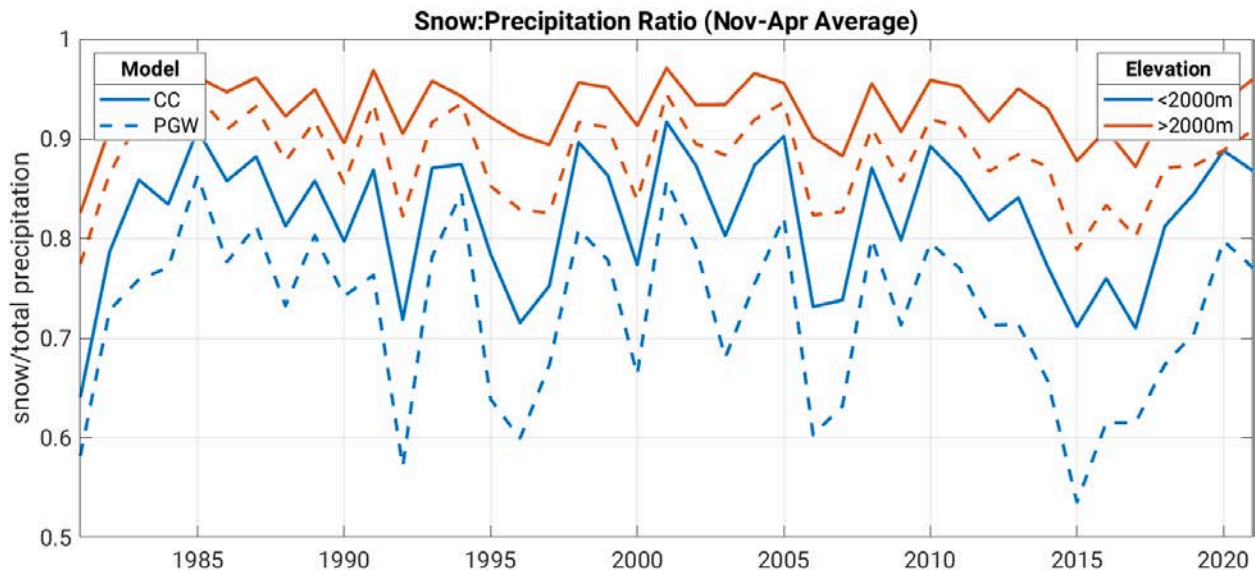


**Figure 4.11.** November to April average fraction of precipitation falling as snow by year. Red (blue) lines indicate data from grid points with elevations greater (less) than 2000 m. Solid lines represent current climate, and dashed lines represent PGW.

### 4.3. Ground-based Seeding Feasibility

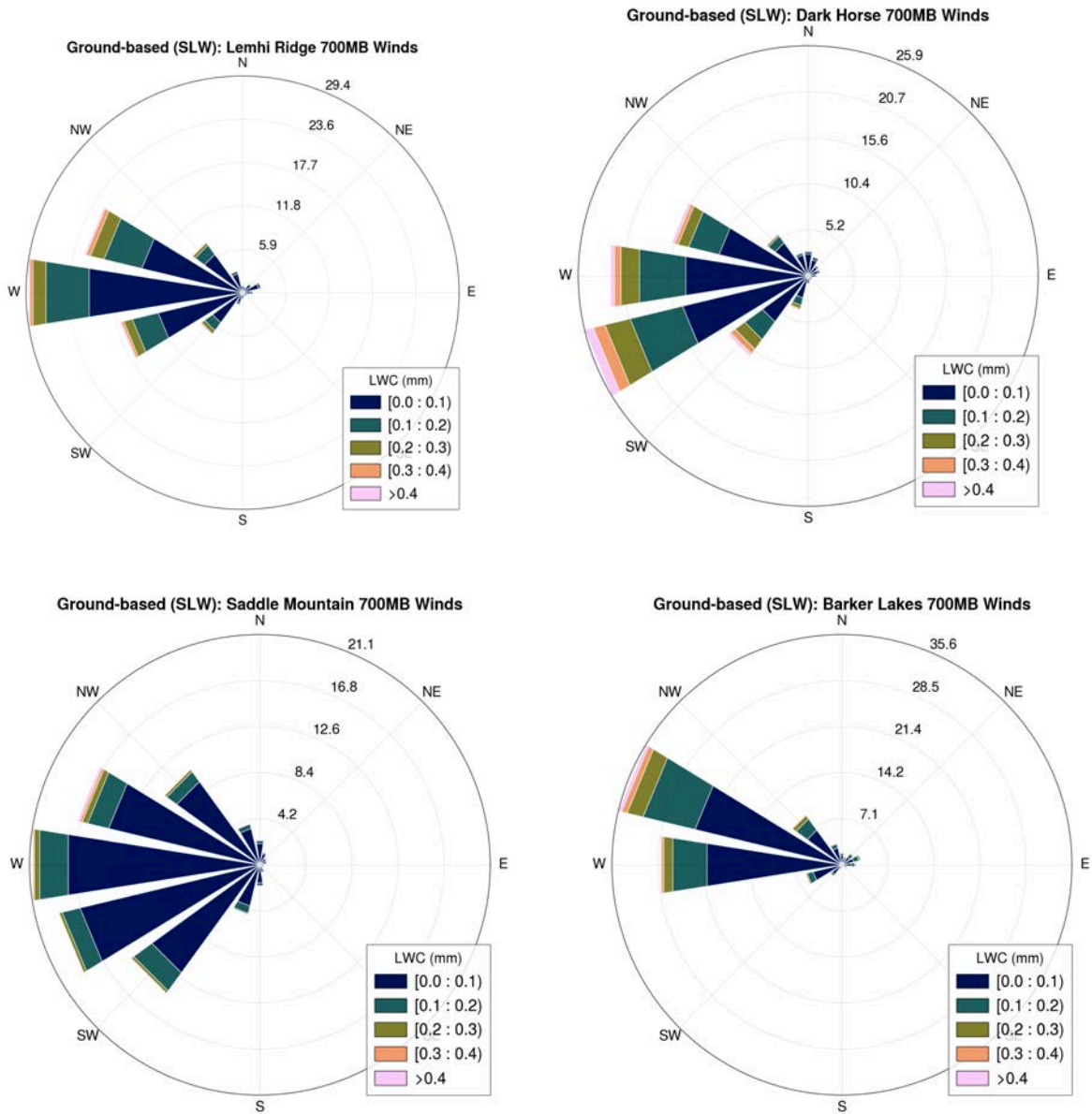
In the following section, ground-based seeding feasibility for the Big Hole Basin region is assessed using the CONUS404 current and future climate simulations. As described in [Section 4.1](#), several approaches were used to estimate the frequency of seedable opportunities in the Big Hole Basin. For ground-based seeding, a representative height range of 0–1 km AGL was used. Maps of layer average LWC, temperature, and frequency of SLW were created from the model dataset. Additionally, target regions were identified and used to calculate monthly and annual frequencies of ground-based seeding opportunities. Ground-based seeding is affected by airflow, so additional analysis was conducted to characterize winds and expected airflow around and over mountain barriers in the region.

#### 4.3.1. CONUS404 Current Climate Simulations

##### Single Site Analysis

Analysis of ground-based conditions was conducted using 700-hPa winds for the Beaverhead Mountains, Anaconda Range, and West and East Pioneer Mountains. Simulated winds at selected grid points associated with SNOTEL locations were used to determine the predominant wind directions when ground-based SLW was present ([Figure 4.12](#)). While the predominant wind direction across the domain ranged from south-westerly to north-westerly, the Beaverhead Mountains experienced more westerly and southwesterly flow on average when SLW was present. The southern portion of the Anaconda Range

experienced varied flow from south-westerly to north-westerly, while the northern side of the range was primarily west to north-westerly. The West Pioneers were dominated by strong westerly component winds, while the East Pioneers saw an increase in a bit more southerly component and also indicated some frequency of north-easterly winds. The greatest amounts of SLW were found in the Beaverhead Mountains under WSW flow in amounts greater than 0.4 mm. Overall, similar results were found when precipitation was present and thus are not shown here for the sake of brevity.



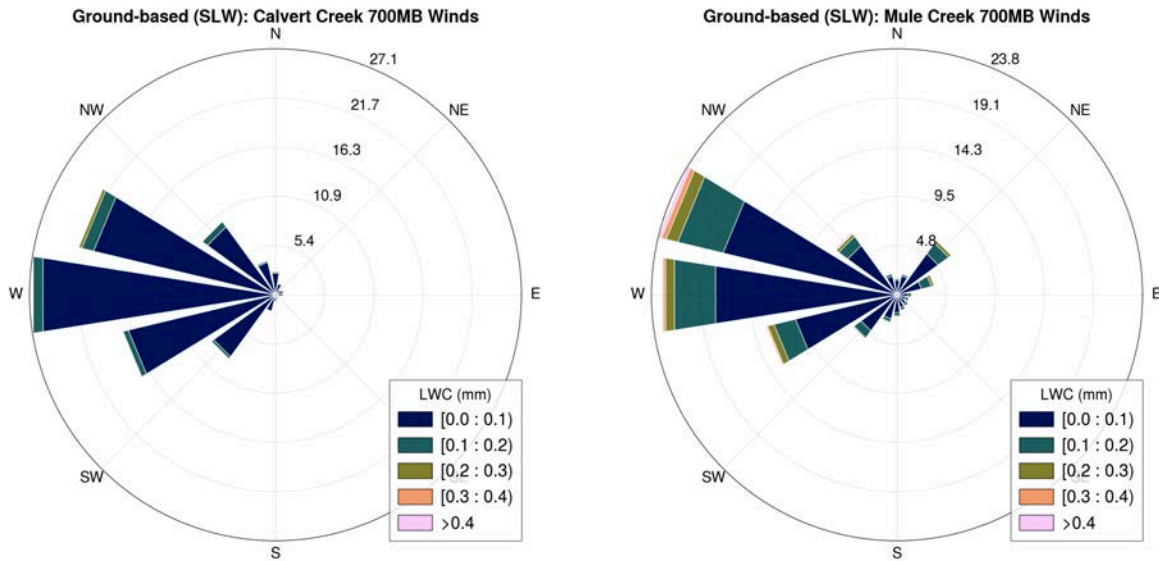
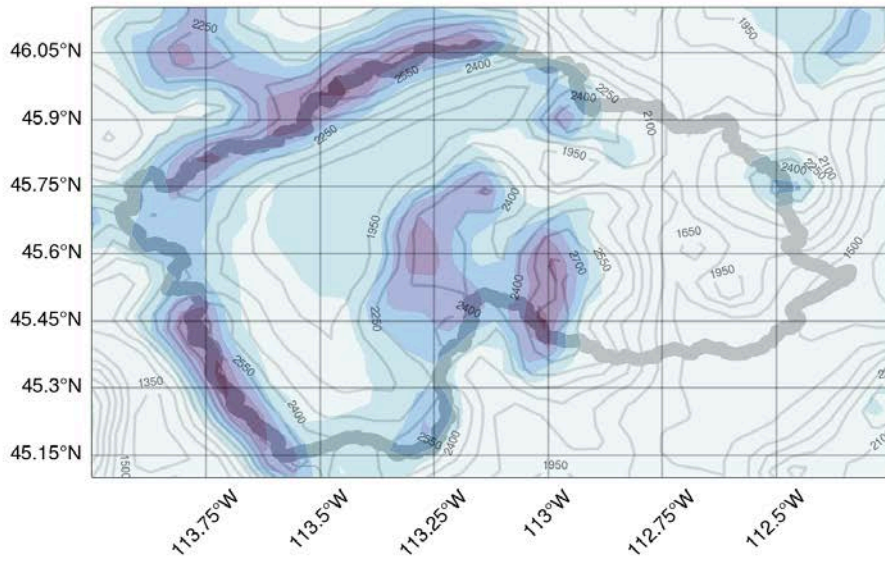


**Figure 4.12.** 700-hPa winds at grid points nearest SNOTELs in the region when ground-based SLW ( $-6^{\circ}\text{C}$  or cooler) is present. Mountain ranges represented are as follows: Beaverhead Mountains (top row), Anaconda Range (middle row), West and East Pioneer Mountains (bottom row).

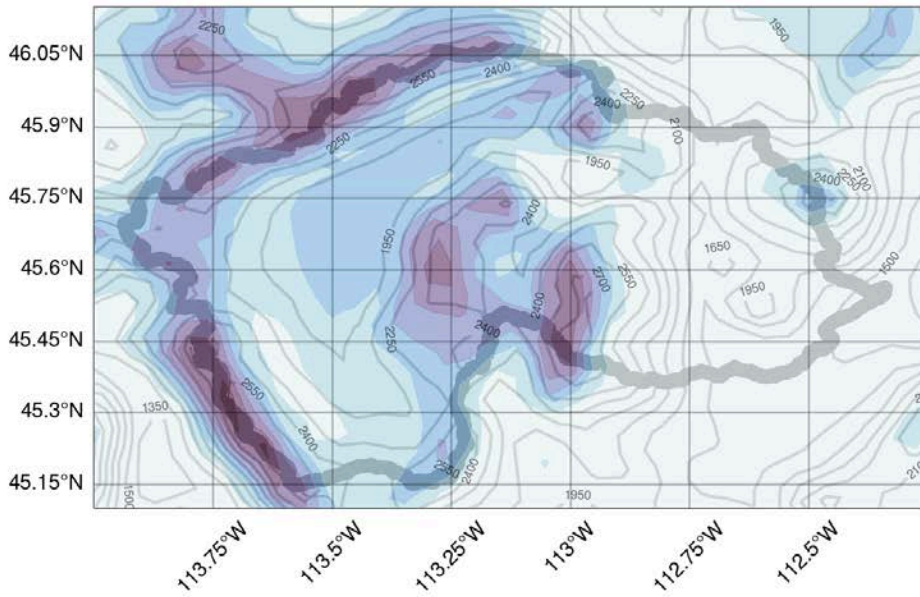
### Spatial Analysis

Maps of simulated 40-year monthly frequencies of seedable conditions (presence of SLW with temperatures between  $-6$  and  $-18^{\circ}\text{C}$ ), average LWC, and average temperature in the target domain within the ground-based layer are shown in [Figure 4.13](#), [Figure 4.14](#), and [Figure 4.15](#), respectively. Frequencies of seedable conditions are large throughout the winter season across the higher elevations of all ranges within the domain, although the greatest frequency of seedable conditions is found from December through February with a secondary peak in April over the lower Beaverhead Mountains, Pioneer and Anaconda Ranges.

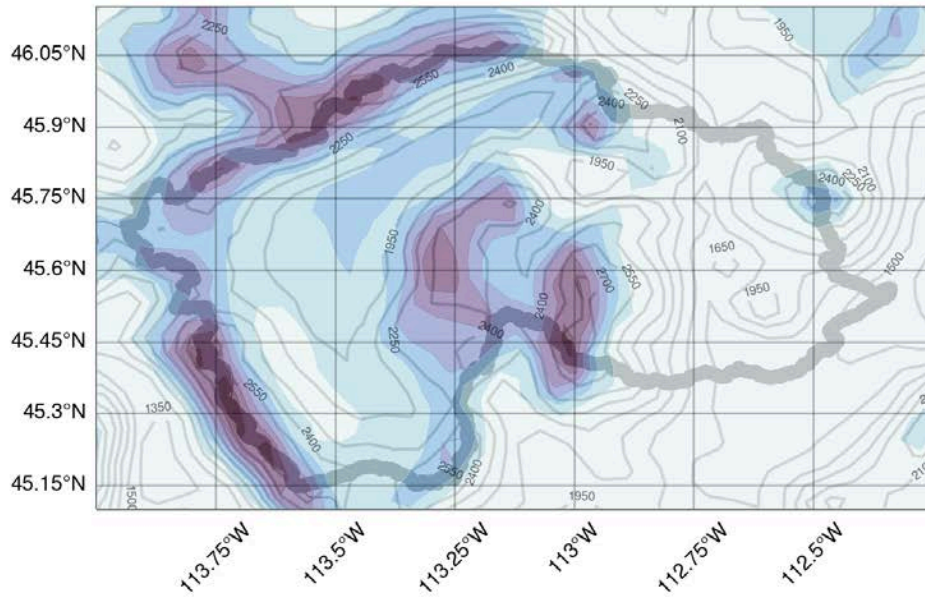
CONUS404 Current Climate  
Ground LWC Frequency (November)



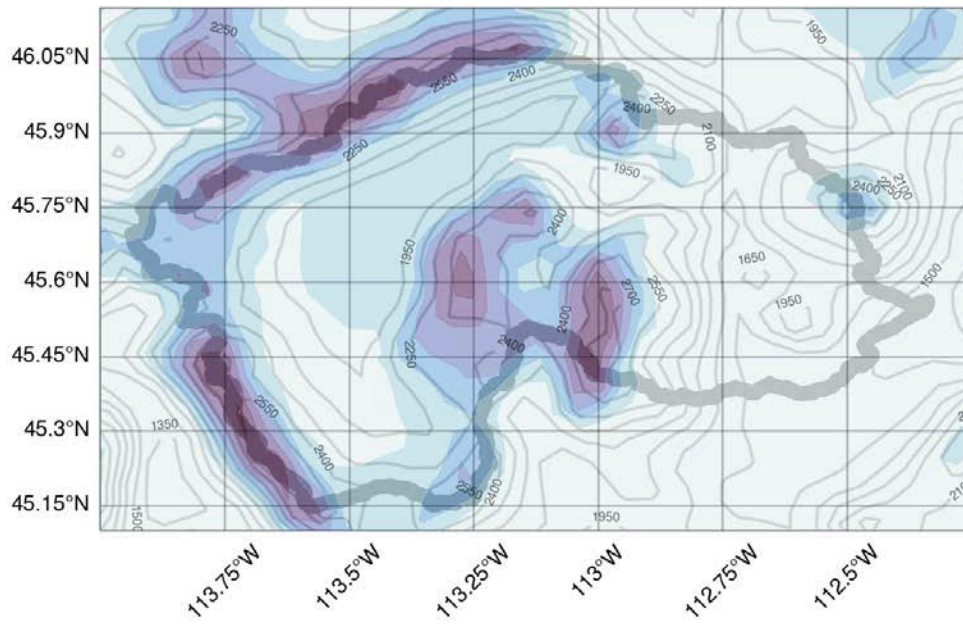
CONUS404 Current Climate  
Ground LWC Frequency (December)



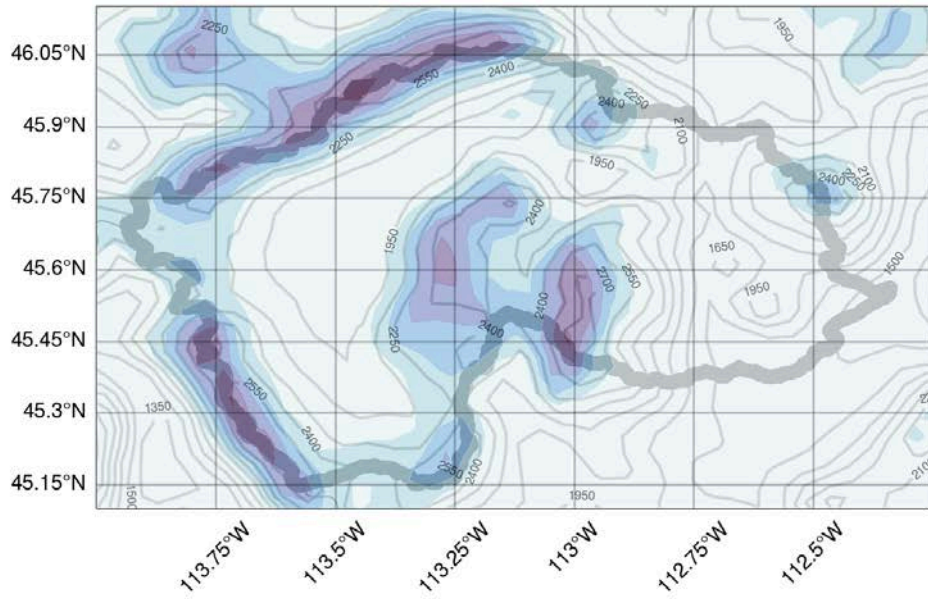
CONUS404 Current Climate  
Ground LWC Frequency (January)



CONUS404 Current Climate  
Ground LWC Frequency (February)



CONUS404 Current Climate  
Ground LWC Frequency (March)



CONUS404 Current Climate  
Ground LWC Frequency (April)

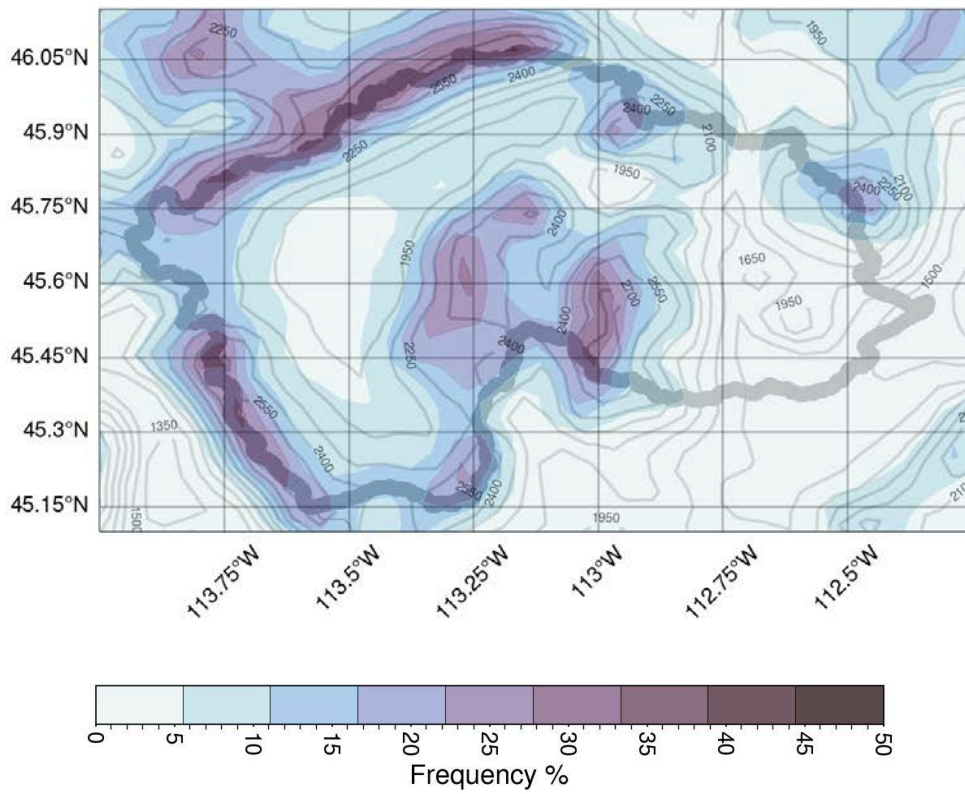
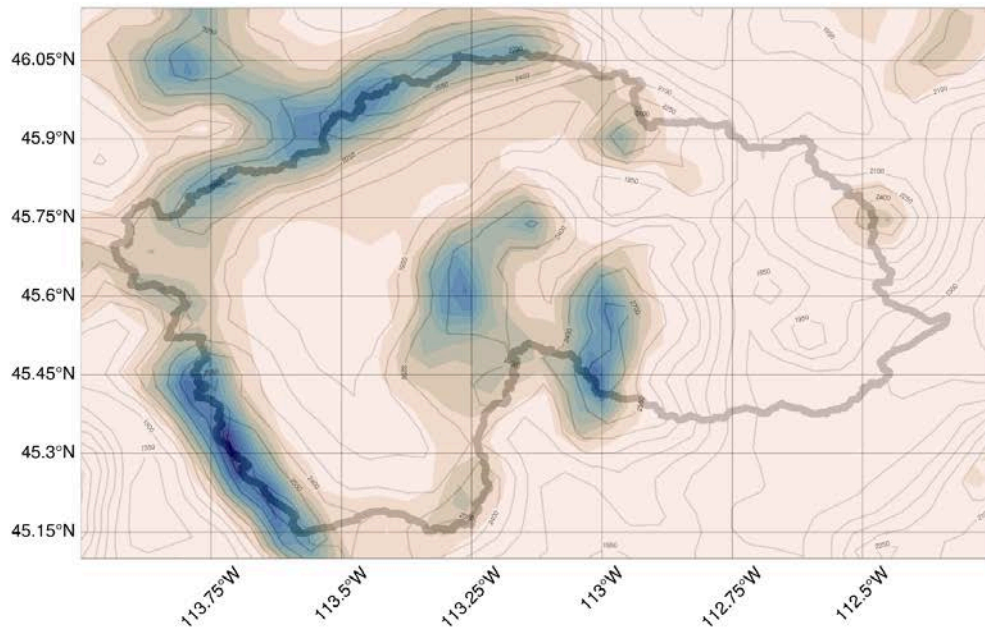


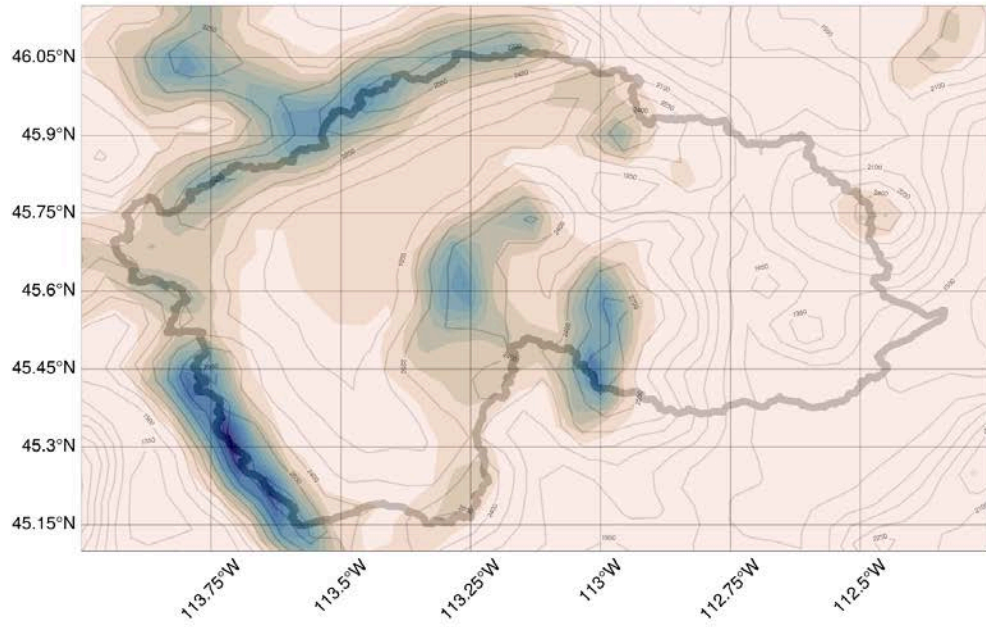
**Figure 4.13.** Frequency of ground-based seedable conditions by month based on presence of LWC > 0.01 g/kg and temperatures between  $-6^{\circ}\text{C}$  to  $-18^{\circ}\text{C}$ .

LWC is present in areas of elevated terrain, with the greatest values over the Beaverhead Mountains in amounts up to 0.075 g/kg (Figure 4.14). The Anaconda and Pioneer Ranges are secondary regions of large LWC with values up to 0.060 g/kg. The average LWC is greatest from November through February with a sharp decline in March and April, especially in the Beaverhead Mountains. However, despite the decline in LWC values in the spring months, values up to 0.035 g/kg remain large enough to be considered seedable. In the calculation of the average frequencies, zero values are included. Therefore, the monthly average values shown in Figure 4.14 are used as a comparison value across space and time.

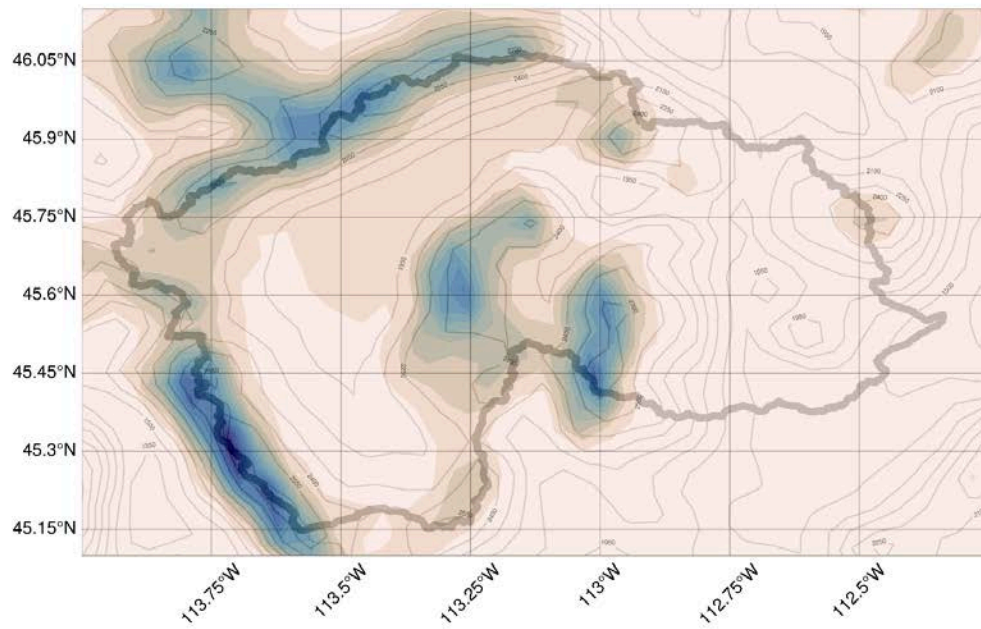
CONUS404 Current Climate  
Ground LWC Average (November)



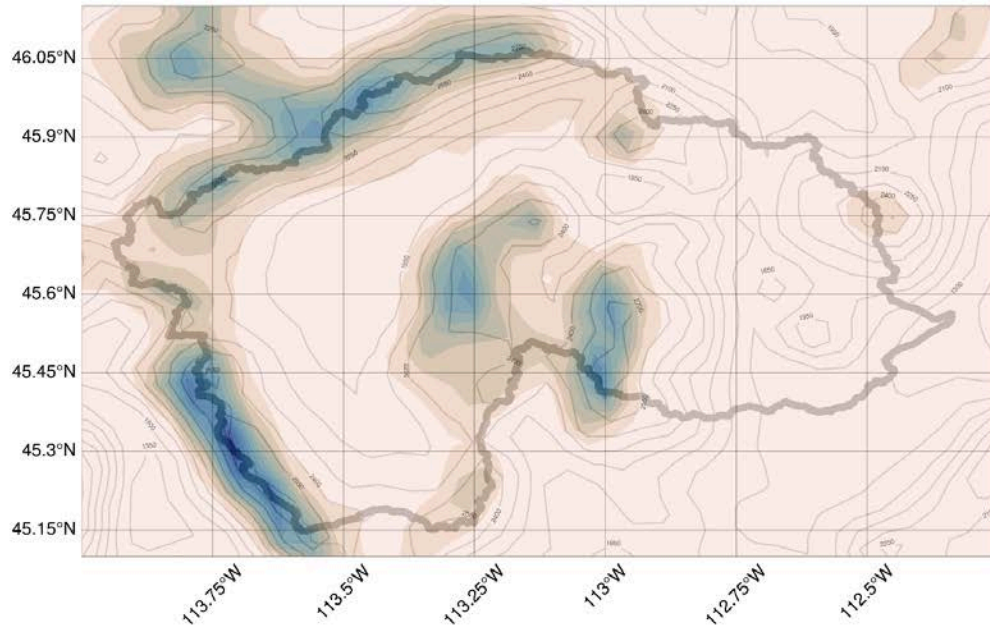
CONUS404 Current Climate  
Ground LWC Average (December)



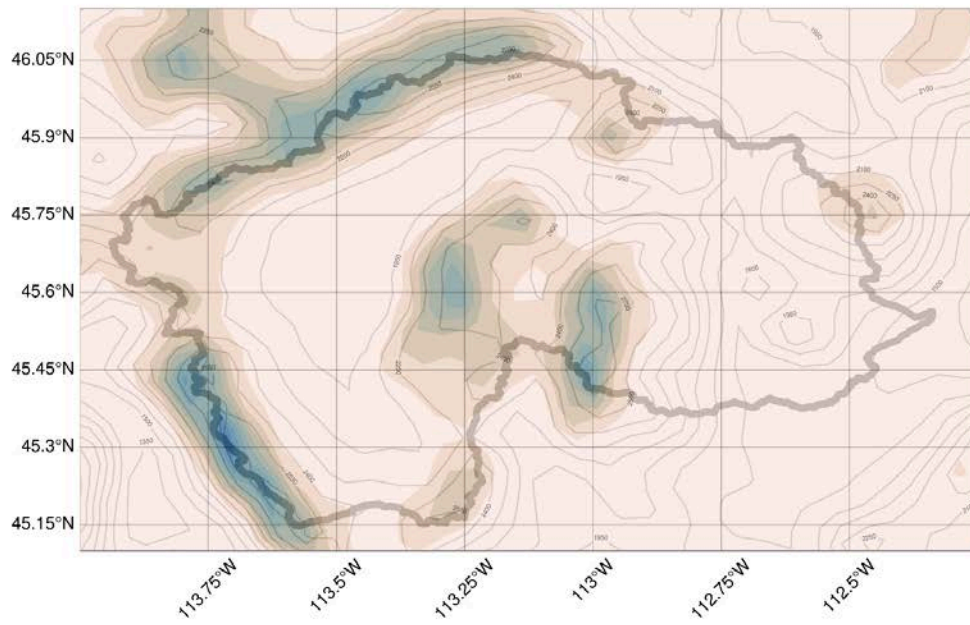
CONUS404 Current Climate  
Ground LWC Average (January)



CONUS404 Current Climate  
Ground LWC Average (February)



CONUS404 Current Climate  
Ground LWC Average (March)



CONUS404 Current Climate  
Ground LWC Average (April)

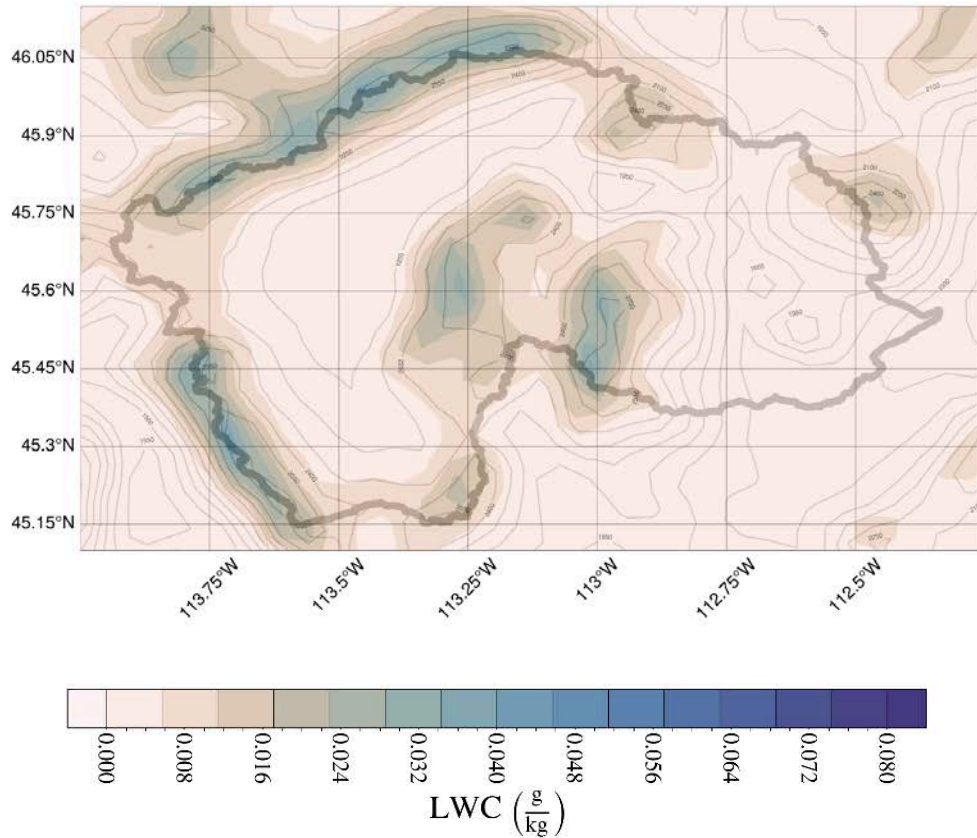
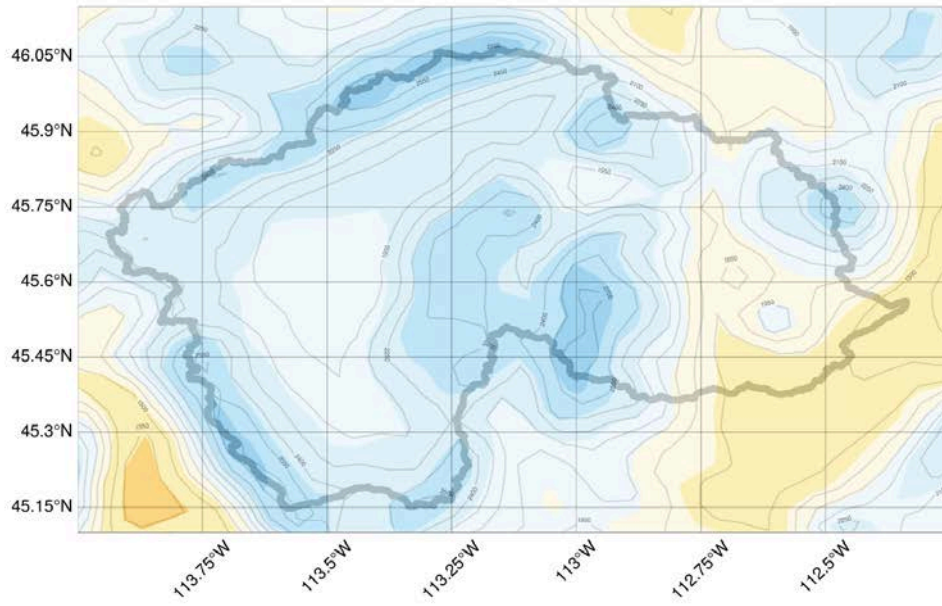


**Figure 4.14.** 40-year average LWC in the ground-seeding layer per month (g/kg).

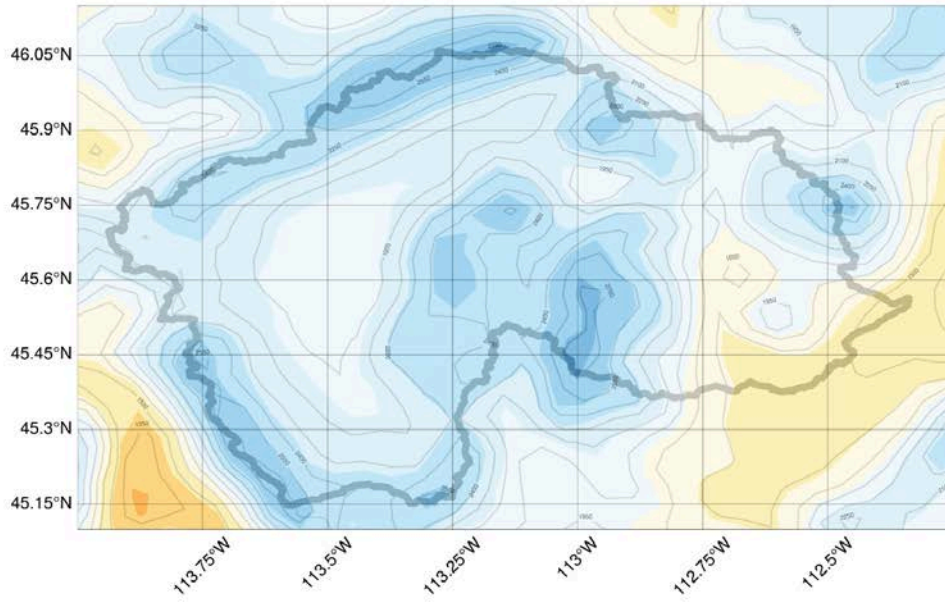
Average temperatures in the target domain within the ground-based layer are shown in [Figure 4.15](#). Monthly average temperature is within the seeding range over the higher elevations of interest from December through February with the coldest temperatures in February. In the months of November and March, temperatures are just barely within the seedable range at higher elevations with temperatures between  $-6^{\circ}\text{C}$  and  $-9^{\circ}\text{C}$ ; however, the valleys between the mountain ranges are too warm. Even at higher elevations, the month of April across the domain is too warm for ground-based seeding operations.



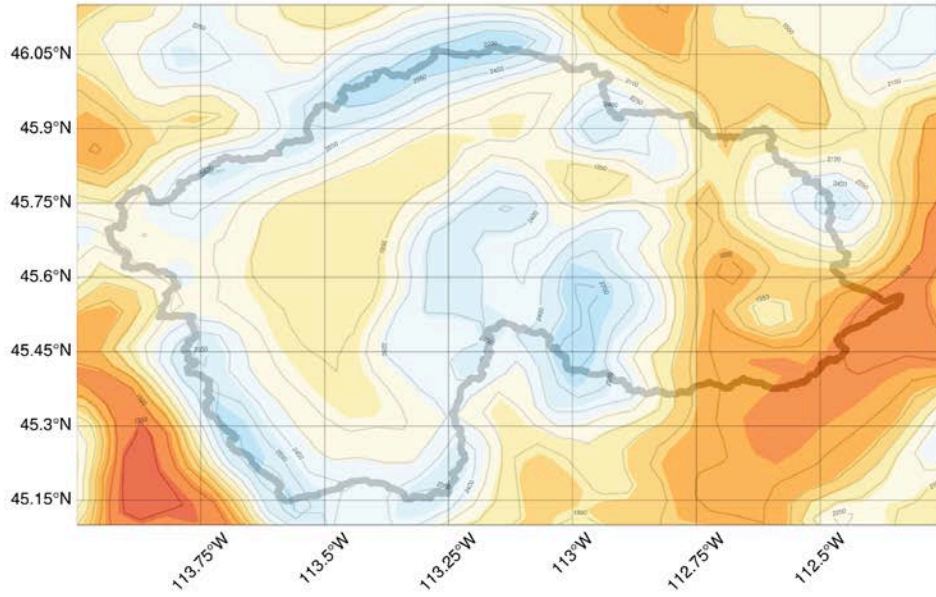
CONUS404 Current Climate  
Ground Temperature Average (January)



CONUS404 Current Climate  
Ground Temperature Average (February)



CONUS404 Current Climate  
Ground Temperature Average (March)



CONUS404 Current Climate  
Ground Temperature Average (April)

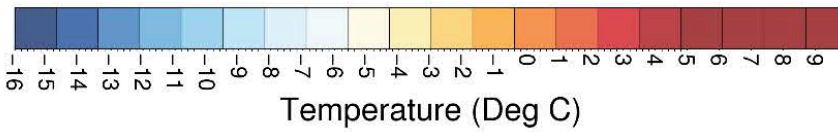
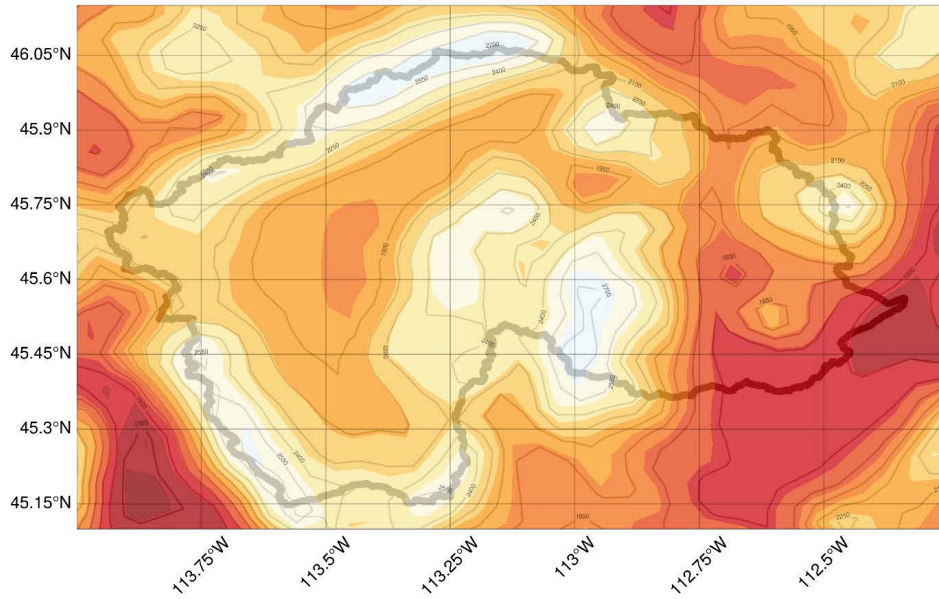
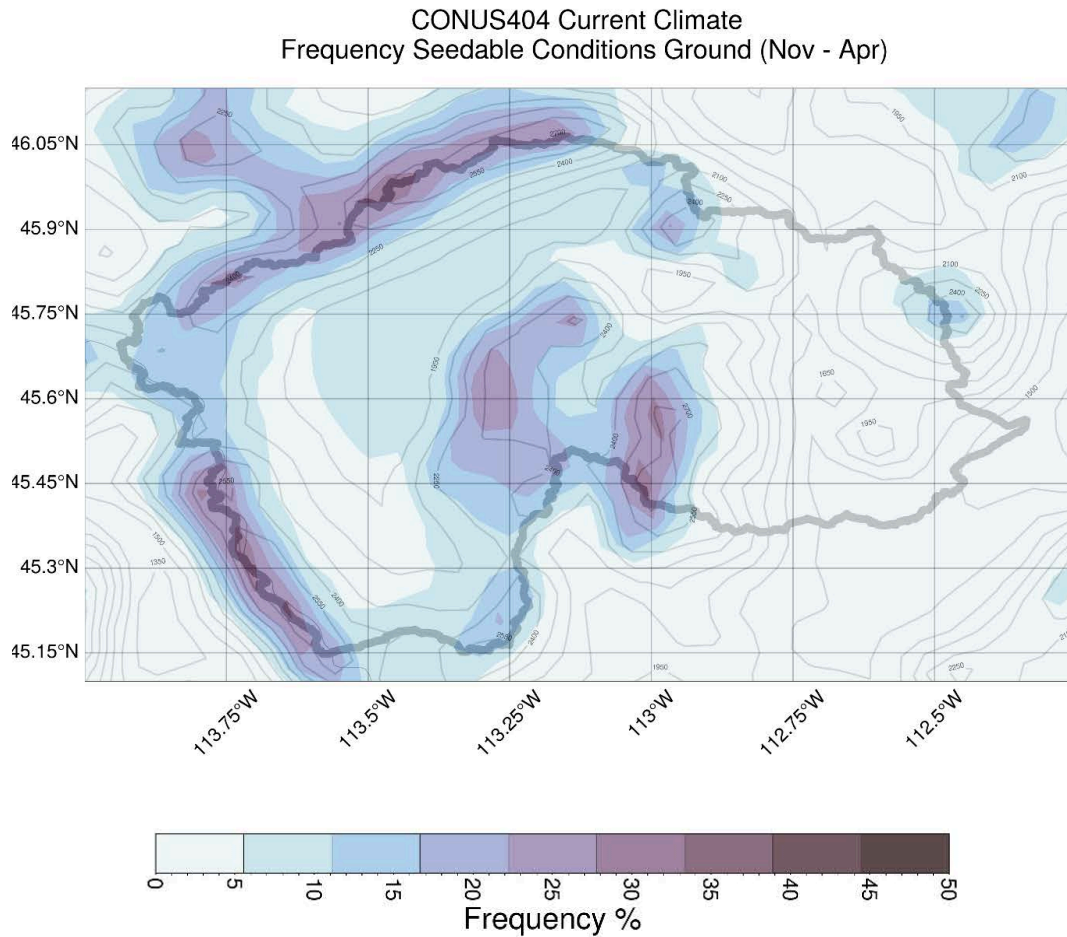


Figure 4.15. 40-year average monthly temperature in the ground-seeding layer (°C).

The overall frequency for the entire seeding season (Nov–Apr) for SLW at seedable temperatures in the ground-based seeding layer indicates that the regions with the greatest frequency of seedable conditions exist over elevated terrain over the Beaverhead Mountains and the north-eastern extent of the Anaconda Range (Figure 4.16). Frequencies are also large over the highest terrain in the Pioneer Mountains. The Highland Mountains show very small frequencies over the entire seeding season and as such are not considered in further analysis.



**Figure 4.16.** 40-year frequency of ground-based seedable conditions over the Nov–Apr seeding season based on presence of  $LWC > 0.01$  g/kg and temperatures between  $-6^{\circ}\text{C}$  to  $-18^{\circ}\text{C}$ .

Figure 4.17 shows the average LWC over the seeding season (Nov–Apr). On average, LWC is the largest over elevated terrain over the Beaverhead Mountains with an average value of 0.70 g/kg. Secondary regions of larger LWC values are noted across the northeastern portion of the Anaconda Range and over the Pioneer Mountains, with average values around 0.045 g/kg. The regions of elevated LWC coincide with the regions of greatest seeding frequency seen in Figure 4.16.

CONUS404 Current Climate  
Ground LWC Average (Nov - Apr)

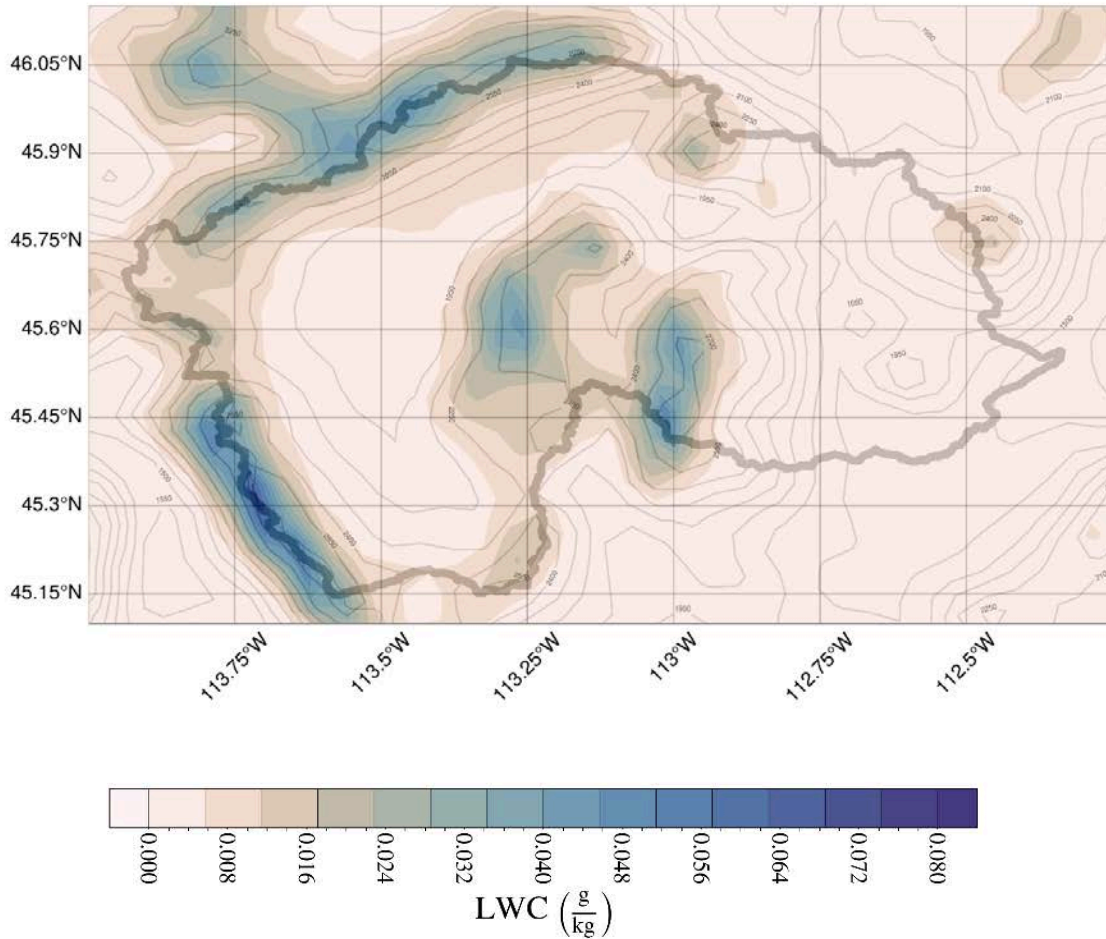


**Figure 4.17.** Average LWC (g/kg) over the Nov–Apr seeding season in the ground-seeding layer.

Across the domain, the average temperature over the seeding season shows values within the seeding range only over high terrain, with an average temperature of  $-9^{\circ}\text{C}$  (Figure 4.18). In the valley regions between the mountain ranges, temperatures are too warm on average for ground-based seeding. While the average temperature across the seeding season appears too high for seeding operations, monthly average temperatures shown in Figure 4.15 show that individual months such as December through February are within the seeding temperature range across the entire domain.

CONUS404 Current Climate  
Ground Temperature Average (Nov - Apr)

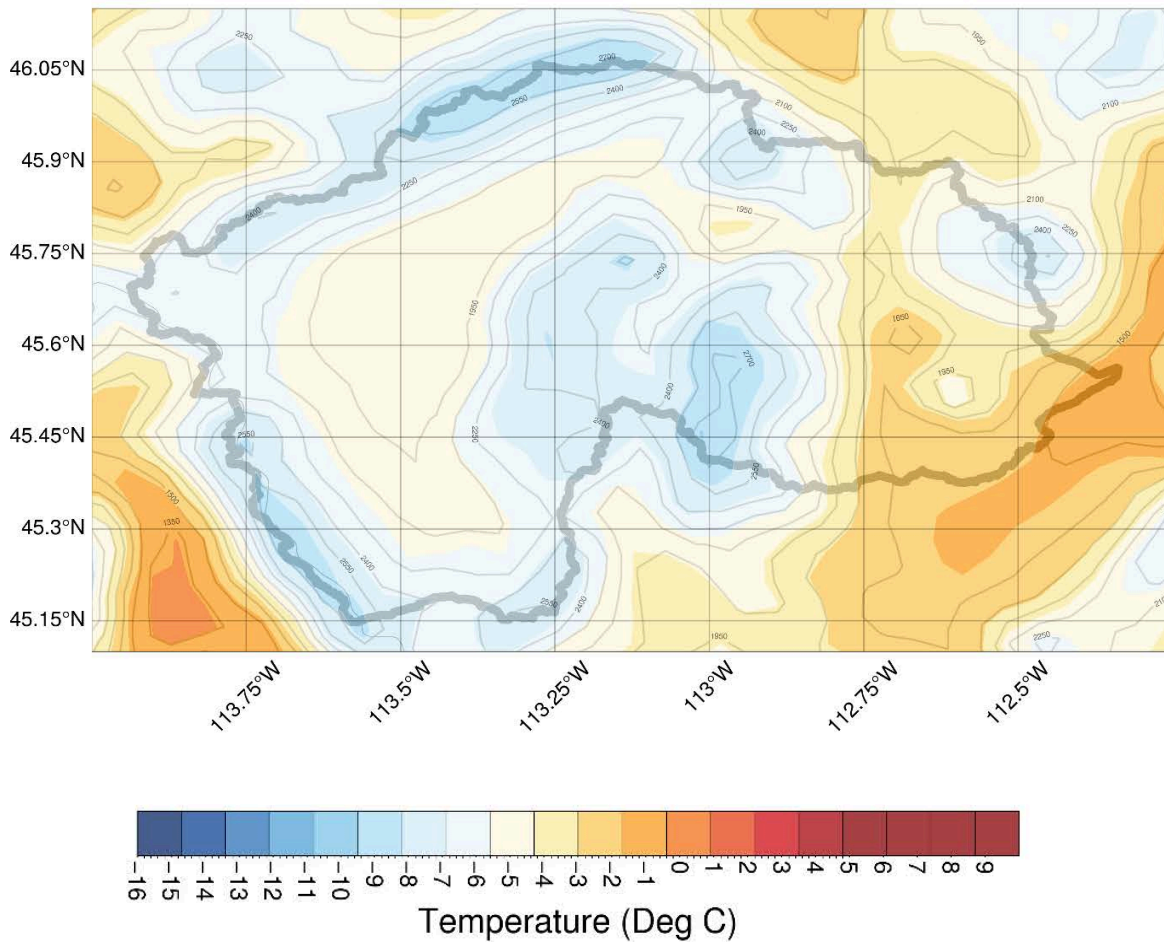


**Figure 4.18.** Average temperature in the ground layer over the Nov–Apr seeding season (°C).

**Area-based Analysis - Monthly**

Monthly 40-year average frequencies of seedable conditions from CONUS404 averaged over each target area (defined in [Figure 4.1](#)) are shown in [Figure 4.19](#). While the basic criteria for seeding opportunities are the same between ground and airborne seeding (i.e. supercooled liquid water and temperature), additional considerations must be taken for ground-based seeding to ensure air flow is conducive to seeding material reaching the target. Modeled winds at each region’s associated surface observation site are used to add additional criteria based upon the Froude number and wind direction to assess seedable opportunities in the ground-based layer ([Table 4.3](#)).

The Froude number is an indication of flow blocking, and is calculated separately for each target range, as range height and orientation are both factors in the calculation. The Froude number expresses the ability of upslope airflow to go over a barrier. The flow will typically be blocked by the barrier when  $Fr < 0.5$ . The flow will freely move over the barrier when  $Fr > 1$ . Froude number is computed from

$$Fr = \frac{U}{N}, \quad (\text{Eq. 1})$$

where  $U$  is the average wind speed perpendicular to the barrier orientation over a depth of  $h$ , and  $N$  is an average of the Brunt-Vaisala frequency between the same depth.  $N$  is expressed as

$$N = \left( \frac{g}{T_v} \frac{\delta\theta_v}{\delta z} \right)^{\frac{1}{2}}, \quad (\text{Eq. 2})$$

where  $g$  is gravitational acceleration,  $T_v$  is the layer average virtual temperature, and  $\frac{\delta\theta_v}{\delta z}$  is the vertical gradient of virtual potential temperature.

The model elevations at each of the sites used to calculate Froude number are shown in [Table 4.3](#). Froude in the Big Hole Basin was calculated assuming a generally north-south orientation for the Beaverhead and Pioneer ranges and a generally west-east orientation for the Anaconda range

**Table 4.3.** Target pairings (SNOTELs and generator groups), wind direction sectors, and range height.

Target	SNOTEL	Generator Group	Wind Direction	Range Height
Beaverhead South	Dark Horse	A	220-280	2641m
Beaverhead North	Saddle Mtn	C	220-320	2500m
Anaconda West	Saddle Mtn	E	220-320	2500m
Anaconda East	Barker Lakes	F	245-320	2627m
Pioneer West	Calvert Creek	I	210-320	2600m
Pioneer East	Mule Creek	J	210-310	2738m

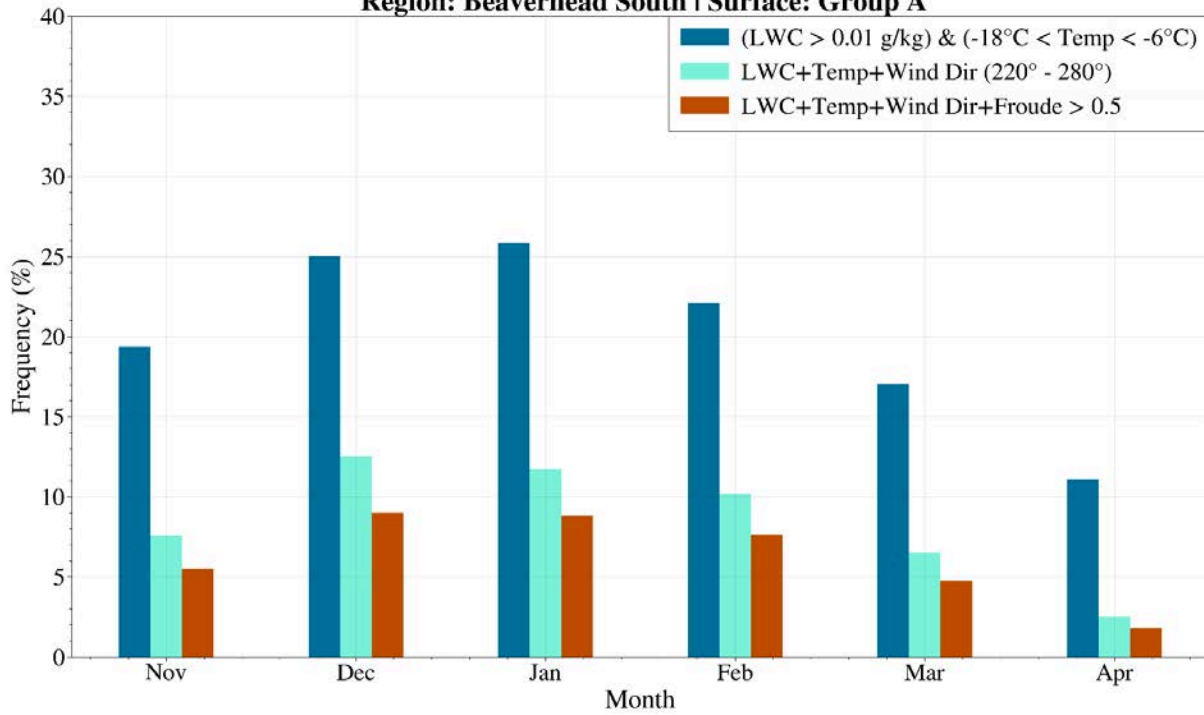
The Froude number is calculated taking into account the orientation of the range as well as the range height. This analysis uses calculated Froude values less than 0.5 at proposed generator sites (denoted by the diamonds in [Figure 4.1](#)) to indicate blocked flow conditions. If the generators are positioned below the elevations for each respective target range and blocking was a factor, the seeding frequency would be further decreased. However, if the generators were positioned higher in elevation they would potentially experience less blocking impact and have greater seeding frequencies.

SNOTEL sites were used to evaluate wind and stability conditions affecting the three ranges upwind of and on the windward side of the ranges. The generator locations were suggested following a combination of the single site analysis of winds summarized above in [Figure 4.4](#) and the model simulations discussed in [Section 5](#). Single site analysis is based on SNOTEL locations shown in [Figure 4.1](#). At SNOTEL sites, wind directions and vertical LWC distribution were analyzed to gain a basic understanding of representative winds and LWC distribution across the domain.

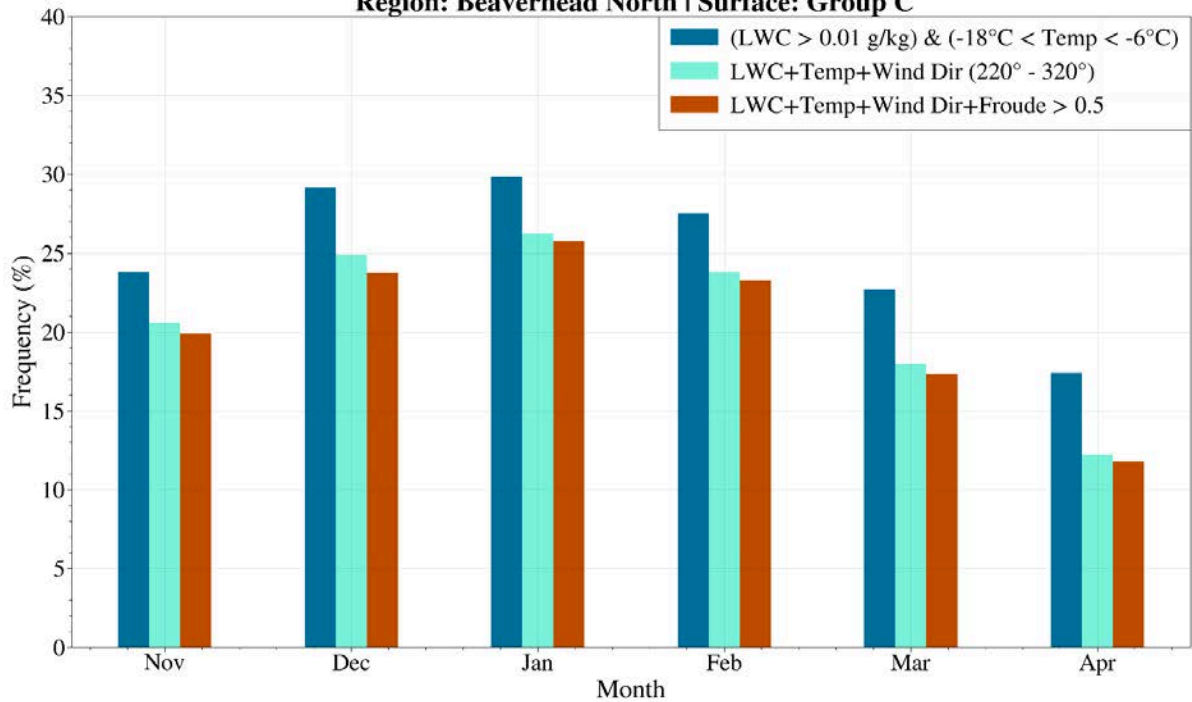
Ground-based seeding opportunities demonstrate notable monthly variability over the winter season, with frequencies typically peaking in December and January ([Figure 4.19](#)). The regions with the greatest

monthly frequency of ground-based seeding potential when considering the basic seeding criteria of LWC and temperature are Beaverhead North with a peak frequency of 30% in January, and Anaconda East with a peak frequencies of 28-29% in December, January, and February. Secondly, Anaconda West and Beaverhead South showed a peak monthly frequencies of 25-26% in December-February. The Pioneer Range peak monthly frequencies were the lowest of the regions, around 22% for both the west and eastern portions of the range. The addition of the wind direction and Froude number criteria decreases seeding potential across every target, although the amount of reduction varies. The Beaverhead North region experiences the most favorable flow conditions, with seedable opportunity frequencies exceeding 20% across most months of the season even when accounting for wind direction and flow blocking. The Anaconda West and Pioneer Range regions also have minimal reductions from the wind flow criteria. The largest reduction in frequency when wind direction and Froude are considered occurs over the Beaverhead South (<10% of each month), which is largely due to the limited wind direction sector used for that region. Anaconda East also exhibits a reduction in frequency with the additional conditions applied, owing mostly to the wind direction sector used; however, the reduction is less than in Beaverhead South. The wind direction sector used in this analysis was selected for targeting the Big Hole Basin; however, if other areas of Montana are also of interest, those regions may have more opportunities if the range of wind directions could be expanded. It should be noted that the Pioneer Range had the least overall frequency of opportunities to begin with, so when wind flow criteria are included, despite only being a modest reduction, their peak frequencies (17-19%) are still slightly less than those from Anaconda East (22%) that had the limited wind direction. Anaconda West was also lower overall, but with wind flow criteria included is very similar to Anaconda East in terms of monthly frequency of seeding opportunities.

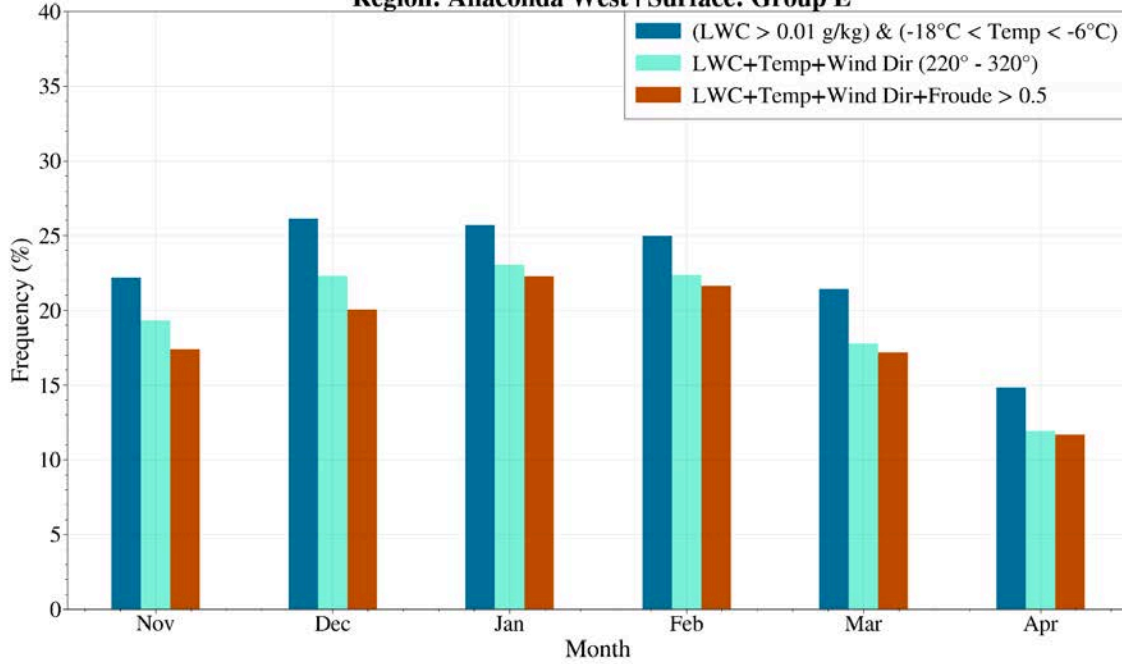
**Ground Monthly Seeding Frequency  
CONUS404 Current Climate  
Region: Beaverhead South | Surface: Group A**



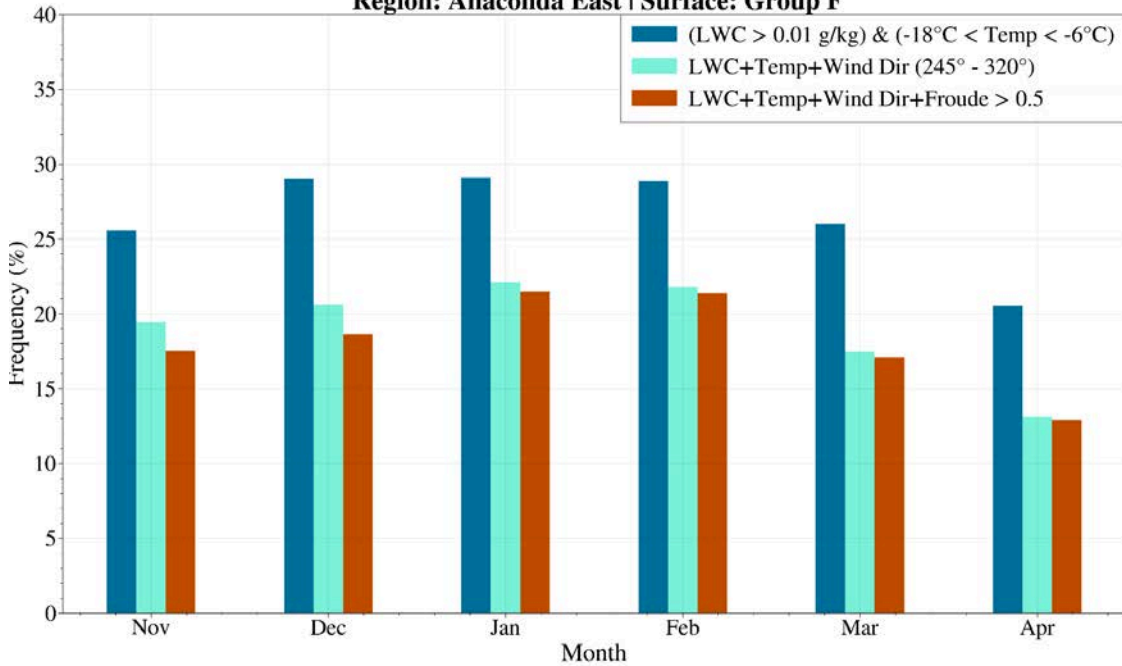
**Ground Monthly Seeding Frequency  
CONUS404 Current Climate  
Region: Beaverhead North | Surface: Group C**



**Ground Monthly Seeding Frequency**  
**CONUS404 Current Climate**  
**Region: Anaconda West | Surface: Group E**



**Ground Monthly Seeding Frequency**  
**CONUS404 Current Climate**  
**Region: Anaconda East | Surface: Group F**



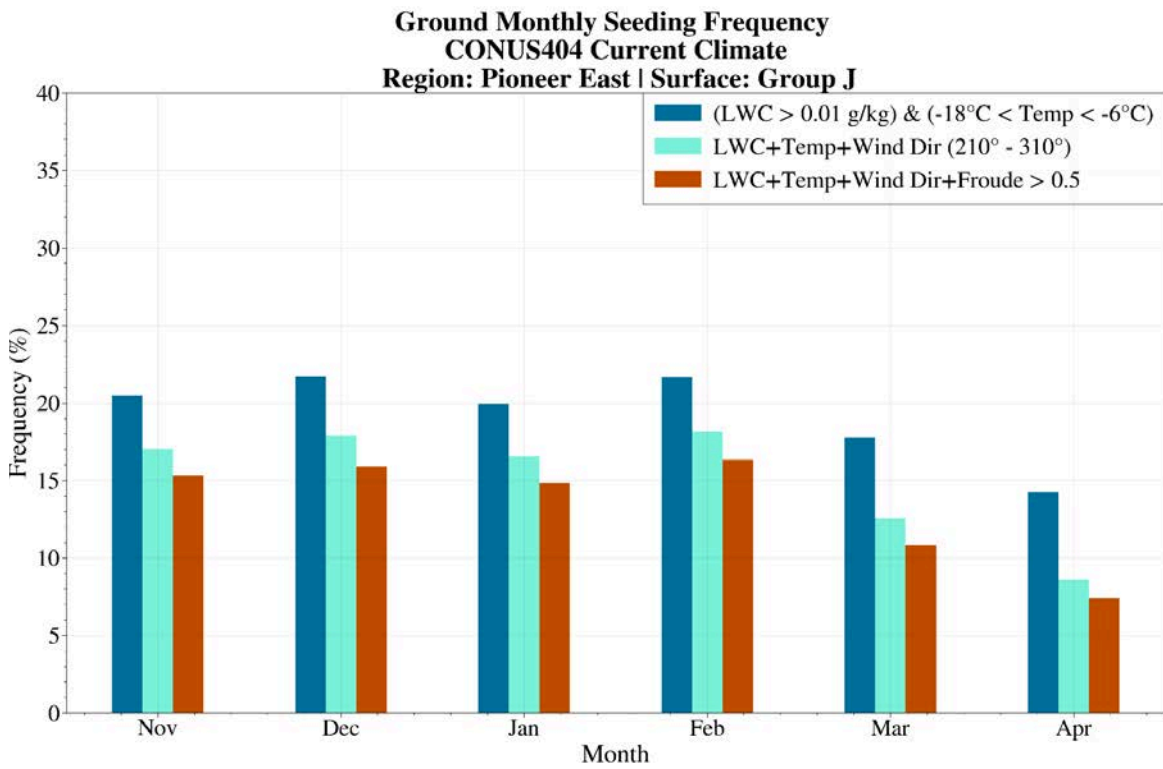
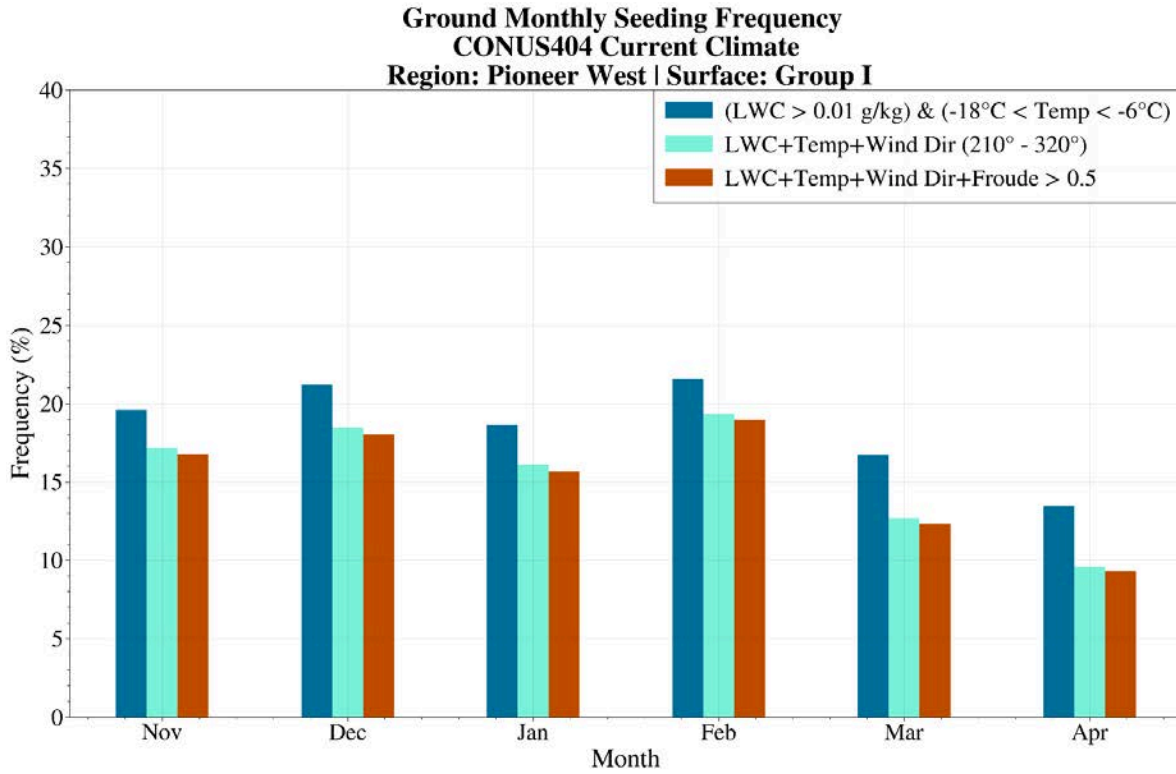


**Figure 4.19.** 40-year average monthly frequency of ground-based seeding. Blue bars indicate frequency based on LWC and temperature, turquoise bars indicate the addition of wind direction, red bars indicate

the addition of the Froude number greater than 0.5. Beaverhead Mountains (plots 1 and 2), Anaconda Range (plots 3 and 4), Pioneer Mountains (plots 5 and 6).

The hourly distribution of seedable frequency by month is shown in [Figure 4.20](#). The scale of frequency is different across all targets, but the diurnal pattern of seedable frequency is similar, and thus only the Anaconda East target is shown. The frequency of seedable conditions generally peaks between the hours of 04 to 15 UTC through the middle of winter. This may be a combination of lower temperatures overnight having a greater frequency of being within the seedable range as well as cloud development due to dropping temperature.

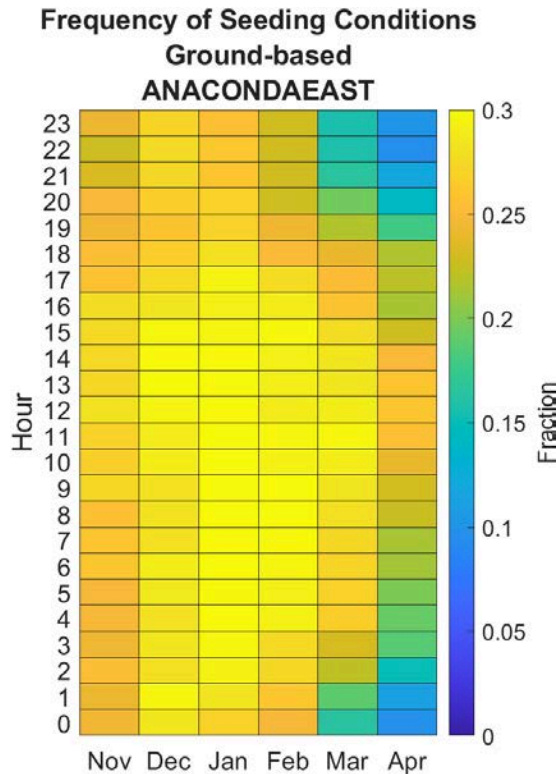
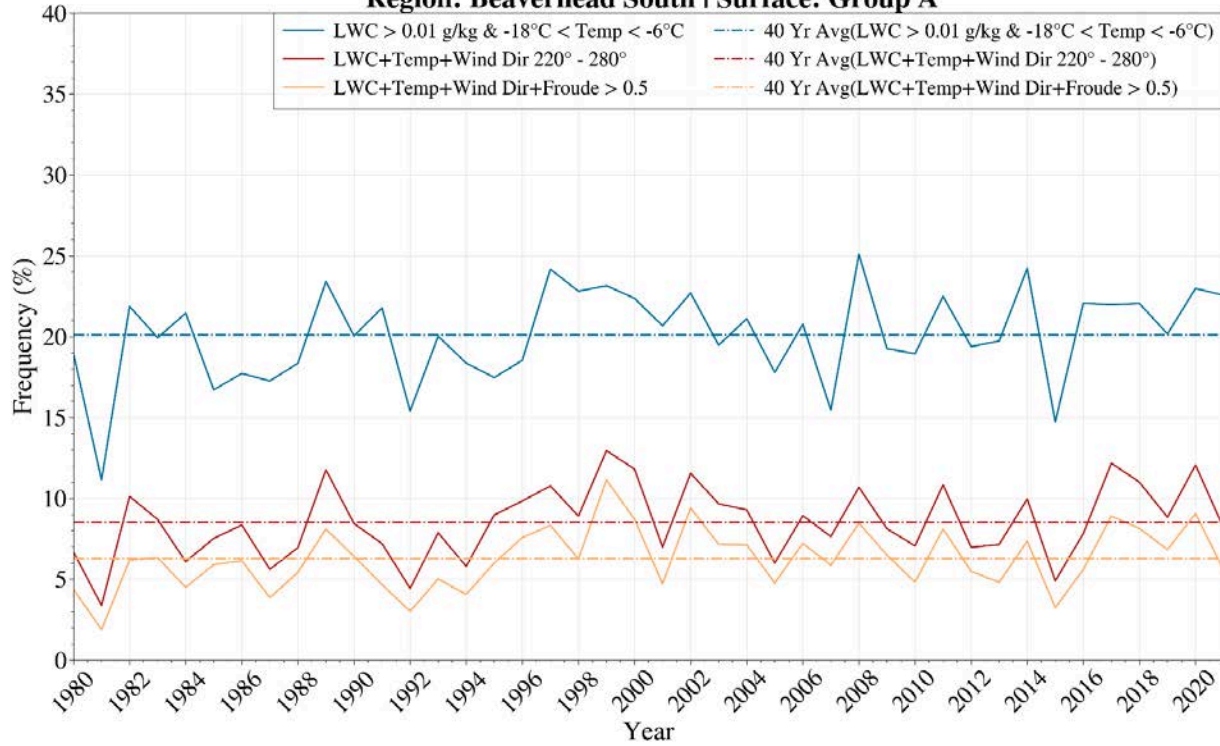


**Figure 4.20.** Hourly distribution of ground-based seedable frequency by month for the Anaconda East target. Time is UTC, and the color represents the fraction of time each hour experiences seedable conditions.

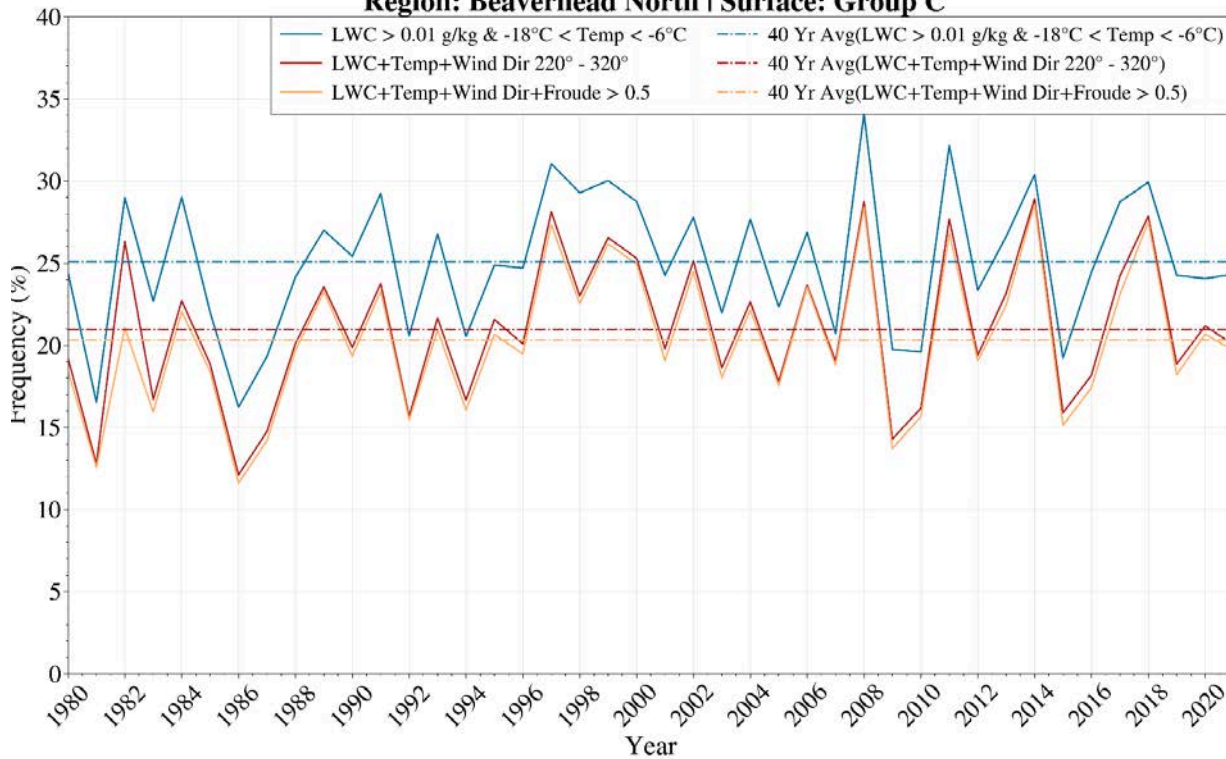
#### Area-based Analysis - Seasonal

The frequency of wintertime (Nov–Apr) seeding opportunities by year for each target region over the 40-year period in CONUS404 is shown in [Figure 4.21](#). Ground-based seeding opportunities exhibit considerable year-to-year variability over the 40-year period. As shown in the monthly analysis ([Figure 4.19](#)), when considering all factors for ground-based seeding opportunities, the Beaverhead North and Anaconda West and East Mountains exhibit the greatest frequency of ground-based seeding opportunities on average (~20%). Beaverhead South has the lowest average frequency (<10%), while the Pioneer Range regions come in around 15%.

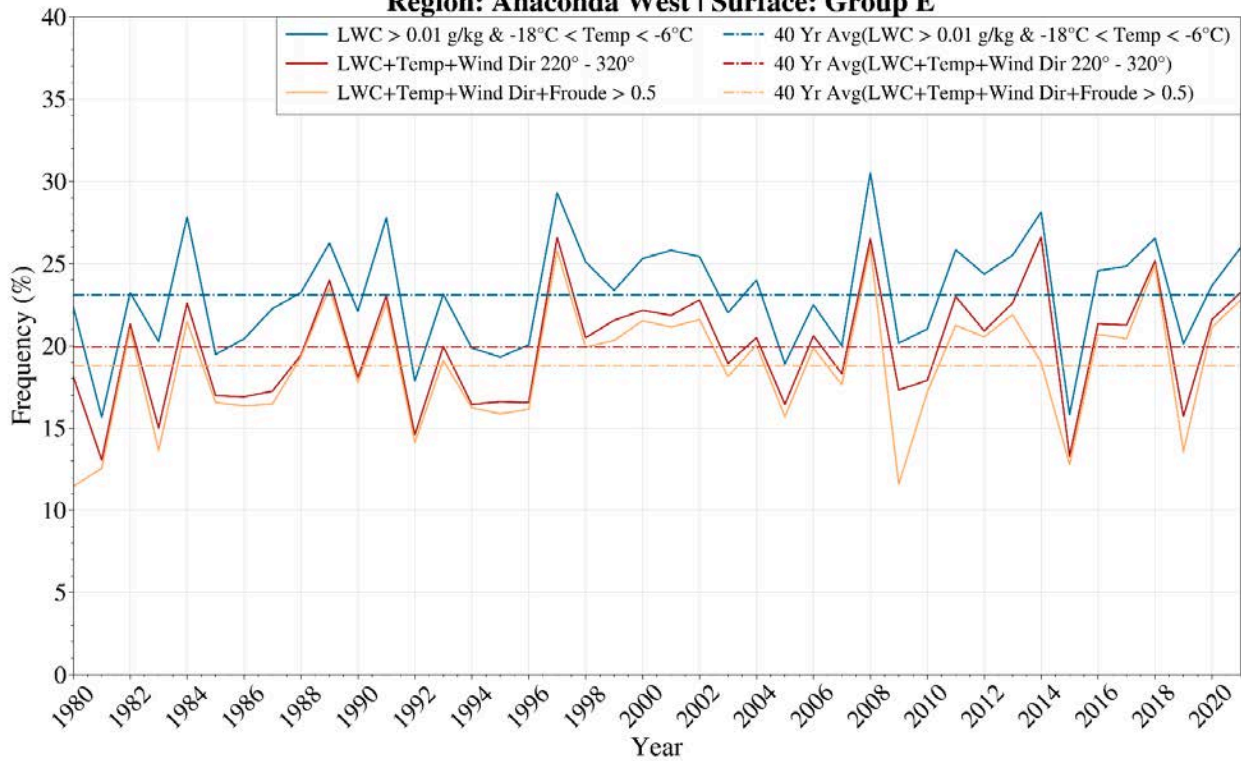
**Ground Yearly Seeding Frequency  
CONUS404 Current Climate  
Region: Beaverhead South | Surface: Group A**



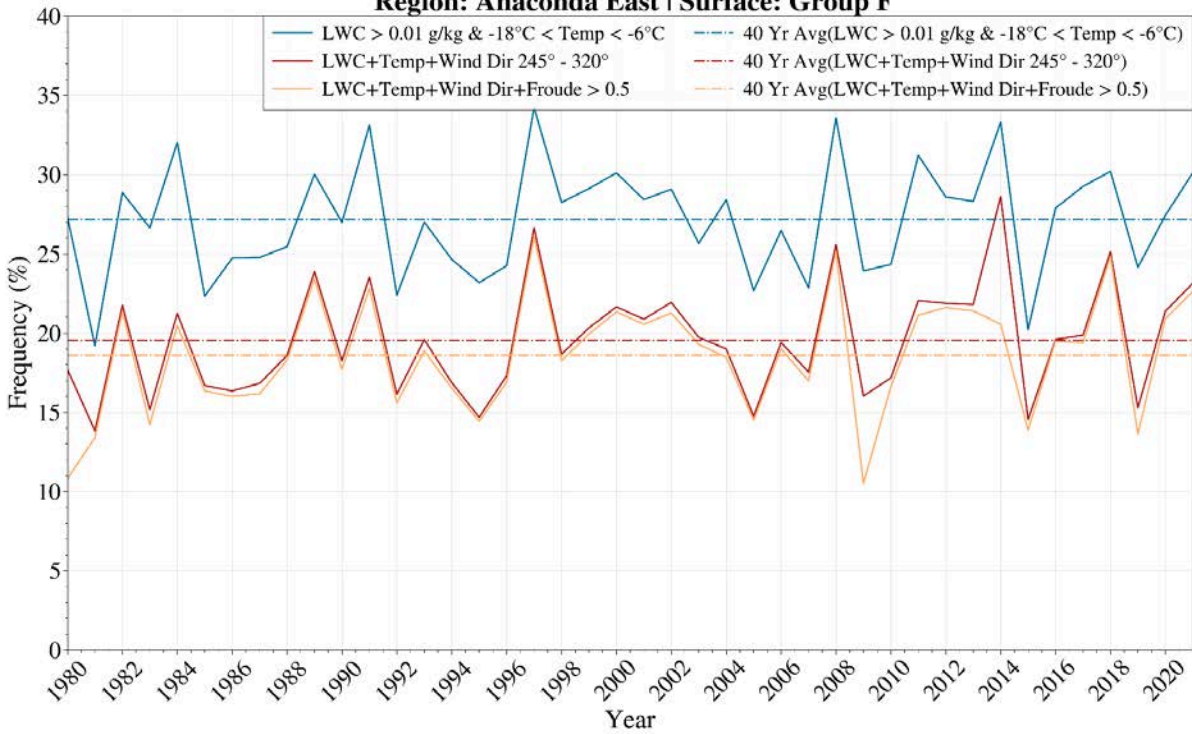
**Ground Yearly Seeding Frequency  
CONUS404 Current Climate  
Region: Beaverhead North | Surface: Group C**



**Ground Yearly Seeding Frequency  
CONUS404 Current Climate  
Region: Anaconda West | Surface: Group E**



**Ground Yearly Seeding Frequency  
CONUS404 Current Climate  
Region: Anaconda East | Surface: Group F**



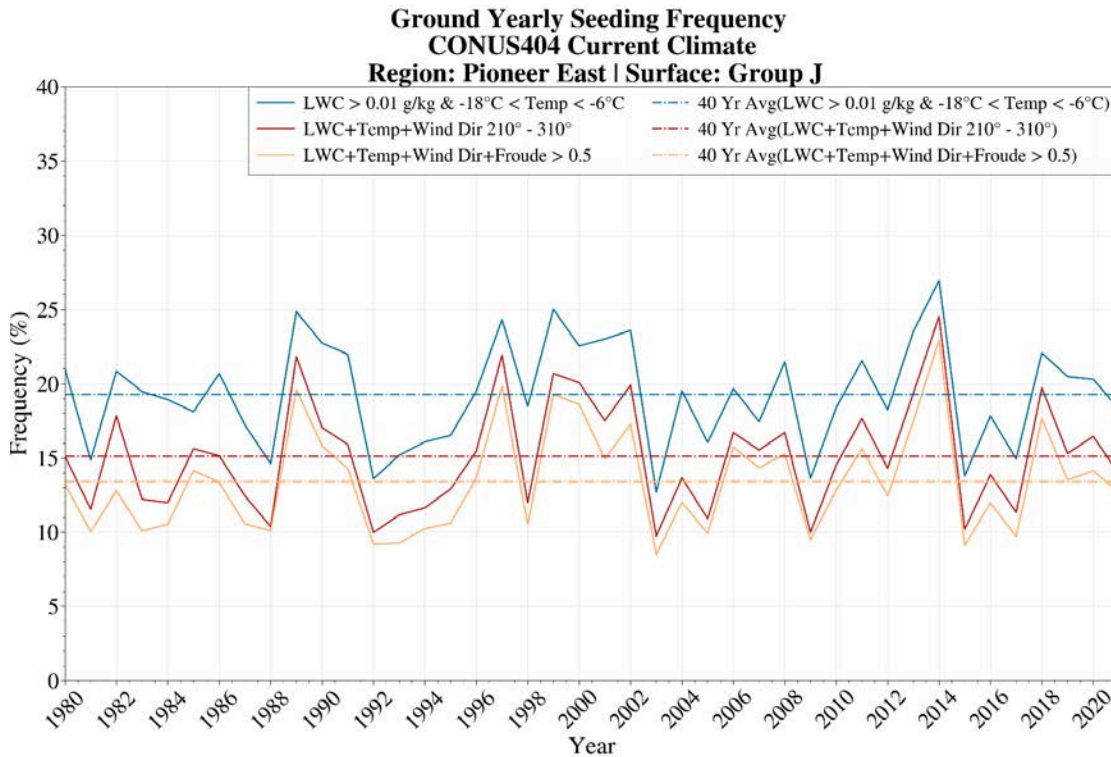
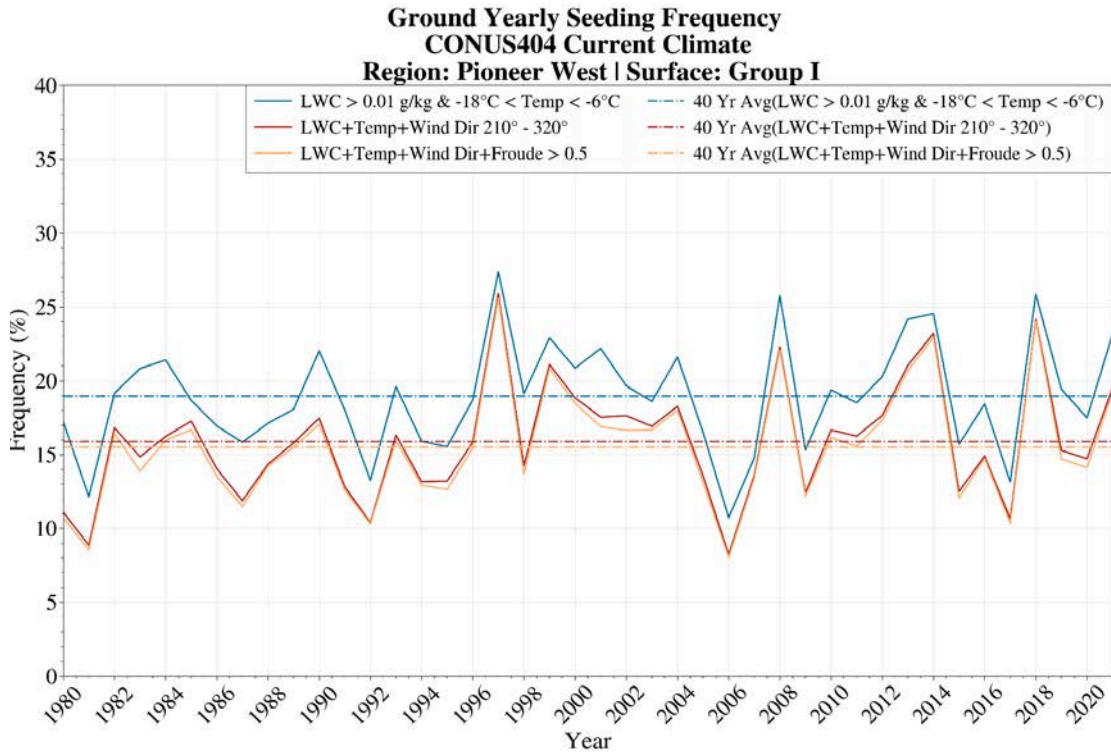


**Figure 4.21.** Seasonal frequency of ground-based seeding opportunities. Blue lines indicate frequency based on LWC and temperature, red lines indicate the addition of wind direction, orange lines indicate the addition of the Froude number greater than 0.5, which is an indicator of unblocked flow. Horizontal

dashed line indicates the 40-year climatological average. Beaverhead Mountains (plots 1 and 2), Anaconda Range (plots 3 and 4), Pioneer Mountains (plots 5 and 6).

### 4.3.2. CONUS404 Future Climate Simulations

#### Spatial Analysis

Output from the CONUS404 PGW simulation was used to construct maps showing the difference in average seeding season seedable opportunity frequency, LWC, and temperature for ground-based conditions between the current and future climate scenarios. The difference in overall frequency ([Figure 4.22](#)) indicates that in the PGW future climate scenario the frequency of seedable conditions decreases across the domain for ground-based seeding. This overall decrease in seeding frequency is due to an increase in temperature in the PGW climate ([Figure 4.23](#)). Although LWC increases in the PGW simulation ([Figure 4.24](#)), especially over higher terrain, the domain-wide temperature increase in the ground-layer, especially over the Beaverhead Mountains makes the region too warm relative to the seeding temperature range and therefore decreases the frequency of seedable conditions for ground-based seeding.

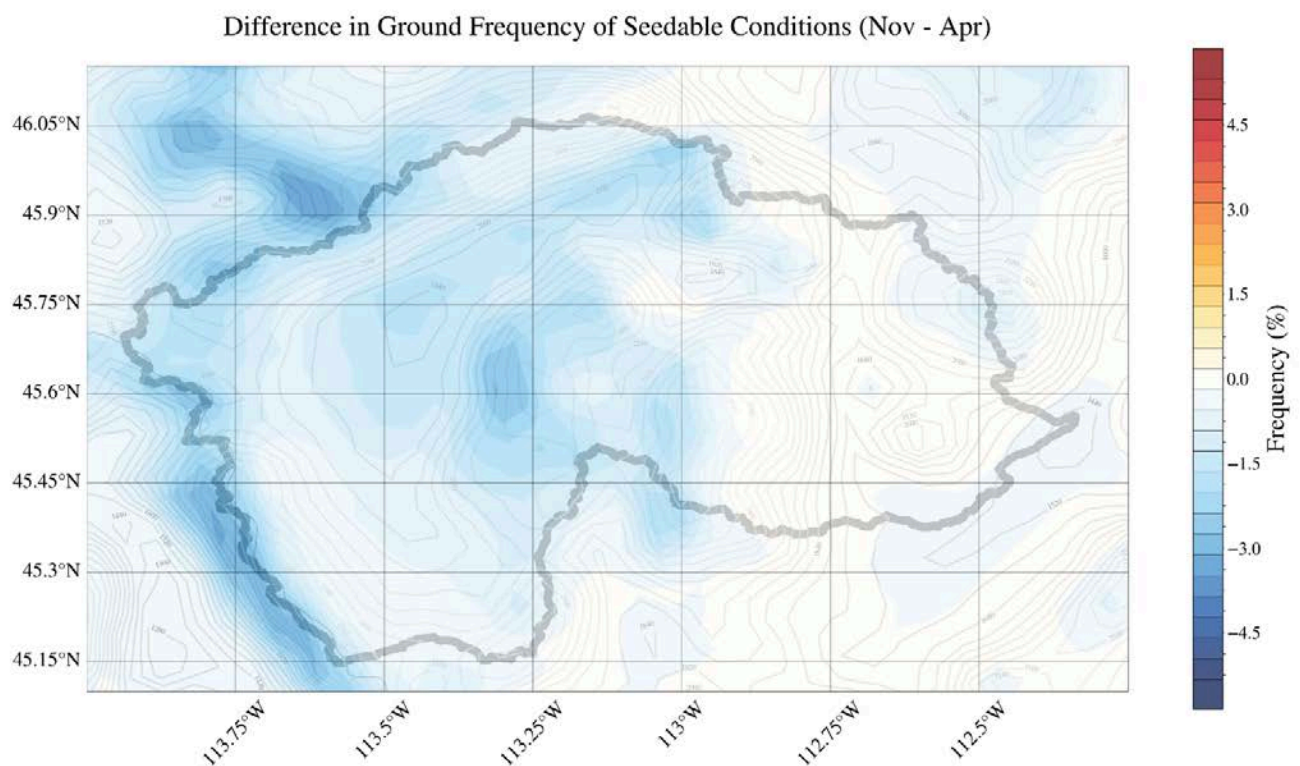


**Figure 4.22.** Difference in wintertime frequency of ground-based seedable conditions: PGW minus CONUS404 current climate based on presence of LWC > 0.01 g/kg and temperatures between  $-6^{\circ}\text{C}$  to  $-18^{\circ}\text{C}$ .

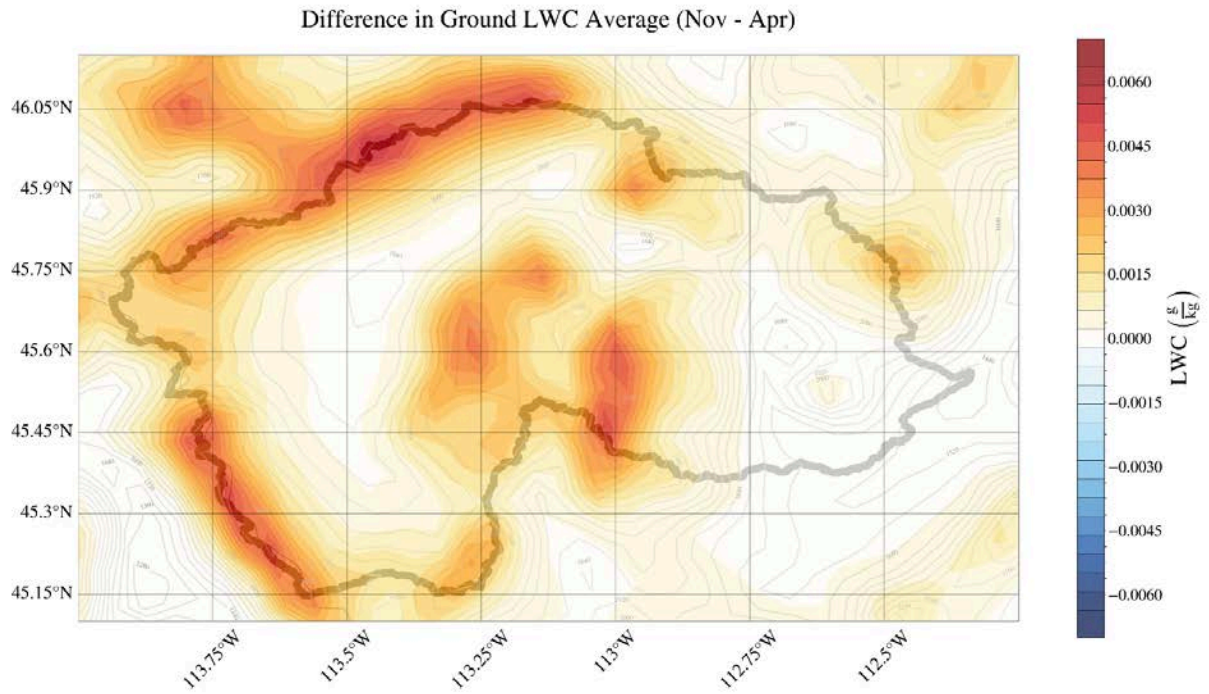


**Figure 4.23.** Difference in ground-based wintertime LWC: PGW minus CONUS404 current climate (g/kg).

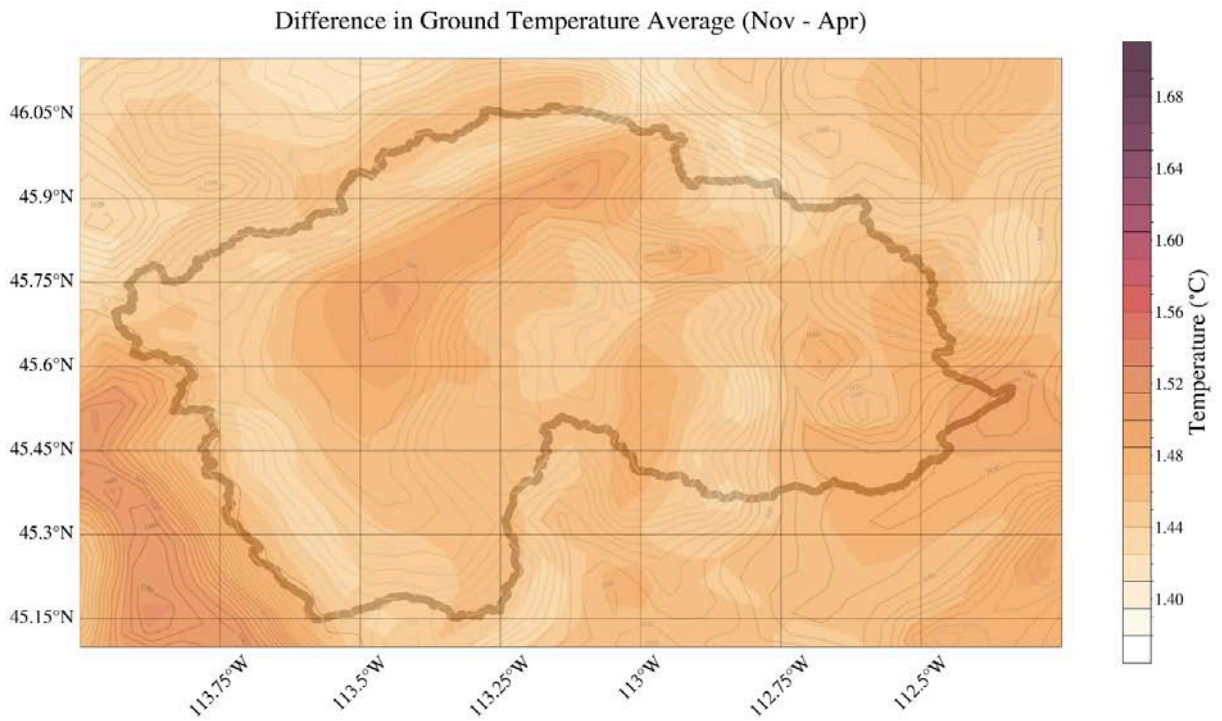
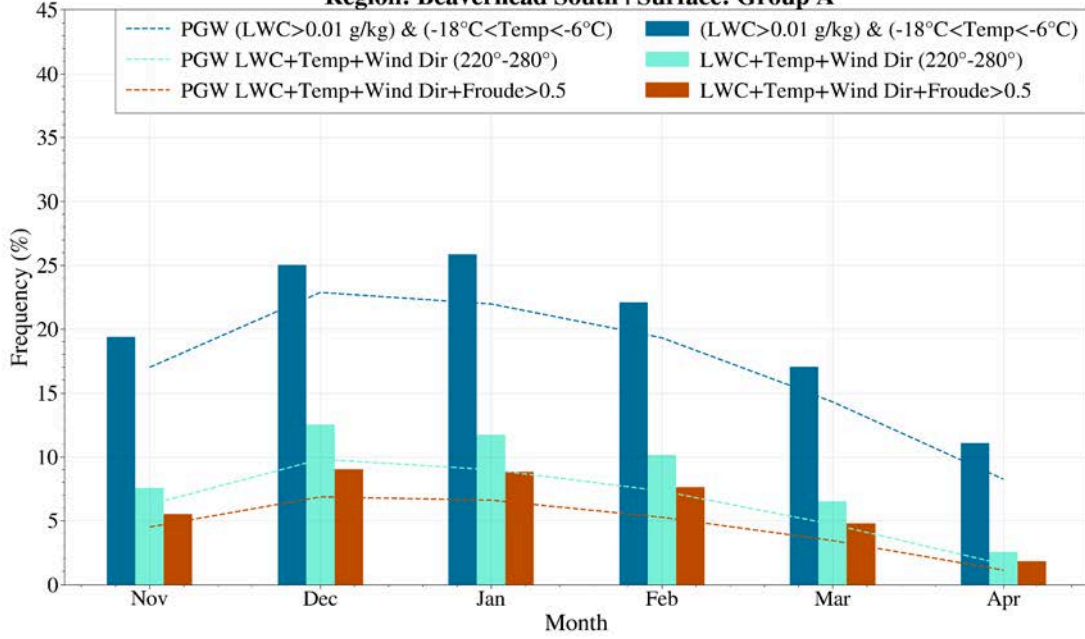


**Figure 4.24.** Difference in wintertime temperature in the ground-layer: PGW minus CONUS404 current climate ( $^{\circ}C$ ). Color bar shows all positive values as there are no decreases in temperature.

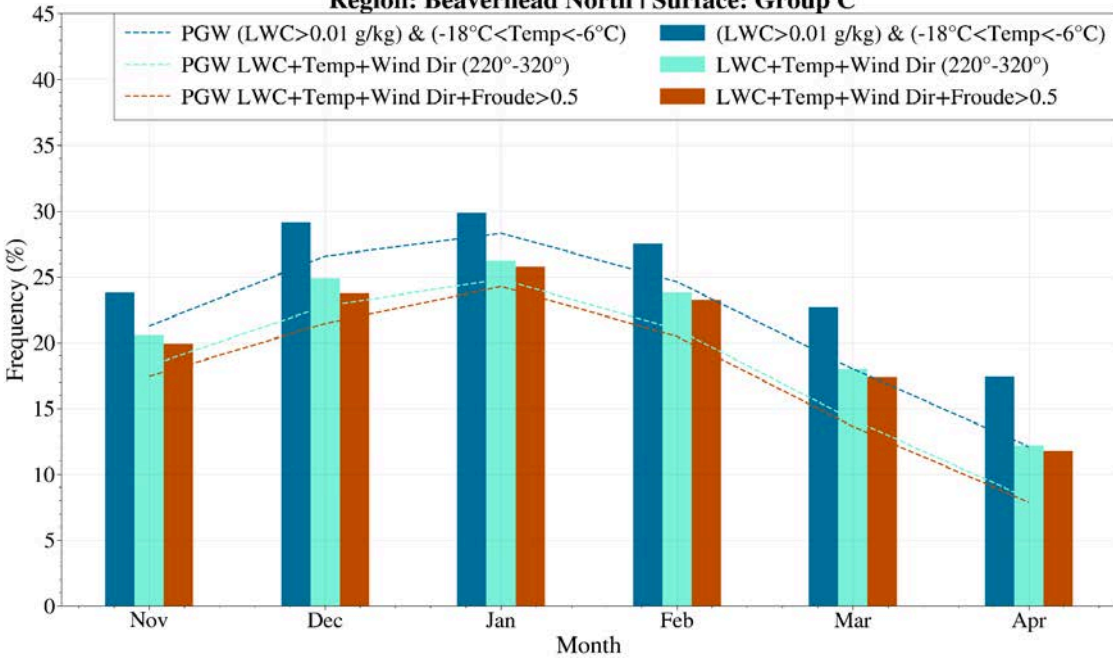
### **Area-based Analysis - Monthly**

Area-averaged monthly frequencies of seedable conditions, using the target regions shown in [Figure 4.1](#), are shown in [Figure 4.25](#) for CONUS404 current climate and PGW analysis. Ground-based seeding frequencies still peak in December through February; however, overall frequencies generally decrease from current climate across most target sites in the domain. In both current and future climate monthly analysis, the regions with the greatest ground-based seeding frequencies are Beaverhead North and the Anaconda Range. These regions exhibit maximum monthly frequencies of 30% and 26-29%, respectively, in current climate, which drops slightly to 28% for Beaverhead North and 25-27% for the Anaconda Range regions in the future climate based on the basic seeding criteria of temperature and SLW alone. The Pioneer West and East regions show frequencies ranging from 14% to 22% in current climate, which increase in the future climate during the months of December and January by a few percent. When the other ground seeding criteria of wind direction and Froude are added, the peak frequencies of seeding potential decrease from current climate to PGW most substantially for the Beaverhead South region as well as Anaconda West.

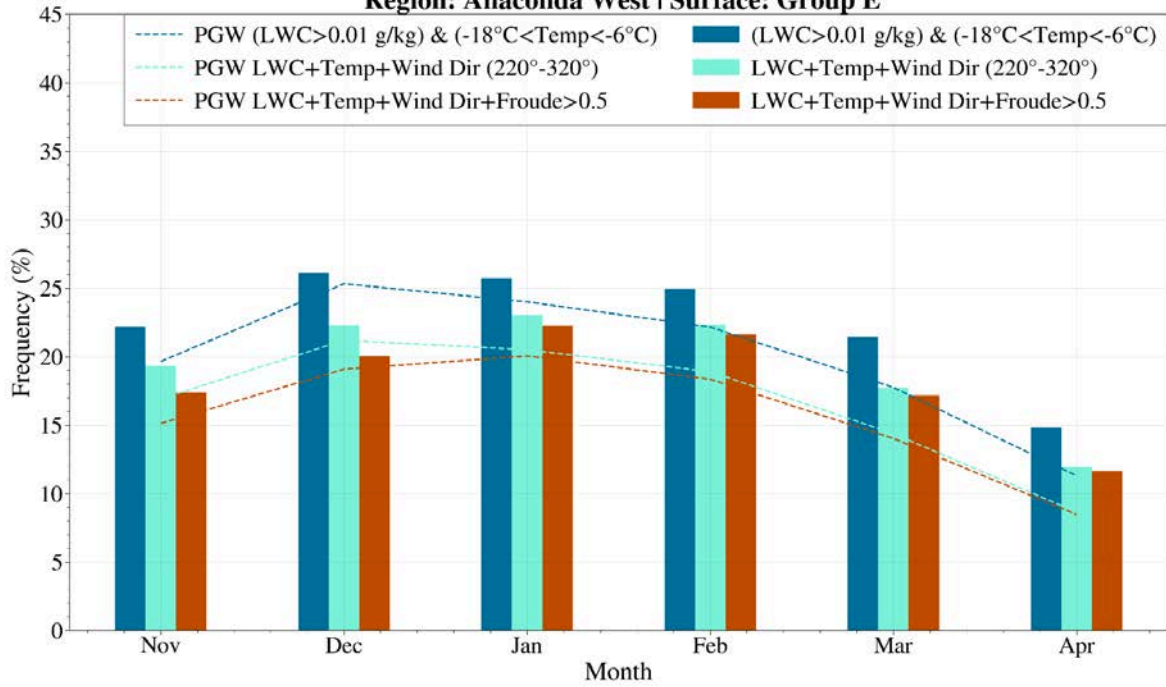
**Monthly Ground Seeding Frequency  
CONUS404 Current and Future Climate  
Region: Beaverhead South | Surface: Group A**



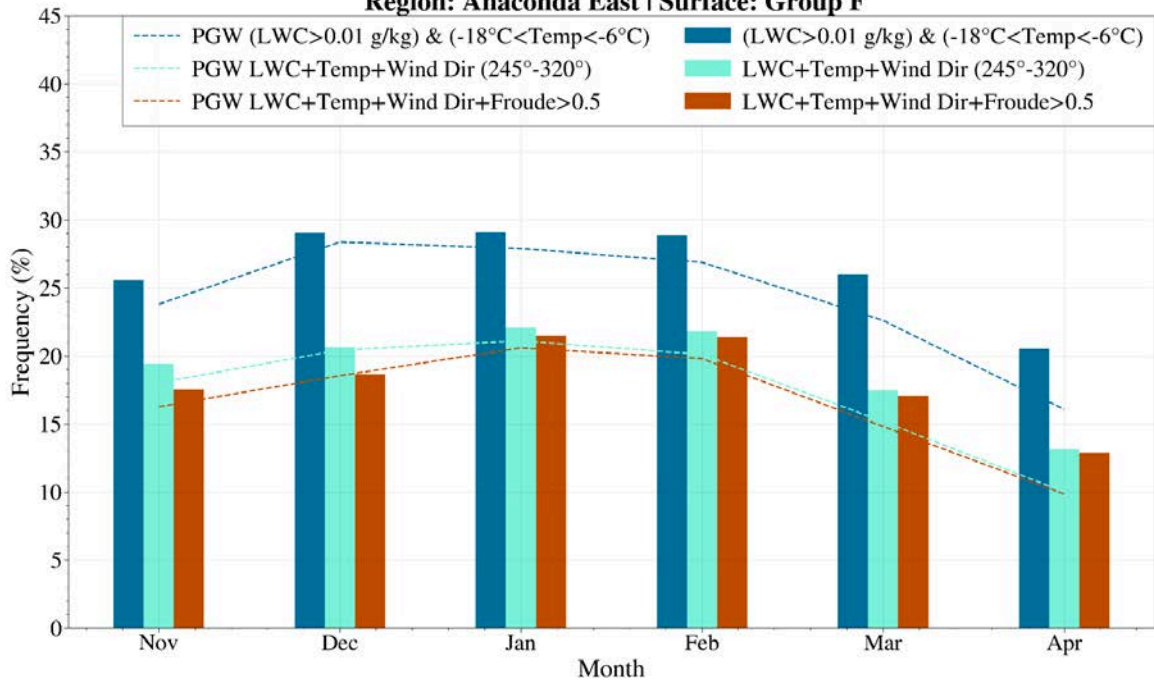
**Monthly Ground Seeding Frequency  
CONUS404 Current and Future Climate  
Region: Beaverhead North | Surface: Group C**



**Monthly Ground Seeding Frequency  
CONUS404 Current and Future Climate  
Region: Anaconda West | Surface: Group E**



**Monthly Ground Seeding Frequency  
CONUS404 Current and Future Climate  
Region: Anaconda East | Surface: Group F**



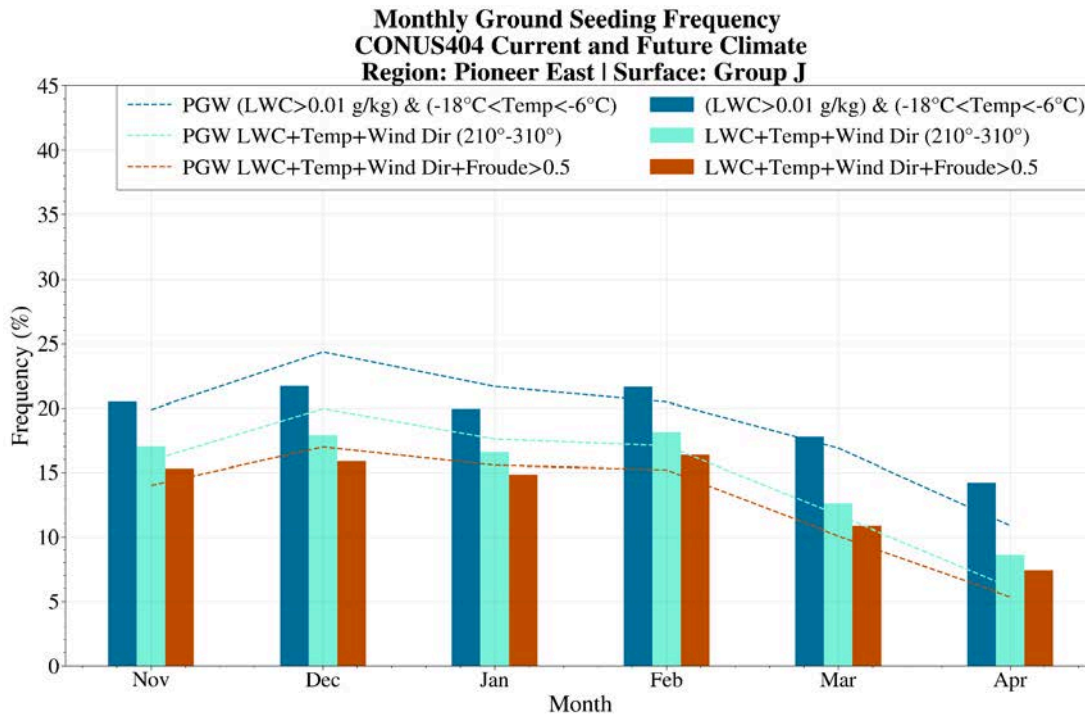
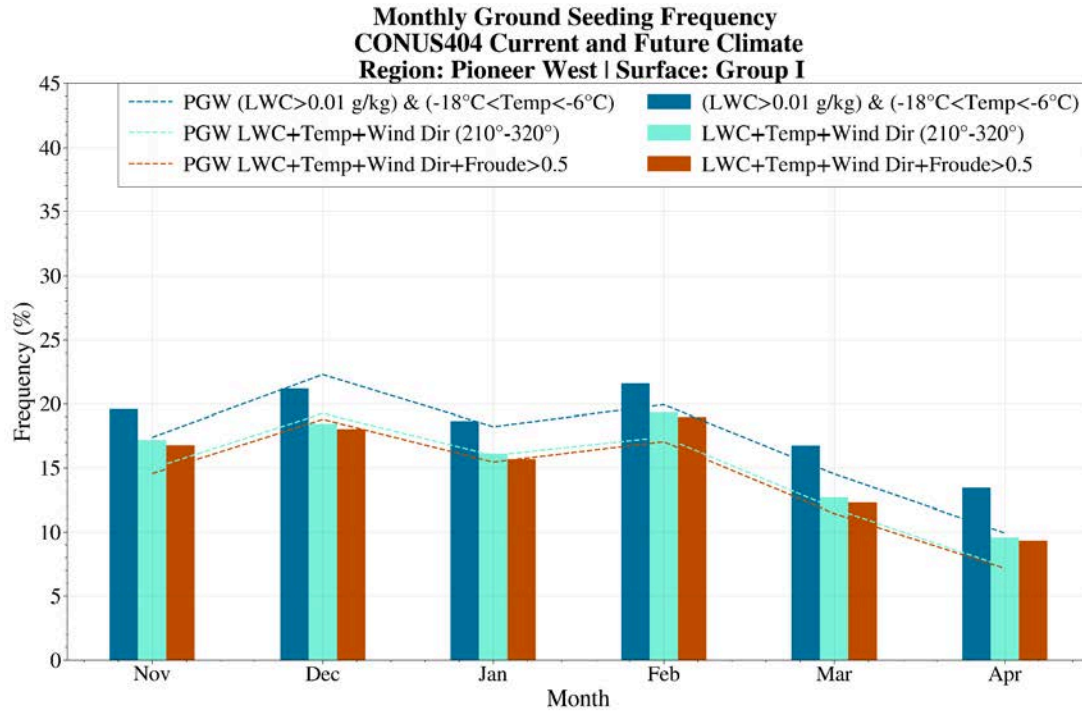
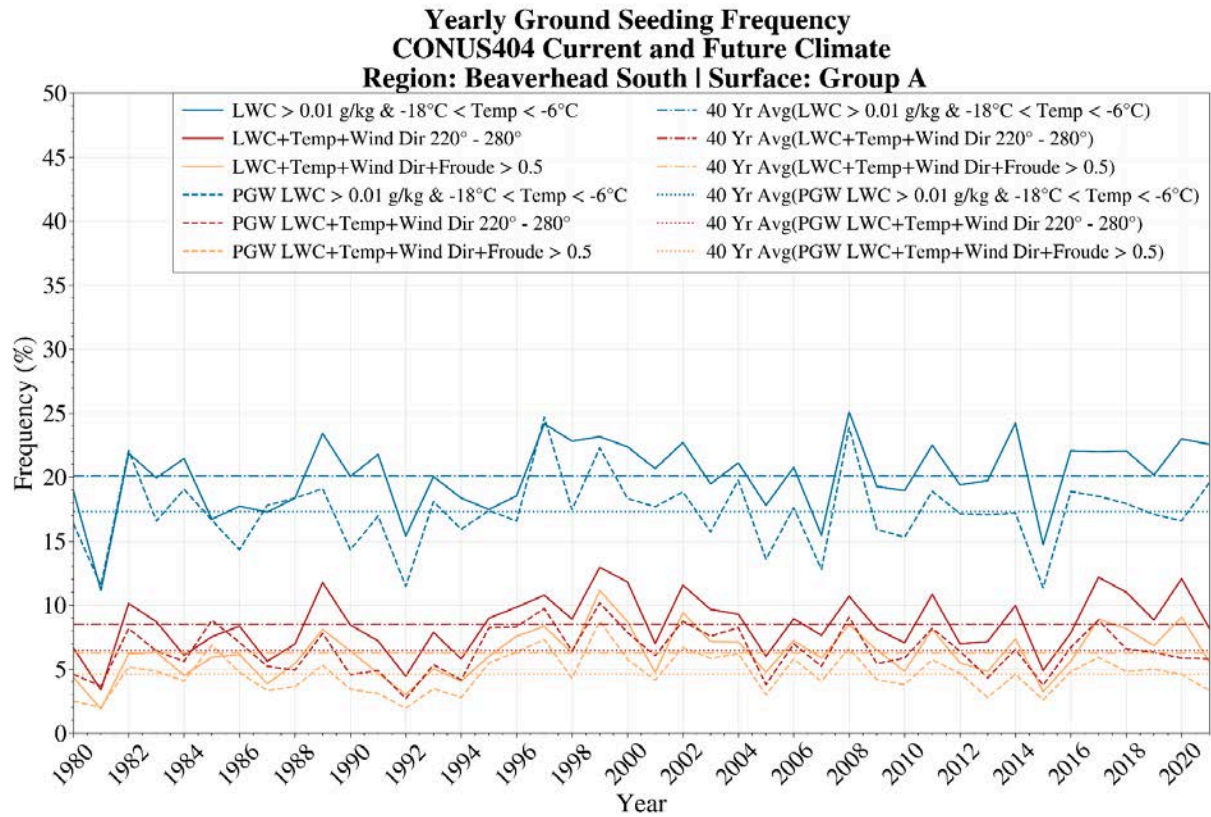


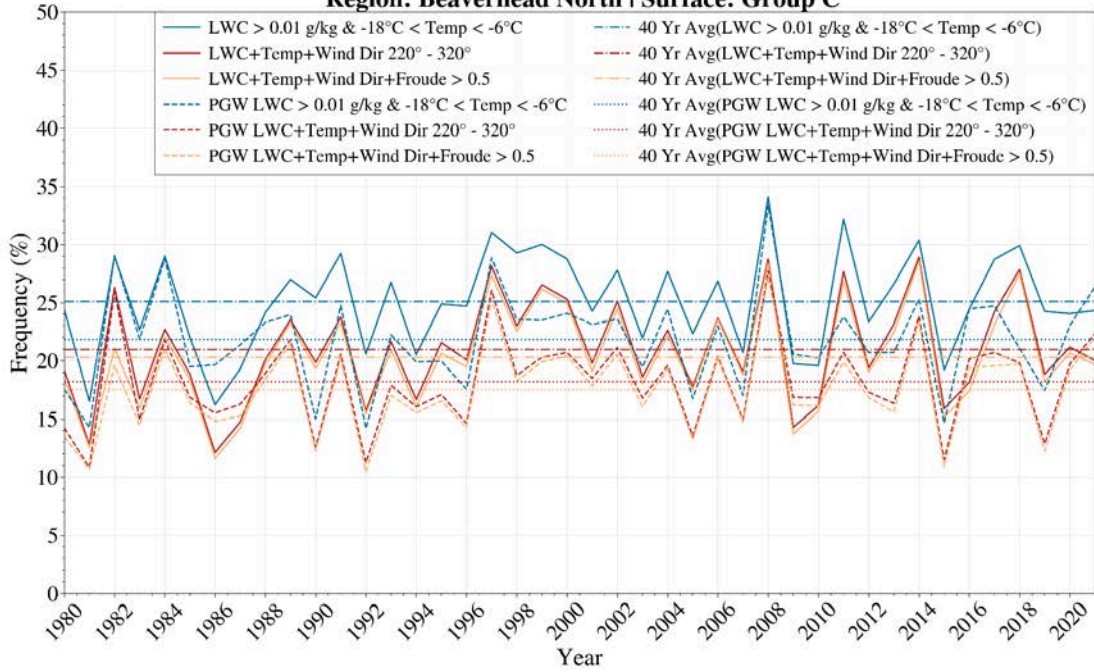
**Figure 4.25.** Seasonal frequencies of ground-based seeding opportunities. Blue indicates frequency based on LWC and temperature, turquoise indicates the addition of wind direction, red indicates the addition of the Froude number greater than 0.5, which is an indicator of unblocked flow. Bars represent current climate and dashed lines indicate PGW. Beaverhead Mountains (plots 1 and 2), Anaconda Range (plots 3 and 4), Pioneer Mountains (plots 5 and 6).

### Area-based Analysis - Yearly

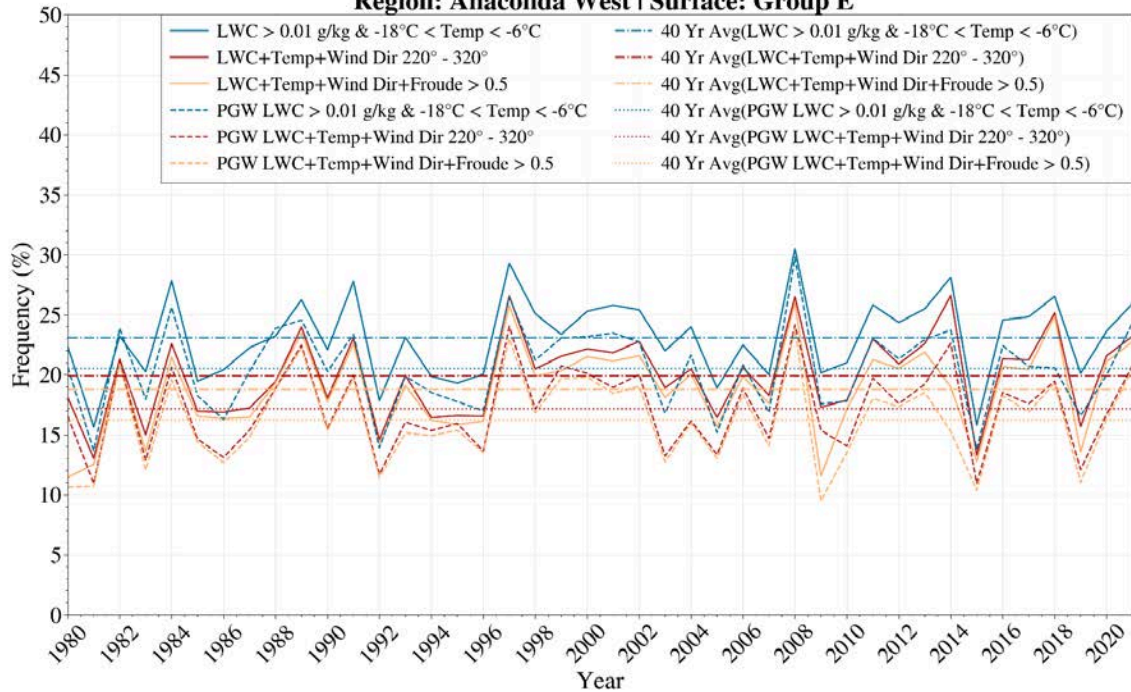
Annual seasonal frequencies for each target region comparing current and future climates are shown in [Figure 4.26](#). Annual analysis reflects the monthly findings shown in [Figure 4.25](#), which indicated that, in general, frequency decreases from current to future climates. Over the 40-year period there is not a noticeable general overall upward or downward trend in frequency in the future climate, but rather there is steady annual variability in minimum and maximum values in frequency.



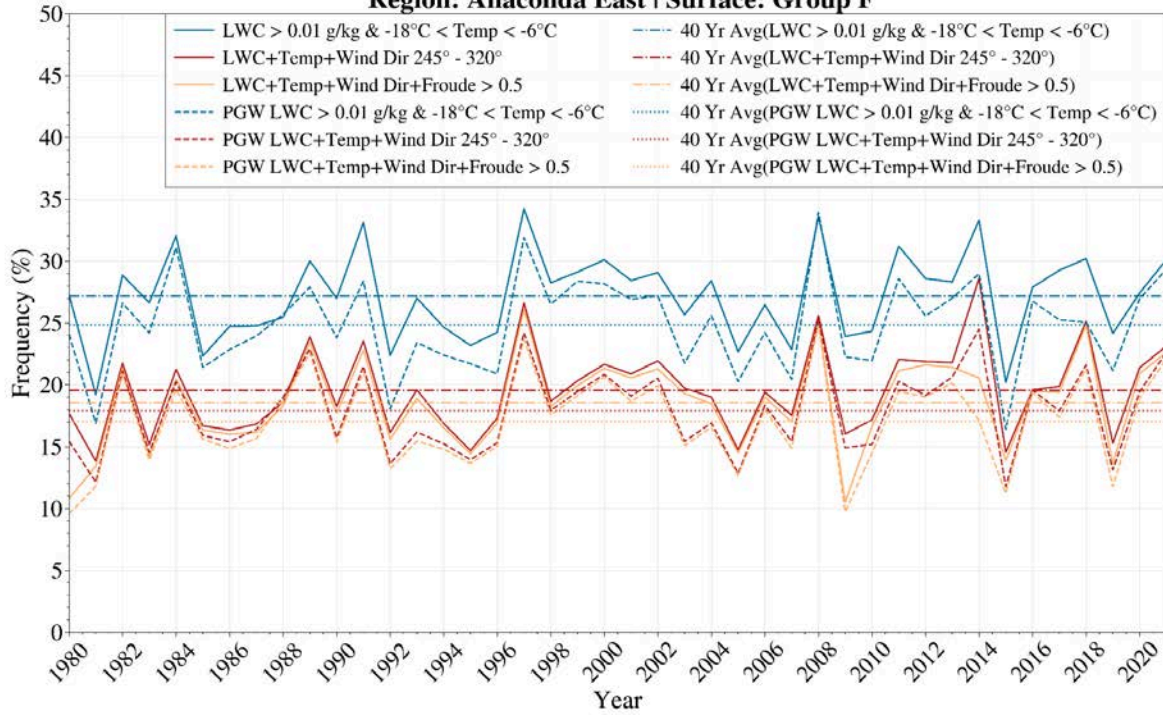
**Yearly Ground Seeding Frequency  
CONUS404 Current and Future Climate  
Region: Beaverhead North | Surface: Group C**



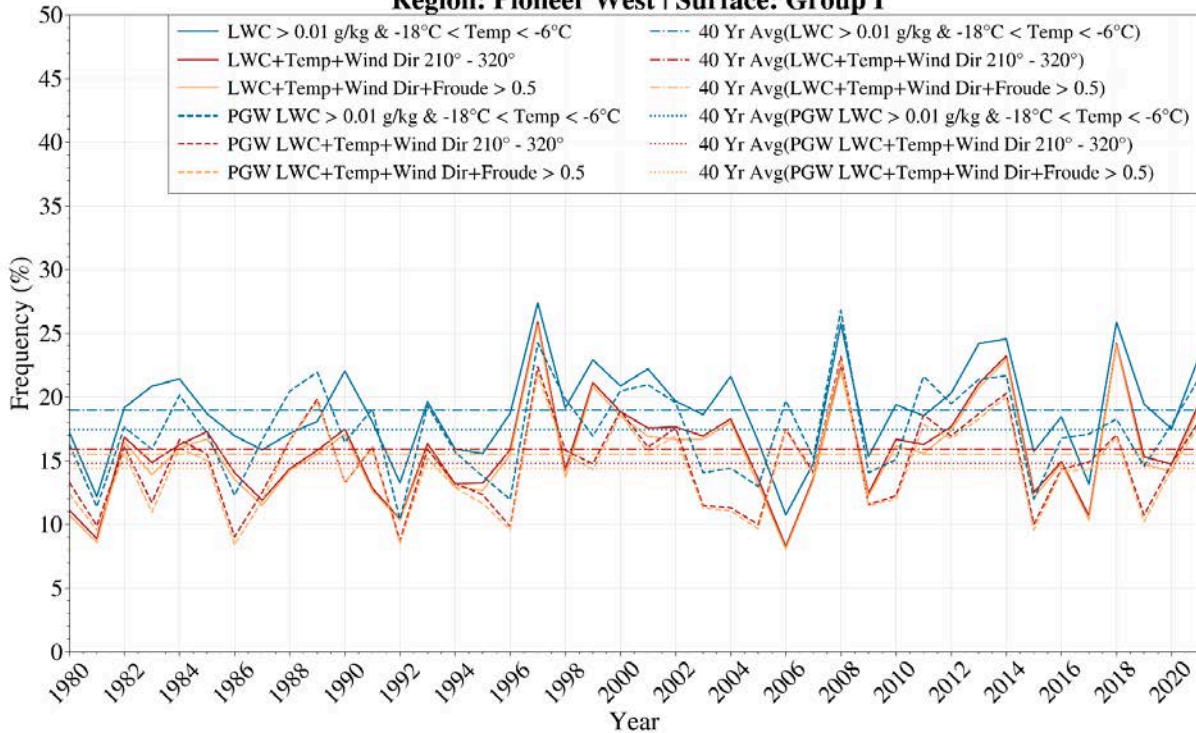
**Yearly Ground Seeding Frequency  
CONUS404 Current and Future Climate  
Region: Anaconda West | Surface: Group E**



**Yearly Ground Seeding Frequency  
CONUS404 Current and Future Climate  
Region: Anaconda East | Surface: Group F**



**Yearly Ground Seeding Frequency  
CONUS404 Current and Future Climate  
Region: Pioneer West | Surface: Group I**



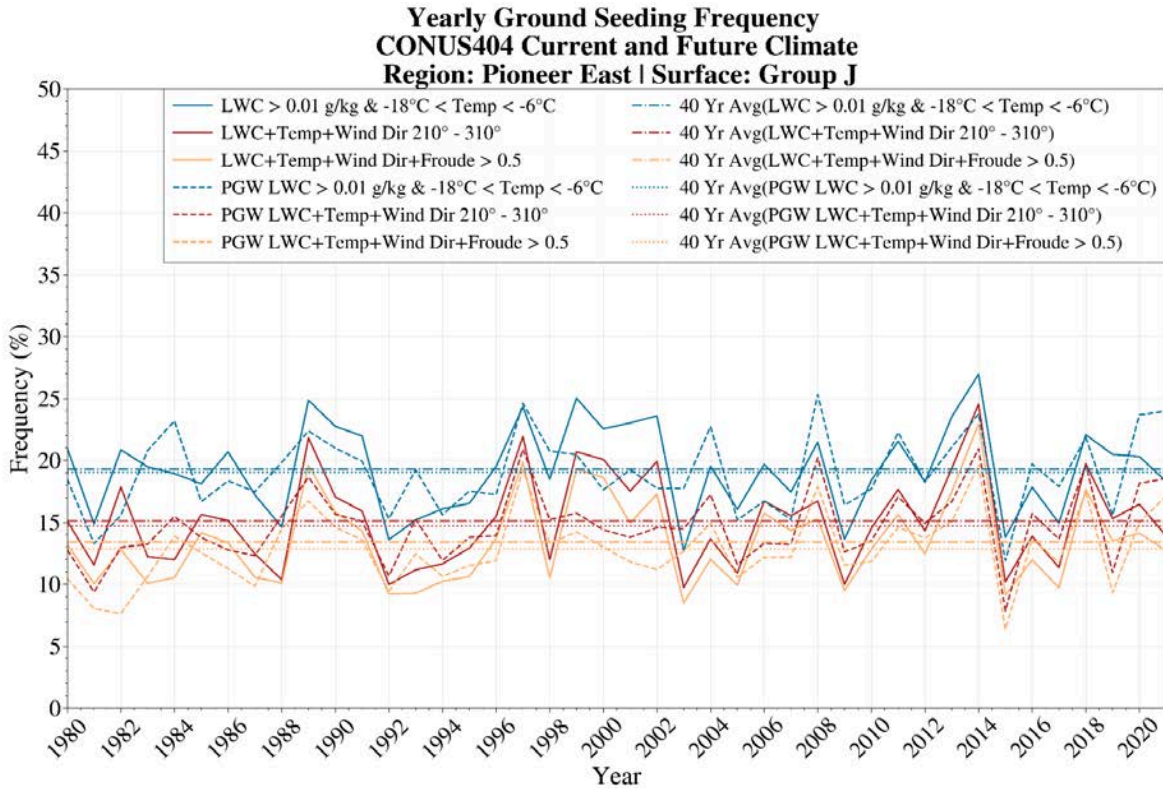


**Figure 4.26.** Annual seasonal frequency of ground-based seeding opportunities. Blue indicates frequency based on LWC and temperature, red indicates the addition of wind direction, orange indicates the addition of the Froude number greater than 0.5. Bars represent current climate and dashed lines indicate PGW. Horizontal dashed lines indicate the 40 year climatological average. Beaverhead Mountains (plots 1 and 2), Anaconda Range (plots 3 and 4), Pioneer Mountains (plots 5 and 6).

## 4.4. Airborne Seeding Feasibility

In the following section, airborne seeding feasibility for the Big Hole Basin region is assessed using the CONUS404 current and future climate simulations. Again, as described in [Section 4.1](#), several approaches were used to estimate the frequency of seedable opportunities in the Big Hole Basin. For airborne seeding, a representative flight height range of 3.5–4.5 km MSL was used, given that an aircraft could fly safely in cloud at that altitude range in this region. Maps of layer average LWC, temperature, and frequency of SLW were created from the CONUS404 model dataset. Additionally, target regions were identified and used to calculate area-based monthly and annual frequencies of seeding opportunities within the airborne seeding layer.

### 4.4.1. CONUS404 Current Climate Simulations

#### Single Site Analysis

To determine the vertical distribution of SLW in the atmosphere as simulated by CONUS404, contoured frequency by altitude diagrams (CFADs) were analyzed ([Figure 4.27](#)). The vertical profile of SLW greater than 0 g/kg from the surface was extracted from CONUS404 from the model grid points nearest the

representative SNOTEL sites in the Beaverhead Mountains, Anaconda Range, and Pioneer Mountains. Overall, across the three ranges, the greatest amount of SLW was seen between 3500 m to 5500 m. There is a sharp decline in larger values of simulated SLW at altitudes greater than 4500m at the Mule Creek and Saddle Mountain SNOTEL locations, but large values of SLW are simulated at higher altitudes in the Dark Horse profile. This suggests that higher flight levels may be suitable for the Beaverhead target.

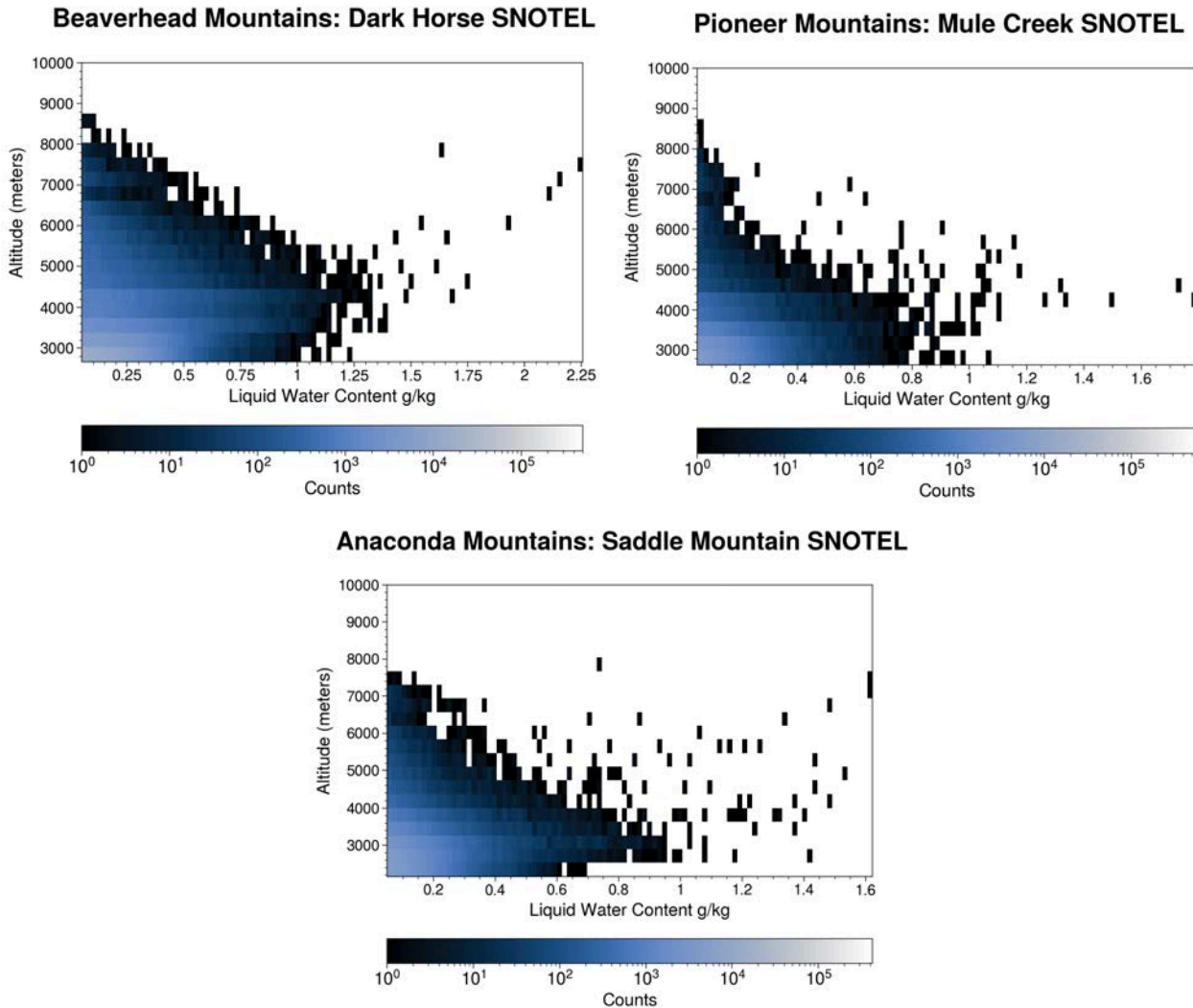


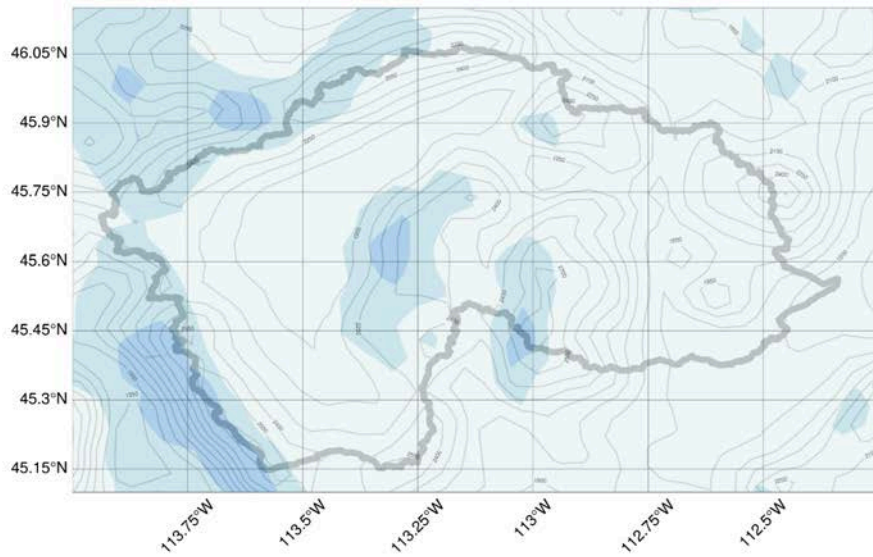
**Figure 4.27.** Contoured frequency by altitude diagrams (CFADs) showing the vertical distribution of SLW at model grid points closest to the associated SNOTEL sites for Beaverhead Mountains (top left), Anaconda Range (top right), and Pioneer Mountains (bottom left).

### Spatial Analysis

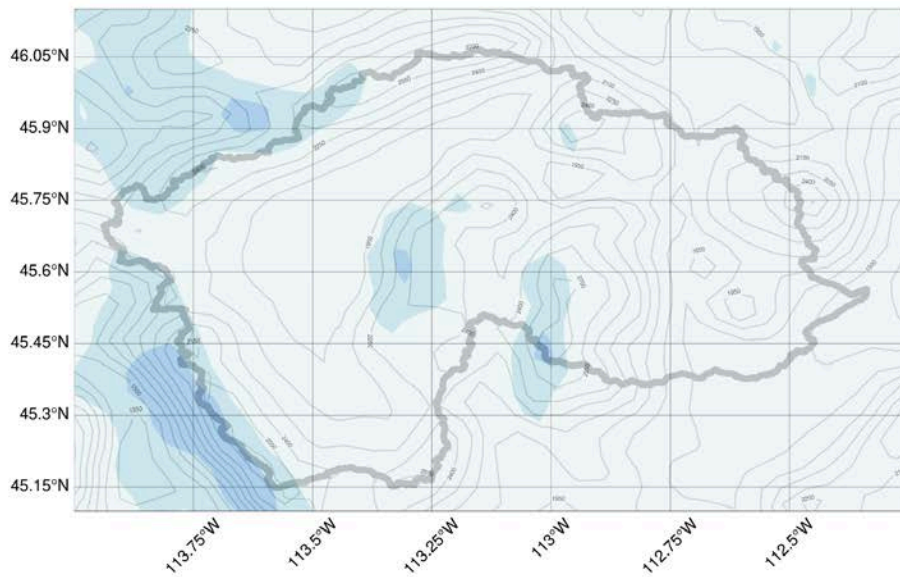
The combined requirements of temperatures between  $-6^{\circ}$  and  $-18^{\circ}\text{C}$  and LWC greater than  $0.01\text{ g/kg}$  are used to determine the 40-year average monthly frequency of airborne seedable conditions shown in [Figure 4.28](#). Frequency of airborne seedable conditions is generally small across the domain. However, the greatest frequency occurs along the ridges of highest terrain over the Beaverhead Mountains. The Anaconda Range and Pioneer Mountains also show areas of elevated frequency. However, as seen with

ground-based analysis, the Highland Mountains show very small frequency across all months and will be excluded from further airborne analysis. In April, frequencies of about 10% are present over a much broader area of the domain due to a slight increase in LWC in April (not shown) as opposed to the more targeted regions of high terrain during the rest of the seeding season.

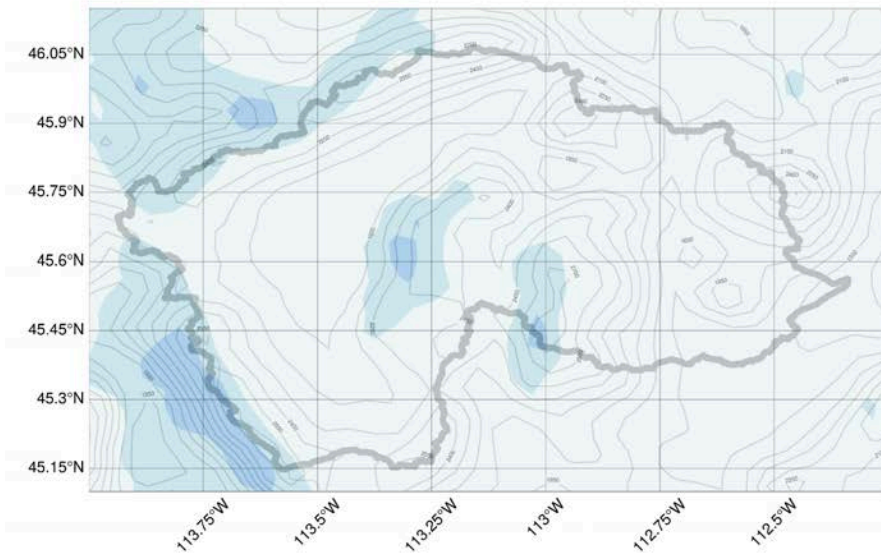
CONUS404 Current Climate  
Airborne Frequency of Seedable Conditions (November)



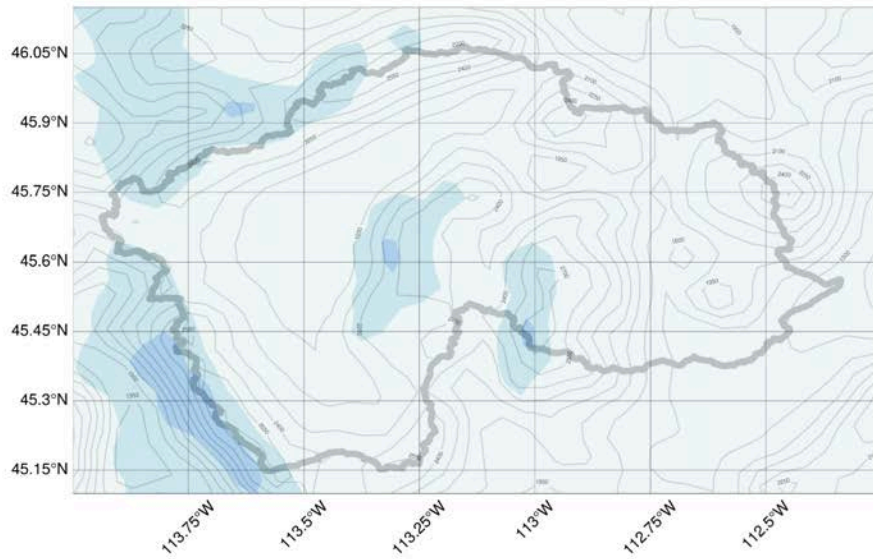
CONUS404 Current Climate  
Airborne Frequency of Seedable Conditions (December)



CONUS404 Current Climate  
Airborne Frequency of Seedable Conditions (January)



CONUS404 Current Climate  
Airborne Frequency of Seedable Conditions (February)



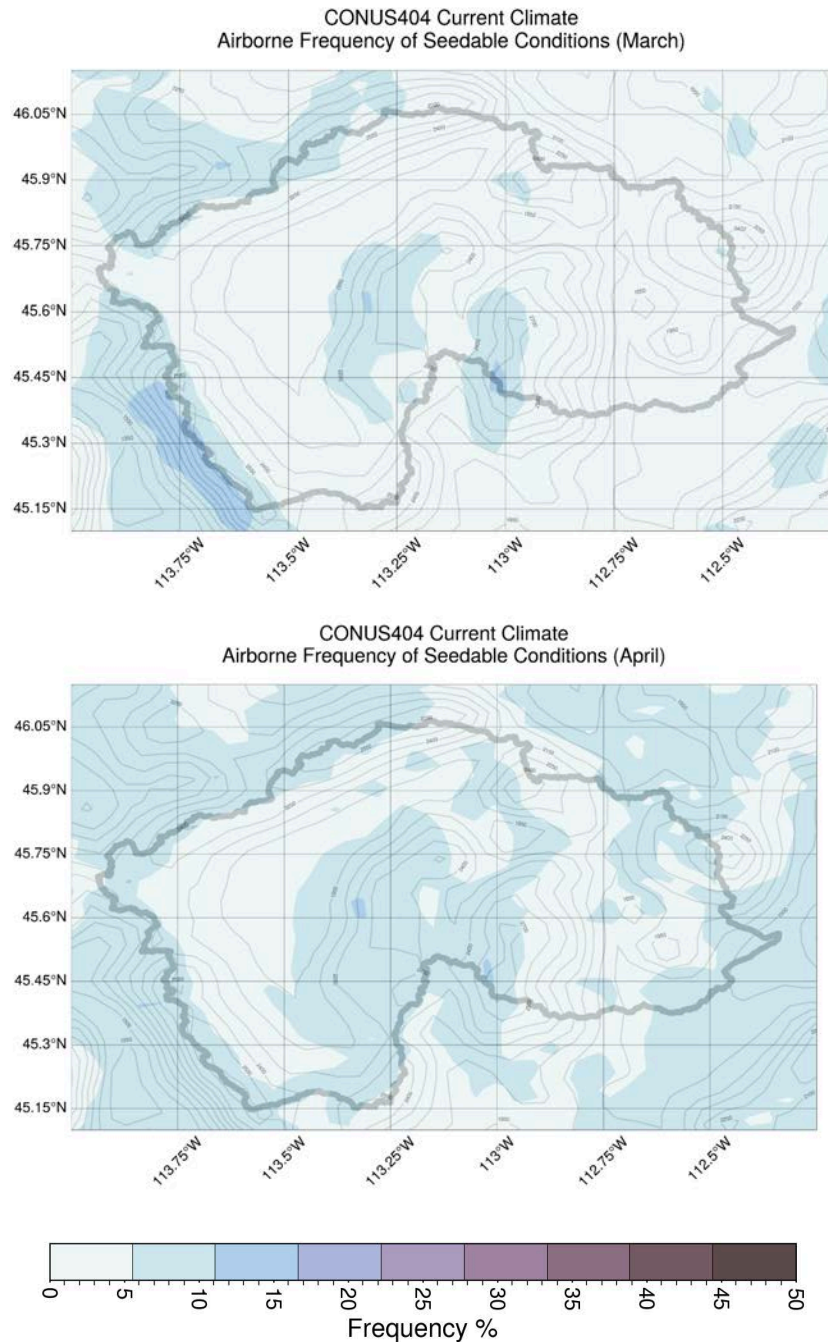


**Figure 4.28.** 40-year average frequency of airborne seedable conditions by month based on presence of  $LWC > 0.01$  g/kg and temperatures between  $-6^{\circ}\text{C}$  to  $-18^{\circ}\text{C}$ .

The 40-year average frequency of airborne seeding conditions for the full Nov–Apr wintertime seeding season is shown in [Figure 4.29](#). Overall, airborne frequencies are substantially smaller than ground-based seeding frequencies ([Figure 4.17](#)). Unlike ground-based frequencies, which showed greater seeding frequencies over all elevated terrain in the domain, airborne seeding frequencies for the seeding season

are greatest over and on the windward side of the Beaverhead Mountains. This is consistent with the vertical profiles of SLW shown in [Figure 4.27](#).

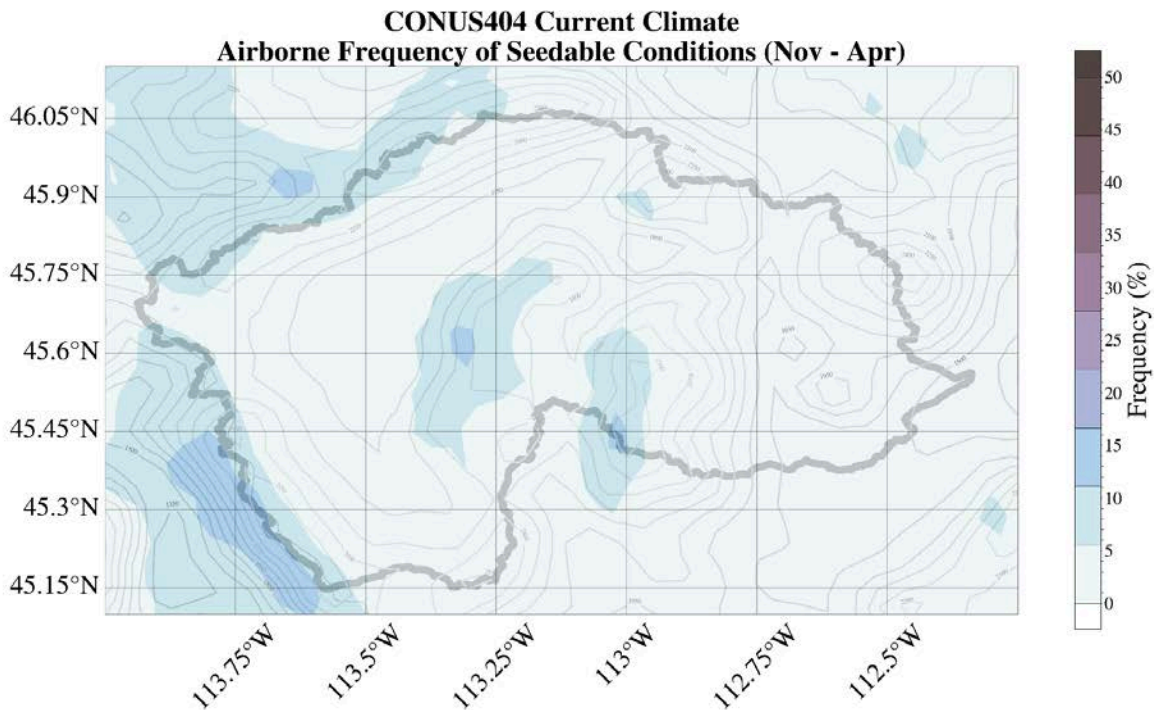


**Figure 4.29.** Frequency of airborne seedable conditions over the Nov–Apr seeding season based on presence of  $LWC > 0.01$  g/kg and temperatures between  $-6^{\circ}\text{C}$  to  $-18^{\circ}\text{C}$ .

In the airborne layer, spatial analysis of average LWC and temperature do not vary substantially by month. Therefore November through April season average maps are presented as representative values of these variables in [Figure 4.30](#) and [Figure 4.31](#).

Through the Nov–Apr season, LWC in the airborne layer is smaller and less distributed spatially ([Figure 4.30](#)) than seen in the ground layer ([Figure 4.17](#)). In the airborne layer, LWC is present only over the Beaverhead Mountains with average values approximately half of what was seen in the ground layer. Outside of the Beaverhead Mountains, LWC is negligible.

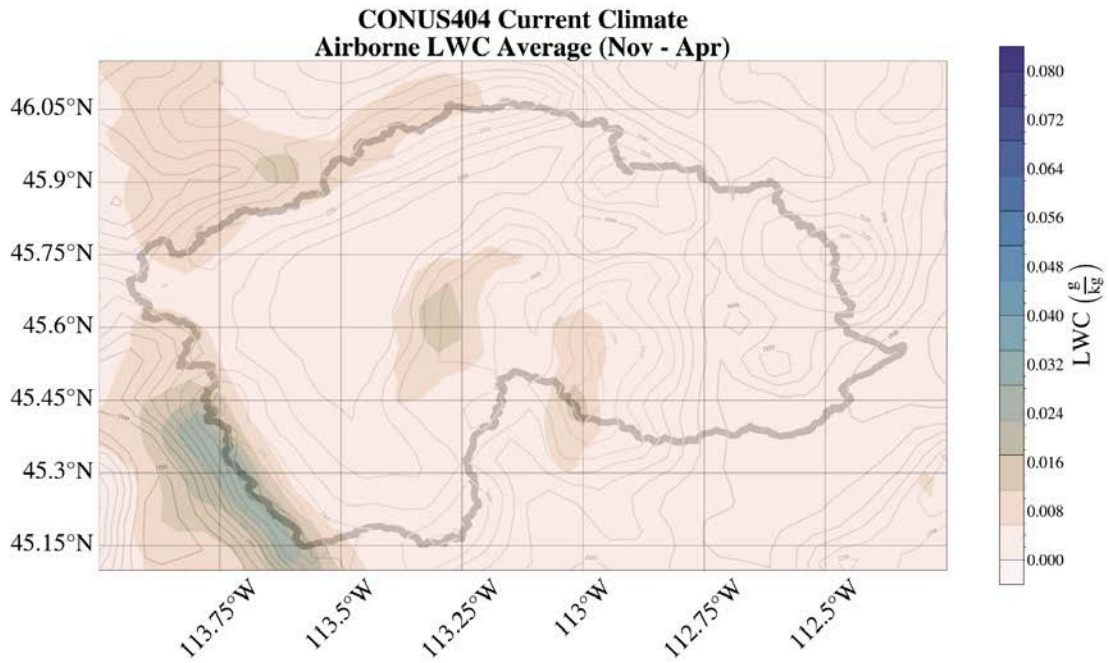


**Figure 4.30.** Average airborne LWC over the Nov–Apr seeding season (g/kg).

The 40-year average temperature for the Nov–Apr seeding season is shown in [Figure 4.31](#). In the airborne layer, temperature does not vary much over the entire domain with an average temperature of  $-14^{\circ}\text{C}$ , which is within the seedable temperature range.

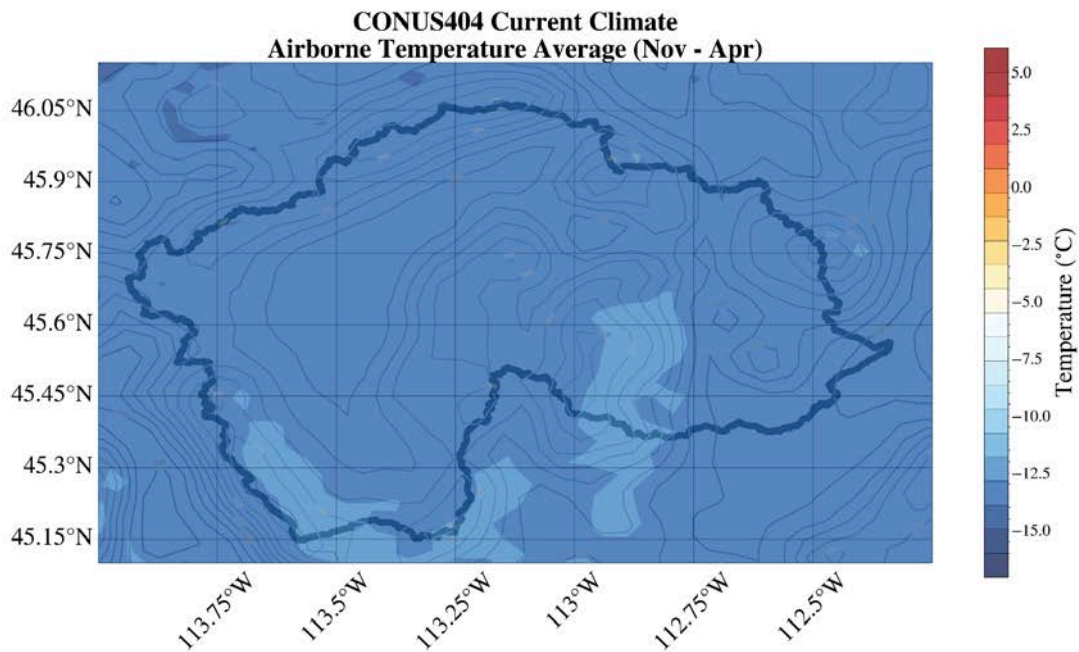
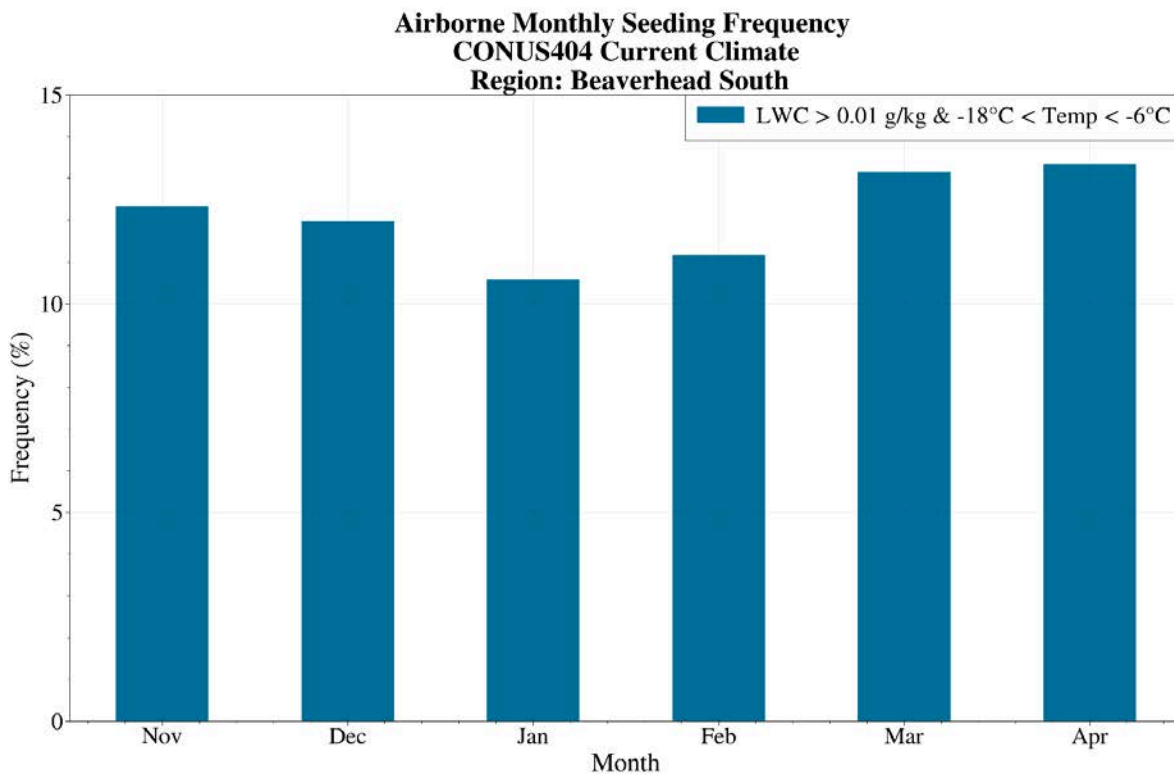


**Figure 4.31.** Average temperature in the airborne layer over the Nov–Apr seeding season ( $^{\circ}\text{C}$ ).

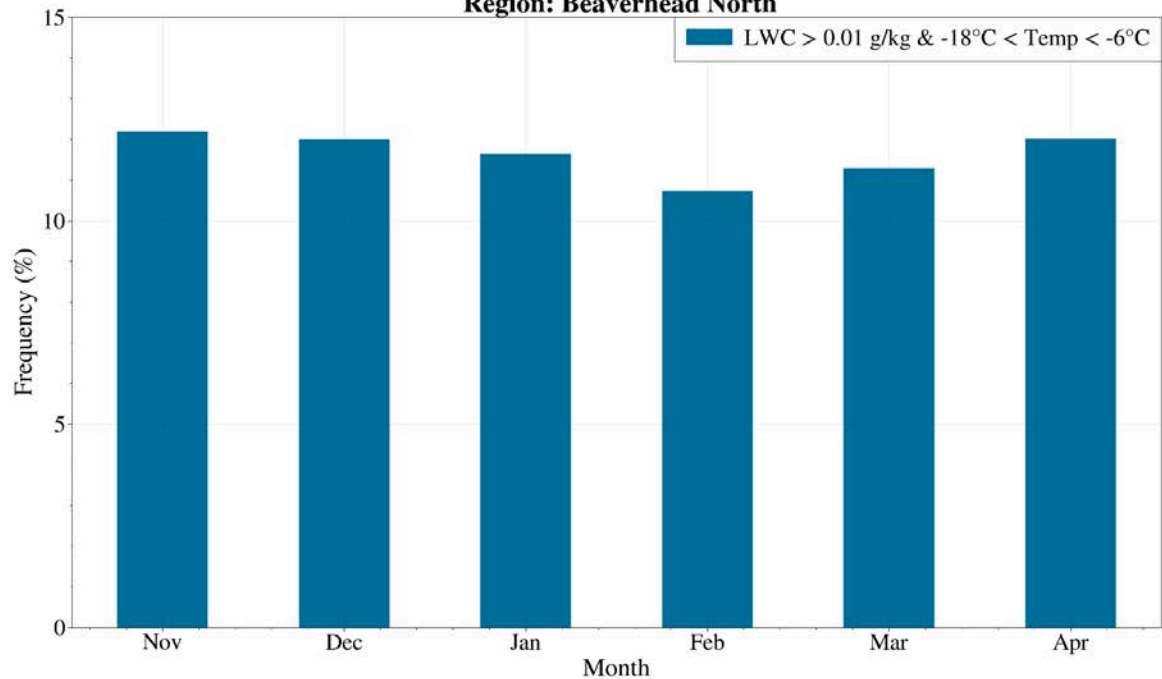
While average temperature is always within the seeding range, the consistently small values of LWC, with only small pockets of sufficient values to be identified as seedable opportunities prevent much of the domain from being feasible for airborne seeding operations. The most favorable target area for airborne seeding is upwind of and over the Beaverhead Mountains.

#### Area-based Analysis - Monthly

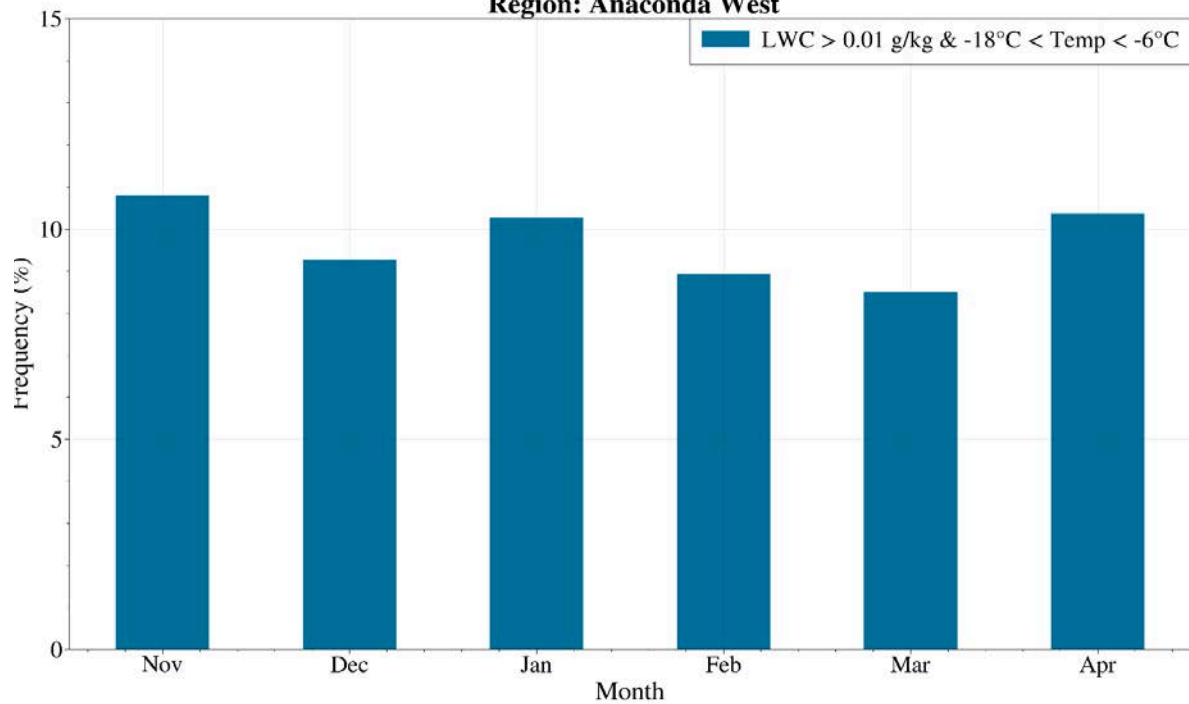
[Figure 4.32](#) provides the area-averaged 40-year average monthly frequencies of airborne seedable conditions, using the target regions as shown in [Figure 4.1](#). For airborne seeding conditions, frequencies only depend on temperature and liquid water; wind direction and blocking are not considered for this analysis. While airborne frequencies are more similar across all winter months as compared to ground-based frequencies, there is a notable mid-season decrease in most regions. While there is generally little variability in airborne frequency across the regions in the domain, the Beaverhead Mountains do show a slightly greater frequency of seeding potential than the other ranges.



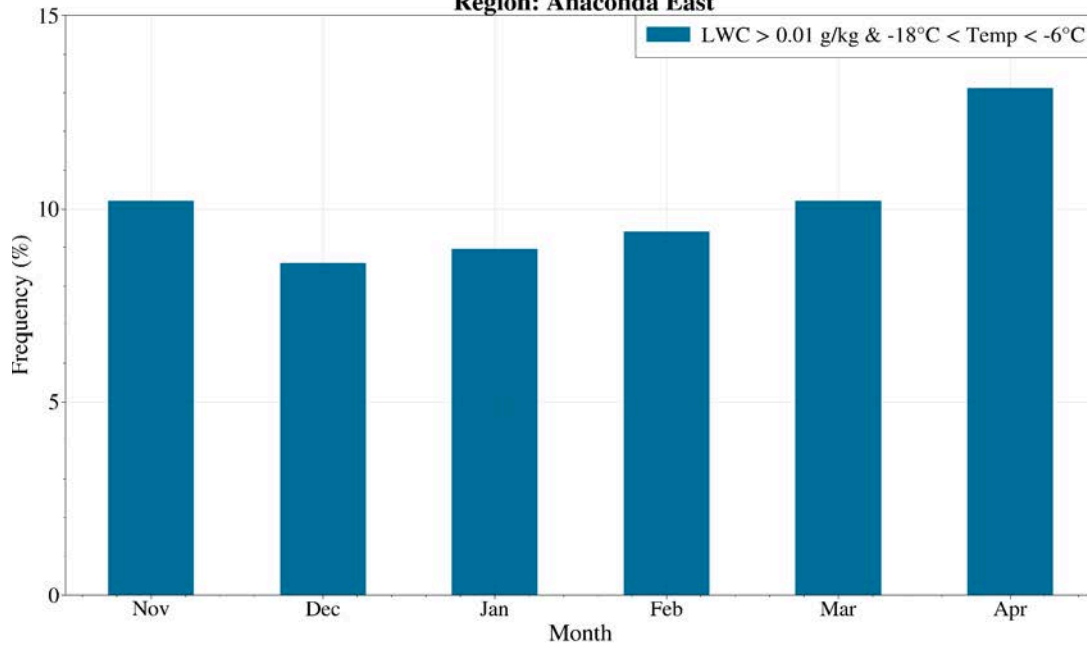
**Airborne Monthly Seeding Frequency**  
**CONUS404 Current Climate**  
**Region: Beaverhead North**



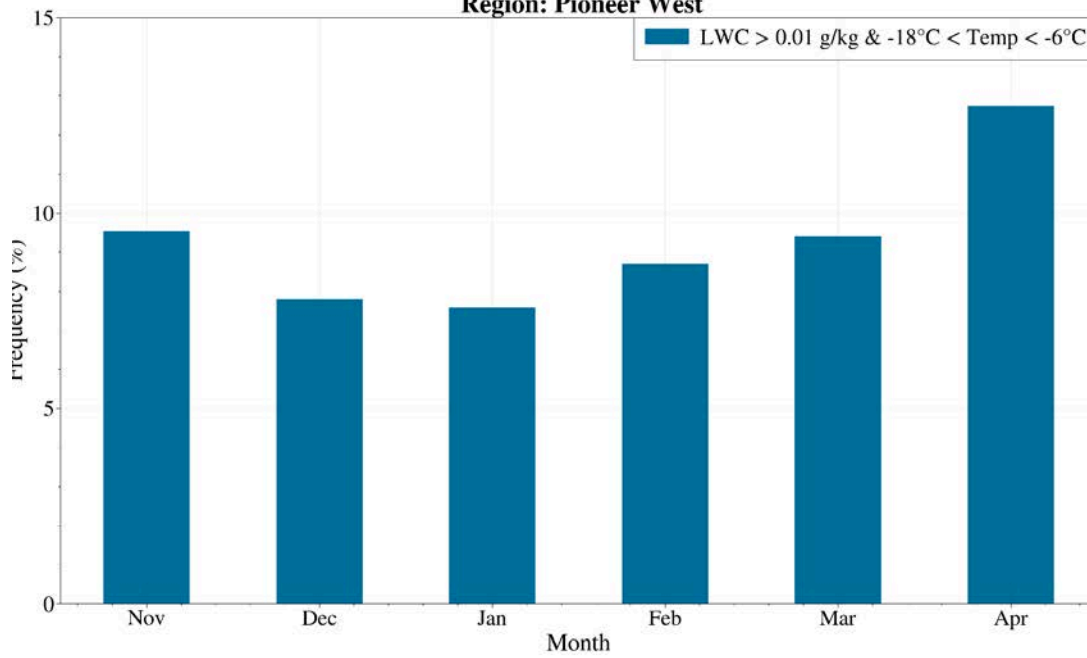
**Airborne Monthly Seeding Frequency**  
**CONUS404 Current Climate**  
**Region: Anaconda West**



**Airborne Monthly Seeding Frequency**  
**CONUS404 Current Climate**  
**Region: Anaconda East**



**Airborne Monthly Seeding Frequency**  
**CONUS404 Current Climate**  
**Region: Pioneer West**



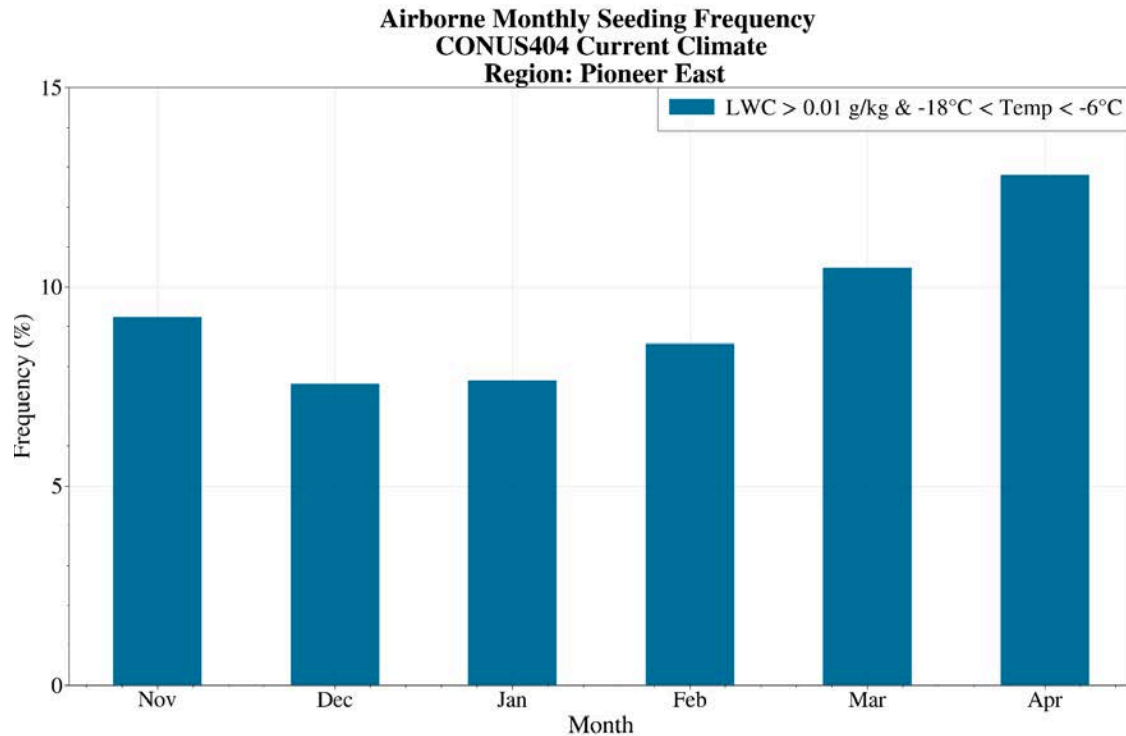


**Figure 4.32.** 40-year average seasonal frequency of airborne seeding. Blue bars indicate frequency based on LWC and temperature. Beaverhead Mountains (plots 1 and 2), Anaconda Range (plots 3 and 4), Pioneer Mountains (plots 5 and 6).

The hourly distribution of seedable frequency by month is shown in [Figure 4.33](#). As with ground-based seeding, the diurnal pattern of seedable frequency is similar across all targets and thus only the Anaconda East target is shown. In contrast to the temporal pattern shown with ground-based seeding, airborne conditions are more frequently met from about 20 to 02 UTC, although as has been already shown, frequencies are much smaller than with ground-based seeding.

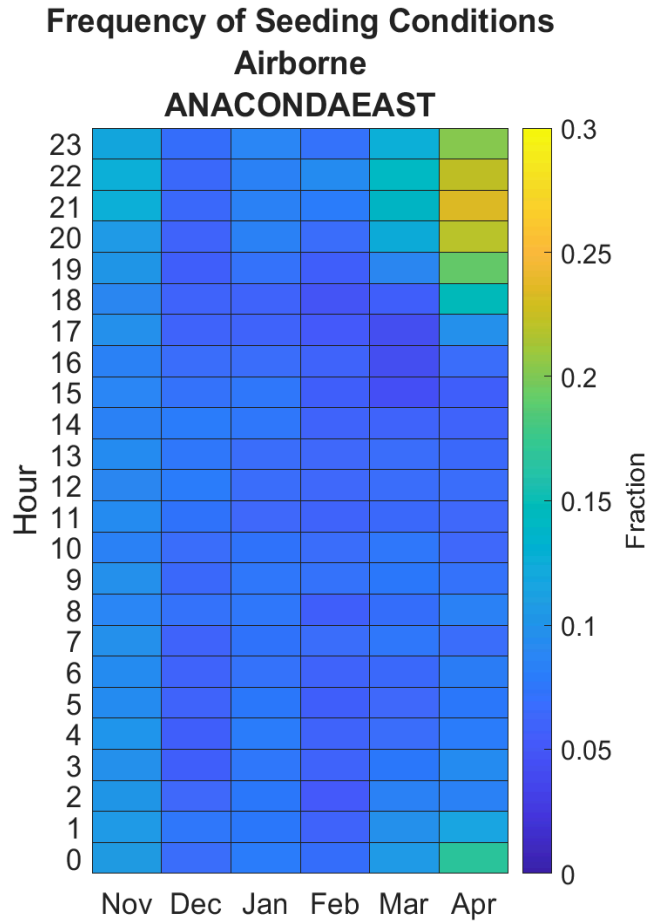


**Figure 4.33.** Hourly distribution of airborne seedable frequency by month for the Anaconda East target. Time is UTC, and the color represents the fraction of time each hour experiences seedable conditions.

#### Area-based Analysis - Seasonal

The interannual frequency of airborne seeding frequency is shown in [Figure 4.34](#). Over the 40-year time span of CONUS404, airborne frequency shows substantial variability from winter to winter. Overall, there is not a noticeable positive or negative trend in frequency of seeding for this region over time. As with monthly analysis in [Figure 4.32](#), the Beaverhead Mountains show the greatest overall frequency of seeding potential with a 40-year average frequency of ~13%.

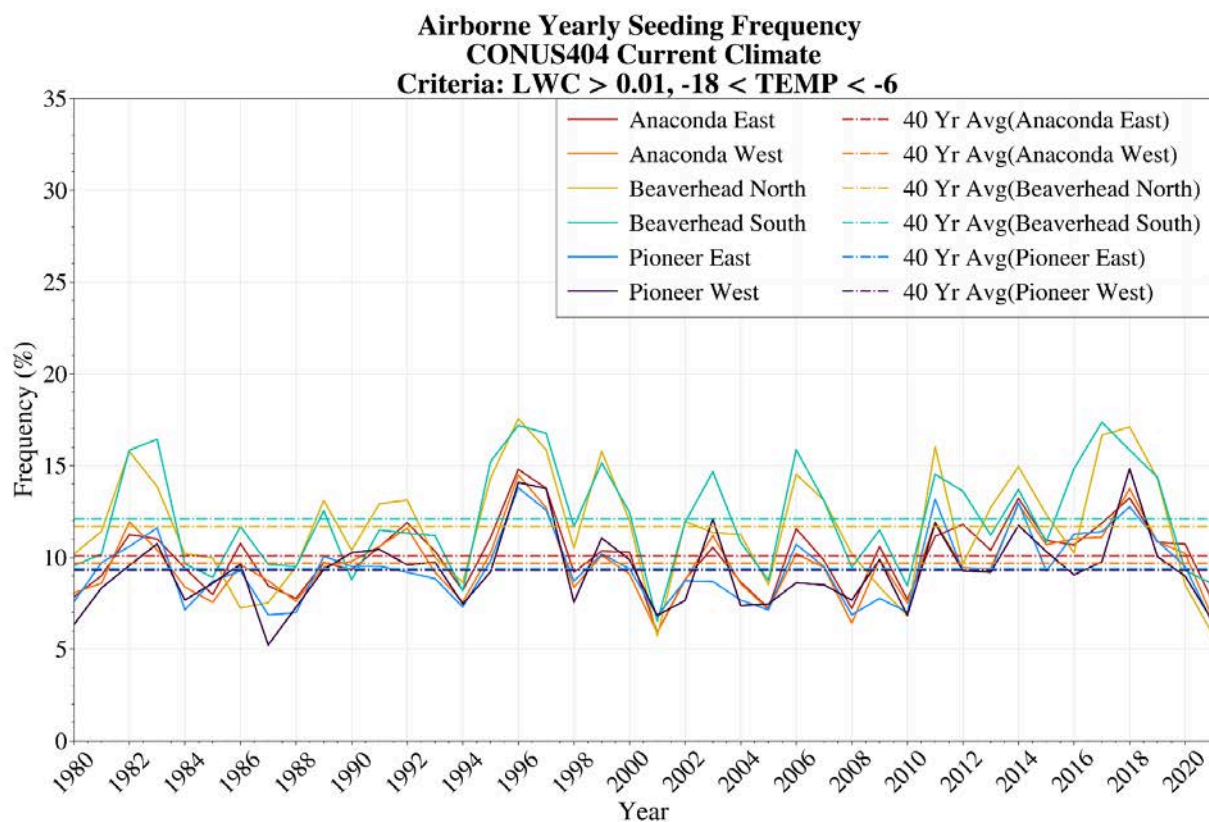


**Figure 4.34.** Annual seasonal frequency of airborne seeding opportunities for all ranges (Beaverhead, Anaconda, and Pioneer).

#### 4.4.2. CONUS404 Future Climate Simulations

##### Spatial Analysis

As with ground layer analysis, the 3.5–4.5 km airborne layer was analyzed using output from CONUS404 PGW simulations. Overall, the frequency of seedable conditions increases slightly between the current and future climates across the entire domain (Figure 4.35). In the future climate scenario, both airborne LWC (Figure 4.36) and temperature (Figure 4.37) increase; however, despite the increase in temperature in the future climate, the temperatures remain within the seeding range (Figure 4.38). Therefore, the increase in airborne LWC and temperatures remaining in the seeding range results in an increase in the frequency of airborne seeding.

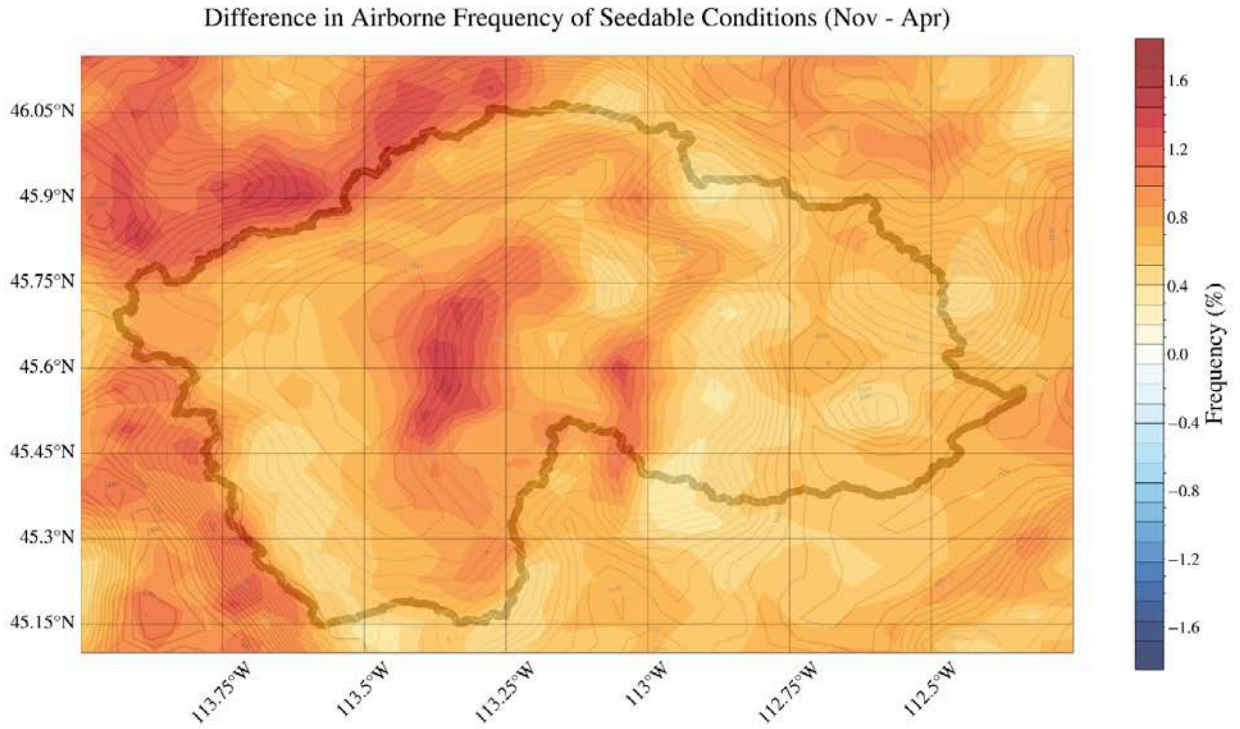


**Figure 4.35.** Difference in wintertime average frequency of airborne seedable conditions: PGW minus CONUS404 current climate based on presence of LWC > 0.01 g/kg and temperatures between  $-6^{\circ}\text{C}$  to  $-18^{\circ}\text{C}$ .

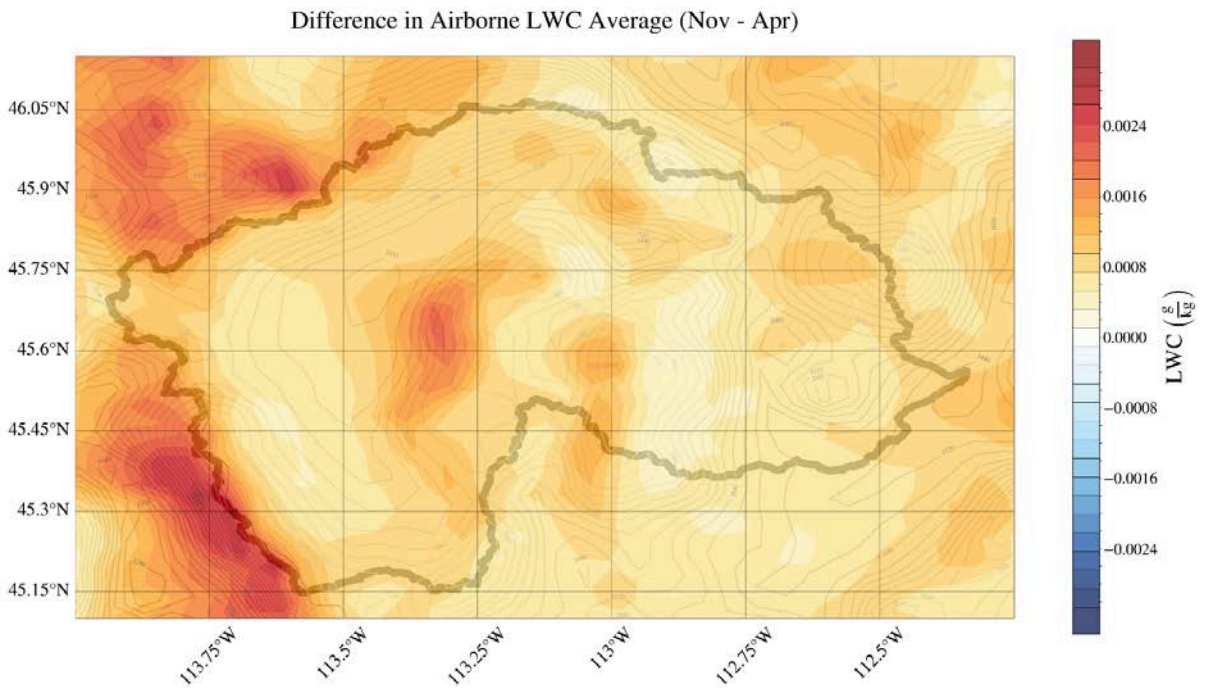


**Figure 4.36.** Difference in wintertime average airborne LWC: PGW minus CONUS404 current climate (g/kg).

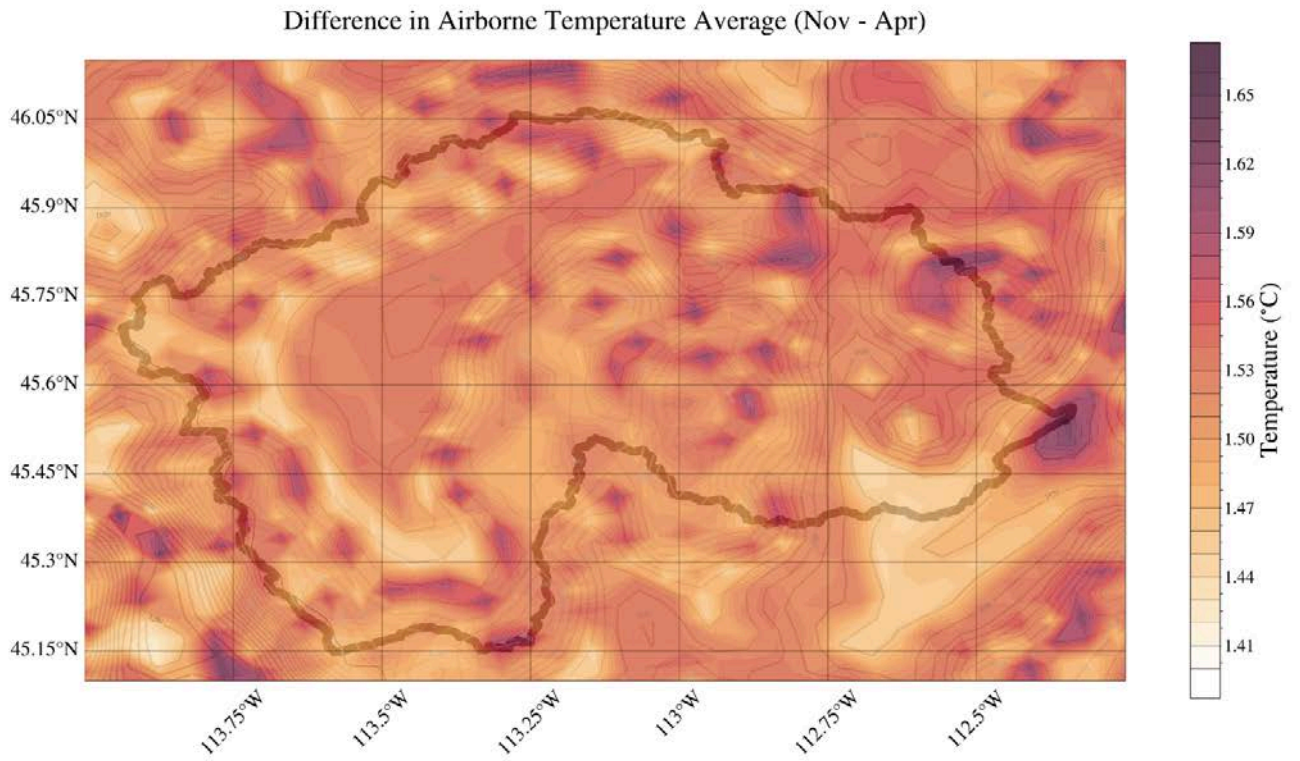


**Figure 4.37.** Difference in wintertime average airborne temperature: PGW minus CONUS404 current climate (°C). Color bar shows all positive values as there are no decreases in temperature.

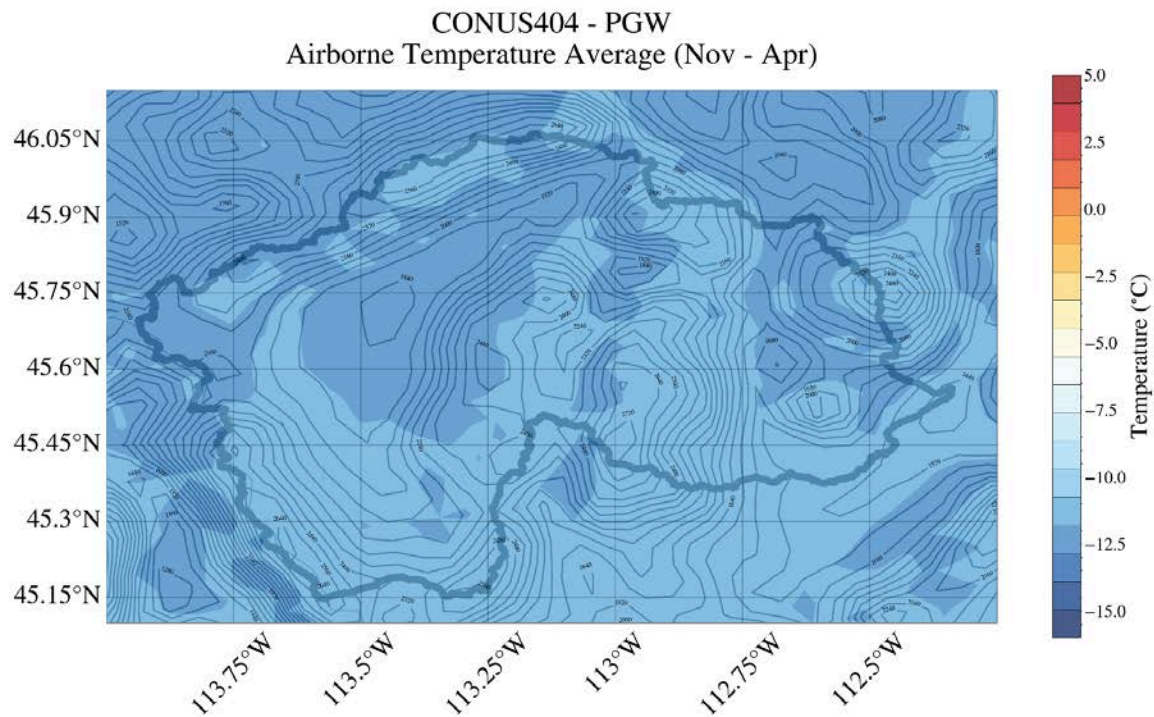
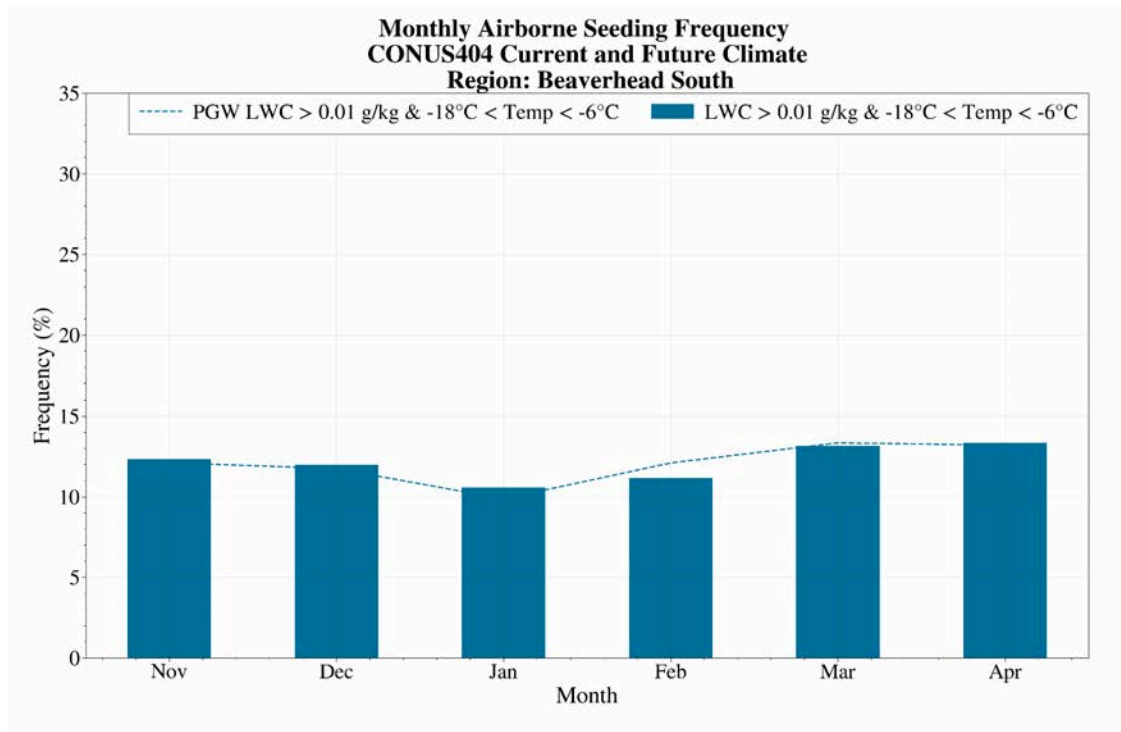


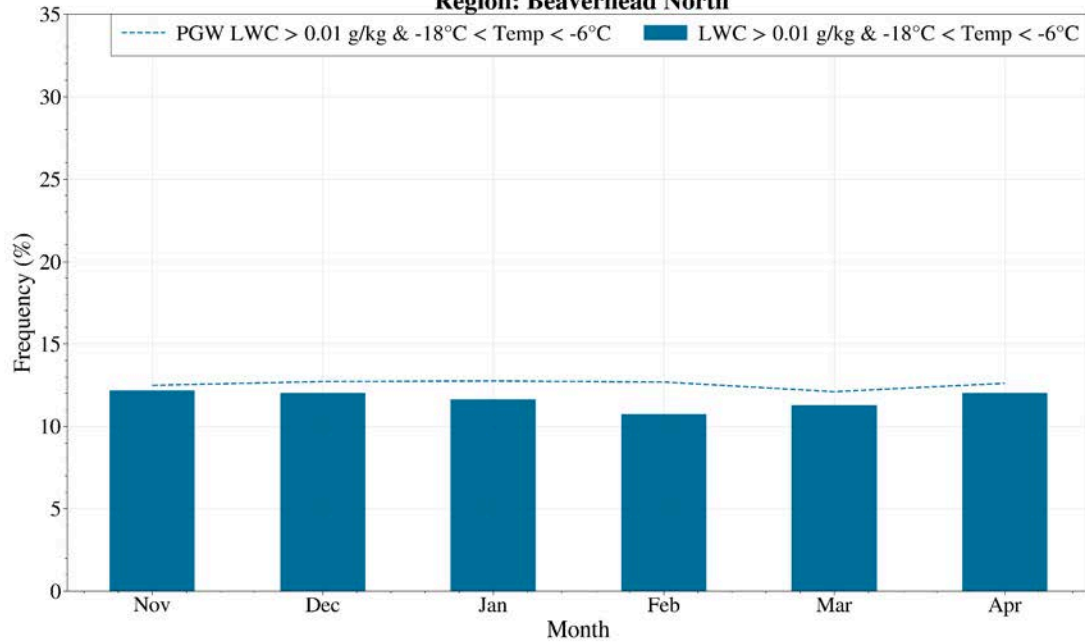
**Figure 4.38.** Average wintertime (Nov–Apr) airborne temperature for CONUS404 PGW (°C).

### Area-based Analysis - Monthly

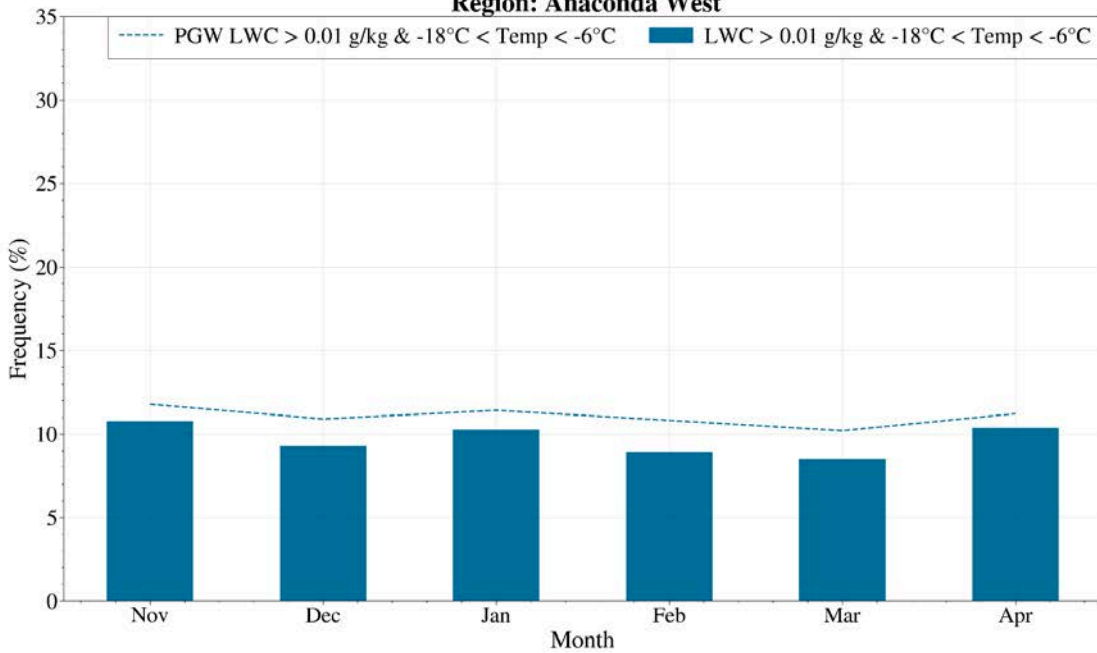
The 40-year average monthly frequencies of seedable conditions for the airborne layer for both the CONUS404 current climate and PGW simulations are shown in [Figure 4.39](#). The airborne analysis shows a more consistent frequency distribution across all target sites, unlike the ground-based analysis that varied significantly depending on additional variables such as wind direction and Froude number. The 40-year average frequency of seedable conditions in the airborne layer in the future climate generally indicates slight increases in frequency in most months ([Figure 4.39](#)). This finding is consistent with the slight increase in frequency seen in the spatial analysis above in [Figure 4.35](#).



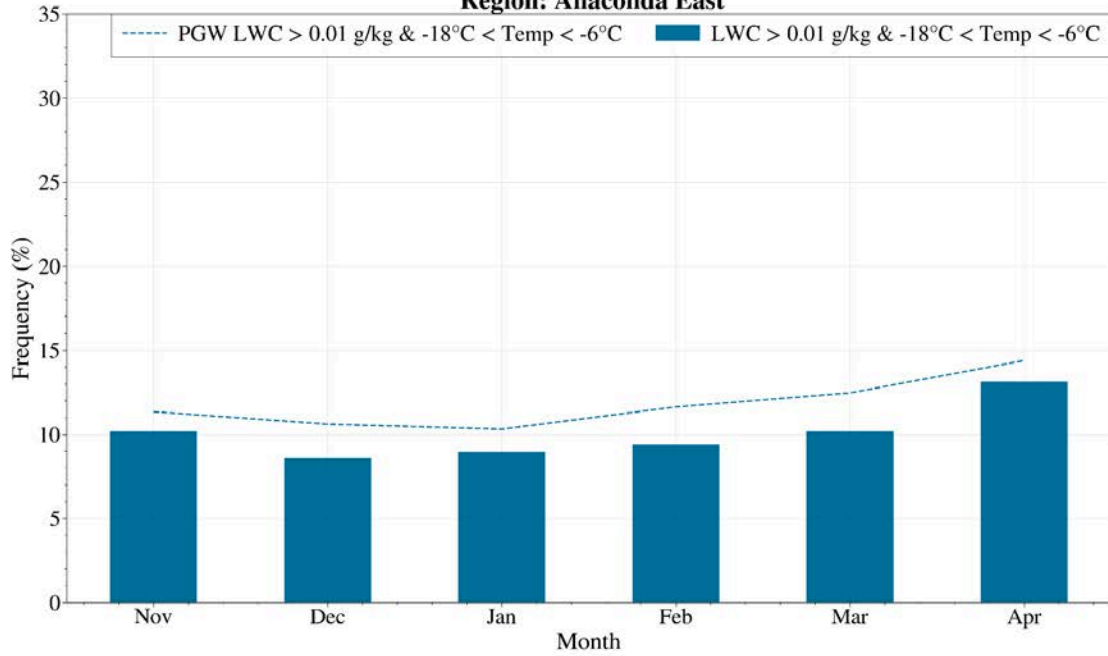
**Monthly Airborne Seeding Frequency  
CONUS404 Current and Future Climate  
Region: Beaverhead North**



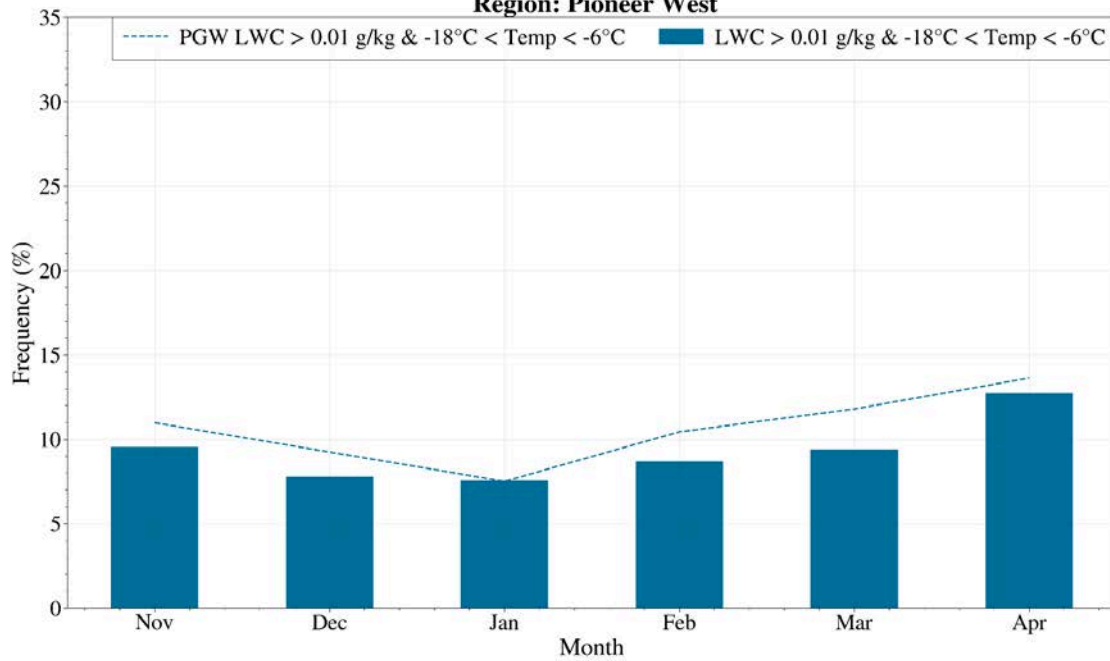
**Monthly Airborne Seeding Frequency  
CONUS404 Current and Future Climate  
Region: Anaconda West**



**Monthly Airborne Seeding Frequency  
CONUS404 Current and Future Climate  
Region: Anaconda East**



**Monthly Airborne Seeding Frequency  
CONUS404 Current and Future Climate  
Region: Pioneer West**



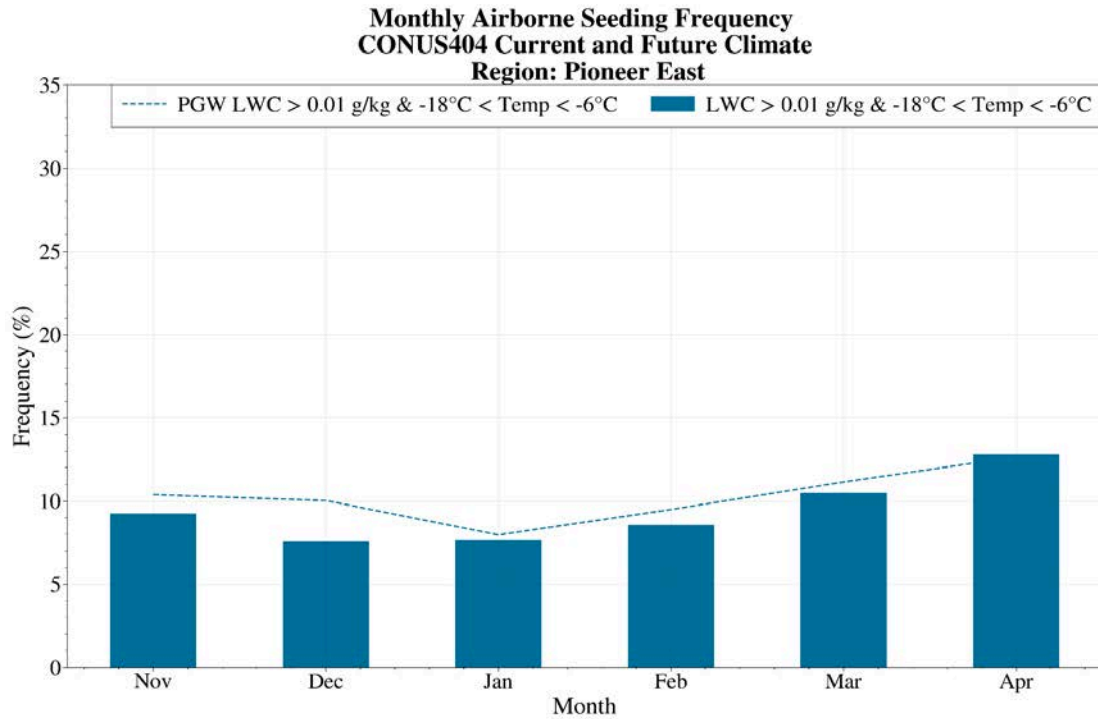
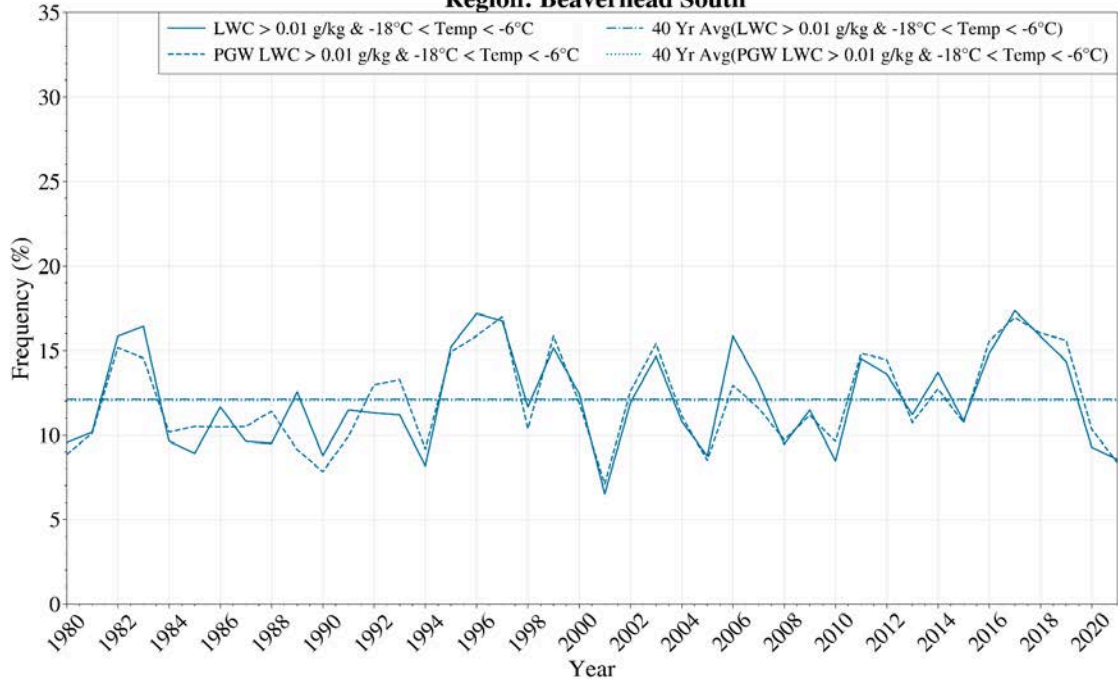


**Figure 4.39.** 40-year average seasonal frequency of airborne seeding opportunities. Bars represent current climate and dashed lines indicate PGW. Beaverhead Mountains (plots 1 and 2), Anaconda Range (plots 3 and 4), Pioneer Mountains (plots 5 and 6).

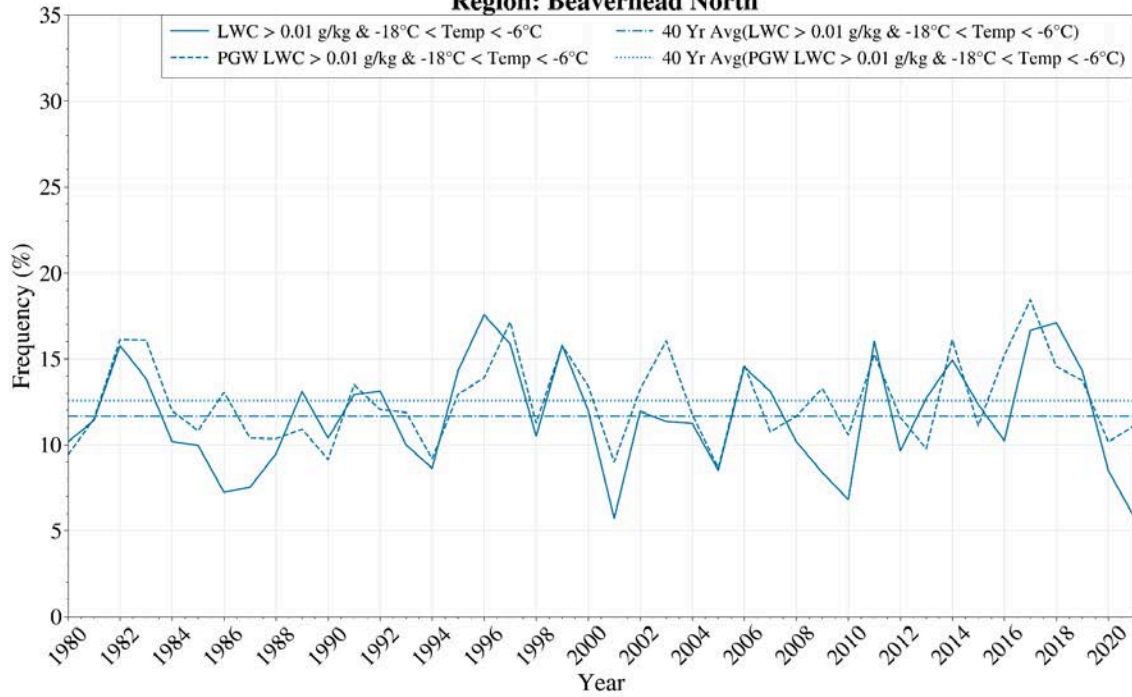
**Area-based Analysis - Yearly**

Seasonal frequencies of airborne seedable conditions for both CONUS404 current and future climate are shown in [Figure 4.40](#). The future climate frequency of airborne seeding potential increases very slightly, but remains between 10% and 15%, across all target regions. Overall, during the 40-year period interannual, variability is present with no notable positive or negative trends. Between the current and future climates, frequencies do not change substantially in the future climate scenario in the airborne layer indicating that airborne seeding operations may not be substantially impacted by a warming climate.

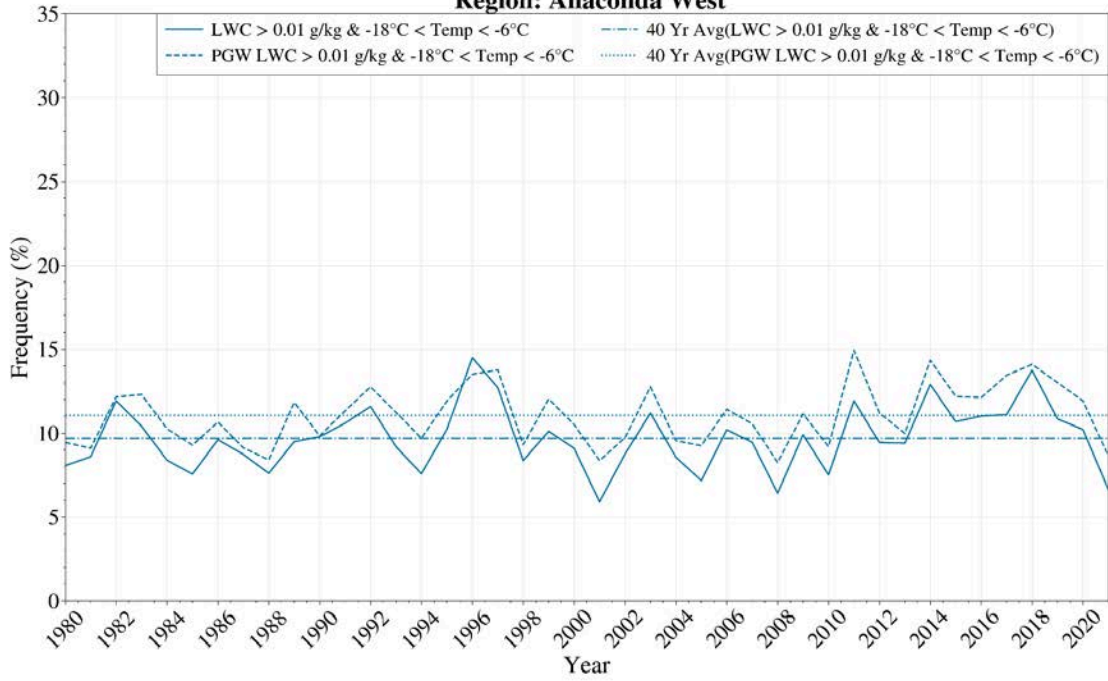
**Yearly Airborne Seeding Frequency  
CONUS404 Current and Future Climate  
Region: Beaverhead South**



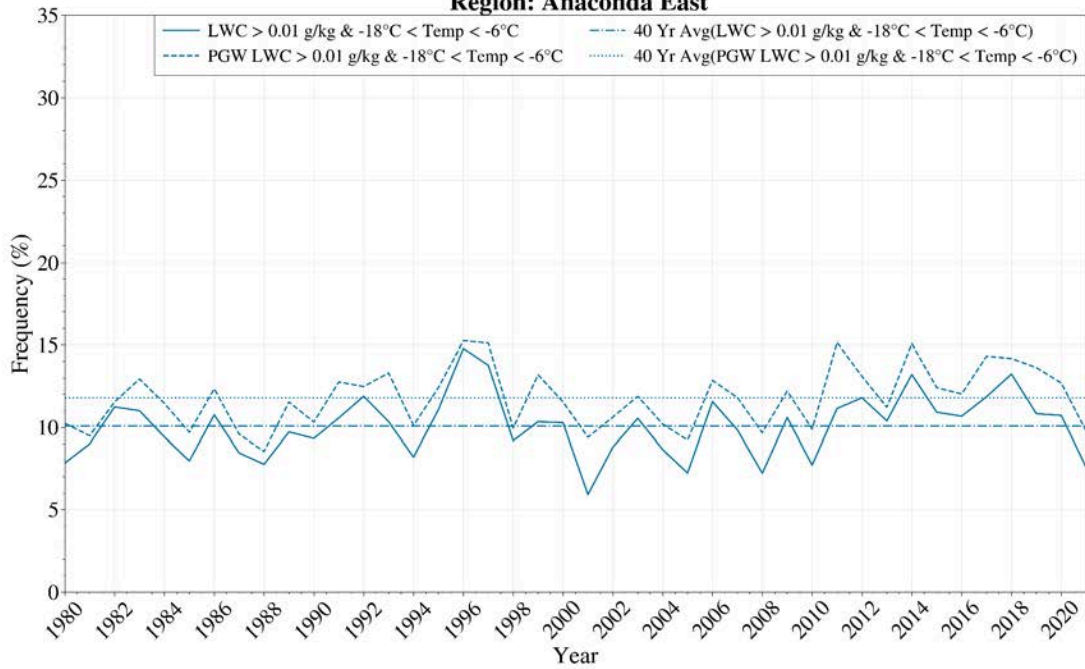
**Yearly Airborne Seeding Frequency  
CONUS404 Current and Future Climate  
Region: Beaverhead North**



**Yearly Airborne Seeding Frequency  
CONUS404 Current and Future Climate  
Region: Anaconda West**



**Yearly Airborne Seeding Frequency  
CONUS404 Current and Future Climate  
Region: Anaconda East**



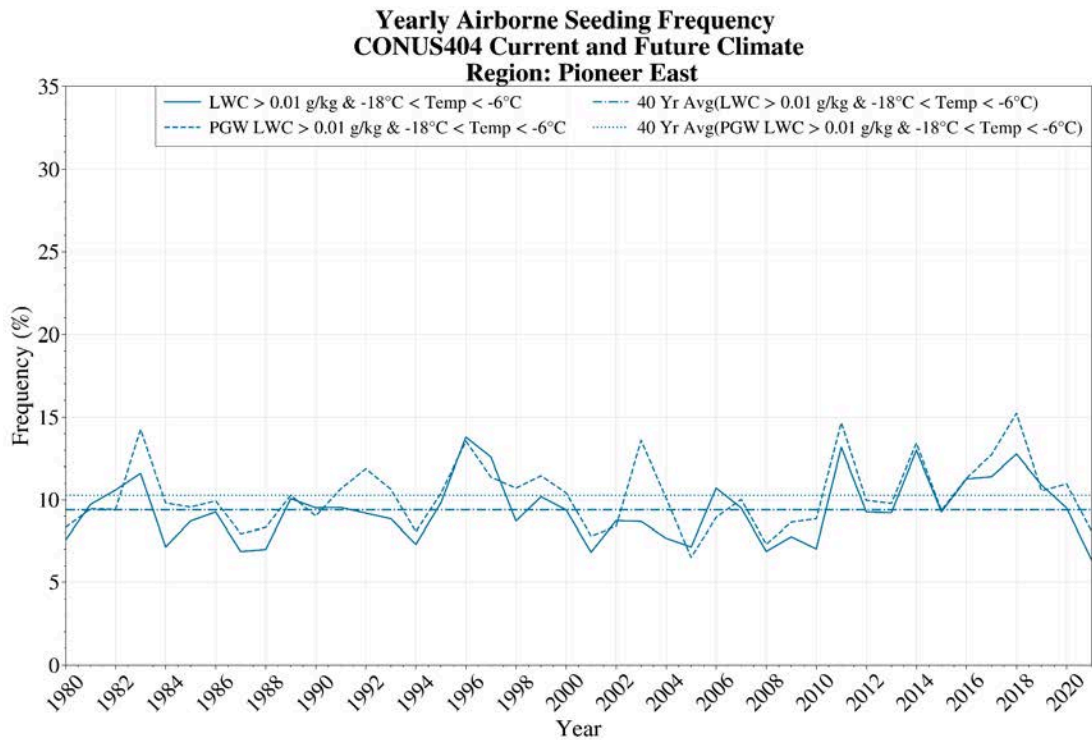
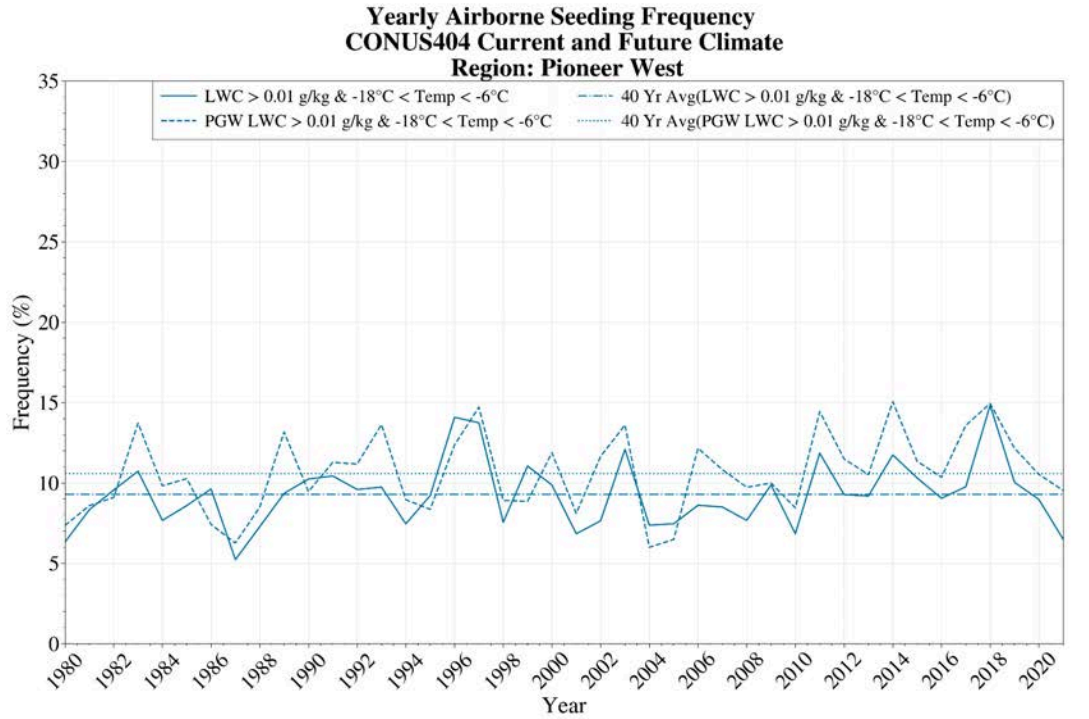


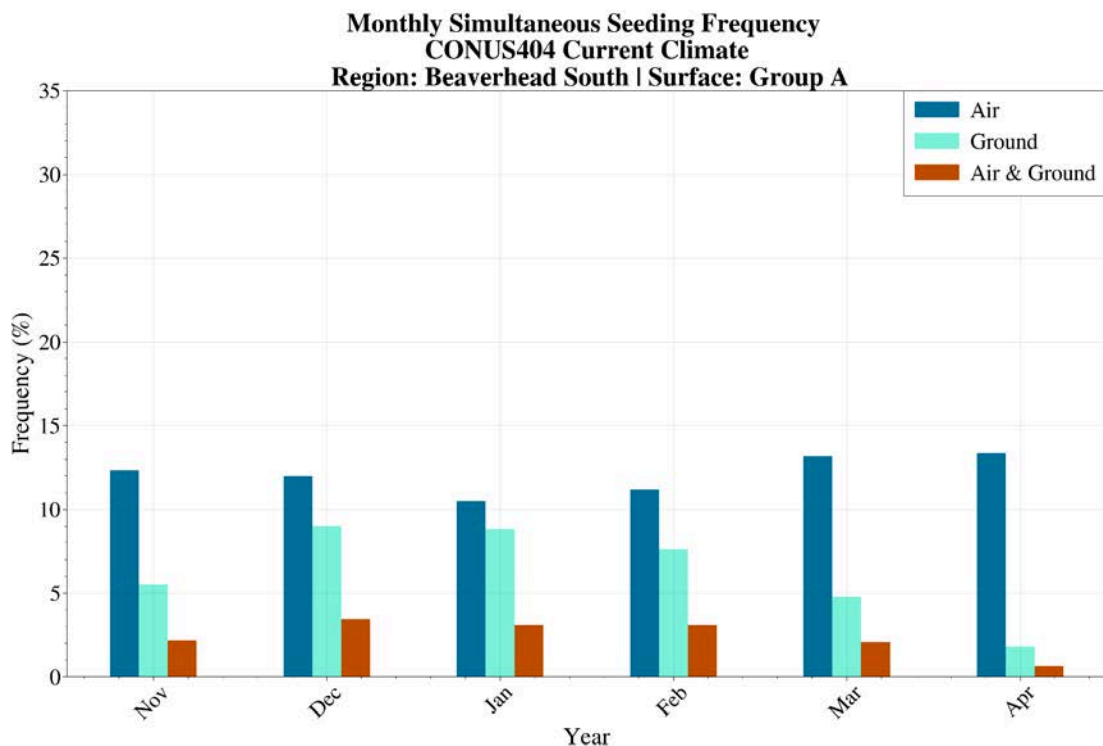
**Figure 4.40.** Annual seasonal frequency of airborne seeding opportunities. Solid lines represent current climate and peaked dashed lines indicate PGW. Horizontal lines indicate 40 year climatological average. Beaverhead Mountains (plots 1 and 2), Anaconda Range (plots 3 and 4), Pioneer Mountains (plots 5 and 6).

## 4.5. Combined Airborne and Ground Seeding Feasibility

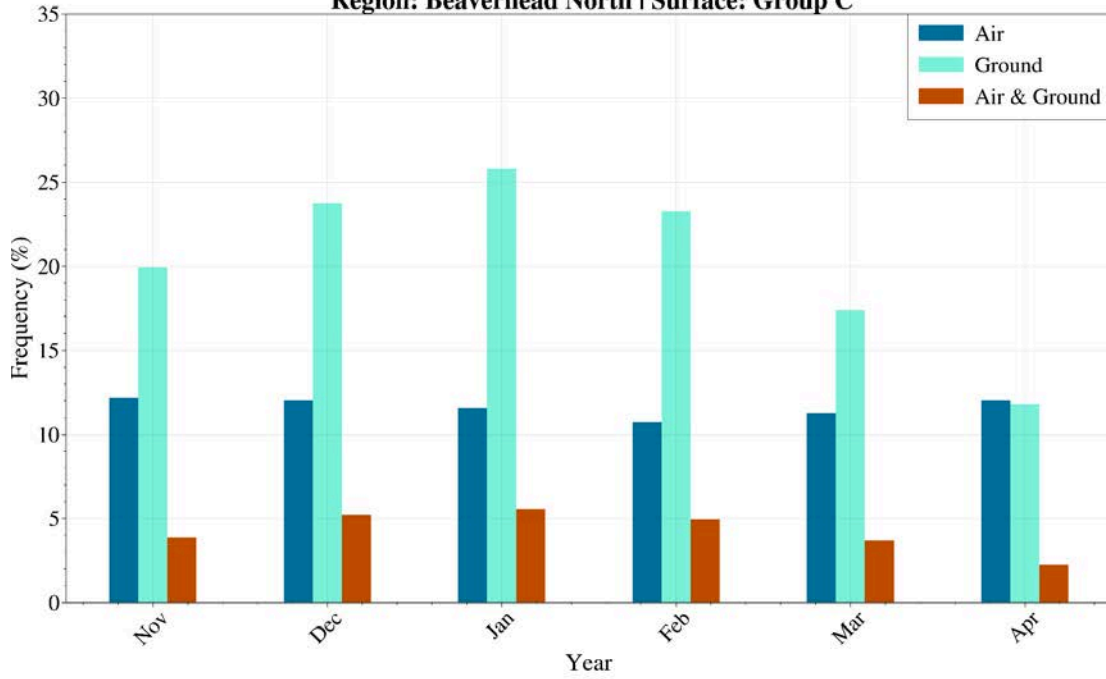
In the following section, combined airborne and ground-based seeding feasibility for the Big Hole Basin region is assessed using the CONUS404 current and future climate simulations. The frequencies of ground-based and airborne opportunities are considered separately, as well as when conditions are occurring at both layers simultaneously, for each of the target regions defined above. The motivation behind this analysis is to provide an estimate of the increase in seeding potential when considering a program that includes both ground-based and airborne seeding activities - a minimal overlap in seedable conditions, shown by the “Simultaneous” (Air & Ground) bars below, indicates that a program operating both will have overall increased opportunities for seeding.

### Current Climate - Area-based Analysis - Monthly

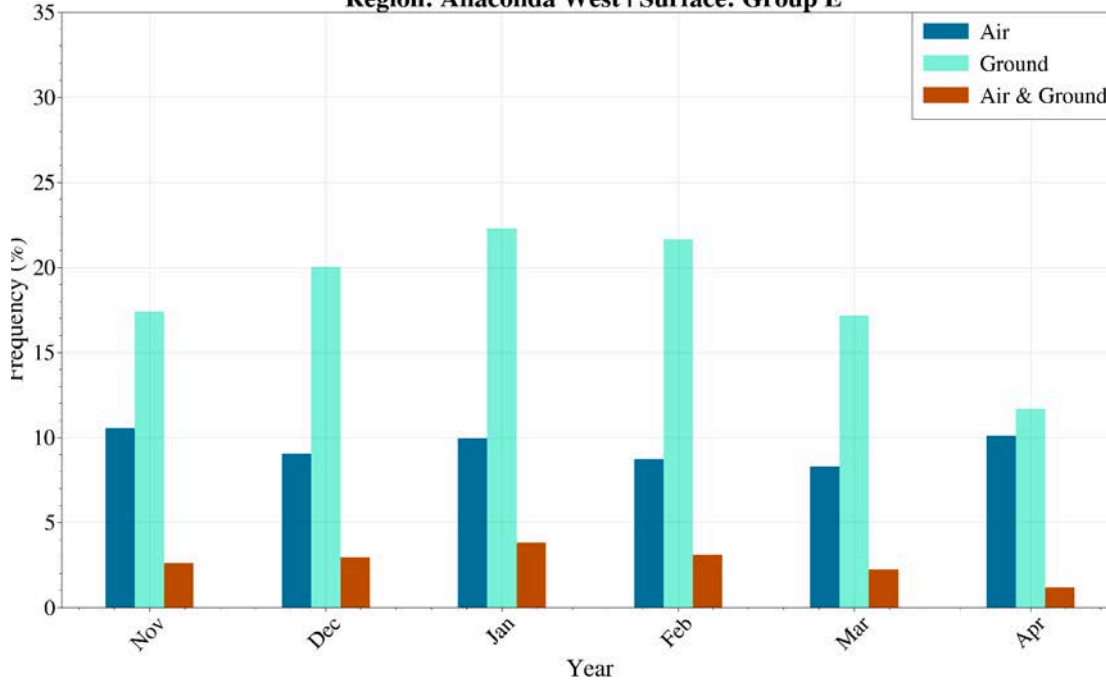
Combined area-averaged monthly frequencies for ground and airborne seeding are shown in [Figure 4.41](#). Ground-based frequencies include wind and Froude variables in addition to the SLW and temperature parameters used in both airborne and ground-based analysis. Across all regions and throughout the seeding season, the times when both ground-based and airborne opportunities occur simultaneously is small. This is consistent with the opposite diurnal patterns of seedable conditions for ground-based and airborne seeding shown in [Figure 4.20](#) and [Figure 4.33](#). The results of the simultaneous air and ground seeding frequencies in [Figure 4.41](#) indicate that independent air and ground operations would be needed in order to maximize seeding opportunities. Other than Beaverhead South, there is a greater frequency of opportunity for seeding with ground seeding than airborne in most months. Only the spring months (April, and for the Pioneers also March) exhibit reduced ground seeding opportunities, to similar or less than airborne.



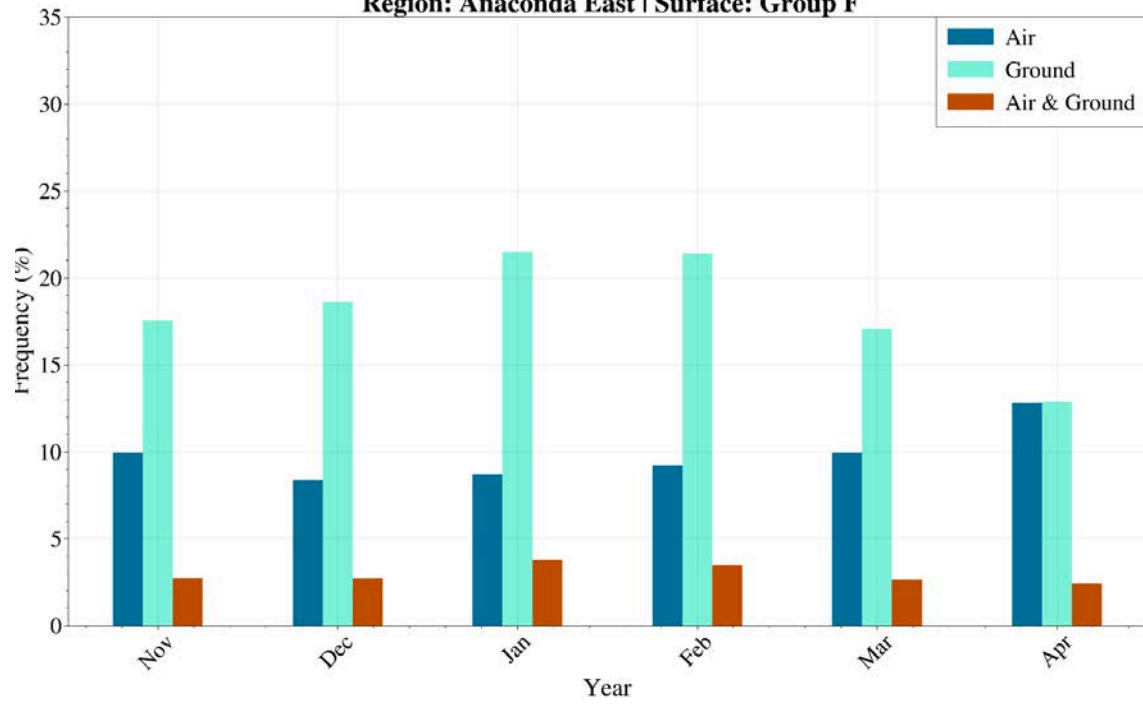
Monthly Simultaneous Seeding Frequency  
 CONUS404 Current Climate  
 Region: Beaverhead North | Surface: Group C



Monthly Simultaneous Seeding Frequency  
 CONUS404 Current Climate  
 Region: Anaconda West | Surface: Group E



Monthly Simultaneous Seeding Frequency  
CONUS404 Current Climate  
Region: Anaconda East | Surface: Group F



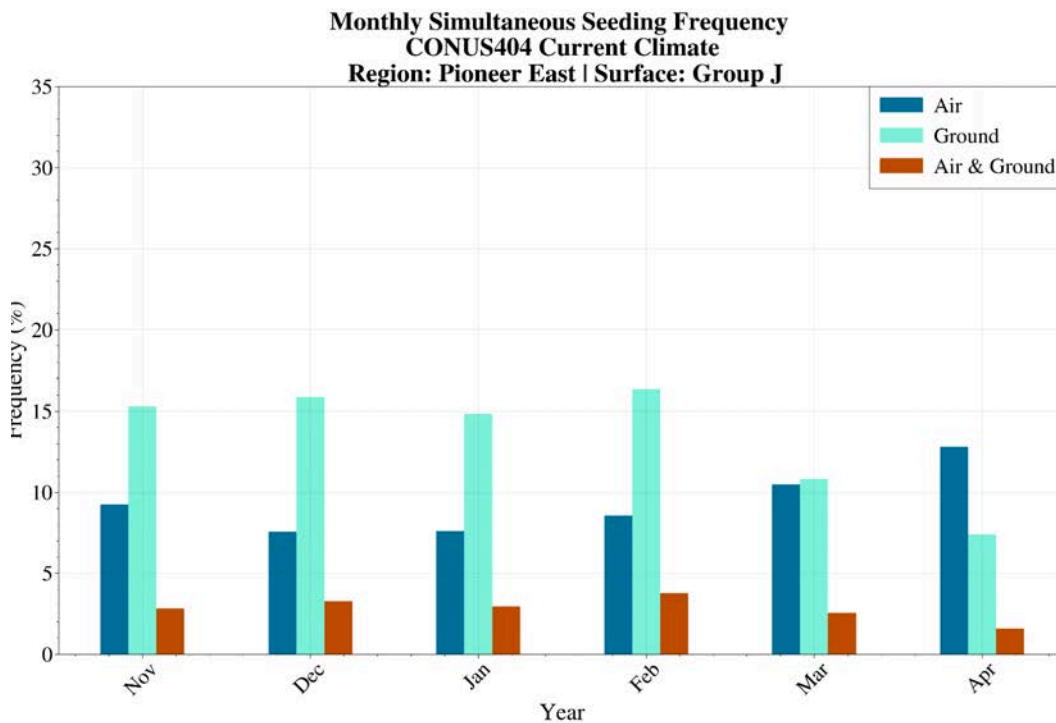
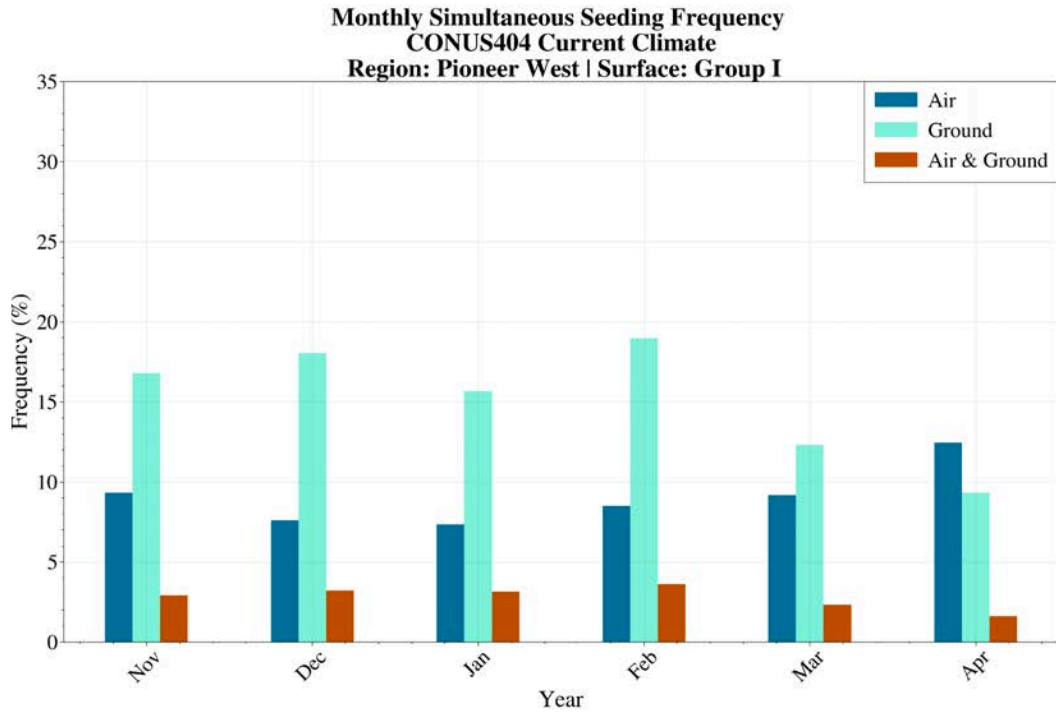
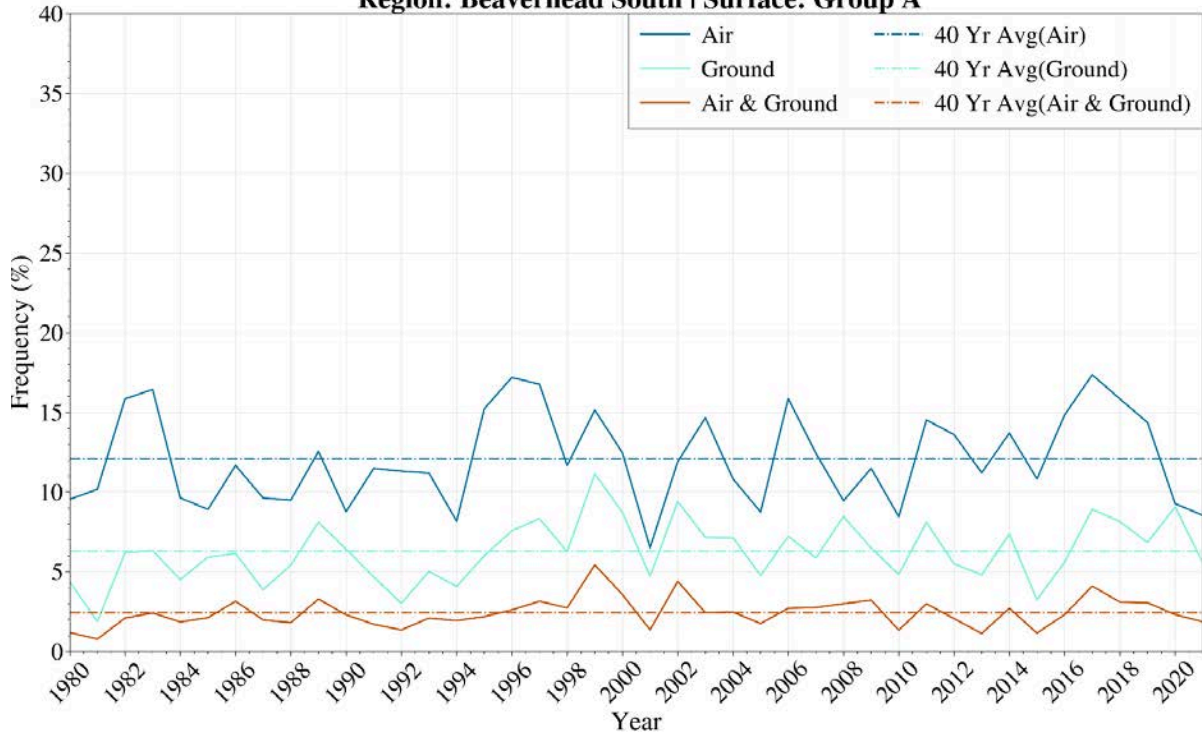


**Figure 4.41.** Monthly frequency of both ground-based and airborne seeding conditions occurring simultaneously. Blue bars indicate airborne frequency based on LWC and temperature, turquoise bars indicate ground-based frequency with the addition of wind direction and Froude number, and red bars indicate the frequency of seedable conditions occurring simultaneously in both layers. Beaverhead Mountains (plots 1 and 2), Anaconda Range (plots 3 and 4), Pioneer Mountains (plots 5 and 6).

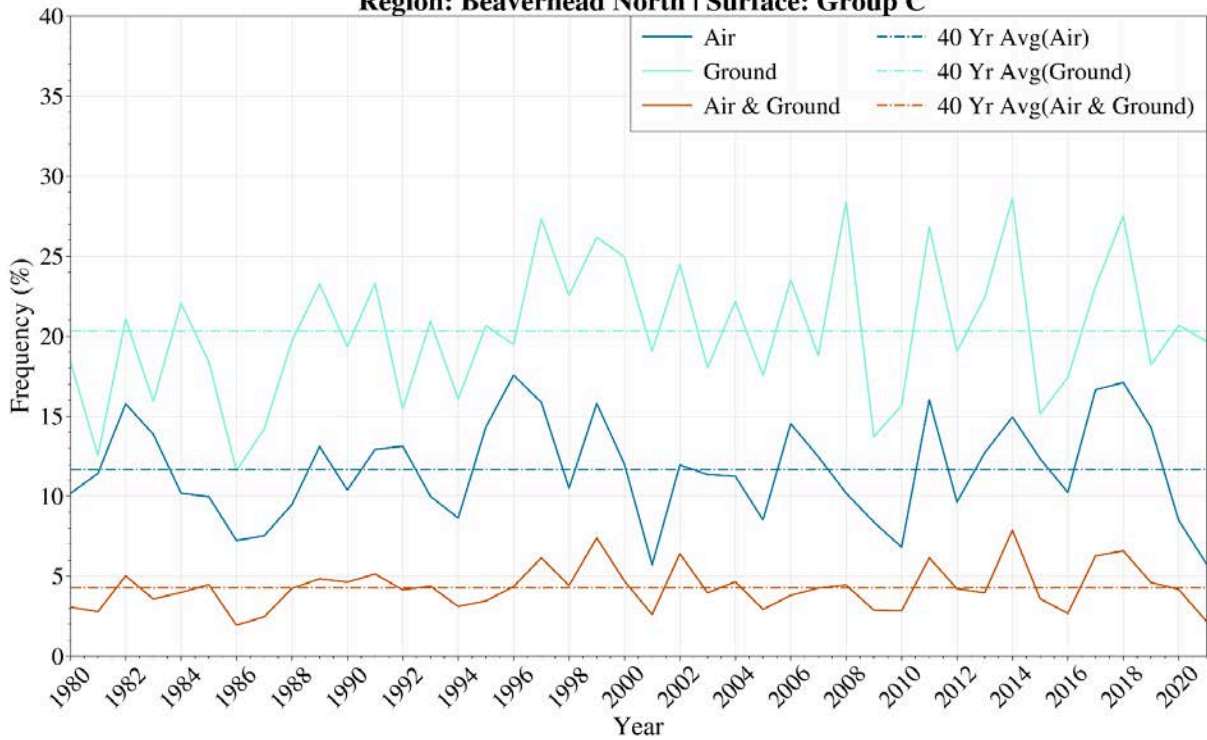
### **Current Climate - Area-based Analysis - Seasonal**

Seasonal frequency of seeding potential for air- and ground-based seeding, as well as the frequency of conditions occurring simultaneously in both levels, is shown in [Figure 4.42](#). As seen with the monthly analysis in [Figure 4.41](#), simultaneous opportunities in the ground-based and airborne layers are infrequent, suggesting that a combined program would consistently be advantageous. There is no noticeable positive or negative trend in frequency over time, but variability across seasons is large. Overall, ground-based seeding has greater frequency of opportunity than airborne, except for the Beaverhead South.

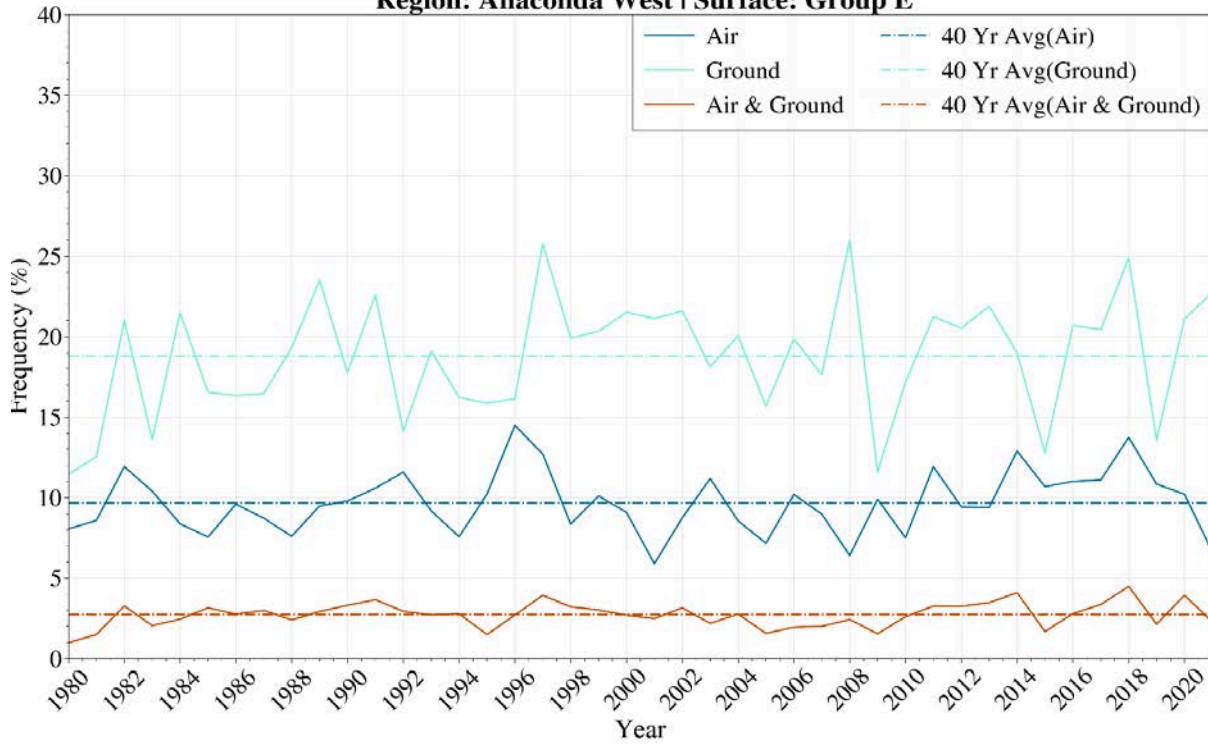
**Yearly Simultaneous Seeding Frequency  
CONUS404 Current Climate  
Region: Beaverhead South | Surface: Group A**



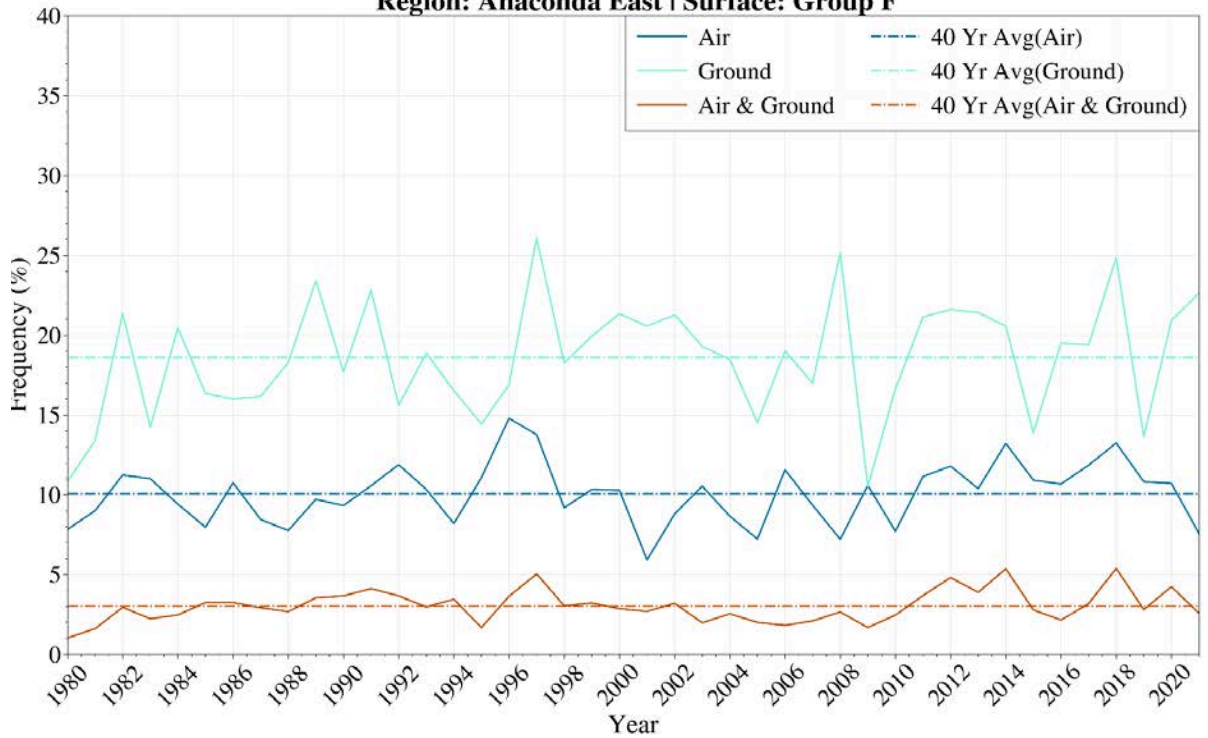
**Yearly Simultaneous Seeding Frequency  
CONUS404 Current Climate  
Region: Beaverhead North | Surface: Group C**



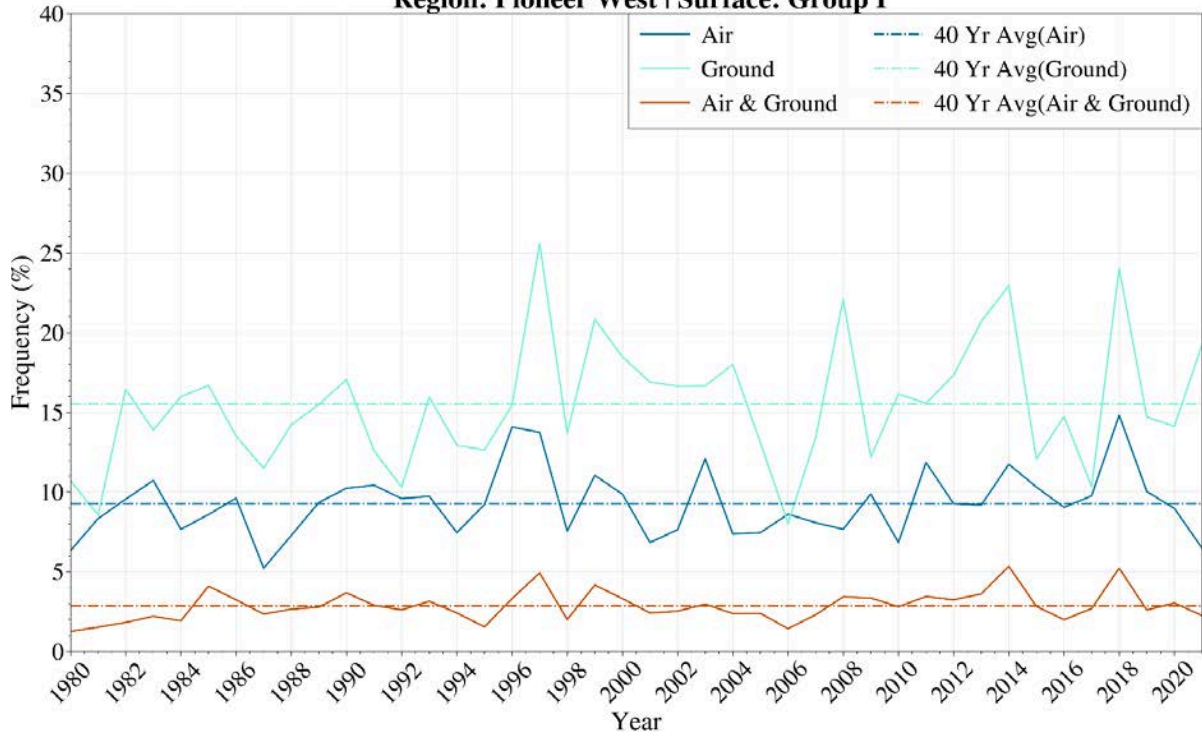
**Yearly Simultaneous Seeding Frequency  
CONUS404 Current Climate  
Region: Anaconda West | Surface: Group E**



**Yearly Simultaneous Seeding Frequency  
CONUS404 Current Climate  
Region: Anaconda East | Surface: Group F**



**Yearly Simultaneous Seeding Frequency  
CONUS404 Current Climate  
Region: Pioneer West | Surface: Group I**



**Yearly Simultaneous Seeding Frequency  
CONUS404 Current Climate  
Region: Pioneer East | Surface: Group J**

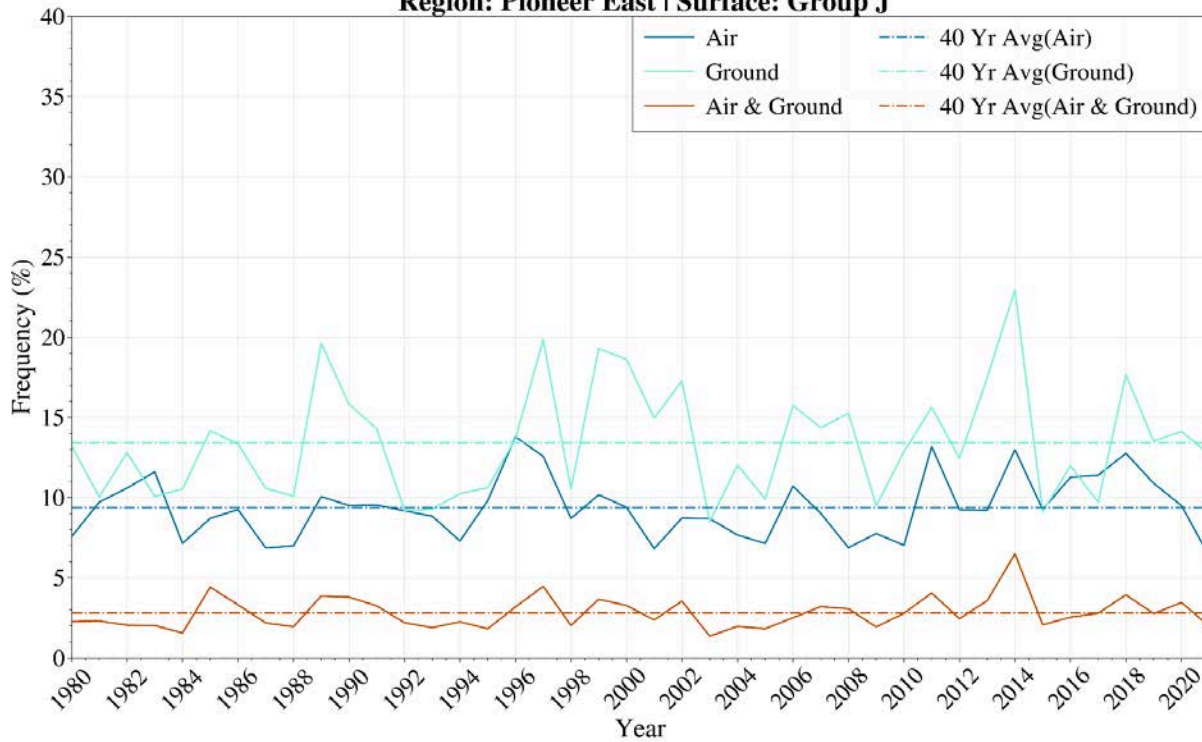
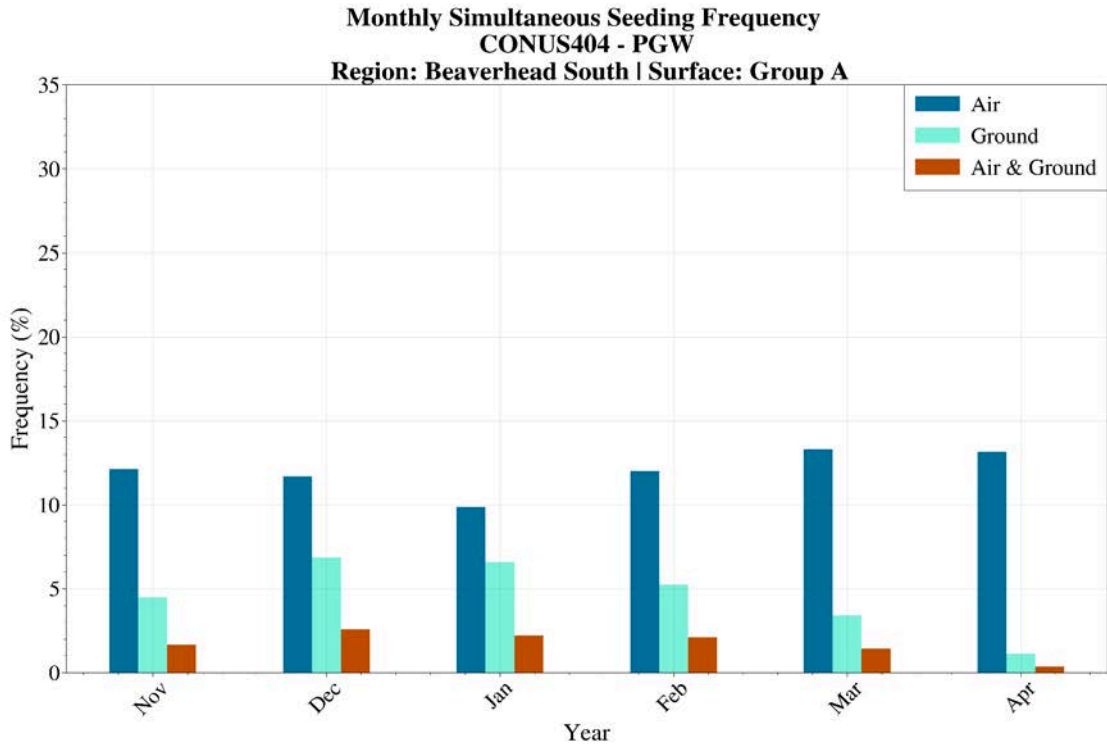


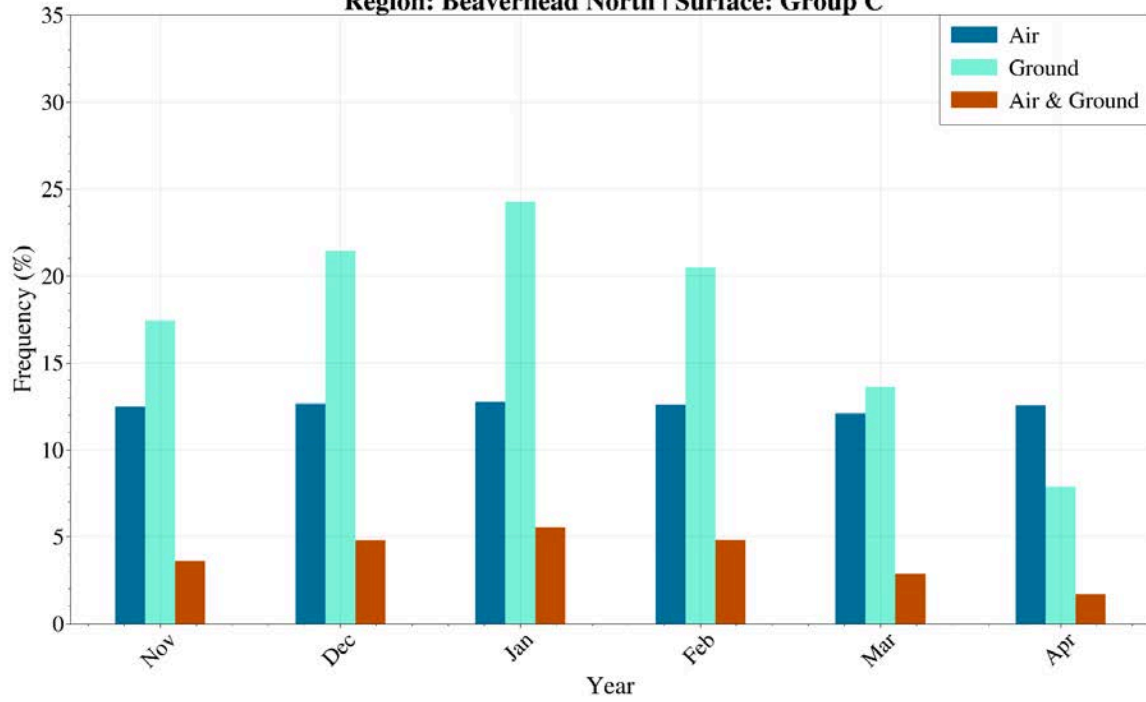
**Figure 4.42.** Seasonal frequency of both ground-based and airborne seeding conditions occurring simultaneously. Blue lines indicate airborne frequency based on LWC and temperature, turquoise lines indicate ground-based frequency with the addition of wind direction and Froude number, red lines indicate the frequency of seedable conditions for both ground and airborne combined. Horizontal dashed lines indicate a 40 year climatological average. Beaverhead Mountains (rows 1 and 2), Anaconda Range (rows 3 and 4), Pioneer Mountains (rows 5 and 6).

**Future Climate - Area-based Analysis - Monthly**

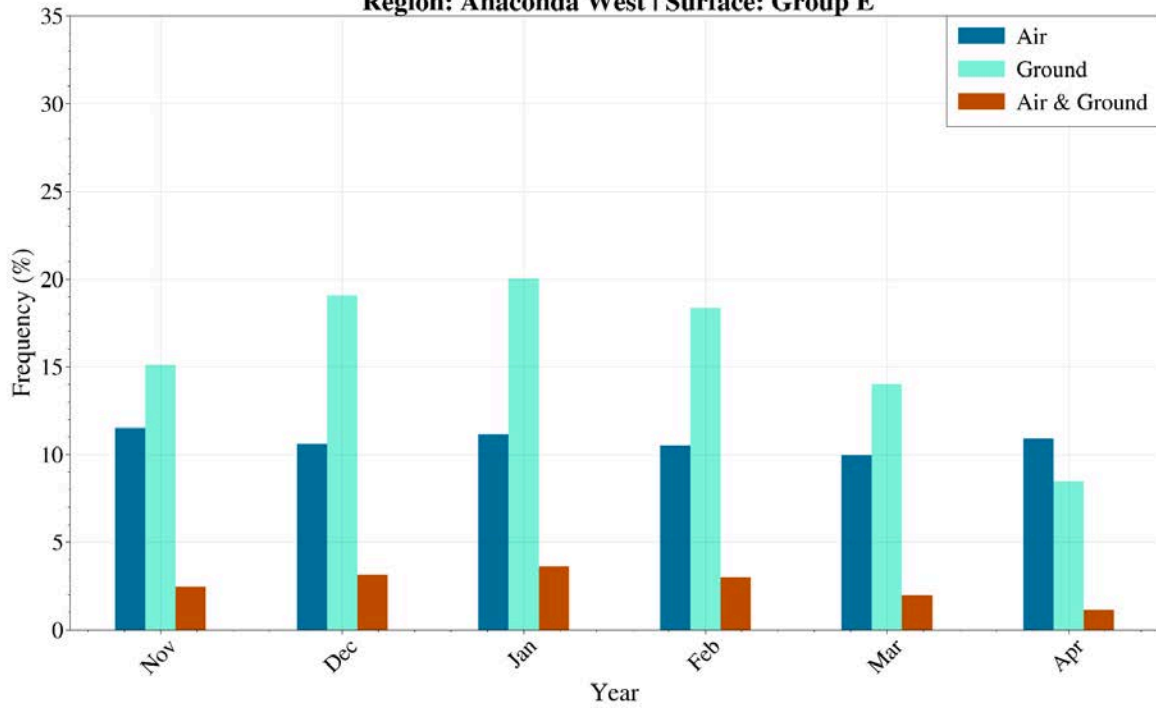
In the future climate scenario, combined area-average monthly frequencies for ground and airborne seeding shown in [Figure 4.43](#) reflect similar patterns as seen for current climate in [Figure 4.41](#). As with current climate, across all regions the coincident occurrences of ground and airborne seeding opportunities is minimal and the biggest reductions in opportunities in the future climate are to ground seeding events. With the minimal or reduced overlap in ground and airborne opportunities, the PGW results show that in the future climate, as with current, ground and airborne operations combined would provide the overall greatest frequency of seeding for the region.



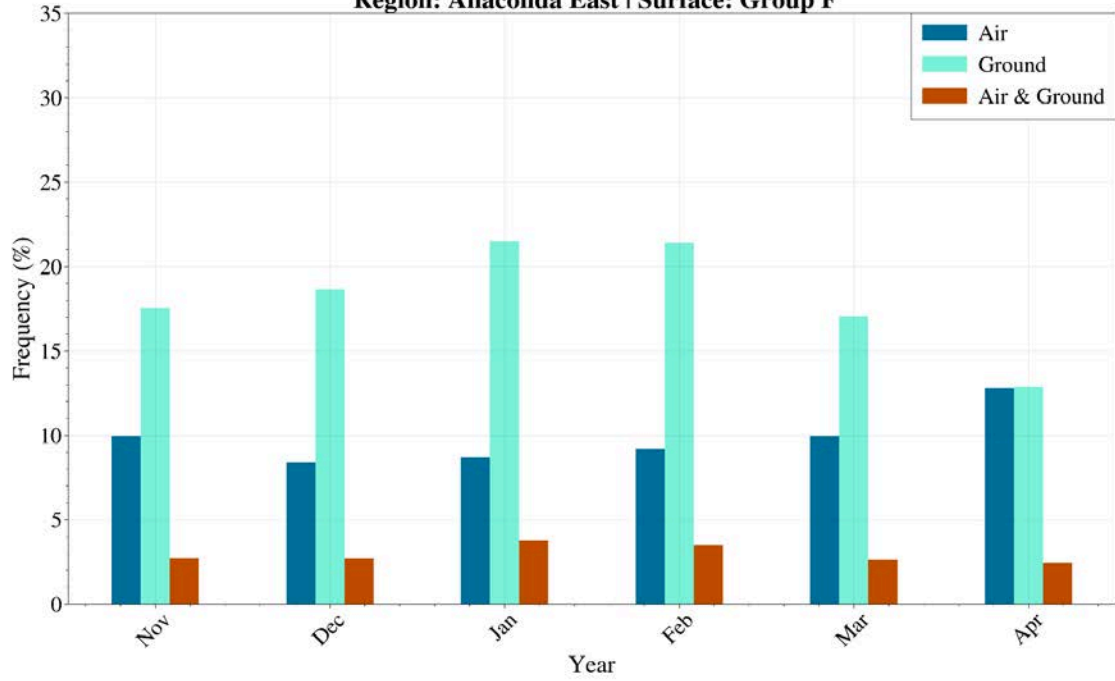
**Monthly Simultaneous Seeding Frequency**  
**CONUS404 - PGW**  
**Region: Beaverhead North | Surface: Group C**



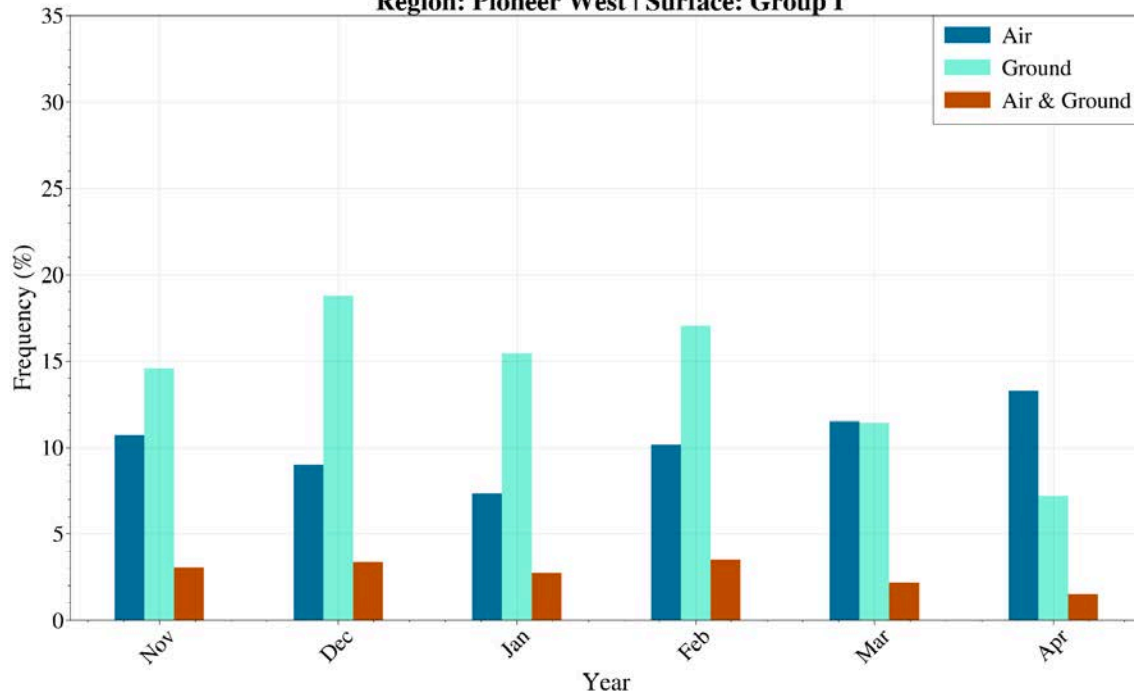
**Monthly Simultaneous Seeding Frequency**  
**CONUS404 - PGW**  
**Region: Anaconda West | Surface: Group E**



**Monthly Simultaneous Seeding Frequency**  
**CONUS404 Current Climate**  
**Region: Anaconda East | Surface: Group F**



**Monthly Simultaneous Seeding Frequency**  
**CONUS404 - PGW**  
**Region: Pioneer West | Surface: Group I**



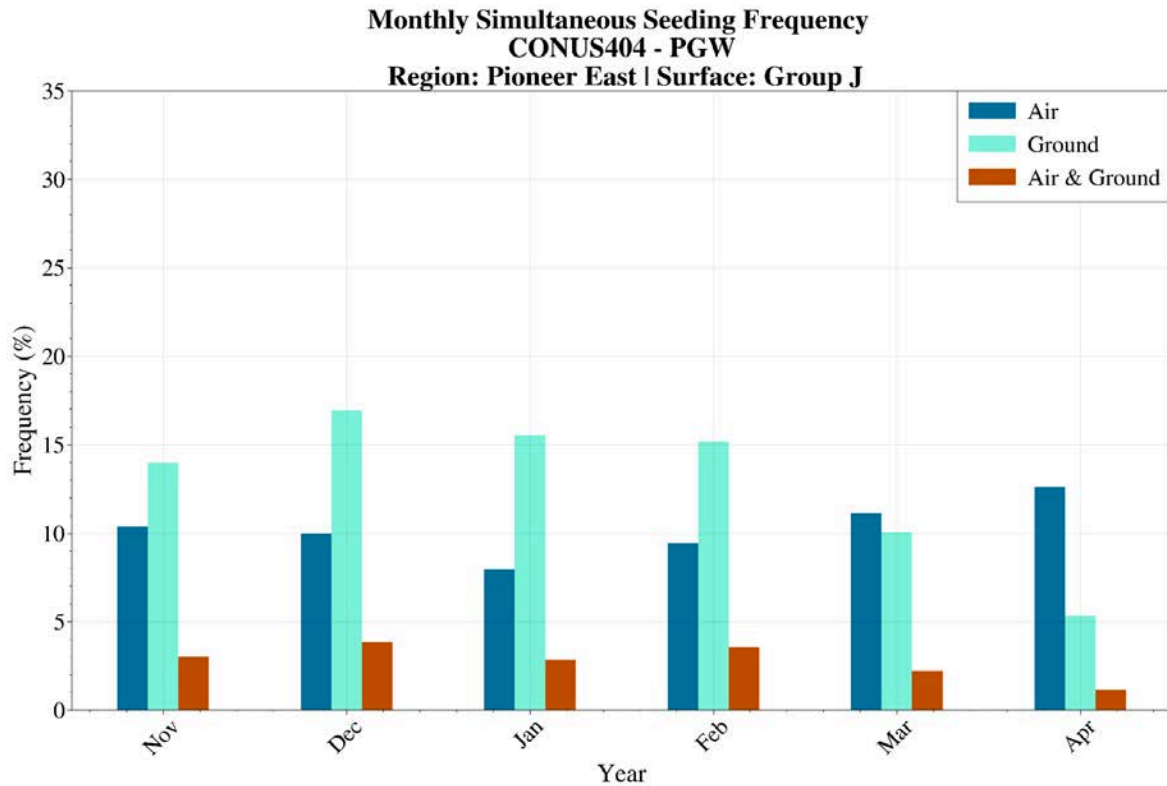
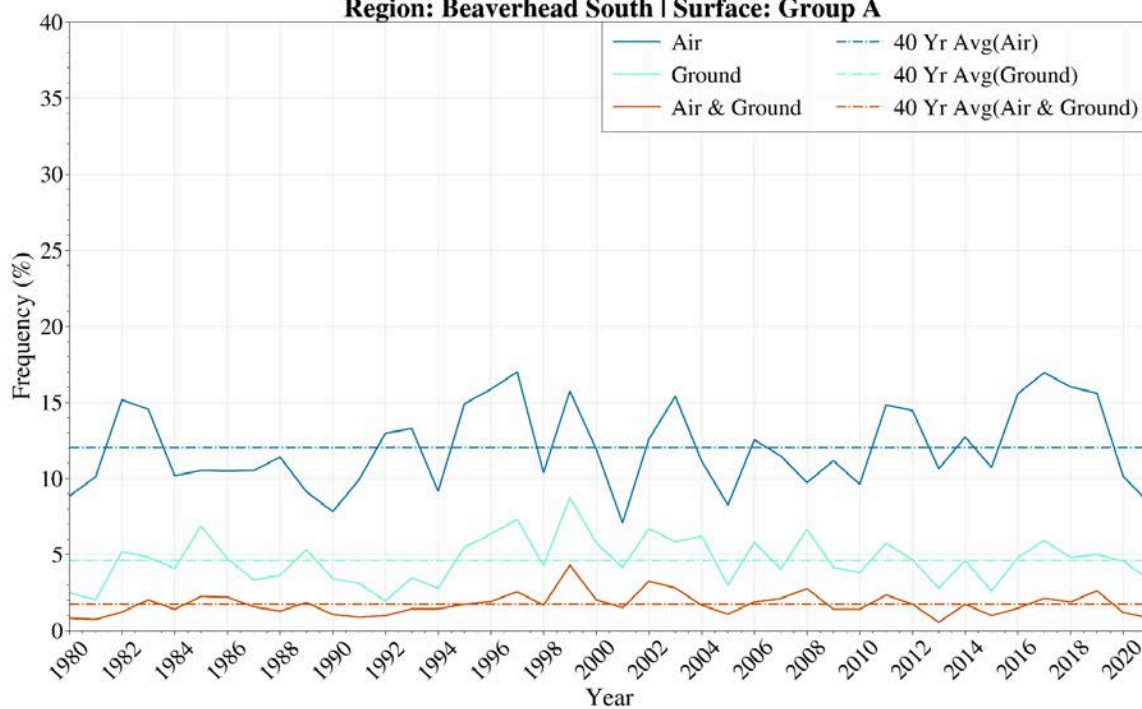


**Figure 4.43.** Monthly frequency of ground-based seeding for airborne and ground-based seeding occurring simultaneously for PGW future climate. Blue bars indicate airborne frequency based on LWC and temperature, turquoise bars indicate ground-based frequency with the addition of wind direction and Froude number, and red bars indicate the frequency of seedable conditions for both ground and airborne combined. Beaverhead Mountains (plots 1 and 2), Anaconda Range (plots 3 and 4), Pioneer Mountains (plots 5 and 6).

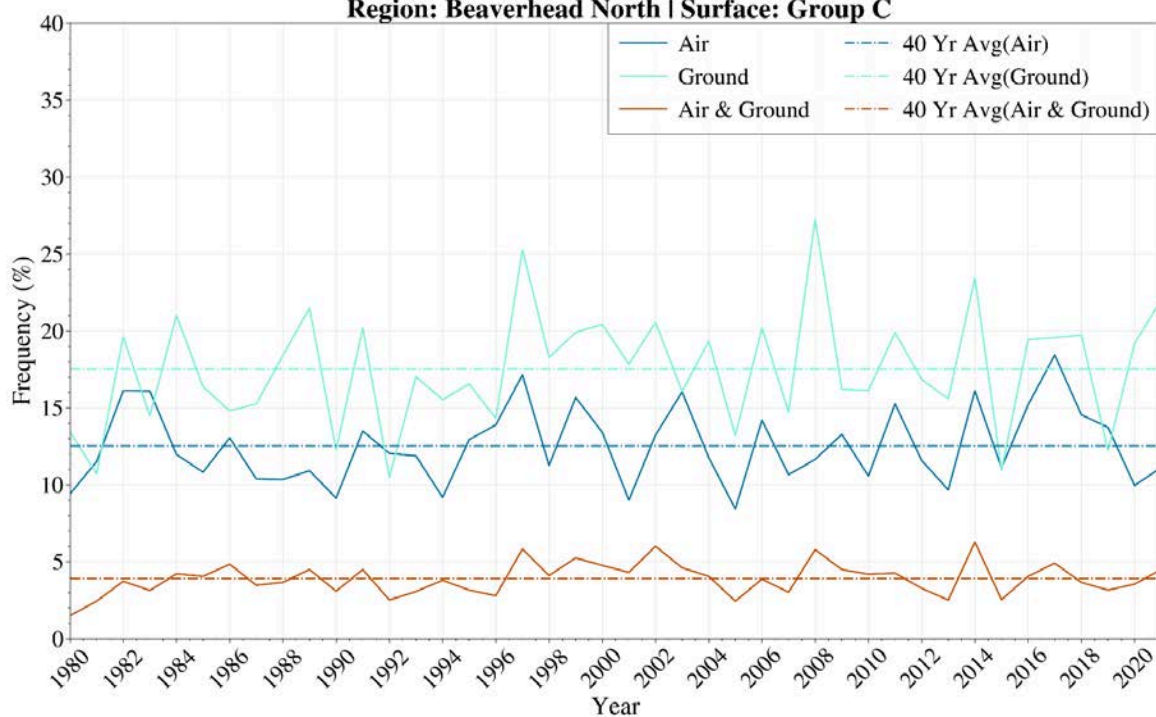
#### Future Climate - Area-based Analysis - Seasonal

As with future climate monthly combined frequency shown in [Figure 4.43](#), the seasonal frequency of seeding potential for air- and ground-based seeding for PGW ([Figure 4.44](#)) shows minimal occurrence of combined opportunities for air and ground-based seeding. Over the 40-year period, variability over the seasons remains large, as seen with current climate. Given the largest reductions in the future climate are to ground seeding opportunities, the overall frequency of opportunity for ground versus airborne seeding is more similar across the regions in a future climate, which is especially noted in the Pioneer East. However, ground seeding frequencies are still greater than airborne in the future climate, except for the Beaverhead South where ground seeding opportunities were less frequent than airborne even in the current climate.

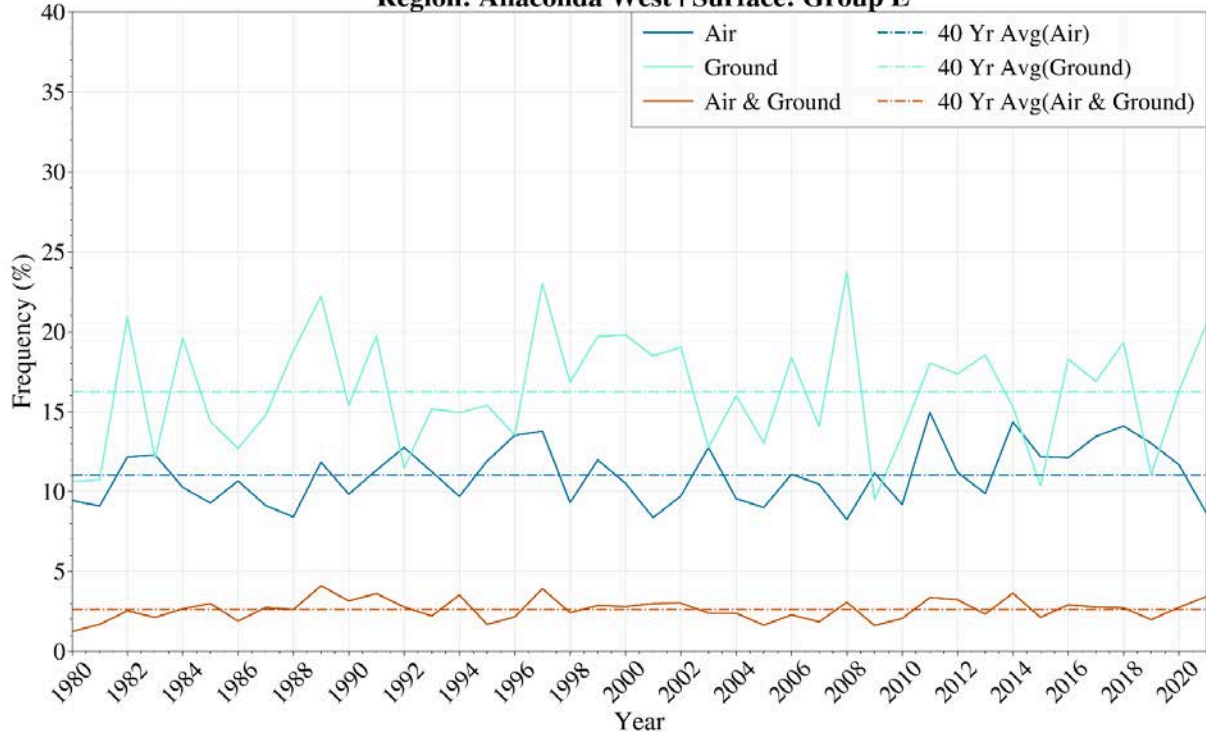
**Yearly Simultaneous Seeding Frequency  
CONUS404 - PGW  
Region: Beaverhead South | Surface: Group A**



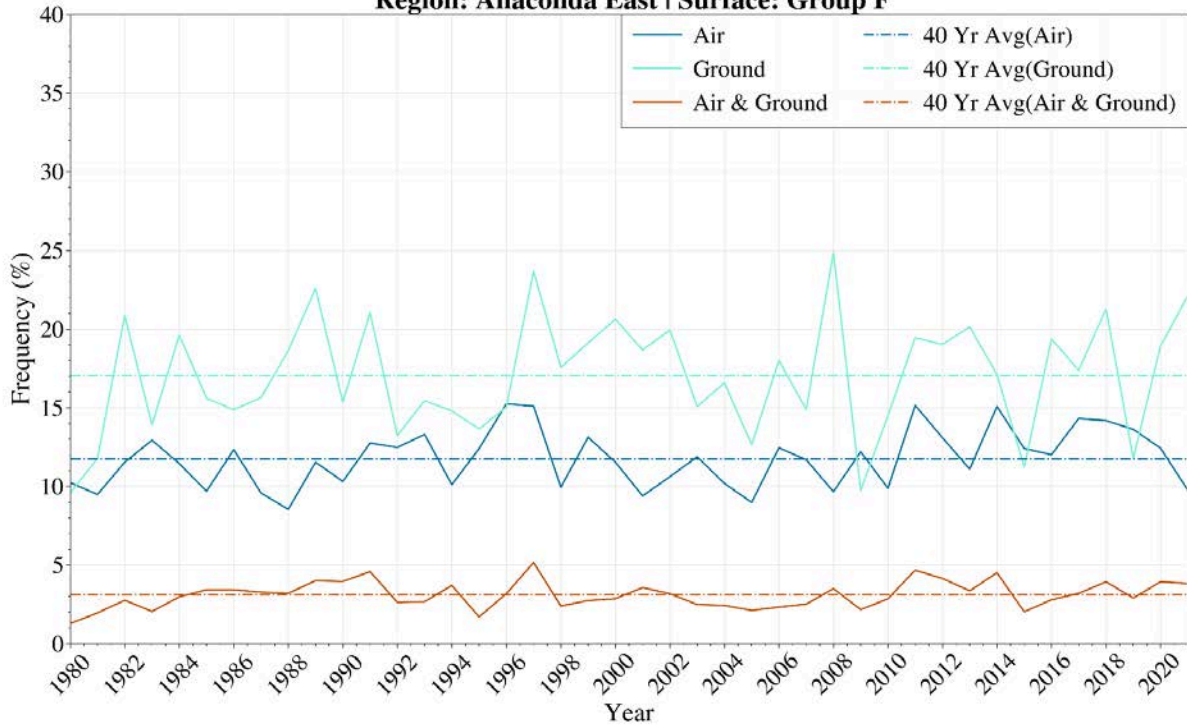
**Yearly Simultaneous Seeding Frequency  
CONUS404 - PGW  
Region: Beaverhead North | Surface: Group C**



**Yearly Simultaneous Seeding Frequency  
CONUS404 - PGW  
Region: Anaconda West | Surface: Group E**



**Yearly Simultaneous Seeding Frequency  
CONUS404 - PGW  
Region: Anaconda East | Surface: Group F**



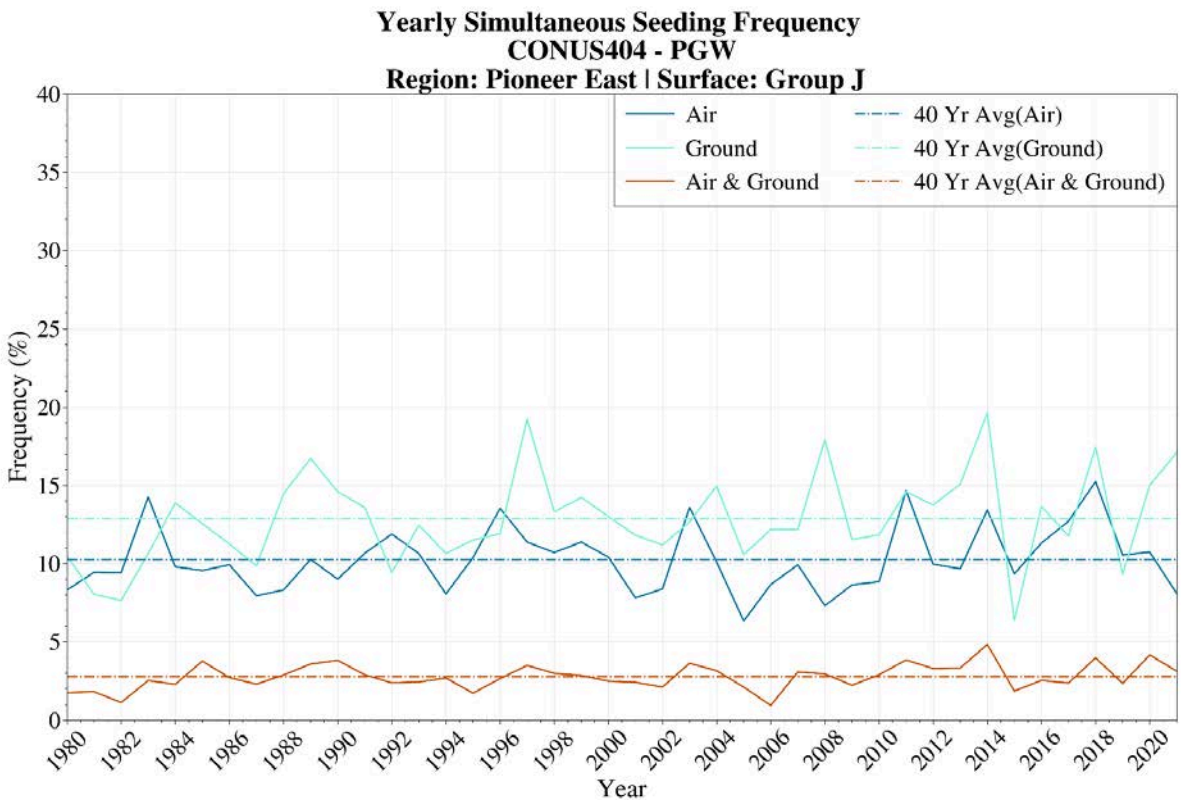
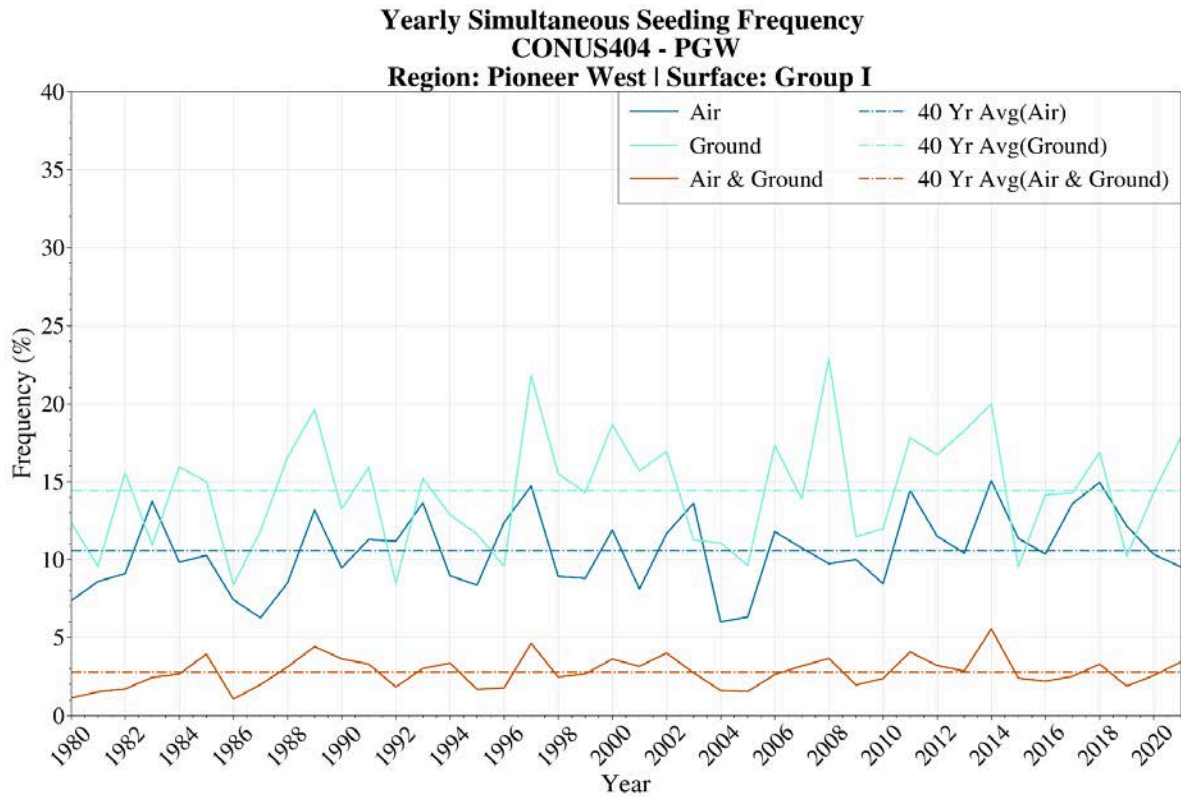


**Figure 4.44.** Seasonal frequency of opportunities for airborne and ground-based seeding occurring simultaneously for PGW. Blue bars indicate airborne frequency based on LWC and temperature,

turquoise bars indicate ground-based frequency with the addition of wind direction and Froude number; red bars indicate the frequency of seedable conditions for both ground and airborne combined. Dashed horizontal lines indicate a 40 year climatological average. Beaverhead Mountains (rows 1 and 2), Anaconda Range (rows 4), Pioneer Mountains (rows 5 and 6).

## 4.6. Fraction of Seedable Precipitation

The previous sections described the frequency (fraction of *time*) that seedable conditions occurred, whereas here we present the fraction of seedable precipitation, which quantifies the portion of the total precipitation that falls under seedable conditions for the ground and airborne layers (Table 4.4). Regions in Figure 4.1 were paired with nearby SNOTELs and generator sites upwind or on the windward slope of the mountain range associated with the region. Over the entire domain, the Beaverhead Mountains experience the greatest fraction of precipitation that falls under seedable conditions, with 37% for Beaverhead North for ground and 41-42% for Beaverhead North and South for airborne. The Anaconda East Mountains had the next largest fraction of ground-based seedable precipitation after Beaverhead North with a value of 31%, followed closely by Anaconda West at 30%. For airborne, after the Beaverhead Mountains, Pioneer West had the next largest fraction of seedable precipitation at ~36%. The Pioneer East and both Anaconda Range regions had the lowest fraction of seedable precipitation for airborne seeding, between 31-33%. However, these are still greater than the lowest fractions of seedable precipitation for ground seeding which were <30% in the Pioneer Mountains.

**Table 4.4.** Fraction of Seedable Precipitation.

Region + Precip site + generator (ground only)	40 year Average Nov-April Total Precipitation (mm)	Average Seasonal Precipitation Ground Seedable (Temp, LWC, Wind, Fr) (mm, %total)	Average Seasonal Precip Air Seedable (Temp, LWC) (mm, % total)
Beaverhead South + Dark Horse + Gen A	543.446mm	156.422mm, 28.78%	228.613mm, 42.07%
Beaverhead North + Saddle Mtn + Gen C	536.242mm	200.158mm, 37.33%	221.95mm, 41.39%
Anaconda West + Saddle Mtn + Gen E	1072.48mm	161.097mm, 30.04%	171.131mm, 31.91%
Anaconda East + Barker Lakes + Gen F	555.057mm	173.073mm, 31.18%	173.934mm, 31.33%
Pioneer West + Calvert Creek + Gen I	714.33mm	103.69mm, 29.02%	130.773mm, 36.61%
Pioneer East + Mule Creek + Gen J	478.907mm	124.929mm, 26.08%	161.958mm, 33.82%

## 4.7. Summary of Climatology Analysis

Climatology analysis across the Big Hole Basin shows that ground-based seeding has a greater frequency of seeding opportunities than airborne. Across the domain, the predominant wind direction ranges from southwesterly to northwesterly. In the 0-1 km AGL ground seeding layer, the greatest amounts of SLW

were found in the Beaverhead Mountains under west to southwesterly flow. Monthly spatial analysis shows that the greatest frequency of ground-based seeding potential is over the high terrain in the Beaverhead, Anaconda and Pioneer mountain ranges from November through February. Overall, the Beaverhead Mountains have the greatest amount of SLW and the greatest frequency of ground-based seedable conditions across the entire domain. The peak in seeding frequency in December through January is due to the entire domain remaining within the seeding temperature range. In the shoulder months, temperatures are only within the seeding range over the highest terrain along mountain ridges.

When considering wind direction and Froude number for ground-based seeding, most regions have reduced frequency of seeding opportunities. However, the Beaverhead North region retains the greatest monthly frequency of seeding opportunities exceeding 20% across most months. This is because the Beaverhead North region is the least blocked region as defined by the Froude number and experiences the most favorable flow conditions, especially for targeting the Big Hole. The Beaverhead South and Anaconda East were the two regions that had reductions when wind direction and Froude were considered, mostly driven by the wind direction constraints for winds that would target the Big Hole Basin. When annual frequencies were analyzed, substantial inter-annual variability was seen with no discernable trend over the 40-year CONUS404 period. The Beaverhead North (22%) and Anaconda West and East (20%) all had the greatest 40-year average frequency of ground-based seeding opportunities when all criteria were considered.

Future climate analysis revealed that ground-based seeding opportunities decrease due to warming temperatures even though SLW increases over high terrain across the Beaverhead, Anaconda and Pioneer mountain ranges. Comparison of monthly frequencies between current and future climate agree with this finding in the spatial analysis and shows there is a slight decrease in frequency across all regions with the exception of the Pioneer Mountains in December and January, which experiences a slight increase in frequency of seedable conditions in the future climate scenario analyzed. Overall, though, in the PGW future climate scenario, ground-based seeding may not be as effective as it is in the current climate.

For the ground layer, it is recommended that the November through February months are targeted focusing on the Beaverhead, with the Anaconda West and Pioneer West regions as secondary targets, as these areas have the most favorable flow and greatest amount of SLW.

Overall, airborne frequency of seedable SLW is substantially less than ground-based seedable SLW with a 40-year average wintertime frequency of 13%; however, when wind flow criteria are considered for ground-based seeding, the Beaverhead South had less ground seeding frequency than airborne. Over the 40-year period, there is considerable interannual variability across all regions for both airborne and ground seeding, with no upward or downward trend. The greatest frequencies for airborne seeding are over the Beaverhead Mountains as this is the region with the greatest amount of SLW. Across the domain, airborne temperatures remain within the seeding range for all months of the seeding season. Area-based analysis by month shows that airborne frequencies do not vary much between November through April and are relatively consistent throughout the season.

Airborne future climate analysis indicates that frequency of seedable conditions increases slightly across the domain due to an increase in airborne SLW. Although airborne temperatures warm slightly in the

PGW simulation, temperatures remain within the seeding range across the entire domain. For the airborne layer, seeding opportunities are greatest over the Beaverhead Mountains and are expected to increase in a warmer, future climate.

In general, the Beaverhead Mountains have the greatest portion of total precipitation that falls under seedable conditions for both ground and airborne seeding. Overall, the airborne seeding conditions occur for a greater portion of total precipitation than for ground seeding across all sites in the domain with the exception of Beaverhead North, which has a comparable fraction for ground and airborne. For a potential pilot program targeting the Big Hole Basin, it is recommended that the Beaverhead Mountains and western slopes of the Anaconda and Pioneer Mountains are targeted for both ground and airborne seeding given the fraction of precipitation that could be seeded from the ground and airborne seeding climatologies. For airborne seeding on its own, all of the mountain ranges can be included, given the versatility of airborne seeding to target various areas and the fraction of seedable precipitation for all of the regions are relatively similar.

## 5. Design for Big Hole Basin Seeding Program

A set of potential program design options were developed based upon the climatology and feasibility analysis. These included multiple groups of hypothetical ground-based generator locations, as well as potential airborne seeding flight tracks. These were tested using the WRF-WxMod model to simulate the impacts of seeding in a selection of case studies to assess the potential for seeding with each option under a variety of environmental conditions. In addition, a preliminary cost-benefit analysis was conducted, using a variety of assumed and calculated conditions, to provide a high-level estimate of the cost per acre foot of precipitation that may be produced by cloud seeding in the region. This section outlines the methods used to test the design options, as well as the designs tested and results for ground-based generator tests, airborne seeding tests, and the cost-benefit analysis.

### 5.1. WRF-WxMod Background

The WRF-WxMod model is a novel capability based on the WRF model (Skamarock et al. 2008) that was developed for evaluating the impacts of cloud seeding on precipitation, designing new or optimizing cloud-seeding initiatives, and/or forecasting cloud-seeding opportunities in a real-time forecast mode. Multiple studies (e.g., Xue et al., 2013 a,b, 2014, 2016, 2017, and 2022) have demonstrated WRF-WxMod is capable of capturing the process of glaciogenic seeding and impacts on wintertime precipitation under both idealized and realistic conditions. By running two simulations with WRF-WxMod – one that is a “control,” where there is no seeding, and another where seeding is simulated – the estimated seeding effect can be calculated both numerically over an area as well as spatial representation, in a controlled way. This set-up can be useful for feasibility and design studies in order to test the sensitivity of potential generator locations and/or airborne seeding tracks.

An important caveat when interpreting the results from this modeling study is that the evaluation took place over 4 case studies, and while it provides a snapshot of individual cases, the seeding effect cannot

be extrapolated over an entire season, given storm type, environmental conditions, etc. can vary on a storm-to-storm basis as well as a season-to-season basis. In addition, WRF-WxMod was run deterministically, providing one possible realization of the seeding effect. Recent studies (e.g., Harrold et al., 2025) have expanded into using an ensemble modeling approach that would allow for quantifying uncertainty and provide a range of possible outcomes, which is critical when understanding and assessing the overall benefits of cloud seeding.

## 5.2. WRF-WxMod Configuration

WRF-WxMod was used to simulate aerial and/or ground-based seeding for 4 total cases. A coarse domain was established over the Western United States ([Figure 5.1](#)) and was used to drive the higher-resolution nested simulations over the Big Hole Basin<sup>8</sup> ([Figure 5.2](#)).

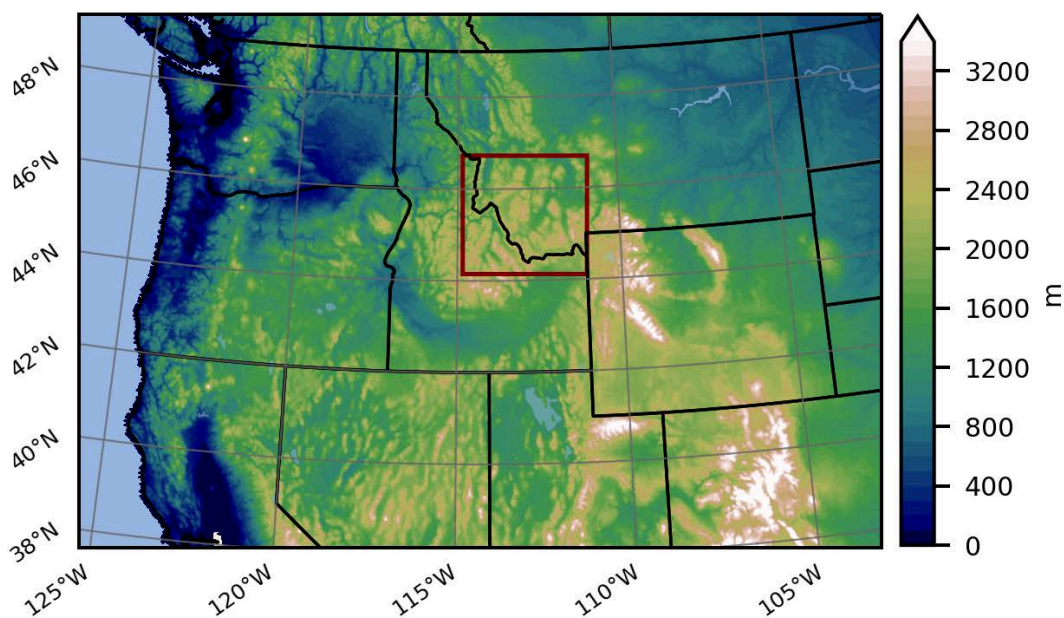


**Figure 5.1.** WRF 2.7-km and 900-m (inner maroon box) computation domains with topography (m). A closer visual of the domain focused over the Big Hole Basin can be seen in [Figure 5.2](#).

---

<sup>8</sup> Due to the coarse grid spacing of the ERA5 forcing dataset to drive the higher-resolution simulations, the 2.7-km domain was necessary as an intermediate step to avoid potential issues with creating undesirable behavior at and near the domain boundaries

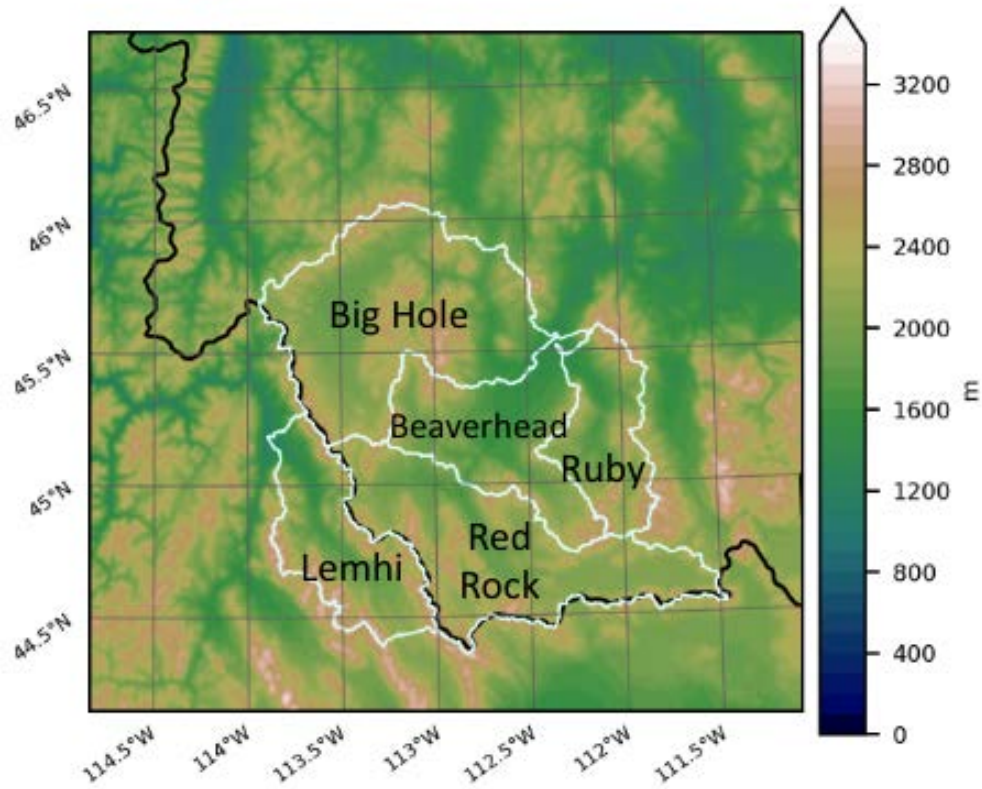


**Figure 5.2.** WRF 900-m computation domain with topography (m). White outlines indicate key river basins, and the black line indicates the Idaho / Montana border.

The high-level model configuration settings that were used in both the 2.7-km and 900-m simulations are listed in [Table 5.1](#).

**Table 5.1.** Model settings used in the WRF-WxMod simulations.

	2.7-km domain	900-m domain
<b>Large-scale forcing data</b>	ERA5	ERA5
<b>Horizontal grid</b>	721 x 481	334 x 319
<b>Vertical coordinate</b>	81 terrain-following ETA levels	81 terrain-following ETA levels
<b>Time step</b>	10 s	5 s
<b>Land Surface Model</b>	Noah-MP	Noah-MP
<b>Radiation schemes</b>	RRTMG longwave and shortwave	RRTMG longwave and shortwave
<b>PBL schemes</b>	MYNN	MYNN
<b>Microphysics schemes</b>	Thompson-Eidhammer	Thompson-Eidhammer with

		cloud-seeding parameterization
<b>Simulation details</b>	Initialized ~12 hours prior to the start of seeding	Initialized ~2-3 hours prior to seeding; simulations ended 3 hours past the seeding end time

### 5.3. Case Study Selection

To select case studies for the WRF-WxMod simulations, SLW events in the CONUS404 dataset from November 2017 - April 2021 were analyzed. Events were defined as time periods with SLW present for 6 or more consecutive hours. Once the full set of events were identified the potential cases were sorted based on wind direction with particular emphasis given to those with wind directions ranging from southwest to northwest, which were the predominant wind directions across the study region as seen in [Figure 4.12](#); cases were stratified by ground-based and airborne potential. For the design study, with exception to Case 2 (2019-12-14; see [Table 5.2](#) below), even if a case was identified as having ground-based *or* airborne potential, it was simulated for both ground-based *and* airborne seeding scenarios with the available HPC resources.

### 5.4. Ground-Based Seeding Design Simulations

For the ground-based seeding experiments, ten potential generator groups were tested. Each generator group ([Figure 5.3](#)) was simulated individually as well as a simulation was run with all generators from groups A-J combined (hereafter ‘all’). This approach allowed for determining the impact of each generator group as well as the full set of generators on the AgI dispersion and ultimately the resulting simulated precipitation. Generator groups A-C in the north Beaverhead Mountains would require operations in the state of Idaho, which may present additional logistical challenges. Since the goal of this study is to provide an optimal design study for the Big Hole Basin, ground-based generators were placed in Idaho. Given current cloud seeding research and initiatives in Idaho, this may offer opportunities on cost sharing with operations in Idaho.

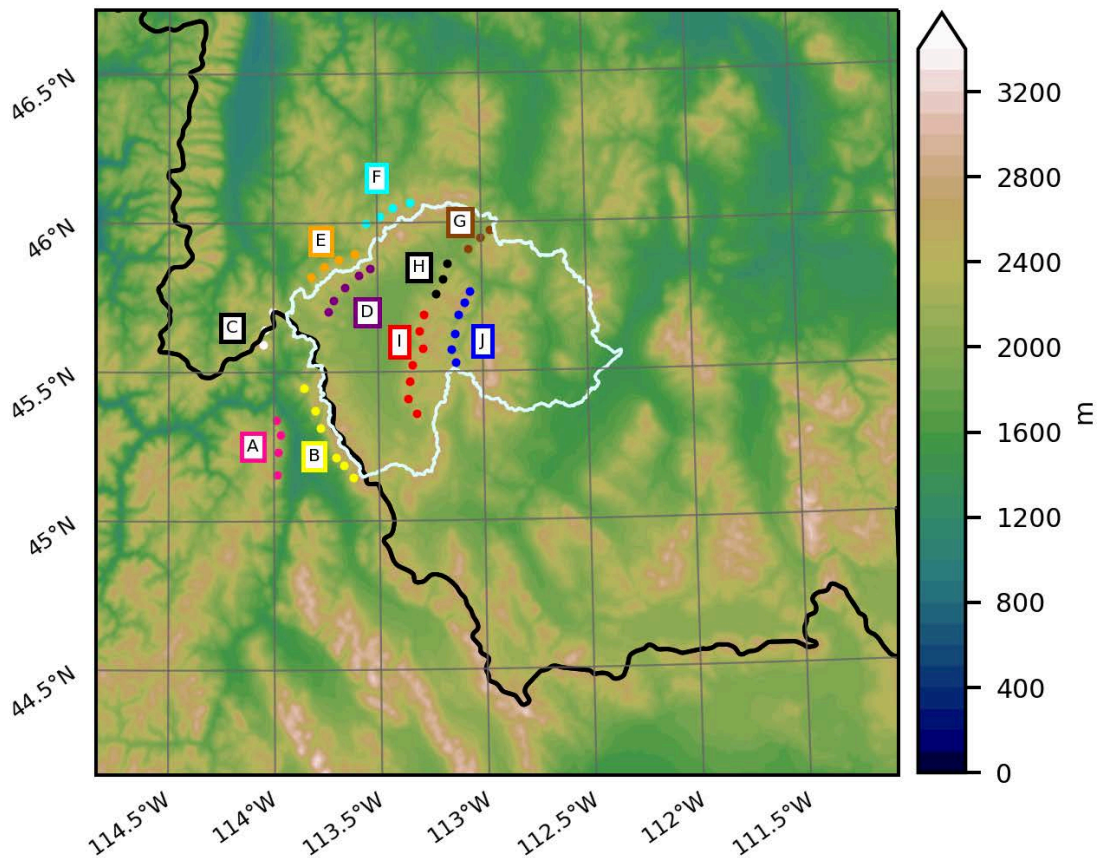


**Figure 5.3.** Location of all ground-based generator groups across the study region used to analyze ground-based case studies.

Five case studies were identified to test the potential generator groups under different weather conditions. [Table 5.2](#) shows a summary of the atmospheric conditions (e.g., wind speed, wind direction, and temperature) for each of the five cases at a height 3500 m above mean sea level, which is a representative level for use in ground-based seeding, as well as the time period that ground seeding was simulated in each case. The following sections contain detailed analyses of the meteorological conditions of each case and results of each generator group tested in each case. For a summary of the results of these case studies, please refer directly to [Section 5.6](#).

**Table 5.2.** Summary of five simulated ground seeding cases. Wind speed (*Wspeed*), wind direction (*WDir*), and temperature (*T*) corresponding to the median value within the seeding period, over the target area centered over the Big Hole Basin, at 3500 m above mean sea level.

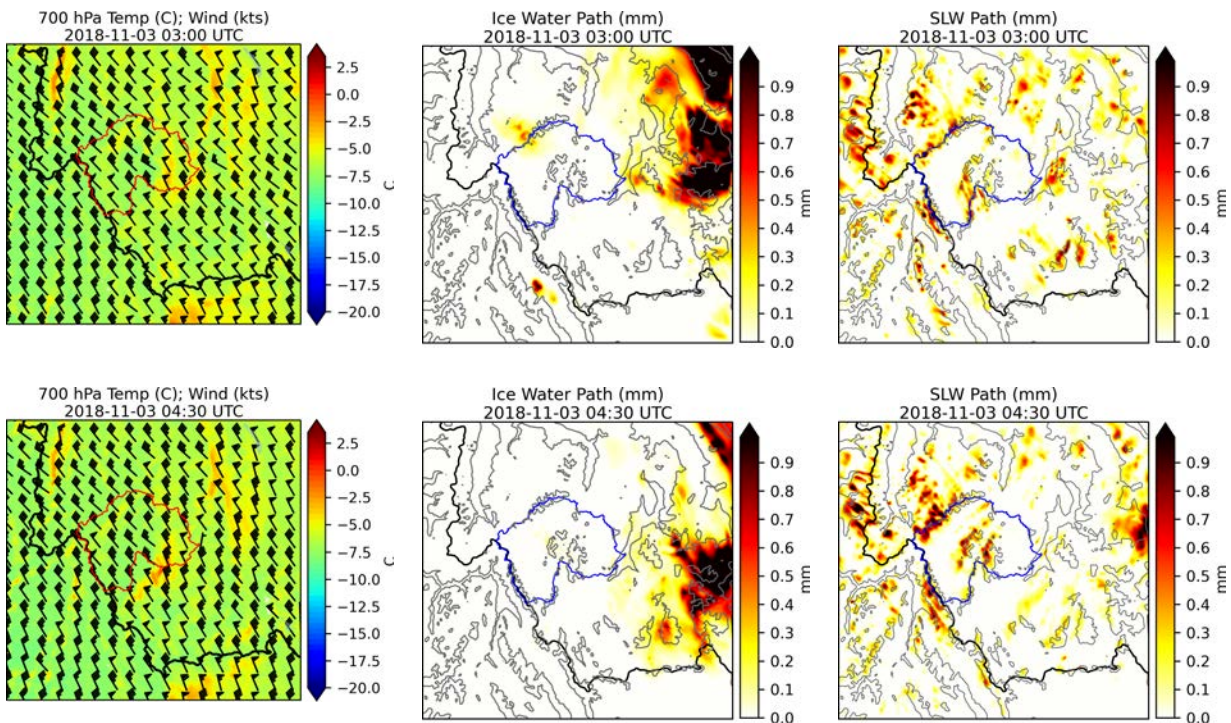
Case ID	Date	Seeding Period	WSpeed [m/s]	WDir[°]	T [°C]
C1	2018-11-02	+1d00 UTC to 09 UTC	21	NW, 317	-10
C2	2019-12-14	11 UTC to 14:30 UTC	3	NW, 310	-18

C3	2020-01-14	12 UTC to 15:30 UTC	19	W, 256	-18
C4	2020-12-19	14 UTC to 19 UTC	28	W, 288	-12
C5	2021-02-28	18 UTC to +1d03 UTC	19	NW, 321	-11

### 5.4.1. Case 1: 2 November 2018

For Case 1, the WRF-WxMod simulation began at 2100 UTC on 2 Nov. 2018. Simulated ground-based seeding commenced at 0000 UTC on 3 Nov. 2018 and lasted 9 h, ending at 0900 UTC. The simulation ended 3 h later at 1200 UTC (in order to allow time for AgI to disperse and activate).

[Figure 5.4](#) provides some of the key environmental conditions at times near the beginning of the simulation (top row), middle (middle row), and the end of the simulation (bottom row). At 0300 UTC on 3 Nov. 2018, wind direction at 700 hPa was NW over the Big Hole Basin, and temperatures at 700 hPa ranged from -2 to -8 °C. Supercooled liquid water path (SLWP) was present over the Beaverhead Mountains, Anaconda Range, and Pioneer Mountains, with some area of local maxima exceeding 0.5 mm. By 0430 UTC on 3 Nov. 2018, the wind direction at 700 hPa is predominantly NW, and temperatures cooled slightly. SLWP increased in coverage and magnitude, and minimal ice water path (IWP) is noted at this time. At 0900 UTC on 3 Nov. 2018, wind direction at 700 hPa is NW/NNW, with temperatures generally from -6 to -9.5 °C. SLWP has decreased from previous times in the simulation, but there is still SLWP over the Beaverhead Mountains and Anaconda Range as well as over portions of the central part of the basin. No significant IWP is seen over the basin.



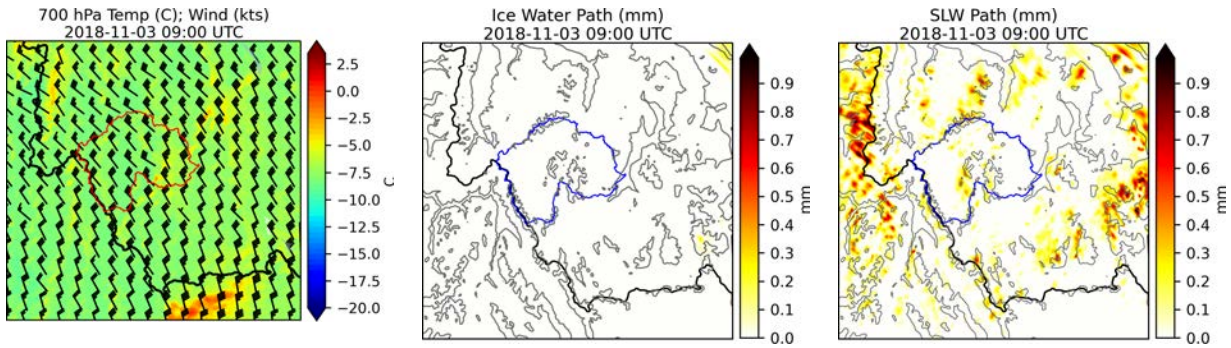


**Figure 5.4.** Temperature ( $^{\circ}\text{C}$ ) and wind barbs (knots) at 700 hPa (left column), IWP (mm; middle column), and SLWP (mm; right column) at 0300 UTC on 3 Nov. 2018 (top row), 0430 UTC on 3 Nov. 2018 (middle row), and 0900 UTC on 3 Nov. 2018 (bottom row) from the control simulation.

The total precipitation from the control simulation for Case 1 is shown in [Figure 5.5](#). Overall, the precipitation generally fell over the highest terrain, with certain areas over Beaverhead Mountains and Anaconda Range seeing  $>10$  mm of precipitation, and the Pioneer Mountains having maximum values  $>5$  mm of precipitation. The precipitation pattern suggests that convective cells within the clouds are contributing to the precipitation, resulting in elongated streaks of precipitation accumulation over the region. In these situations, the WRF-WxMod simulations investigating the difference between seeding and control simulations may experience some numerical noise, due to slight dislocations of the location of these convective scales between the two simulations (Ancell et al., 2018).

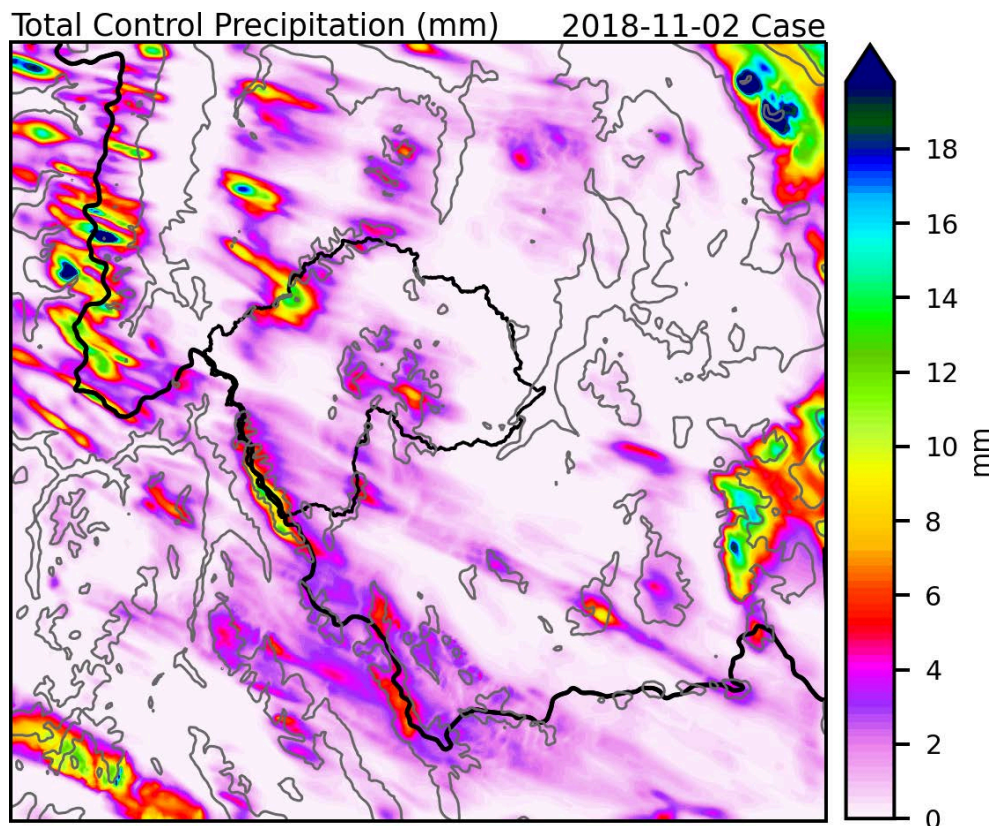
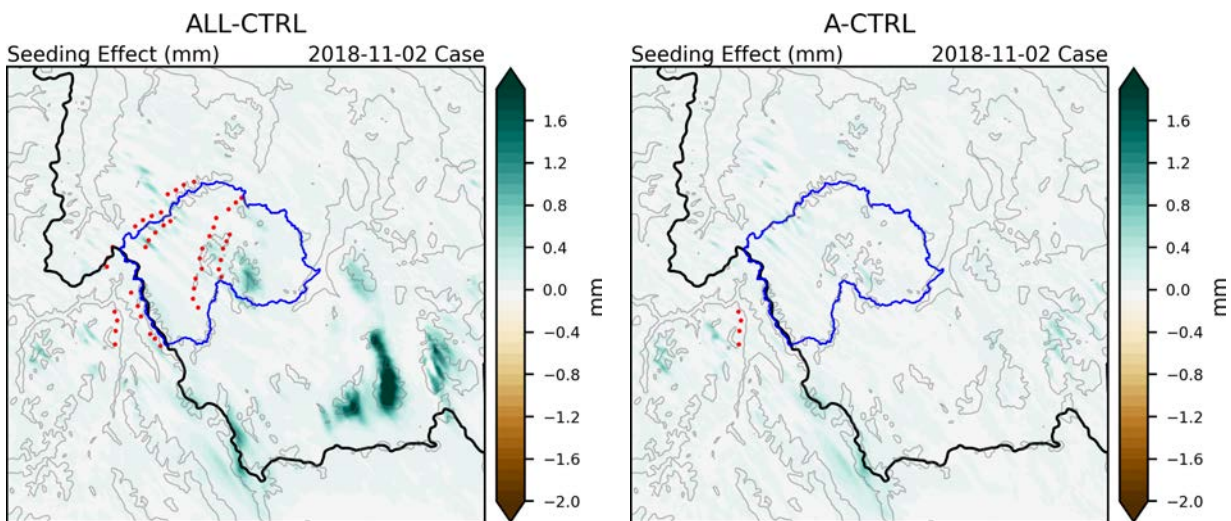


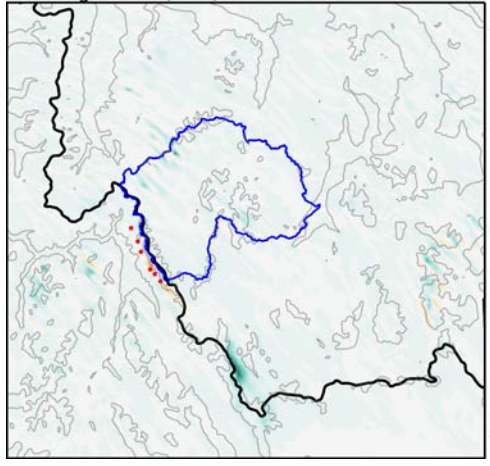
**Figure 5.5.** Total control precipitation (mm) for the 2 Nov. 2018 case (2100 UTC 2 Nov. - 1200 UTC 3 Nov. 2018).

The change in precipitation accumulation from the seeding simulation minus the control simulation, also referred to as the simulated seeding effect, for the 2 Nov. 2018 case for all generators and each individual generator are shown in [Figure 5.6](#). Overall, the simulated seeding effect for all individual generator groups was small over the Big Hole Basin, with the Pioneer Mountains showing the largest signal of simulated precipitation enhancement within the basin (see [Table 5.3](#)). Generator groups C, D, E, and I (33 AF, 25 AF, 32 AF, and 18 AF) had a modest, positive simulated seeding effect in the Big Hole Basin. Despite greater SLW values over the highest peaks in and around the Big Hole Basin, simulated seeding effects were less in this case, and even some simulated decreases in precipitation occurred, perhaps due to the convective nature of this case causing some numerical noise and/or indicating the SLW was more elevated above the near-ground surface. While the simulated seeding effect was less overall in the Big Hole Basin, precipitation enhancements were simulated further downstream over the Madison Mountains and other areas of high terrain, suggesting that the AgI may have dispersed downwind before encountering SLW for precipitation enhancement. Generator groups F and G had the largest domain-wide totals of precipitation enhancement at 793 AF and 715 AF, respectively.

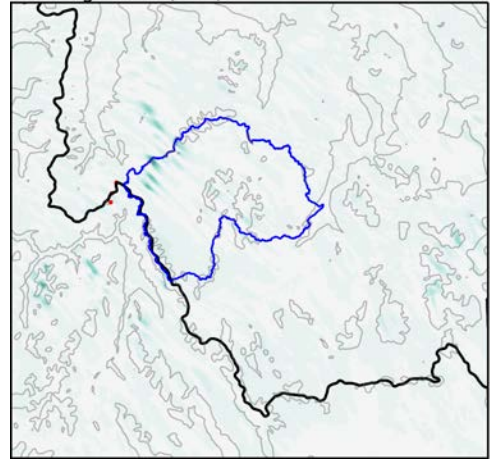
Appendix A highlights additional testing to investigate sensitivities to simulated precipitation. Of note, by simply adding "noise" to a control simulation (i.e., where no there is no seeding), differences are seen between the original simulation and the "noisy" simulation. While these differences are often small, they can lead to net positive or negative simulated precipitation differences over the domain. Extending these findings to seeding simulations, the numerical instabilities are usually small compared to the physical impacts of seeding. For example, in the simulated seeding effect maps in [Figure 5.6](#), it is difficult to visually discern any negative values over the Big Hole Basin; however, when a numerical sum is taken over the basin, there are small net negative values for some generator groups (see [Table 5.3](#)). These results are generally considered to be in the noise.



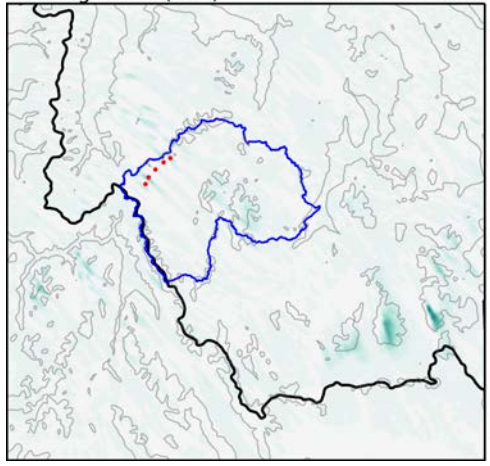
B-CTRL  
Seeding Effect (mm) 2018-11-02 Case



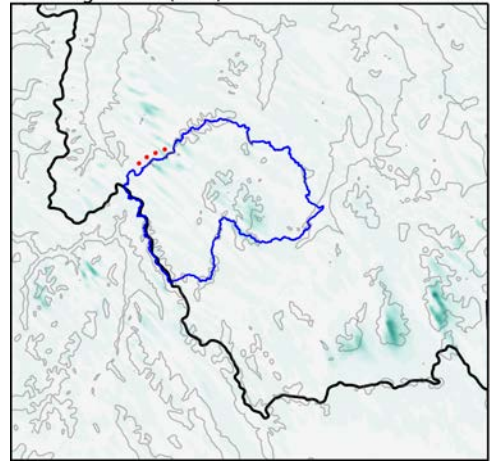
C-CTRL  
Seeding Effect (mm) 2018-11-02 Case



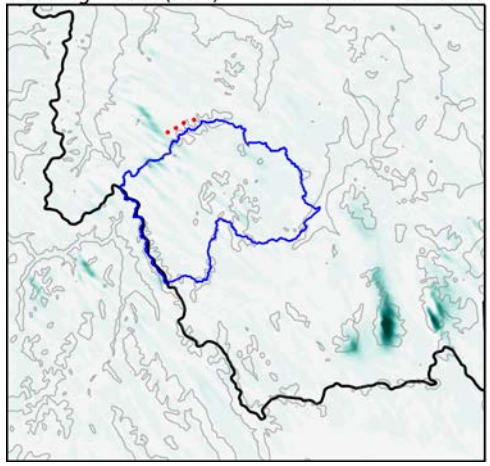
D-CTRL  
Seeding Effect (mm) 2018-11-02 Case



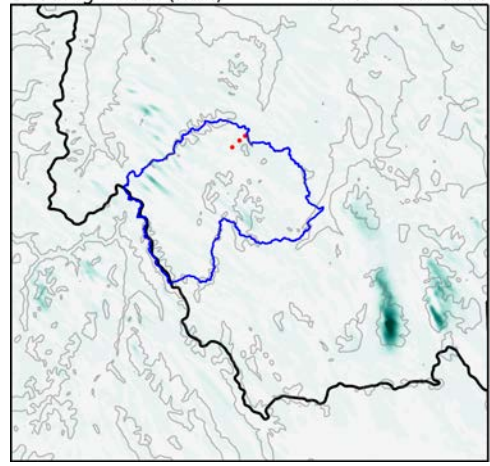
E-CTRL  
Seeding Effect (mm) 2018-11-02 Case



F-CTRL  
Seeding Effect (mm) 2018-11-02 Case



G-CTRL  
Seeding Effect (mm) 2018-11-02 Case



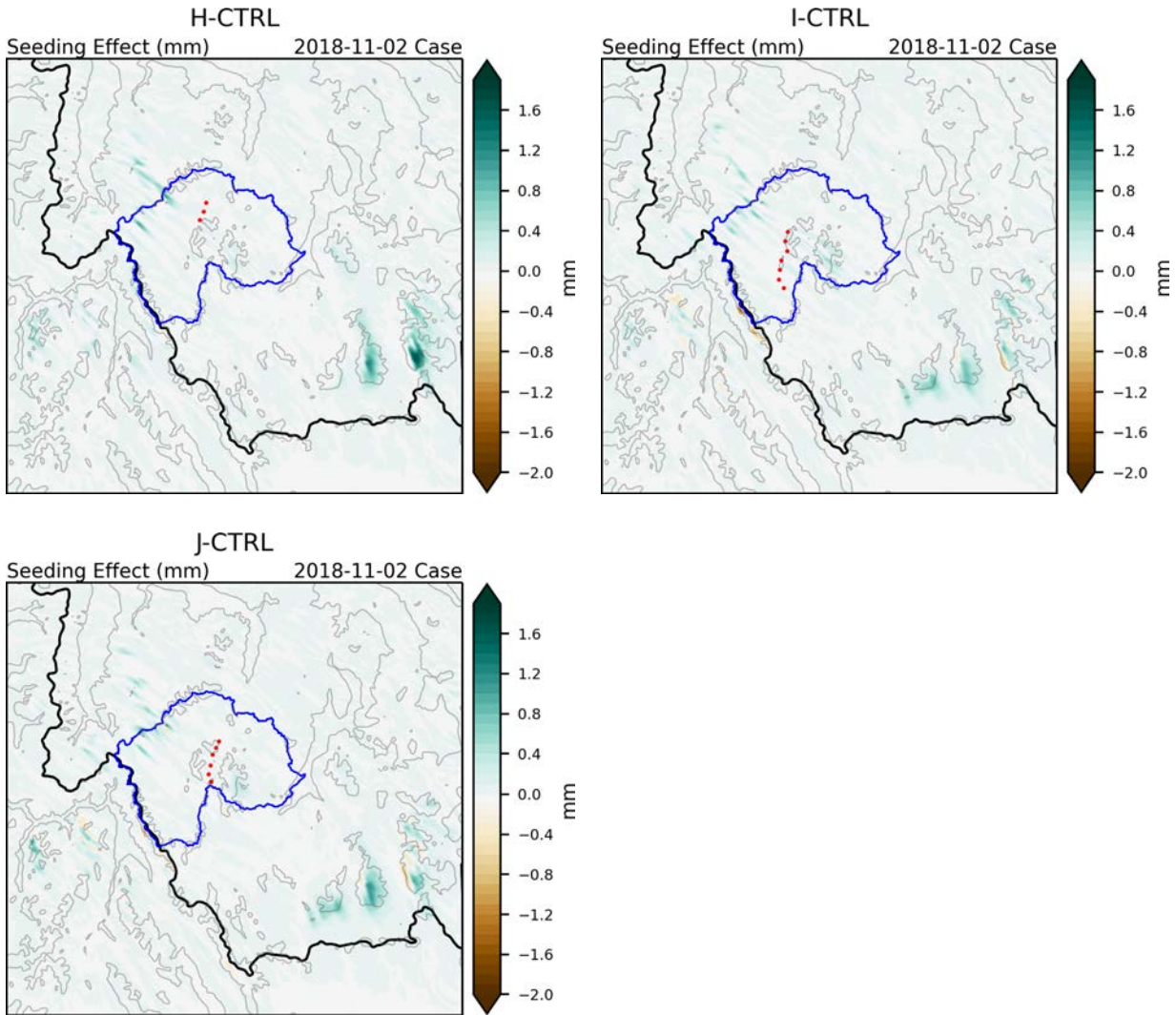


**Figure 5.6.** Simulated seeding effect from all generator groups (A-J) and each individual generator group for the 2 Nov. 2018 case study. Green hues indicate an increase in simulated precipitation due to seeding; brown hues indicate a decrease in simulated precipitation in the seeding simulations relative to the control simulation.

**Table 5.3.** Simulated seeding effect for individual ground-based generator groups A-J and all generators from groups A-J combined ('All') in Case 1.

		Simulated Seeding Effect for 2018-11-02 [AF]										
		gA	gB	gC	gD	gE	gF	gG	gH	gI	gJ	All
<b>Big Hole</b>		-8	-17	33	25	32	-14	-41	-25	18	-7	238
<b>Domain</b>		391	200	51	348	511	793	715	402	239	432	2766

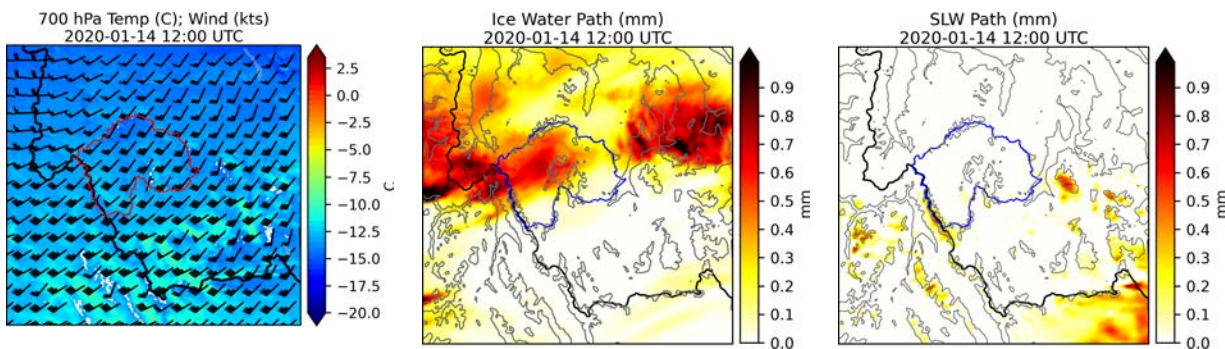
### 5.4.2. Case 2: 14 December 2019

For Case 2, the WRF-WxMod simulation began at 0900 UTC on 14 Dec. 2019. Simulated ground-based seeding commenced at 1200 UTC on 14 Dec. 2019 and lasted 3.5 h, ending at 1530 UTC. The simulation ended 3 h later at 1830 UTC. Overall, the simulated seeding effect for all individual generator groups was minor – both over the Big Hole Basin and across the entire domain. This was likely driven by the primarily NNW flow, presence of diffuse areas of IWP and minimal SLWP over the Big Hole Basin. The results of this case are fully documented in Appendix B, but are omitted from the main report for brevity.

### 5.4.3. Case 3: 14 January 2020

The 14 Jan. 2020 case was identified as a case conducive to ground-based seeding with prolonged periods of LWC in the region. The WRF-WxMod simulation for this case began at 0900 UTC on 14 Jan. 2020, and seeding commenced at 1200 UTC on 14 Jan. 2020. The ground-based seeding lasted 3.5 h, ending at 1530 UTC, and the simulation ended 3 h later at 1830 UTC (in order to allow time for AgI to disperse and activate).

[Figure 5.7](#) highlights some of the key environmental conditions throughout the control simulation. At 1200 UTC on 14 Jan. 2020, wind direction at 700 hPa was predominantly SW over the Big Hole Basin, with temperatures around  $-14^{\circ}\text{C}$  at 700 hPa. SLWP was present over the Beaverhead Mountains, but minimal SLWP was noted over the Big Hole Basin. Generally greater IWP was simulated over the north and west portions of the Big Hole Basin; however, the SW area of the basin, where the SLWP was present, had much smaller IWP. At 1530 UTC on 14 Jan. 2020, winds at 700 hPa shifted to a more westerly component within the basin and temperatures at 700 hPa cooled slightly. The Beaverhead Mountains continued to have SLWP present, and the West and East Pioneer Mountains also began to show SLWP over the higher terrain. While IWP generally decreased over the Big Hole Basin at this time, IWP was noted over portions of the Beaverhead Mountains. By the end of the simulation, winds at 700 hPa were predominantly westerly over the basin and temperatures at 700 hPa continued to cool. Some areas of SLWP were noted over the West Pioneer Mountains, but generally, low-to-zero SLWP was present over the Big Hole Basin. Some streaks of larger IWP were seen over the basin at this time and were associated with more convective features.



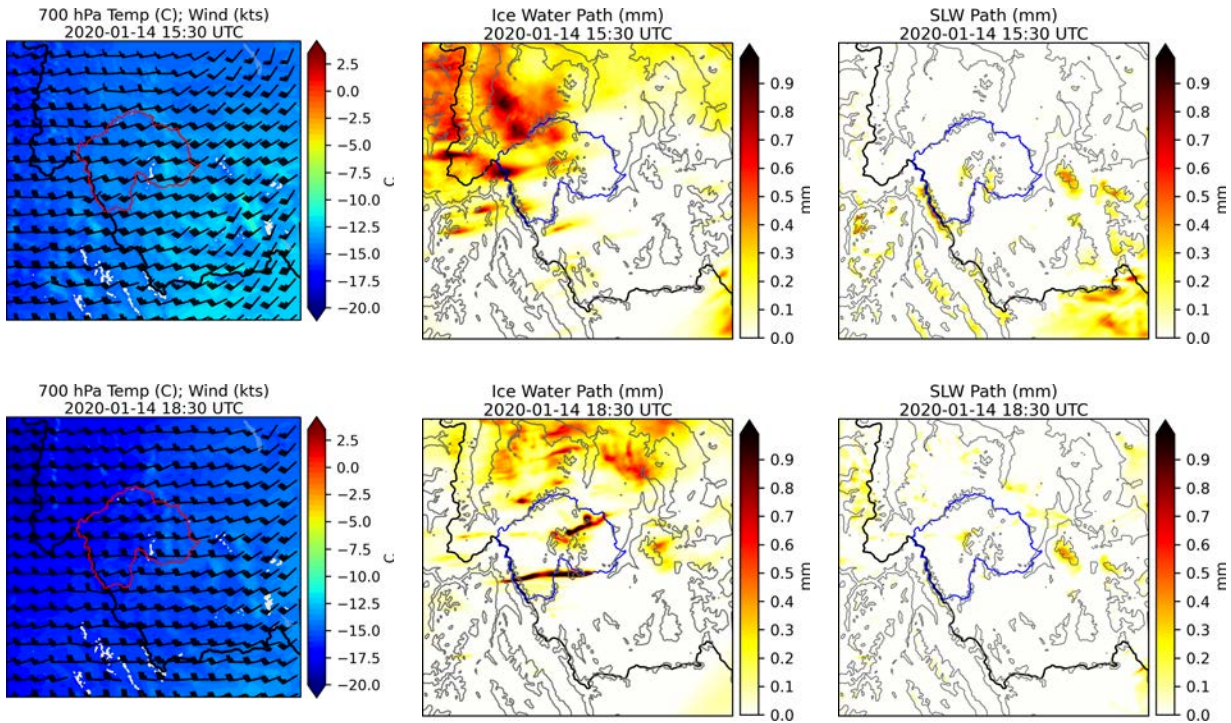


**Figure 5.7.** Temperature ( $^{\circ}\text{C}$ ) and wind barbs (knots) at 700 hPa (left column), IWP (mm; middle column), and SLWP (mm; right column) at 1200 UTC on 14 Jan. 2020 (top row), 1530 UTC on 14 Jan. 2020 (middle row), and 1830 UTC on 14 Jan. 2020 (bottom row) from the control simulation.

The total precipitation from the control simulation for Case 3 is shown in [Figure 5.8](#). Precipitation in and near the Big Hole Basin tended to be associated with the highest terrain; the Anaconda Range had areas  $>15$  mm, the Pioneer and Northern Beaverhead Mountains had local maxima  $>10$  mm. Widespread areas in the northern portion of the Big Hole domain had  $>5$  mm of precipitation.

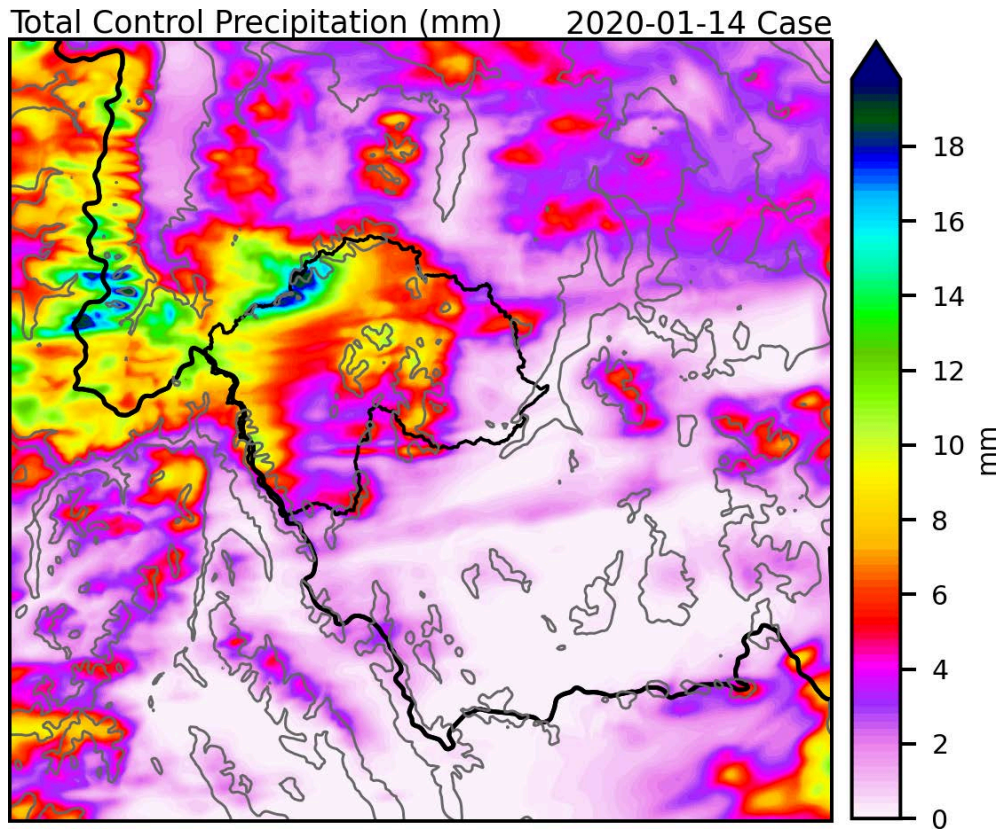
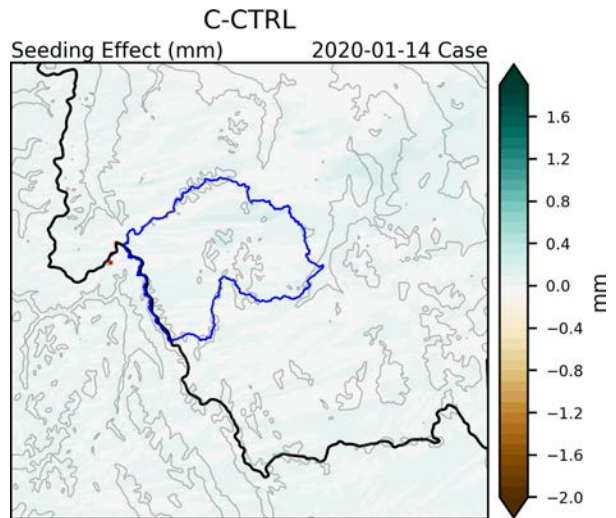
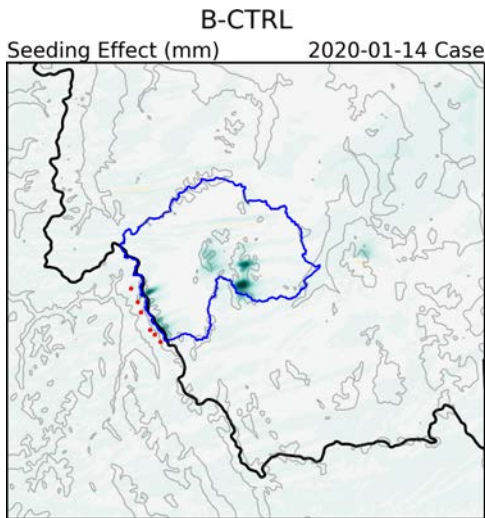
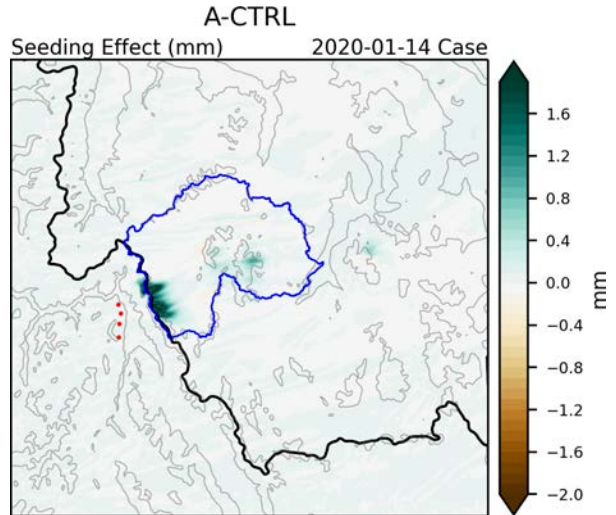
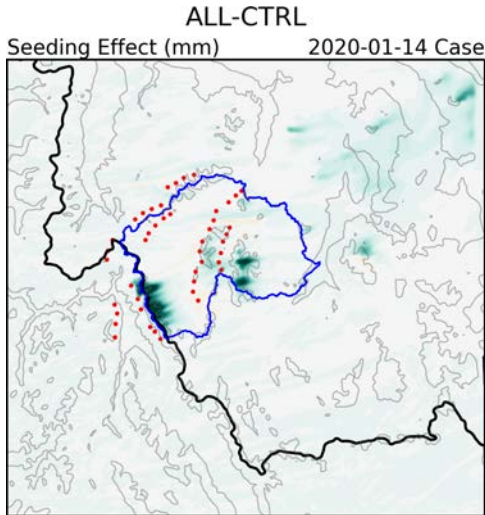


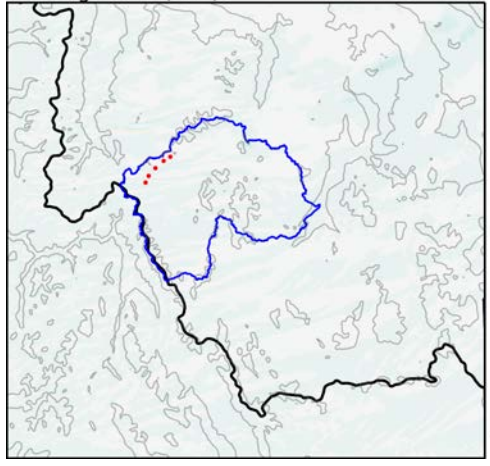
**Figure 5.8.** Total control precipitation (mm) for the 14 Jan. 2020 case (0900 UTC 14 Jan. - 0900 UTC 15 Jan. 2020).

The simulated seeding effects for the 14 Jan. 2020 case for all generators and each individual generator are shown in [Figure 5.9](#). In the simulation with all generators being used, the largest positive simulated effect is seen over the Beaverhead Mountains and East Pioneer Mountains, with areas of smaller positive simulated seeding effect over the West Pioneer Mountains and Anaconda Range. More diffuse areas of positive simulated seeding effect are seen downwind, outside of the Big Hole Basin, where the AgI plume spread. Due to the winds at 700 hPa having predominantly a southwesterly and westerly component, the orientation of certain generator groups was more favorable for positive simulated seeding effects (see [Table 5.4](#)). Generator group A had positive simulated seeding effects over the northern and central Beaverhead Mountains. In addition, smaller positive simulated seeding effects were seen further downwind over the Pioneer Mountains. Generator group B exhibited smaller, more localized positive simulated seeding effects over the Beaverhead Mountains, but positive simulated seeding effects were seen over the highest peaks in the Pioneer Mountains. Group A was sited for upwind of the Beaverhead Mountains as compared to group B, which was sited at the base of the Beaverhead Mountains. Due to the more southwest-northeast orientation of groups C-H, in combination with those generators occurring in areas of smaller SLWP and larger IWP and SW/W flow, minimal simulated seeding effects were noted. Group I, upwind of the Pioneer Mountains, showed the largest positive simulating seeding effects over the Pioneer Mountains, with some positive simulated seeding effect farther downwind, outside of the Big Hole due to the dispersion of the AgI plume. Group J, which is nestled between the West and East Pioneer Mountains did exhibit some positive simulated seeding effect over the East Pioneer Mountains, but it was

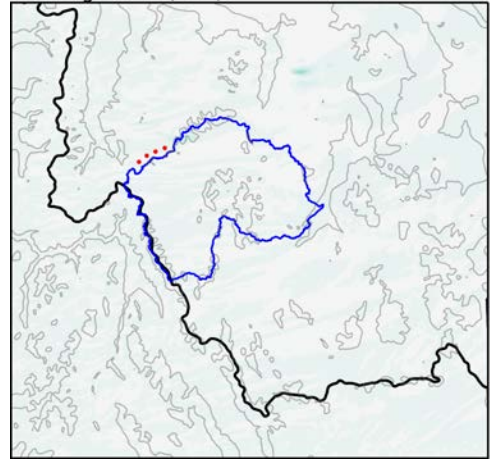
more muted compared to group I; group J also saw positive simulated seeding effect farther downwind, outside of the Big Hole.



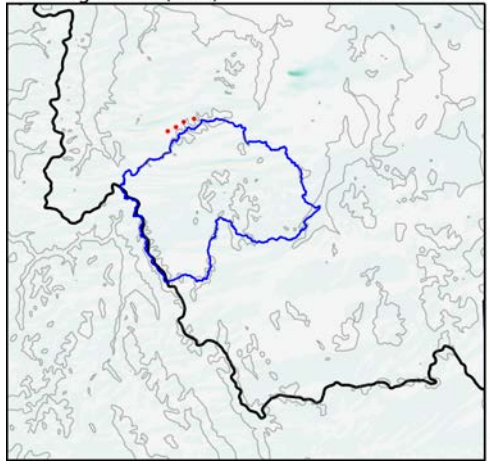
D-CTRL Seeding Effect (mm) 2020-01-14 Case



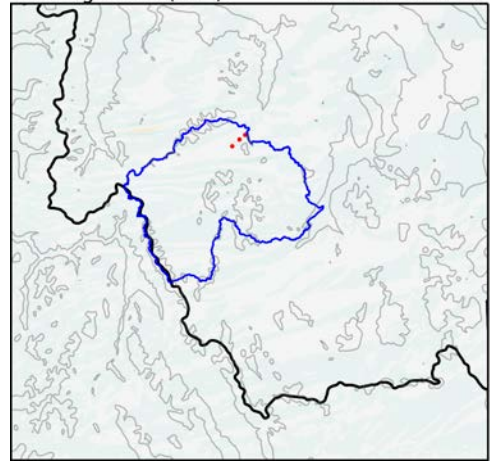
E-CTRL Seeding Effect (mm) 2020-01-14 Case



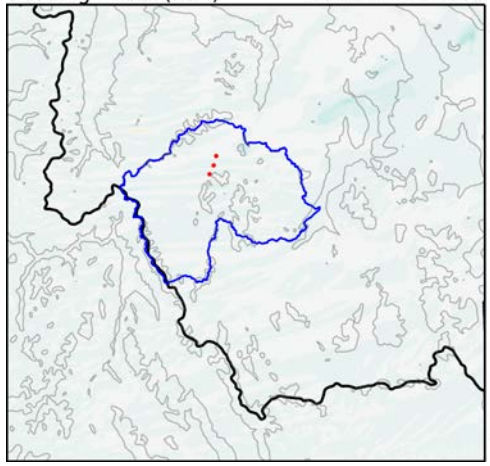
F-CTRL Seeding Effect (mm) 2020-01-14 Case



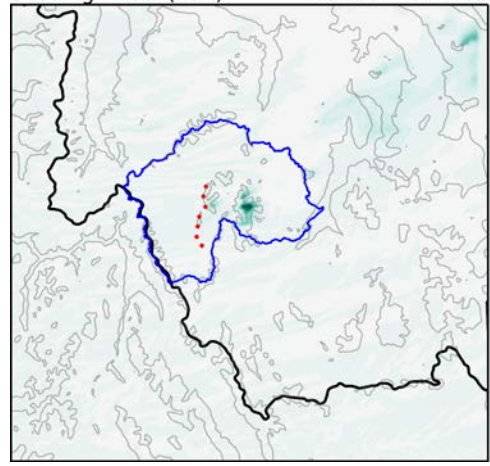
G-CTRL Seeding Effect (mm) 2020-01-14 Case



H-CTRL Seeding Effect (mm) 2020-01-14 Case



I-CTRL Seeding Effect (mm) 2020-01-14 Case



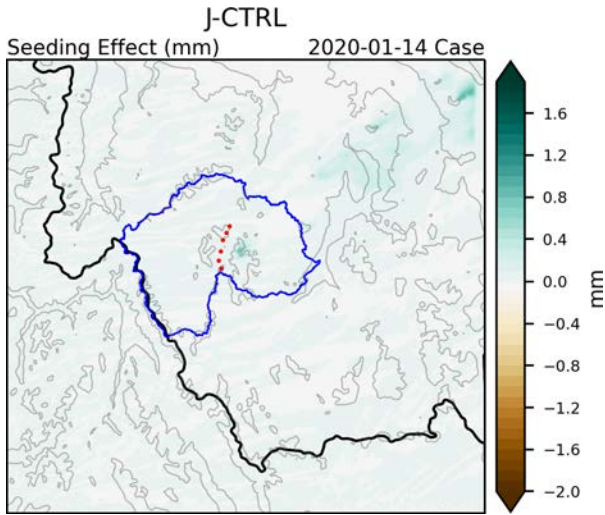


**Figure 5.9.** Simulated seeding effect from all generator groups (A-J) and each individual generator group for the 14 Jan. 2020 case study. Green hues indicate an increase in simulated precipitation due to seeding; brown hues indicate a decrease in simulated precipitation due to seeding.

**Table 5.4.** Simulated seeding effect for individual ground-based generator groups A-J and all generators from groups A-J combined ('All') in Case 3.

		Simulated Seeding Effect for 2020-01-14 [AF]										
		gA	gB	gC	gD	gE	gF	gG	gH	gI	gJ	All
<b>Big Hole</b>	<b>Basin</b>	426	337	67	12	7	-1	1	12	146	31	693
<b>Domain</b>		521	588	314	145	78	46	21	235	643	559	1493

#### 5.4.4. Case 4: 19 December 2020

[Figure 5.10](#) highlights some of the key environmental conditions for Case 4 at various times throughout the control run. Winds at 700 hPa remain generally westerly throughout the entirety of the simulation period (left column). At 1400 UTC on 19 Dec. 2020, larger IWP values were present over most of the Big Hole Basin, but they decreased to near zero by 1630 UTC (middle column). SLWP was present throughout the simulation period but generally decreased with time (right column). At 1400 UTC on 19 Dec. 2020, SLWP values in the Northern Beaverhead Mountains exceeded 0.5 mm, with other areas of enhanced SLWP over the southwestern portion of the Anaconda Range and the Pioneer Mountains. At 1630 UTC, SLWP maxima shifted slightly northward, with increased values in the Anaconda Range, with SLWP decreased in and around the entire Big Hole Basin by the end of the forecast period.

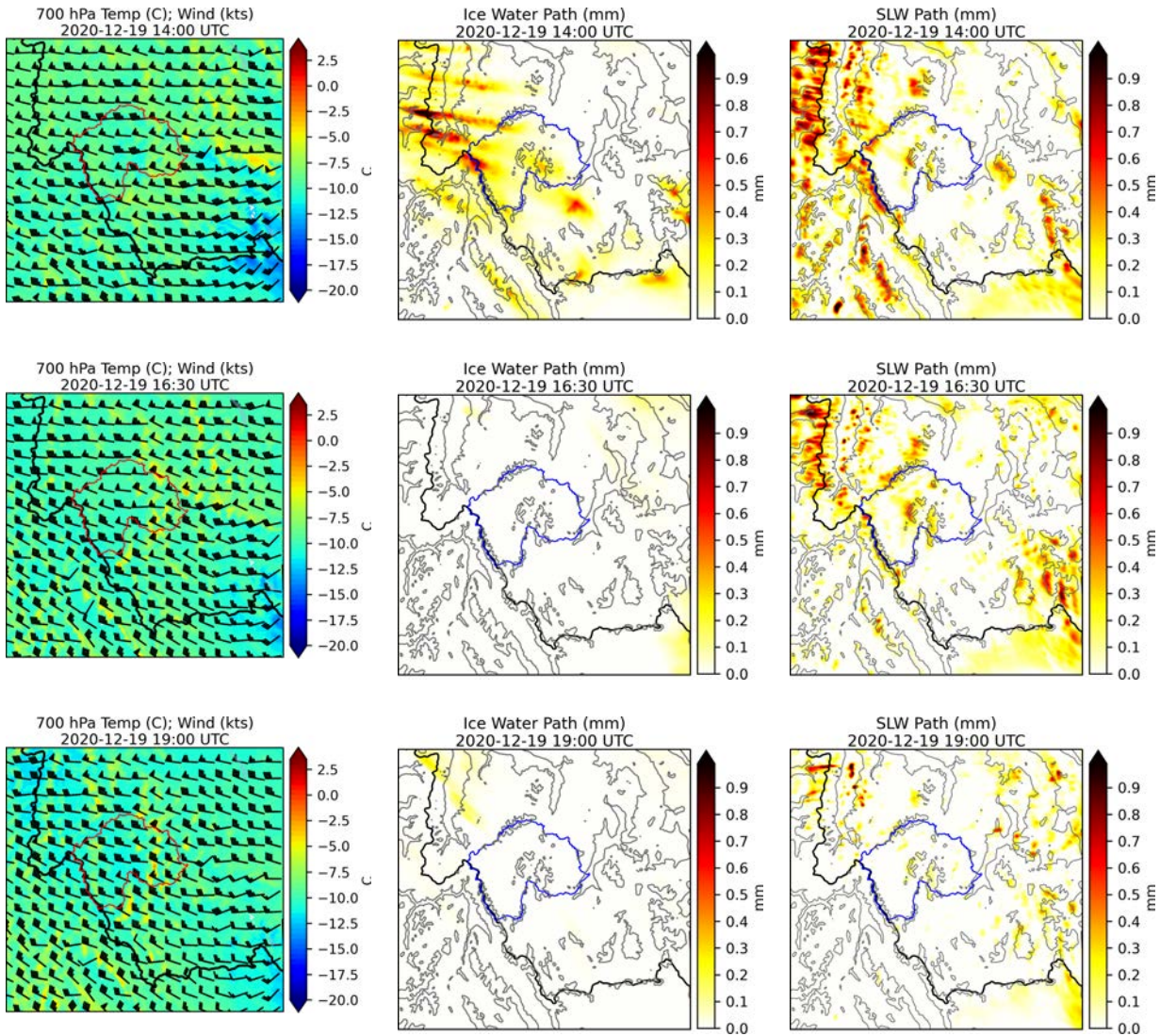


**Figure 5.10.** Temperature (°C) and wind barbs (knots) at 700 hPa (left column), SLWP (mm; middle column), and ice water path (mm; right column) at 1400 UTC on 19 Dec. 2020 (top row), 1630 UTC on 19 Dec. 2020 (middle row), and 1900 UTC on 19 Dec. 2020 (bottom row) from the control simulation.

The total precipitation from the control simulation for Case 4 is shown in [Figure 5.11](#). Overall, the area of maximum precipitation is in the north and west portions of the computational domain. In the Big Hole Basin, the largest precipitation amounts are over the higher terrain of the Northern Beaverhead Mountains, Anaconda Range, and Pioneer Mountains, with maximum precipitation over 30 mm in the most northern part of the Beaverhead Mountains and local maximums near 15 mm over the Pioneer Mountains.

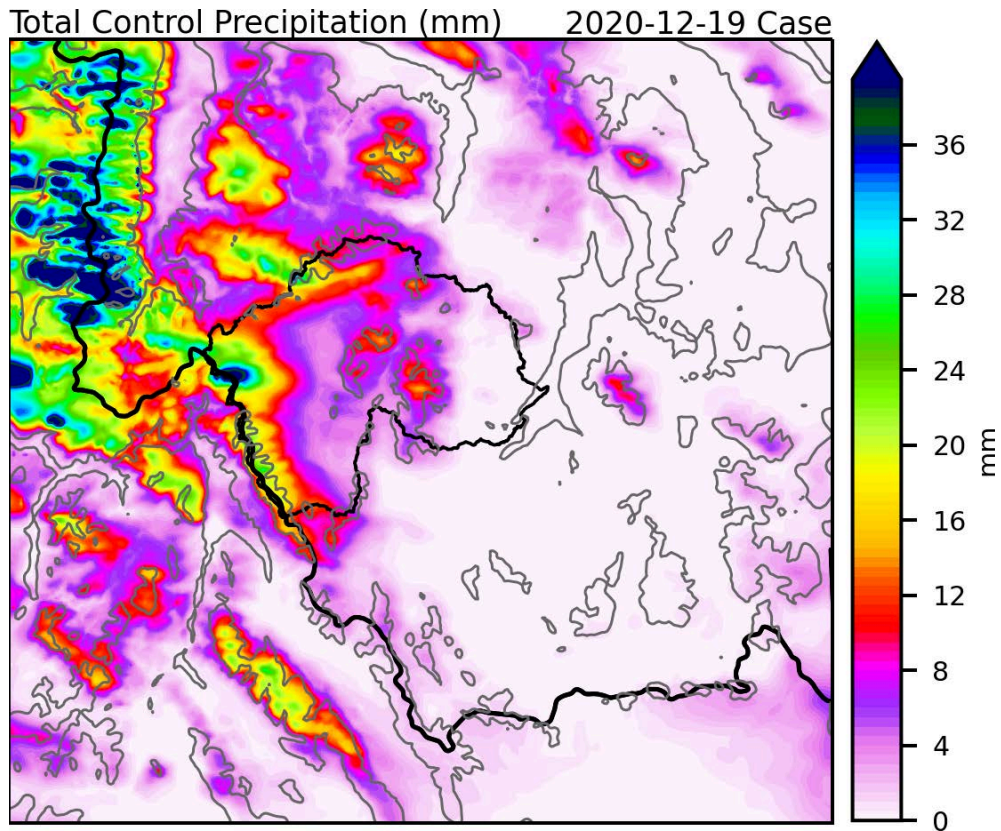
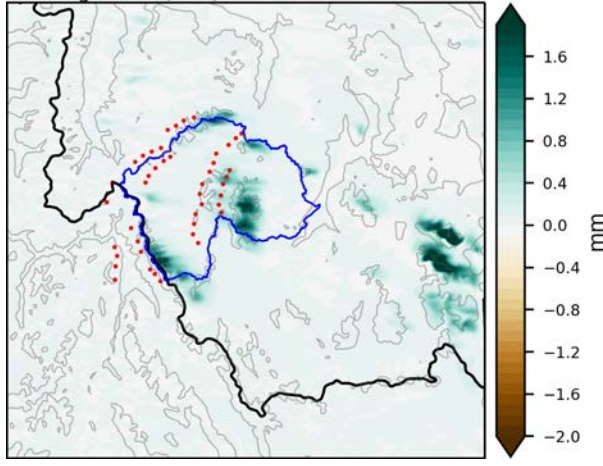


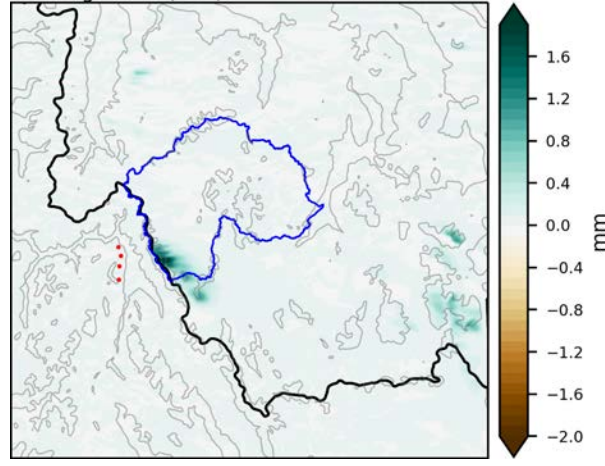
**Figure 5.11.** Total control precipitation (mm) for the 19 Dec. 2020 case (1200 UTC 19 Dec. - 1800 UTC 20 Dec. 2020).

The simulated seeding effects for the 19 Dec. 2020 case for all generators and each individual generator are shown in [Figure 5.12](#). Generators in group A demonstrated a positive simulated seeding effect over the Northern Beaverhead Mountains (271 AF over the Big Hole Basin). Similarly, generators from groups C, I, and J contributed to a positive simulated seeding effect over the Pioneer Mountains (450 AF, 218 AF, and 76 AF over the Big Hole Basin, respectively; see [Table 5.5](#)). Generator groups A and C are the furthest west and have the largest simulated seeding effect, more so than the more eastward generator groups. In addition, generator group B is located right up against the windward side of the Northern Beaverhead Mountains and has minimal local seeding effect; however, positive simulated seeding effect is noted further downstream over the Madison Mountains, suggesting that location to barriers and time for AgI to disperse affects seeding potential. Additionally, downstream positive seeding effects near or over the Madison Mountains were also observed from generator sites A, C, I, and J.

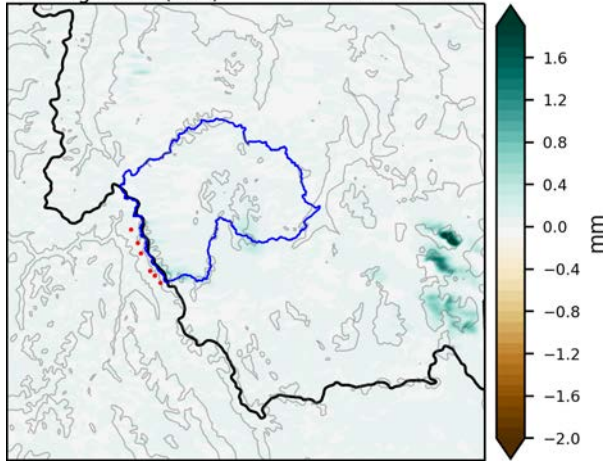
ALL-CTRL  
Seeding Effect (mm) 2020-12-19 Case



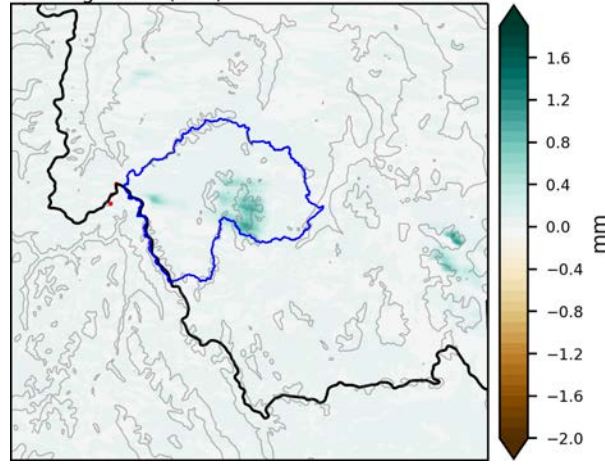
A-CTRL  
Seeding Effect (mm) 2020-12-19 Case



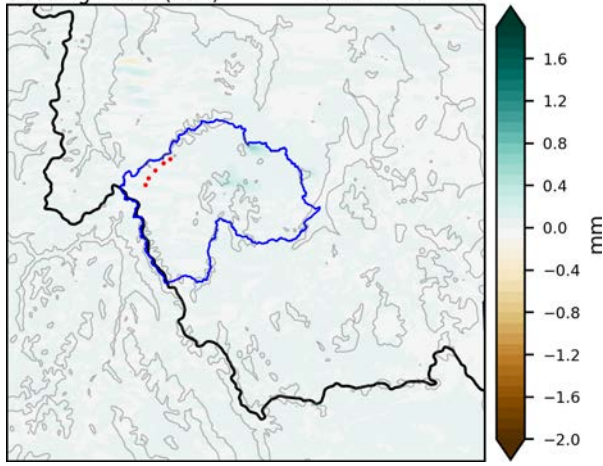
B-CTRL  
Seeding Effect (mm) 2020-12-19 Case



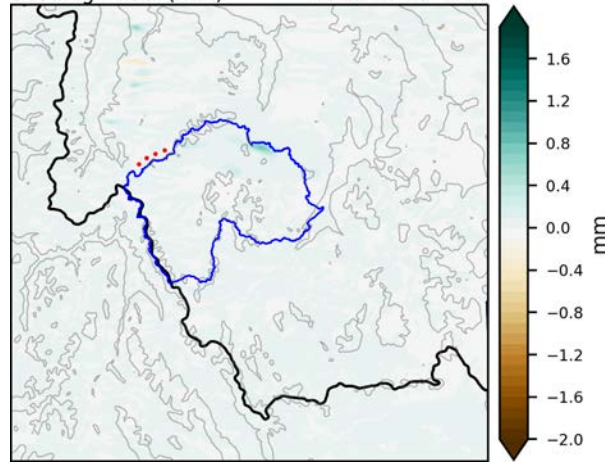
C-CTRL  
Seeding Effect (mm) 2020-12-19 Case



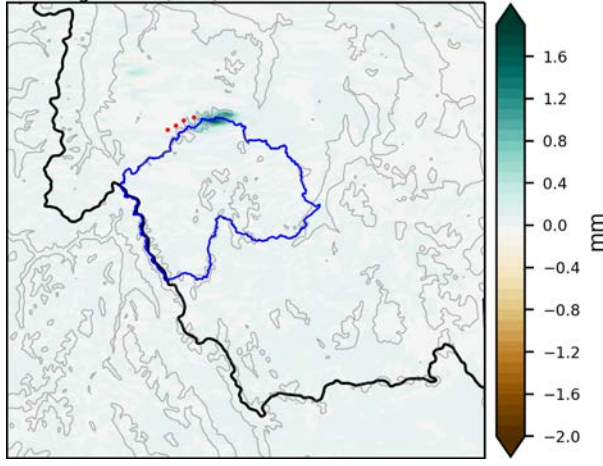
D-CTRL  
Seeding Effect (mm) 2020-12-19 Case



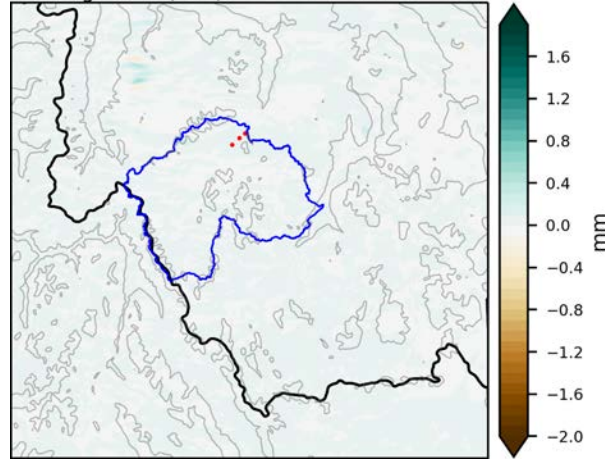
E-CTRL  
Seeding Effect (mm) 2020-12-19 Case



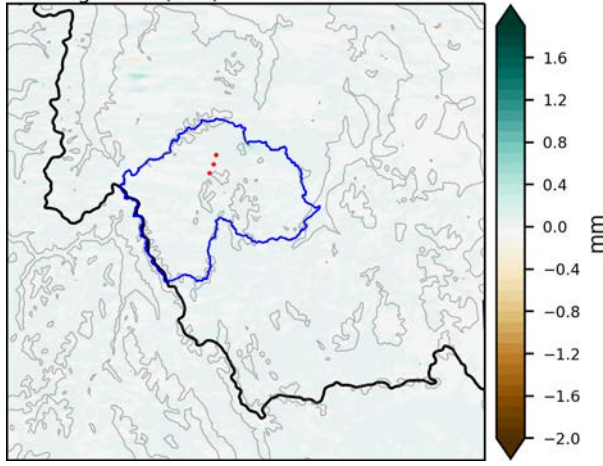
F-CTRL  
Seeding Effect (mm) 2020-12-19 Case



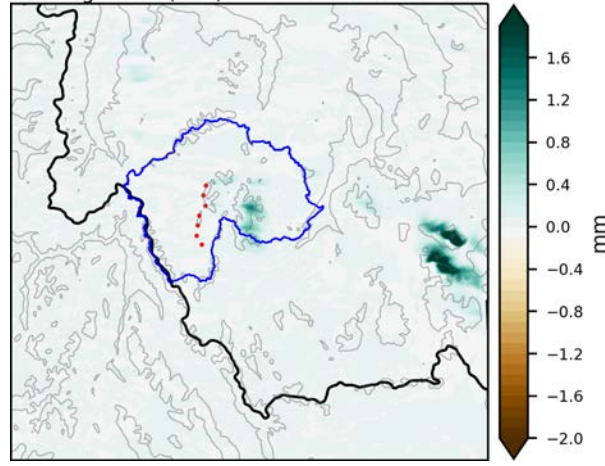
G-CTRL  
Seeding Effect (mm) 2020-12-19 Case



H-CTRL  
Seeding Effect (mm) 2020-12-19 Case



I-CTRL  
Seeding Effect (mm) 2020-12-19 Case



J-CTRL  
Seeding Effect (mm) 2020-12-19 Case

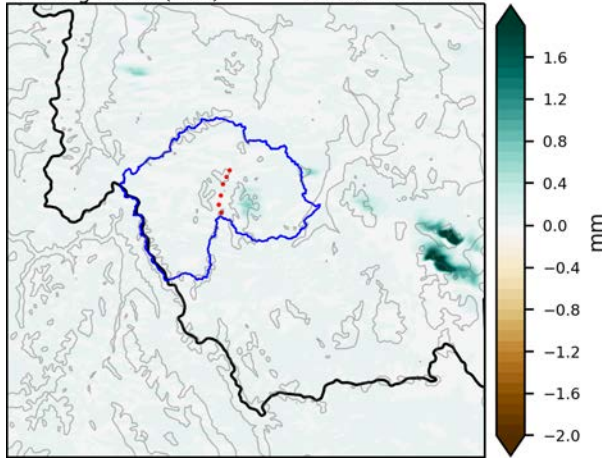


**Figure 5.12.** Simulated seeding effect from all generator groups (A-J) and each individual generator group for the 19 Dec. 2020 case study. Green hues indicate an increase in simulated precipitation due to seeding; brown hues indicate a decrease in simulated precipitation due to seeding.

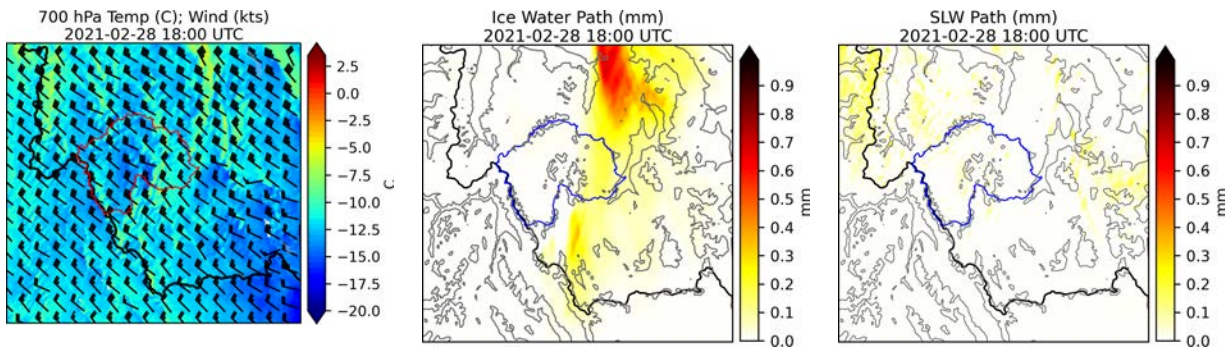
**Table 5.5.** Simulated seeding effect for individual ground-based generator groups A-J and all generators from groups A-J combined ('All') in Case 4.

		Simulated Seeding Effect for 2020-12-19 [AF]										
		gA	gB	gC	gD	gE	gF	gG	gH	gI	gJ	All
Big Hole		271	153	450	99	100	89	8	21	218	76	1251
Domain		893	948	651	112	112	174	16	17	1212	883	3371

### 5.4.5. Case 5: 28 February 2021

The 28 Feb. 2021 case was identified as a case conducive to ground-based seeding with periods of greater LWC over the central portions of the Big Hole Basin. The WRF-WxMod simulation for this case began at 1600 UTC on 28 Feb. 2021, and simulated ground seeding commenced at 1800 UTC on 28 Feb. 2021. The ground-based seeding lasted 9 h, ending at 0300 UTC on 1 March 2021, and the simulation ended 3 h later at 0600 UTC.

[Figure 5.13](#) provides an overview of key environmental conditions for Case 5 at various times throughout the control run. Winds at 700 hPa were generally from the NW throughout the entirety of the simulation period (left column). At 1800 UTC on 28 Feb. 2021, IWP was seen over the eastern portion of the Big Hole Basin, but then decreased to near zero throughout the remainder of the simulation (middle column). At 1800 UTC on 28 Feb. 2021, SLWP was simulated over the Anaconda Range and Pioneer Mountains; however, the greatest SLWP values fell outside the Big Hole Basin (right column). By 2230 UTC on 28 Feb. 2021, SLWP increased in coverage and magnitude over the Big Hole before decreasing by 0300 UTC on 1 March 2021.



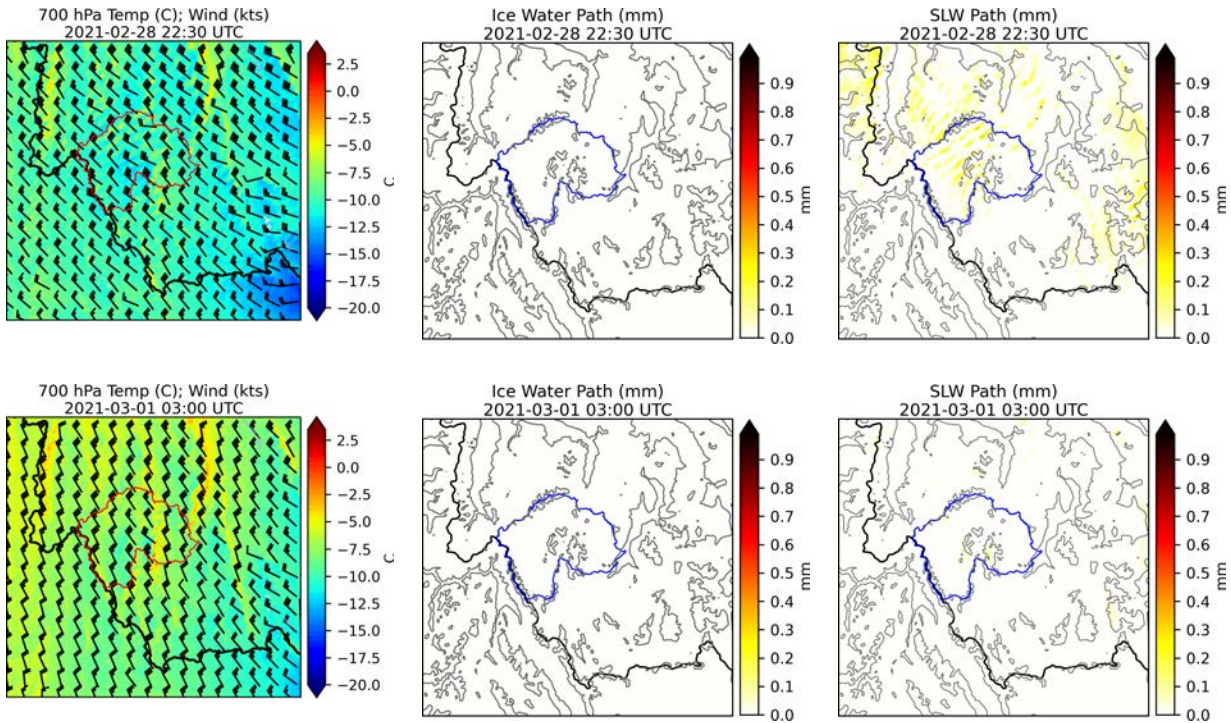


**Figure 5.13.** Temperature ( $^{\circ}\text{C}$ ) and wind barbs (knots) at 700 hPa (left column), SLWP (mm; middle column), and ice water path (mm; right column) at 1800 UTC on 28 Feb. 2021 (top row), 2230 UTC on 28 Feb. 2021 (middle row), and 0300 UTC on 1 March 2021 (bottom row) from the control simulation.

The total precipitation from the control simulation for Case 5 is shown in [Figure 5.14](#). Overall, this case produced very little simulated precipitation, especially over the target area. The area of maximum precipitation is in the north and east portions of the computational domain, outside of the Big Hole Basin. In and near the Big Hole Basin, the largest precipitation amounts are over the higher terrain of the Anaconda Range and Pioneer Mountains, with maximum precipitation  $<0.2$  mm.

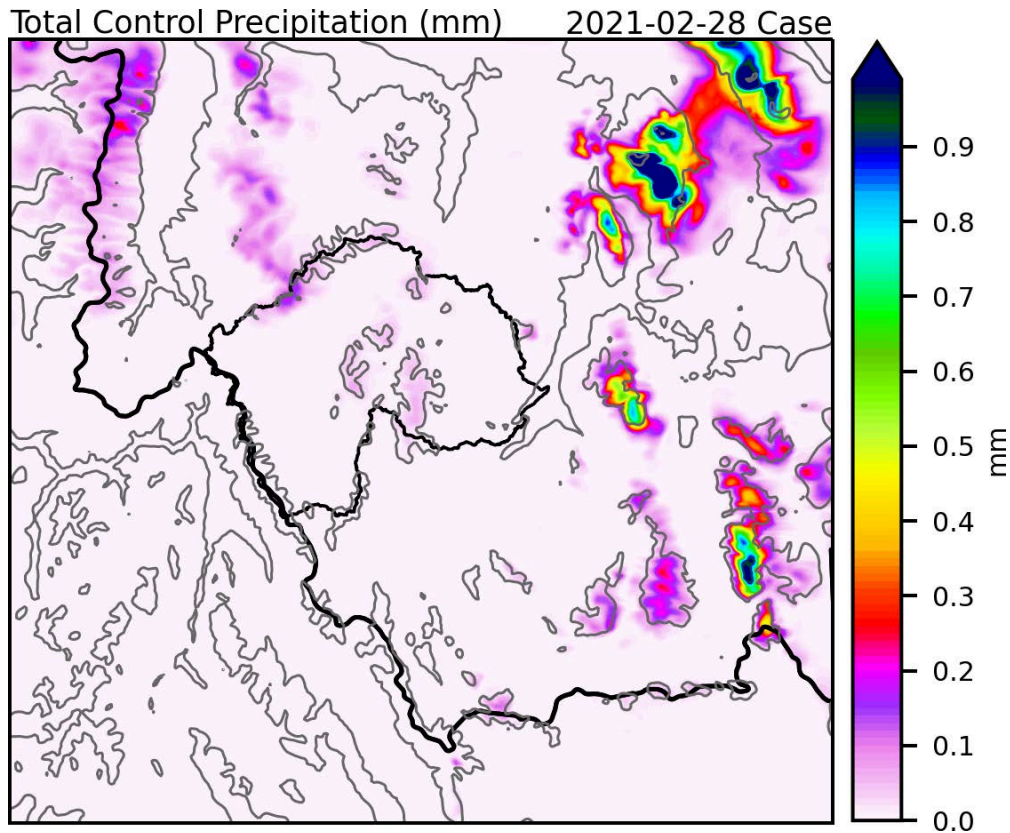
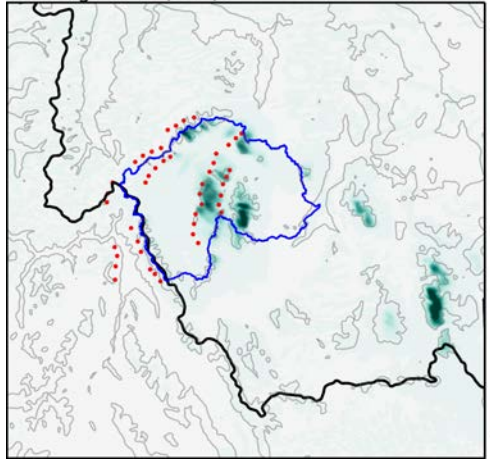


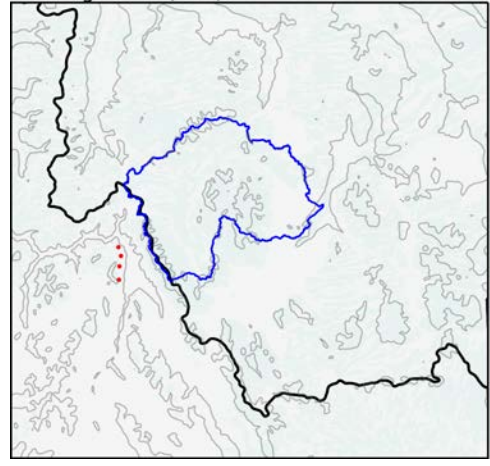
**Figure 5.14.** Control precipitation (mm) for the 28 Feb. 2021 case (1600 UTC 28 Feb. - 0600 UTC 1 Mar. 2021).

The simulated seeding effects for the 28 Feb. 2021 case for all generators and each individual generator are shown in [Figure 5.15](#). Over the Big Hole Basin, the largest simulated seeding effect was produced from the D, E, F, I, and J generator groups (451 AF, 303 AF, 203 AF, 205 AF, and 146 AF, respectively; see [Table 5.6](#)). Generator groups D and E, being located further west, successfully targeted both the western and eastern peaks in the Pioneer Mountains, Generator groups I and J have a more concentrated simulated seeding effect over the East Pioneer Mountains. Due to the NW wind direction at 700 hPa, location of generators, and minimal SLWP in the region, only a small, simulated seeding effect was noted for generator groups A and B in both the Big Hole Basin as well as the full domain. Generator groups G and H had negligible simulated seeding effects in the Big Hole Basin, likely due to minimal SLWP in the vicinity, but did simulate modest positive seeding effects over the full domain (82 AF and 202 AF, respectively). Additionally, downstream positive seeding effects near or over the Madison Mountains were also observed from generator sites D, E, F, H, I and J. Given that the control simulated precipitation was less over the Big Hole Basin (see [Figure 5.14](#)), ground seeding, with select generator groups, proved efficient at enhancing precipitation.

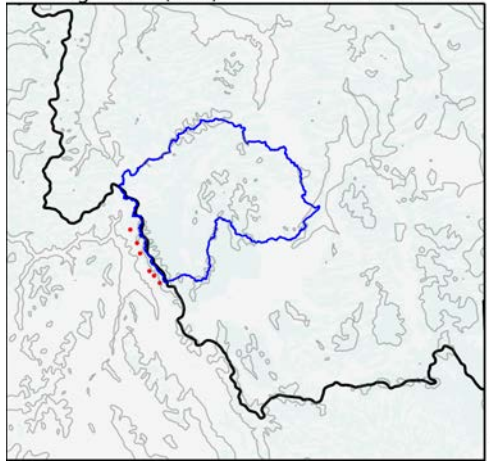
ALL-CTRL  
Seeding Effect (mm) 2021-02-28 Case



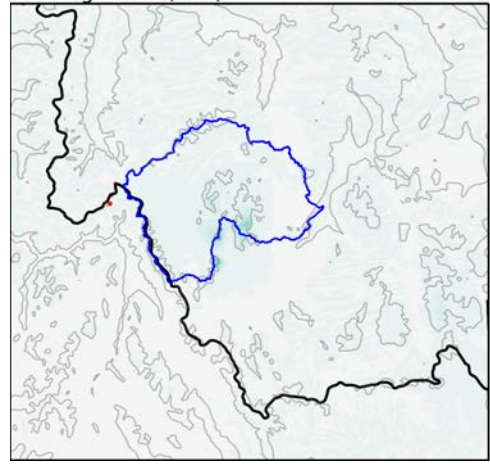
A-CTRL  
Seeding Effect (mm) 2021-02-28 Case



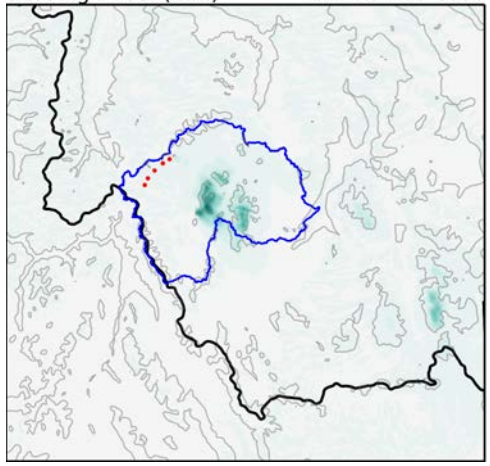
B-CTRL  
Seeding Effect (mm) 2021-02-28 Case



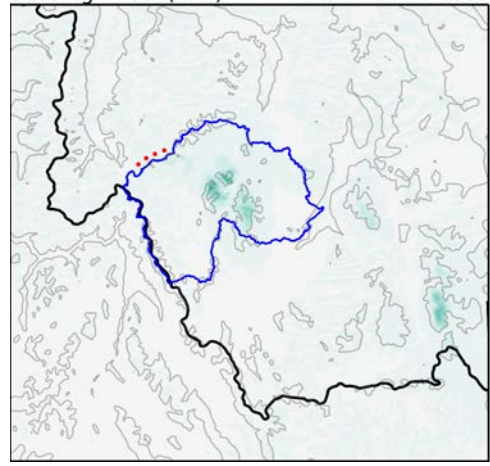
C-CTRL  
Seeding Effect (mm) 2021-02-28 Case



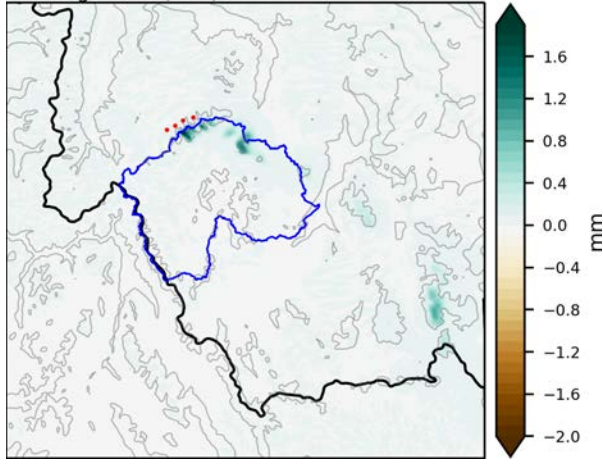
D-CTRL  
Seeding Effect (mm) 2021-02-28 Case



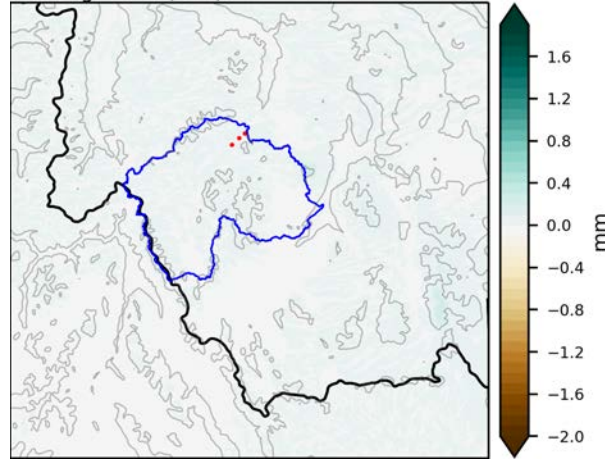
E-CTRL  
Seeding Effect (mm) 2021-02-28 Case



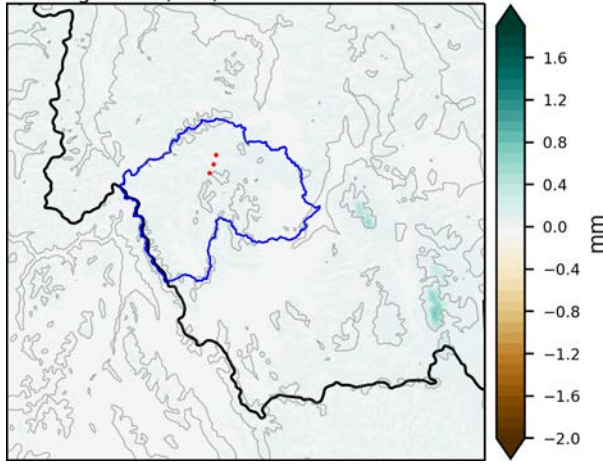
F-CTRL  
Seeding Effect (mm) 2021-02-28 Case



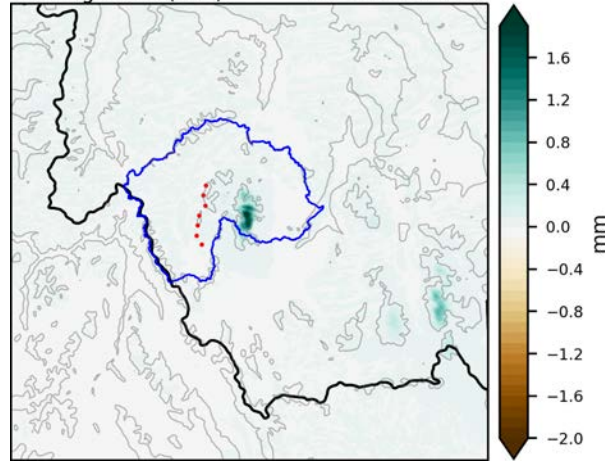
G-CTRL  
Seeding Effect (mm) 2021-02-28 Case



H-CTRL  
Seeding Effect (mm) 2021-02-28 Case



I-CTRL  
Seeding Effect (mm) 2021-02-28 Case



J-CTRL  
Seeding Effect (mm) 2021-02-28 Case

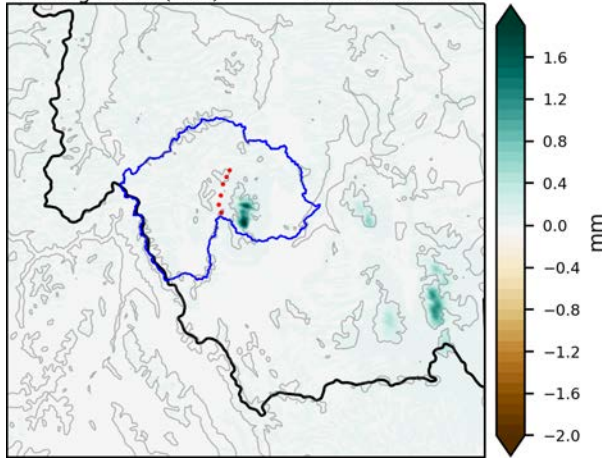


**Figure 5.15.** Simulated seeding effect from all generator groups (A-J) and each individual generator group for the 28 Feb. 2021 case study. Green hues indicate an increase in simulated precipitation due to seeding; brown hues indicate a decrease in simulated precipitation due to seeding.

**Table 5.6.** Simulated seeding effect for individual ground-based generator groups A-J and all generators from groups A-J combined ('All') in Case 5.

		Simulated Seeding Effect for 2021-02-28 [AF]										
		gA	gB	gC	gD	gE	gF	gG	gH	gI	gJ	All
<b>Big Hole</b>		14	12	126	451	303	203	1	3	205	146	944
<b>Domain</b>		24	30	245	705	509	491	82	202	452	491	1808

## 5.5. Airborne Seeding Design Simulations

This section examines the simulated effects of airborne cloud seeding in Montana’s Big Hole Basin. It contains detailed analysis of the meteorological conditions of each case and results of each potential flight track tested in each case. For a summary of the results of these case studies, please refer directly to Section 5.6.

Based on the climatology of prevailing wind directions as well as the selected case studies, multiple flight tracks were tested to evaluate the simulated impacts of airborne cloud seeding. Five tracks were chosen for westerly wind scenarios, 3 tracks were chosen for southwesterly scenarios, and 3 tracks were chosen for northwesterly scenarios ([Figure 5.16](#)). [Table 5.7](#) lists the coordinates for each flight track used in the simulated seeding experiments. The flight tracks chosen for each of the model simulations considered several factors, including predominant wind speed and direction, temperature at 700 hPa, and the presence of SLW and IWP. Note, since there is only one aircraft flying one hypothetical track at one time, there is no ‘All’ simulation as with the ground generator experiments.

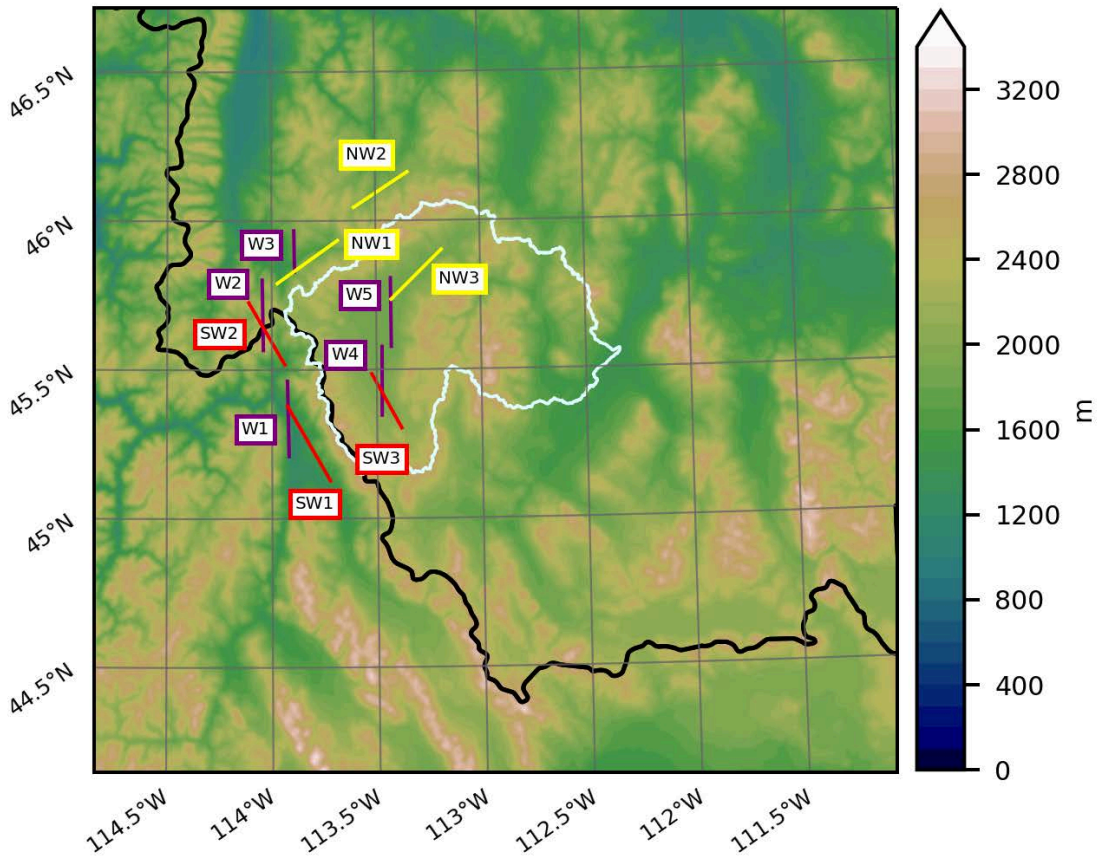


**Figure 5.16.** Simulated airborne cloud-seeding flight tracks; western flight tracks are in purple, southwestern flight tracks are in red, and northwestern flight tracks are in yellow.

**Table 5.7.** Summary of flight track coordinates for the 5 western tracks, 3 southwestern tracks, and 3 northwestern tracks.

Track	Starting Coordinates (Longitude, Latitude)	Ending Coordinates (Longitude, Latitude)
W1	(113.92W, 45.21N)	(113.93W, 45.46N)
W2	(114.04W, 45.57N)	(114.05W, 45.80N)
W3	(113.89W, 45.83N)	(113.89W, 45.97N)
W4	(113.48W, 45.35N)	(113.47W, 45.58N)
W5	(113.43W, 45.58N)	(113.43W, 45.81N)
SW1	(113.72W, 45.13N)	(113.93W, 45.38N)
SW2	(113.94W, 45.52N)	(114.11W, 45.73N)

SW3	(113.38W, 45.30N)	(113.52W, 45.49N)
NW1	(113.97W, 45.79N)	(113.68W, 45.93N)
NW2	(113.60W, 46.04N)	(113.34W, 46.16N)
NW3	(113.43W, 45.74N)	(113.19W, 45.90N)

[Table 5.8](#) summarizes the four simulated airborne seeding cases (same cases as simulated for ground seeding, except not Case 2) and the average meteorological conditions. Each airborne seeding period lasted for three hours, with the simulated seeding effect calculated from the beginning of the seeding window until three hours after the end of the seeding period to allow for time for the AgI to disperse and activate.

**Table 5.8.** Summary of simulated airborne seeding cases. Wind speed (*WSpeed*), wind direction (*WDir*), and temperature (*T*) corresponding to the median value within the seeding period, over the target area centered over the Big Hole Basin, at 3750 m and 4250 m above mean sea level.

Case ID	Date	Seeding Period	Track	WSpeed [m/s]	WDir[°]	T [°C]
C1	2018-11-02	+1d03 UTC to 06 UTC	NW1 3750	19	NW, 315	-13
			NW1 4250	17	NW, 327	-16
			NW2 3750	17	NW, 327	-12
			NW2 4250	16	NW, 330	-16
			NW3 3750	20	NW, 326	-12
			NW3 4250	20	NW, 329	-15
C3	2020-01-14	12:15 UTC to 14:45 UTC	SW1 3750	21	W, 253	-20
			SW1 4250	21	W, 253	-21
			SW2 3750	15	W, 259	-20
			SW2 4250	14	W, 255	-24
			SW3 3750	21	W, 256	-20
			SW3 4250	20	W, 255	-23
		15:15 UTC to 18:15 UTC	W1 3750	14	W, 262	-23
			W1 4250	15	W, 255	-27
			W2 3750	14	W, 263	-23
			W2 4250	13	W, 251	-27
W3 3750	15	W, 261	-23			
W3 4250	14	W, 256	-26			
W4 3750	14	W, 264	-21			

			W4 4250	14	W, 253	-26
C4	2020-12-19	14:30 UTC to 17:30 UTC	W1 3750	23	NW, 293	-14
			W1 4250	26	NW, 292	-16
			W2 3750	27	W, 290	-13
			W2 4250	29	NW, 294	-14
			W3 3750	26	W, 287	-13
			W3 4250	28	W, 292	-15
			W4 3750	27	NW, 298	-11
			W4 4250	28	NW, 303	-14
C5	2021-02-28	20:30 UTC to 23:30 UTC	NW1 3750	18	NW, 328	-10
			NW1 4250	21	N, 346	-12
			NW2 3750	19	NW, 329	-11
			NW2 4250	21	N, 339	-13
			NW3 3750	20	NW, 328	-11
			NW3 4250	22	N, 340	-12

### 5.5.1. Case 1: 2 November 2018

The WRF-WxMod simulation began at 2100 UTC on 2 Nov. 2018, and airborne seeding commenced at 0300 UTC on 3 Nov. 2018 along the northwesterly flight tracks. Seeding lasted 3 h, ending at 0600 UTC, and the simulation ended 3 h later at 0900 UTC. This case was identified as a case conducive to airborne seeding based on prolonged periods of enhanced SLW within a representative flight height range of 3.5–4.5 km MSL.

The simulated seeding effects for the 2 Nov. 2018 case for each of the 6 different permutations of NW flight track simulations are shown in [Figure 5.17](#). Overall, flight tracks at 3750 m have more positive simulated seeding effect than the flight tracks at 4250 m (see [Table 5.9](#)). The largest positive simulated seeding effects in the Big Hole Basin are seen in the NW2 tracks (1245 AF at 3750 m and 1279 AF at 4250 m). Both NW2 tracks have positive simulated seeding effects on the downstream side of the Anaconda Range, with a large positive seeding effect swath extending over and downstream of the Pioneer Mountains. The NW3 track at 3750 m has a large positive simulated seeding effect over the Pioneer Mountains and then extending downstream; the NW3 flight track at 4250 m has less positive simulated seeding effect over the tallest peaks of the Pioneer Mountains but does see positive differences on the leeward side. While the NW1 track does produce positive simulated seeding effects in the basin (580 AF at 3750 m and 385 AF at 4250 m), larger seeding effects occur outside of the basin (1109 AF at 3750 m and 936 AF at 4250 m). Some areas outside of the Big Hole Basin that are downstream of NW2 and NW3 tracks also see positive simulated seeding effects.

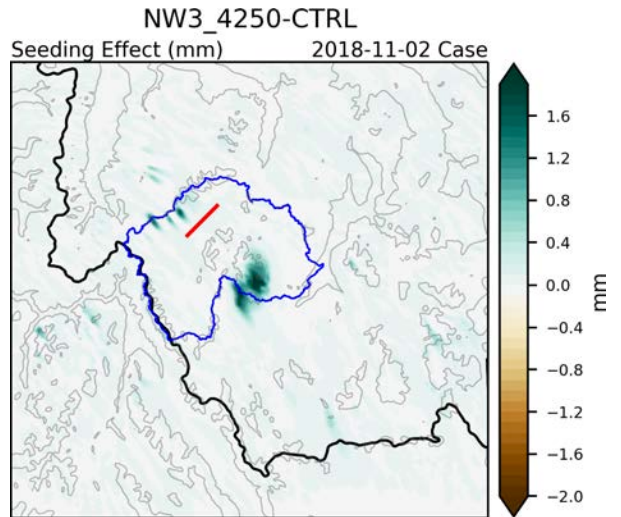
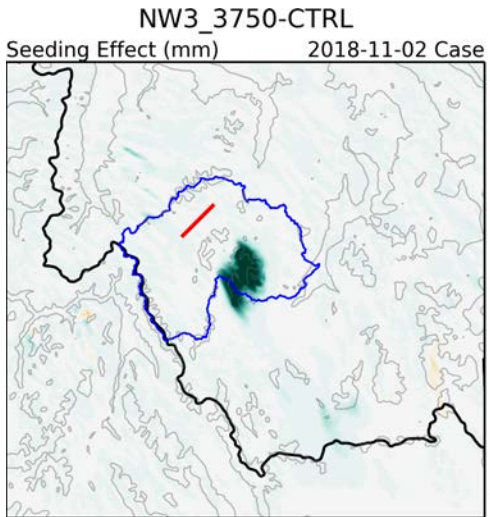
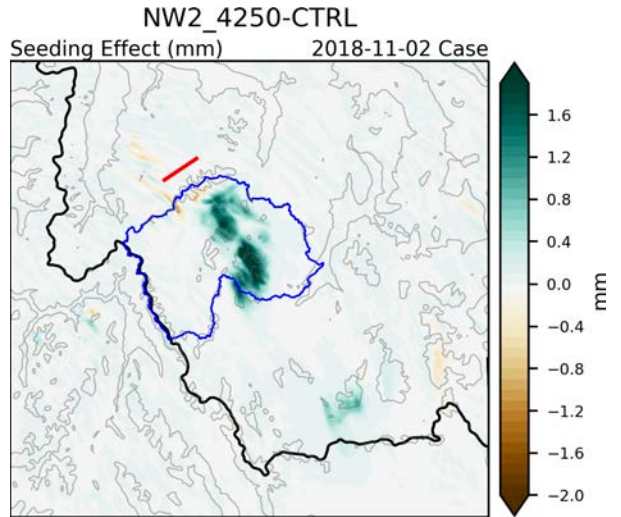
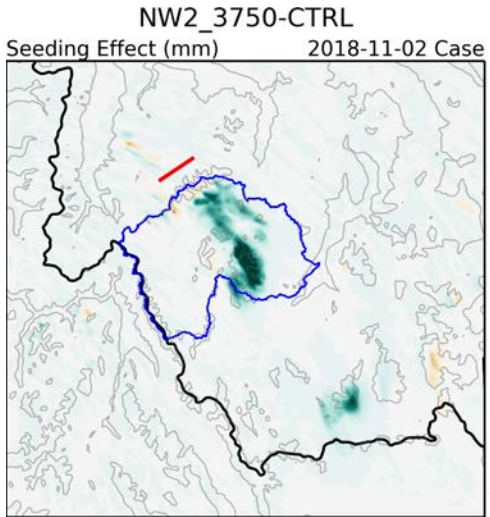
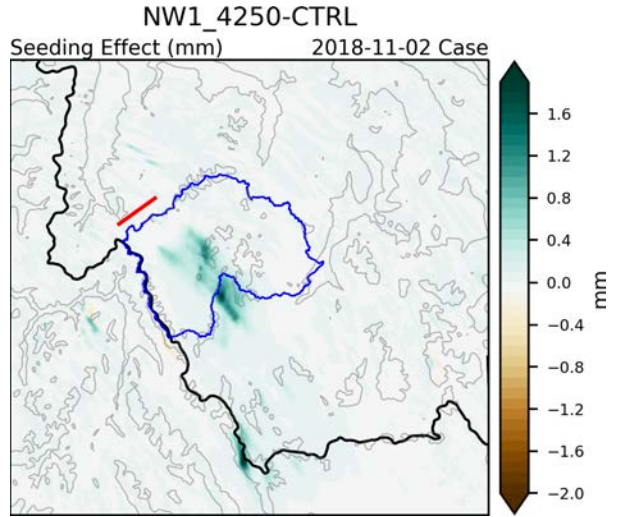
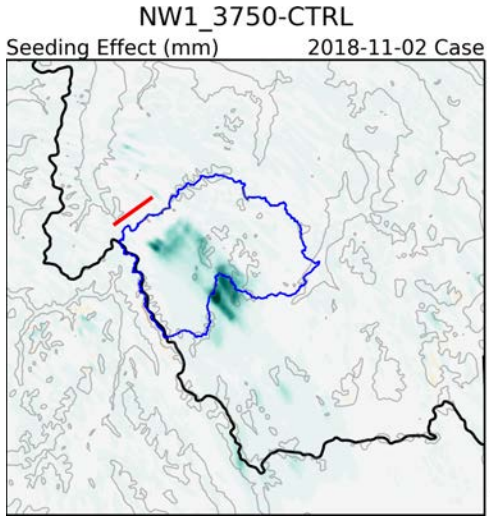


**Figure 5.17.** Simulated seeding effect from airborne seeding along the NW1 track (top), NW2 track (center), and NW3 track (right) for the 3750 m above mean sea level (left) and 4250 m above mean sea level (right) for the 2 Nov. 2018 case study. Green hues indicate an increase in simulated precipitation due to seeding; brown hues indicate a decrease in simulated precipitation due to seeding.

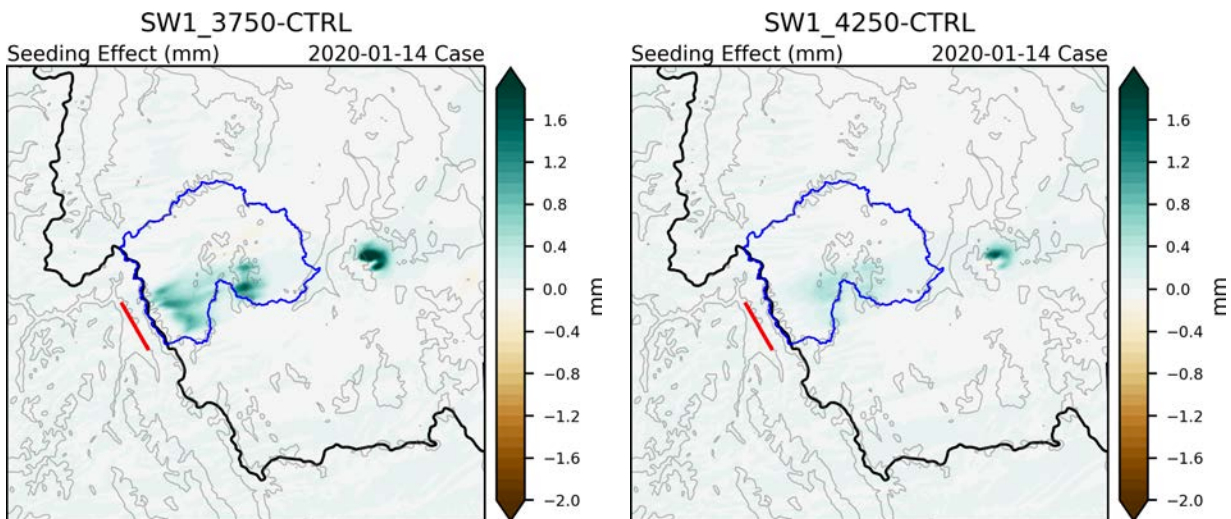
**Table 5.9.** Simulated seeding effect for airborne tracks in Case 1.

		Seeding Effect for 2018-11-02 [AF]		
		NW1	NW2	NW3
3750m	BigHole	580	1245	919
	Domain	1109	1476	1194
4250m	BigHole	385	1279	338
	Domain	936	1428	491

### 5.5.2. Case 3: 14 January 2020

As shown in [Figure 5.7](#), the winds direction at 700 hPa shifted from southwesterly to westerly during the simulation window during this case; therefore, the WRF-WxMod simulation began at 0900 UTC on 14 Jan. 2020, and airborne seeding was conducted on SW tracks from 1215 – 1445 UTC on 14 Jan. 2020 and W tracks from 1515 – 1815 UTC on 14 Jan. 2020.

Overall, for both SW and W tracks, airborne seeding at 3750 m yielded a larger positive seeding effect than at 4250 m ([Figure 5.18](#) and [Figure 5.19](#); see [Table 5.10](#)). The better environment with respect to greater SLWP and less IWP was noted over the Northern Beaverhead and Pioneer Mountains (see [Figure 5.7](#)); therefore, the flight tracks targeting these areas yielded the greater simulated seeding effects (i.e., SW1, SW3, W1, and W4), with the SW1 track simulated the largest seeding effect (693 AF) within the Big Hole Basin. In addition, downstream of the Big Hole Basin, there were large positive simulated seeding effects near and over the Tobacco Root Mountains.



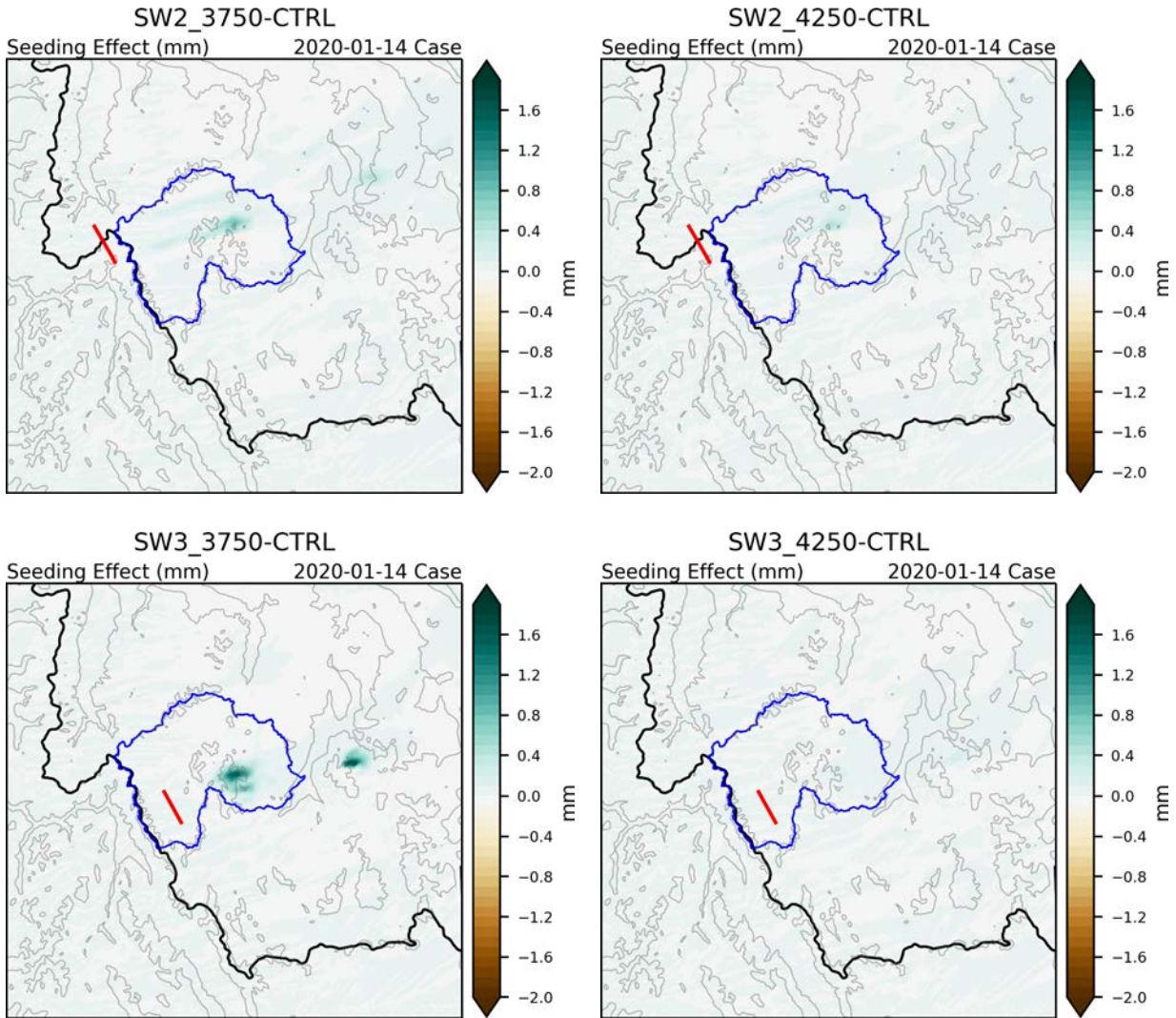
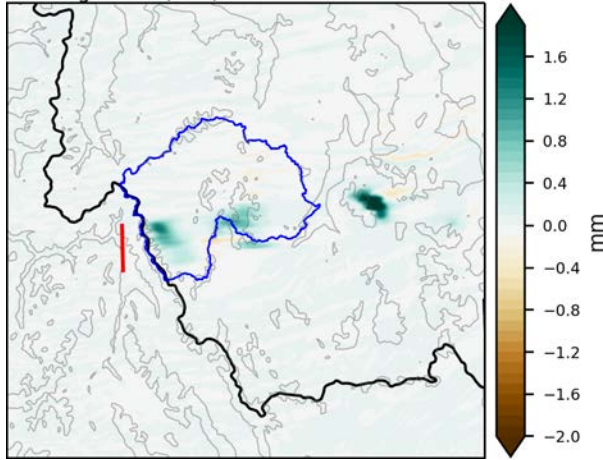
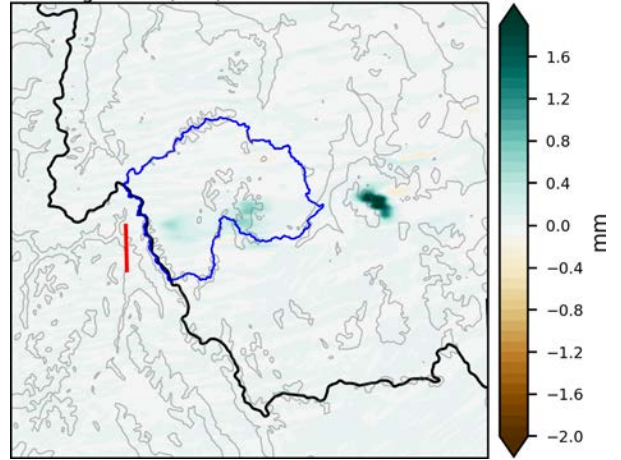


**Figure 5.18.** Simulated seeding effect from airborne seeding along the SW1 track (top), SW2 track (center), and SW3 track (right) for the 3750 m above mean sea level (left) and 4250 m above mean sea level (right) for the 14 Jan. 2020 case study, where simulated seeding occurred from 1215 – 1445 UTC on 14 Jan. 2020. Green hues indicate an increase in simulated precipitation due to seeding; brown hues indicate a decrease in simulated precipitation due to seeding.

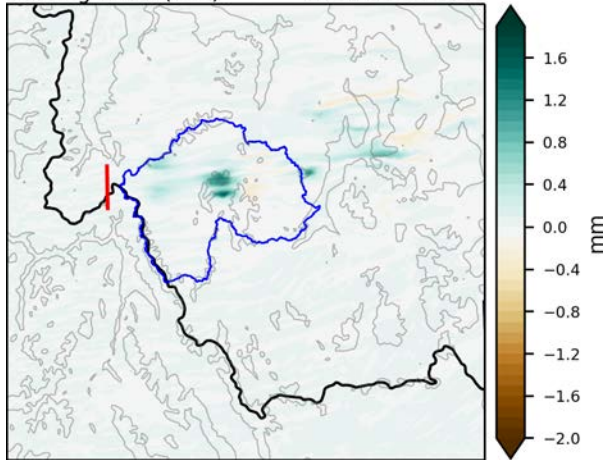
W1\_3750-CTRL  
Seeding Effect (mm) 2020-01-14 Case



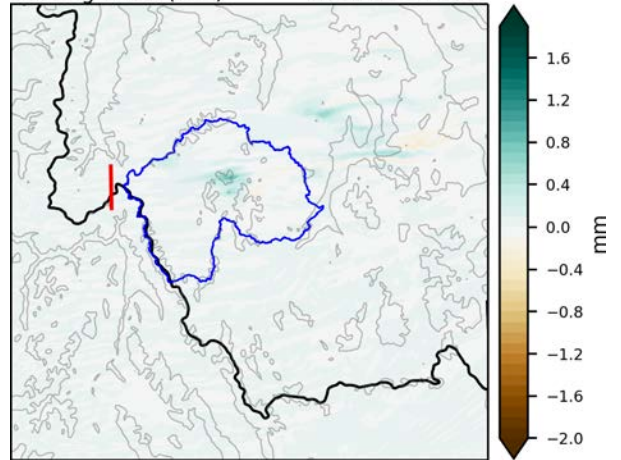
W1\_4250-CTRL  
Seeding Effect (mm) 2020-01-14 Case



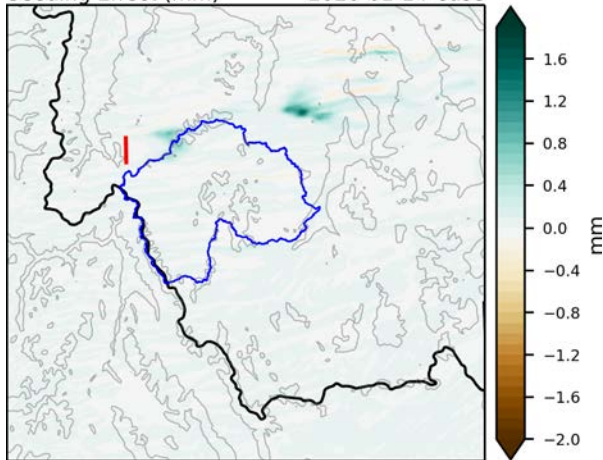
W2\_3750-CTRL  
Seeding Effect (mm) 2020-01-14 Case



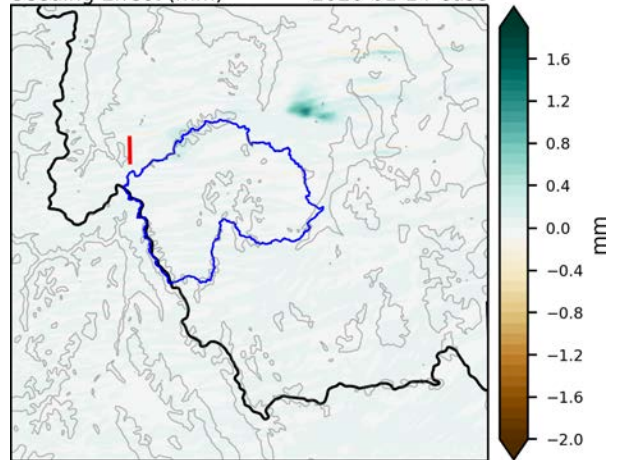
W2\_4250-CTRL  
Seeding Effect (mm) 2020-01-14 Case



W3\_3750-CTRL  
Seeding Effect (mm) 2020-01-14 Case



W3\_4250-CTRL  
Seeding Effect (mm) 2020-01-14 Case



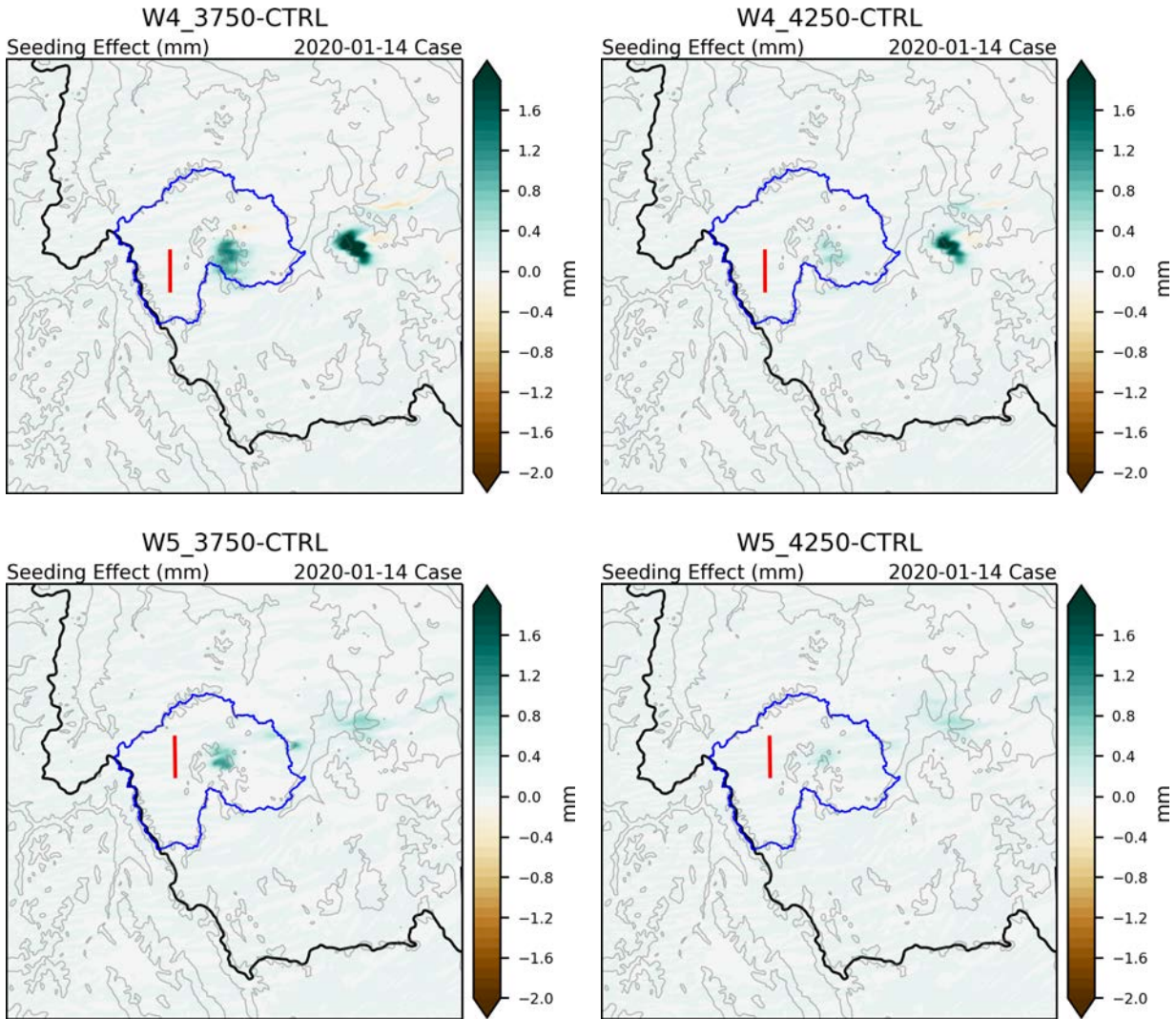


**Figure 5.19.** Simulated seeding effect from airborne seeding along the W1 track (first row), W2 track (second row), W3 track (third row), W4 track (fourth row), and W5 (fifth row) for the 3750 m above mean sea level (left) and 4250 m above mean sea level (right) for the 14 Jan. 2020 case study, where simulated seeding occurred from 1515 – 1815 UTC on 14 Jan. 2020. Green hues indicate an increase in simulated precipitation due to seeding; brown hues indicate a decrease in simulated precipitation due to seeding.

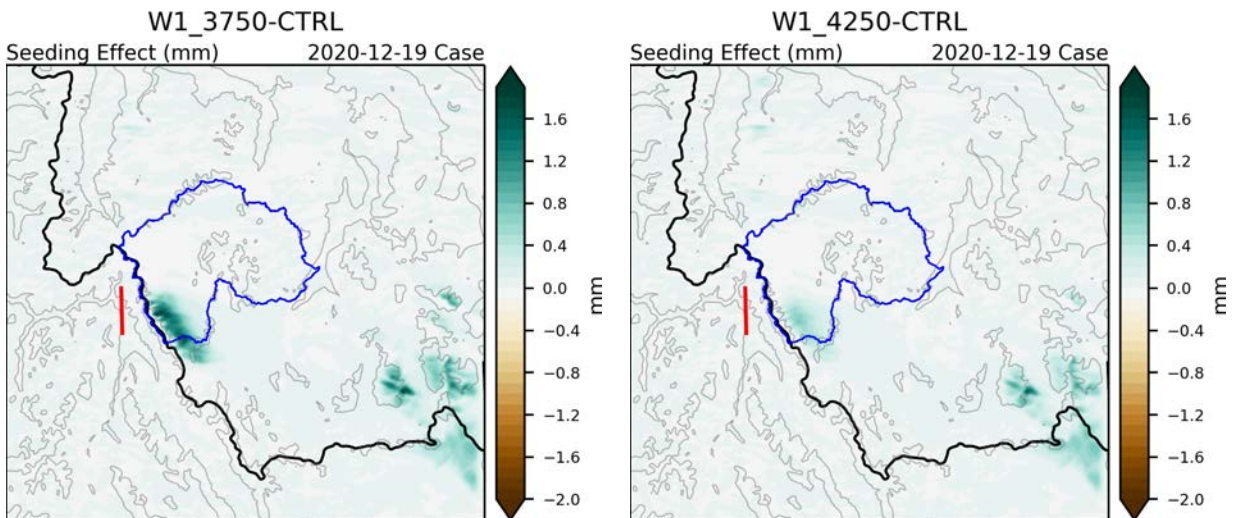
**Table 5.10.** Simulated seeding effect for airborne tracks in Case 3.

		Seeding Effect for 2020-01-14 [AF]							
		SW1	SW2	SW3	W1	W2	W3	W4	W5
3750m	BigHole	693	153	282	329	284	21	244	120
	Domain	923	276	376	536	315	239	601	252
4250m	BigHole	271	105	21	186	104	-2	72	33
	Domain	438	121	72	380	132	169	309	140

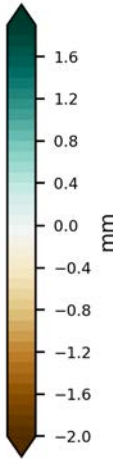
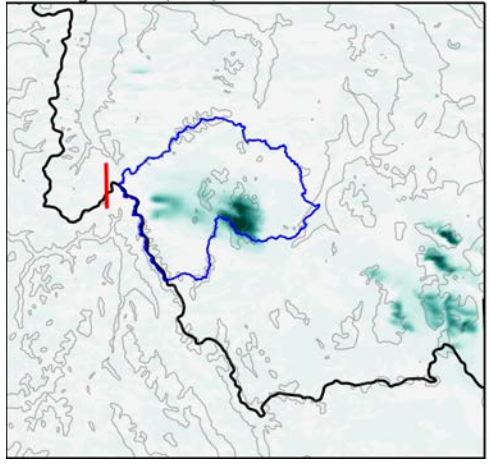
### 5.5.3. Case 4: 19 December 2020

For Case 4, the WRF-WxMod simulation began at 1200 UTC on 19 Dec. 2020, and airborne seeding commenced along westerly flight tracks at 1430 UTC. Seeding lasted 3 h, ending at 1730 UTC, and the simulation ended 3 h later at 2030 UTC. This case was identified as a case conducive to airborne seeding based on prolonged periods of enhanced SLW within a representative flight height range of 3.5–4.5 km MSL.

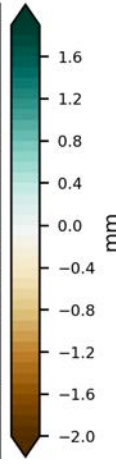
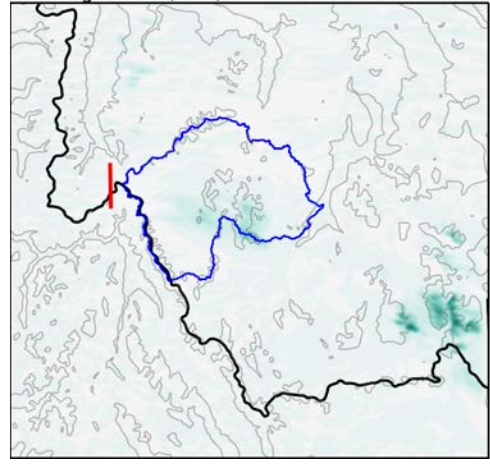
The simulated seeding effect was sensitive to a combination of track orientation and meteorological conditions; larger SLW values were noted over the Northern Beaverhead and Pioneer Mountains, and the Anaconda Range, and winds at 700 hPa were generally WNW. Airborne seeding at 3750 m consistently yielded a larger positive seeding effect than at 4250 m for all 5 westerly flight tracks (Figure 5.20; see Table 5.11), with W2 and W3 flights tracks at 3750 m producing the largest seeding effect in the Big Hole Basin (1003 and 919 AF, respectively). W5 flight tracks simulated positive seeding effects over the Pioneer Mountains (538 AF over the Big Hole Domain at 3750 m); however, it is worth noting that the W2 flight tracks produced a similar seeding effect over the Pioneer Mountains but also had additional positive simulated seeding effect over the Big Hole Basin west of the Pioneer Mountains. This might indicate that for westerly winds, the further upstream or westerly airborne tracks might be preferable. While positive simulated seeding effects are noted in the Big Hole Basin for all flight tracks, large downstream seeding effects over the Madison Mountains are seen outside of the basin, as well, with W2 and W5 flight tracks (3750 m) simulated 2314 AF and 2424 AF, respectively.



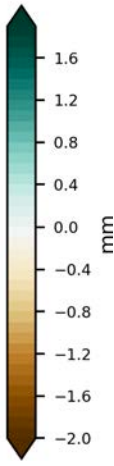
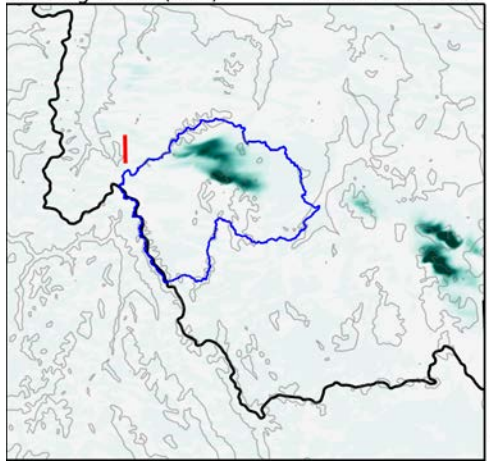
W2\_3750-CTRL  
Seeding Effect (mm) 2020-12-19 Case



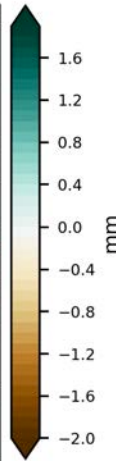
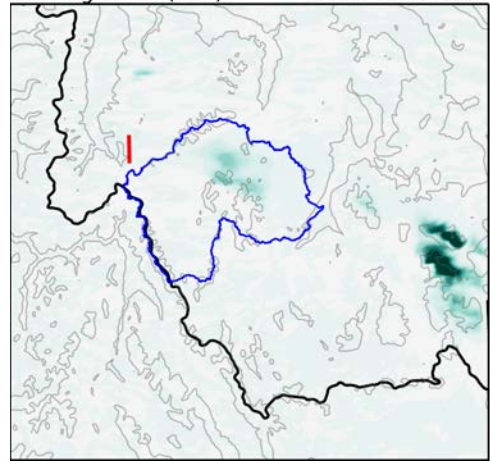
W2\_4250-CTRL  
Seeding Effect (mm) 2020-12-19 Case



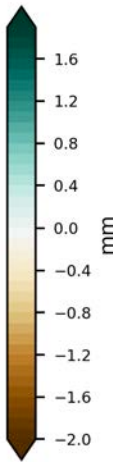
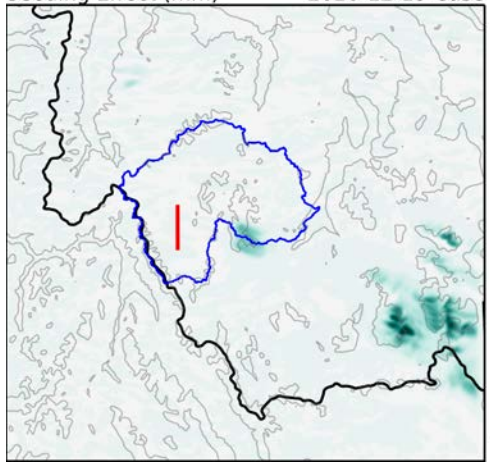
W3\_3750-CTRL  
Seeding Effect (mm) 2020-12-19 Case



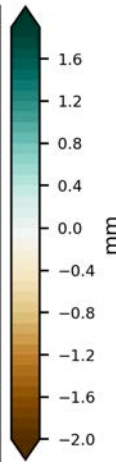
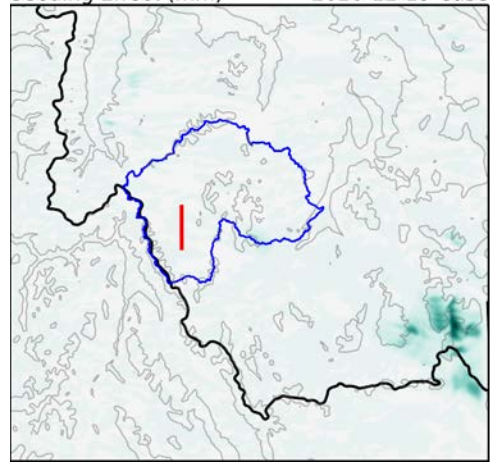
W3\_4250-CTRL  
Seeding Effect (mm) 2020-12-19 Case



W4\_3750-CTRL  
Seeding Effect (mm) 2020-12-19 Case



W4\_4250-CTRL  
Seeding Effect (mm) 2020-12-19 Case



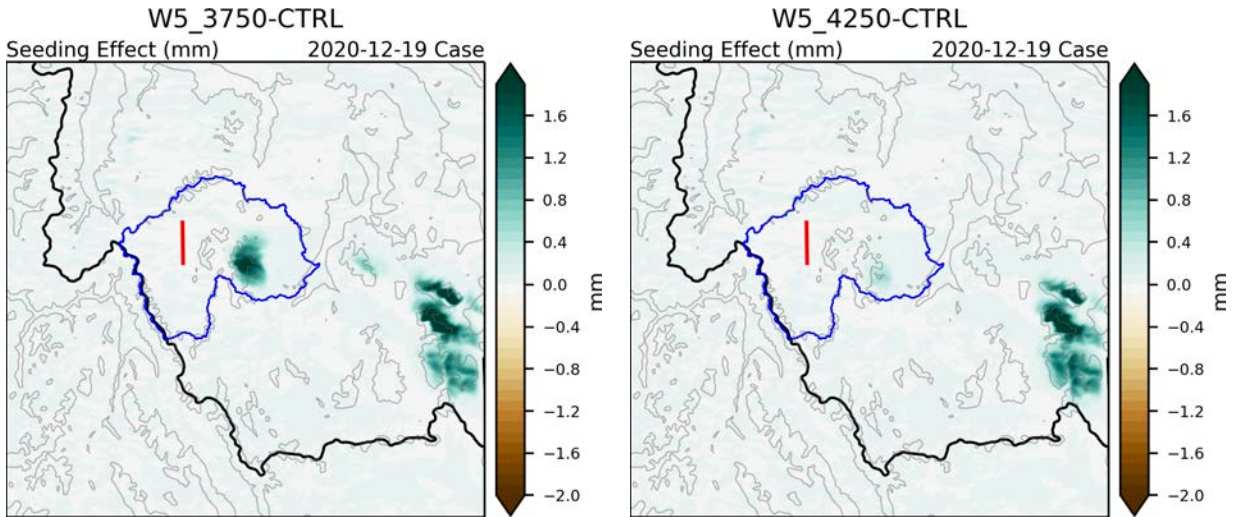


**Figure 5.20.** Simulated seeding effect from airborne seeding along the W1 track (first row), W2 track (second row), W3 track (third row), W4 track (fourth row), and W5 (fifth row) for the 3750 m above mean sea level (left) and 4250 m above mean sea level (right) for the 19 Dec. 2020 case study. Green hues indicate an increase in simulated precipitation due to seeding; brown hues indicate a decrease in simulated precipitation due to seeding.

**Table 5.11.** Simulated seeding effect for airborne tracks in Case 4.

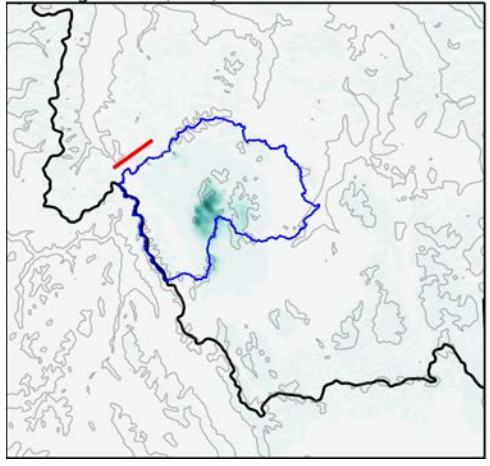
		Seeding Effect for 2020-12-19 [AF]				
		W1	W2	W3	W4	W5
3750m	BigHole	446	1003	919	94	538
	Domain	1936	2314	2016	1857	2424
4250m	BigHole	185	293	339	24	89
	Domain	1275	1210	1643	1160	1976

#### 5.5.4. Case 5: 28 February 2021

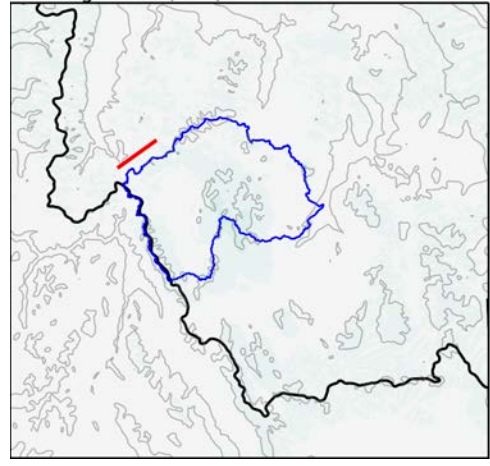
For case 5, the WRF-WxMod simulation began at 1600 UTC on 28 Feb. 2020, and airborne seeding commenced along northwesterly flight tracks at 2030 UTC. Seeding lasted 3 h, ending at 2330 UTC, and the simulation ended 3 h later at 0230 UTC on 1 March 2020.

Consistent with the other cases, airborne seeding at 3750 m yielded a larger positive seeding effect than at 4250 m for all flight tracks (Figure 5.21; see Table 5.12); in addition, most of the positive simulated seeding effect is concentrated within the Big Hole Basin, with minimal downstream seeding effect noted. The largest positive simulated seeding effect was from the NW1 track at 3750 m (411 AF in the Big Hole Basin; 524 AF in the domain). Generally, the smallest seeding effect was seen in the NW3 track, which is located within the Big Hole Basin, targeting the Pioneer Mountains. Similar to other airborne cases, flight tracks upstream and outside of the western edge of the Big Hole Basin tend to produce larger simulated seeding effects.

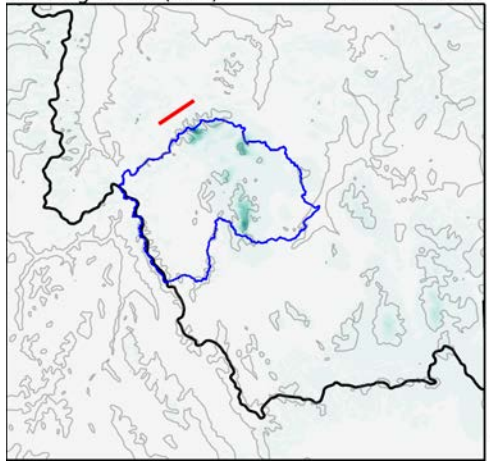
NW1\_3750-CTRL  
Seeding Effect (mm) 2021-02-28 Case



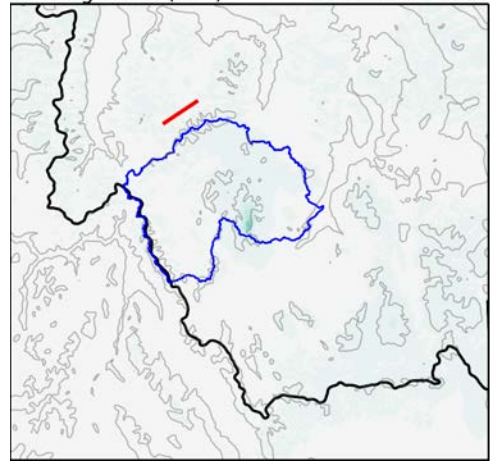
NW1\_4250-CTRL  
Seeding Effect (mm) 2021-02-28 Case



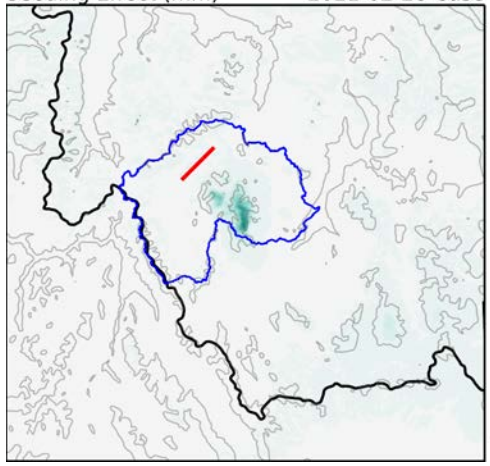
NW2\_3750-CTRL  
Seeding Effect (mm) 2021-02-28 Case



NW2\_4250-CTRL  
Seeding Effect (mm) 2021-02-28 Case



NW3\_3750-CTRL  
Seeding Effect (mm) 2021-02-28 Case



NW3\_4250-CTRL  
Seeding Effect (mm) 2021-02-28 Case

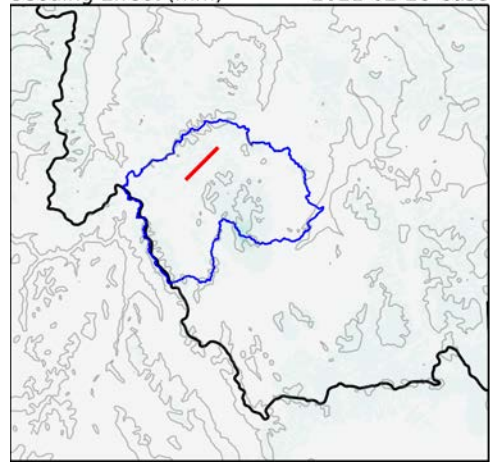


**Figure 5.21.** Simulated seeding effect from airborne seeding along the NW1 track (top), NW2 track (center), and NW3 track (right) for the 3750 m above mean sea level (left) and 4250 m above mean sea level (right) for the 28 Feb. 2021 case study. Green hues indicate an increase in simulated precipitation due to seeding; brown hues indicate a decrease in simulated precipitation due to seeding.

**Table 5.12.** Simulated seeding effect for airborne tracks in Case 5.

		Seeding Effect for 2021-02-28 [AF]		
		NW1	NW2	NW3
3750m	BigHole	411	282	246
	Domain	524	420	312
		NW1	NW2	NW3
4250m	BigHole	46	75	30
	Domain	83	114	57

## 5.6. Summary of Case Study Simulation

The effectiveness of cloud-seeding operations in Montana’s Big Hole Basin was examined using five case studies for ground seeding, with four of these cases also presenting favorable conditions for airborne seeding: 2018-11-02 (C1), 2019-12-14 (C2, no favorable airborne seeding condition), 2020-11-14 (C3), 2020-12-19 (C4), 2021-02-18 (C5). These cases were analyzed to determine the resulting impact of meteorological conditions, such as wind patterns and the presence of SLW and IWP, in the success of simulated cloud seeding missions. The overall program design recommendations detailed in [Section 6](#) are based on the simulated seeding effect with respect to the total mass of AgI, because it allows us to take into account the number of generators and seeding duration.

The ground-based simulation experiments evaluated 10 distinct generator groups (sets of 3 to 7 generators per group), and a reference experiment with all groups combined (45 generators in total). The simulated seeding effects from groups placed along the westward side of the Big Hole Basin (A, B, C, D, E, F) are more favorable for precipitation enhancements targeting the region than groups farther east. *The simulations for these groups indicate the effects are highly dependent on the wind direction and location of SLW.* For example, Group F is located at the northernmost side of the Big Hole Basin, and so its seeding potential to impact the target region decreases when wind directions are not predominantly from the NW. Groups C, D, and E, which are located further west, show greater simulated seeding effects in the case studies with W and NW wind directions.

- Groups A and C were the top performing generator groups for targeting the Big Hole Basin ([Table 5.13](#), top) and more broadly the full domain ([Table 5.13](#), bottom), although their effects decrease in wind directions with a predominantly N component (> 300 deg) as illustrated by Cases 1, 2 and 5.
- Group A showed the greatest total simulated seeding effect due to its efficiency in Case 3 for the Big Hole Basin and the full domain ([Table 5.14](#)), whereas groups A and C showed similarly large simulated effects in Case 4 over the full domain ([Table 5.14](#), bottom). This result reflects a combination of optimal wind direction for these groups’ locations combined with the location of the SLW in these simulations.

- [Figure 5.22](#) shows the AgI dispersion for groups A, B, and C in Cases 3, 4, and 5. Although Cases 3 and 4 show westerly wind directions (256 deg and 288 deg, respectively), the figure illustrates that a slight variation in the N-S components can substantially affect AgI dispersion. In Case 3, a mild southerly component favors the simulated seeding effect of groups A and B, whereas in Case 4, the dispersion from group C covers the Big Hole more broadly. In Case 5, the more prominent northerly component (321 deg) relative to the other cases is more favorable to group C (and also to groups D and E, not shown in the figure) than groups A and B. In any of these cases, the seeding effect ultimately depends on whether the AgI dispersion reaches the locations of available SLW, allowing ice and snowflakes to form, grow, and precipitate downwind.

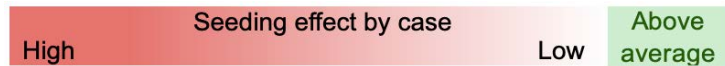
Even though generator groups G, H, I, and J show modest simulated seeding effects in some of the cases, the location of these groups (further east in the Big Hole Basin) leads to simulated seeding effects beyond the catchment of the Big Hole. This result is illustrated in the tables by the relatively greater seeding effect over the full simulation domain in comparison to the Big Hole Basin alone.

Finally, it should be noted that the convective nature of the precipitation, especially in Case 1, led to some numerical noise and dislocations of convective cells between the seeding and control simulations, which resulted in some simulations indicating potential decreases in precipitation accumulation over the Big Hole Basin. It is likely these are due to numerical noise; however, this warrants further investigation into the model-based methodology being employed herein (see [Appendix A](#)).

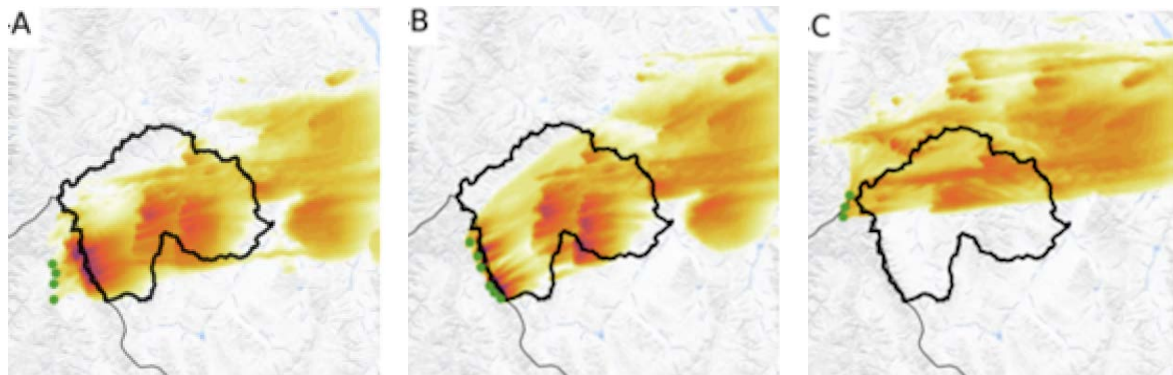
**Table 5.13.** *Simulated seeding effect normalized by mass of AgI for the Big Hole Basin (top) and total over the full simulation domain (bottom). The table rows show the different generator groups run independently as well as all groups run together ('all'), and the columns show the simulated case studies, including the total simulated seeding effect for all cases combined in the last column.*

		Agl-Normalized Seeding Effect [AF/kg]					
Group		C1	C2	C3	C4	C5	Total
		2018110221	2019121409	2020011409	2020121912	2021022816	
BigHole	gA	-11	-20	1520	678	19	2,188
	gB	-16	98	803	256	11	1,151
	gC	61	25	317	1500	232	2,136
	gD	28	231	34	197	501	991
	gE	44	100	24	250	421	839
	gF	-20	129	-2	222	281	611
	gG	-76	32	3	26	1	-13
	gH	-46	32	56	71	5	117
	gI	15	99	298	311	163	884
	gJ	-6	122	73	126	135	450
	All	29	61	220	278	116	705

		Agl-Normalized Seeding Effect [AF/kg]					
Group		C1	C2	C3	C4	C5	Total
		2018110221	2019121409	2020011409	2020121912	2021022816	
Domain	gA	543	934	1861	2232	33	5,603
	gB	186	296	1400	1580	28	3,490
	gC	95	453	1497	2172	454	4,670
	gD	387	155	415	224	784	1,965
	gE	710	101	277	280	708	2,075
	gF	1101	125	163	435	682	2,507
	gG	1324	32	100	53	152	1,661
	gH	744	26	1118	57	373	2,318
	gI	189	181	1313	1731	358	3,773
	gJ	400	127	1331	1471	455	3,783
	All	341	180	474	749	223	1,968



Case 3, 2020-01-14



Case 4, 2020-12-19

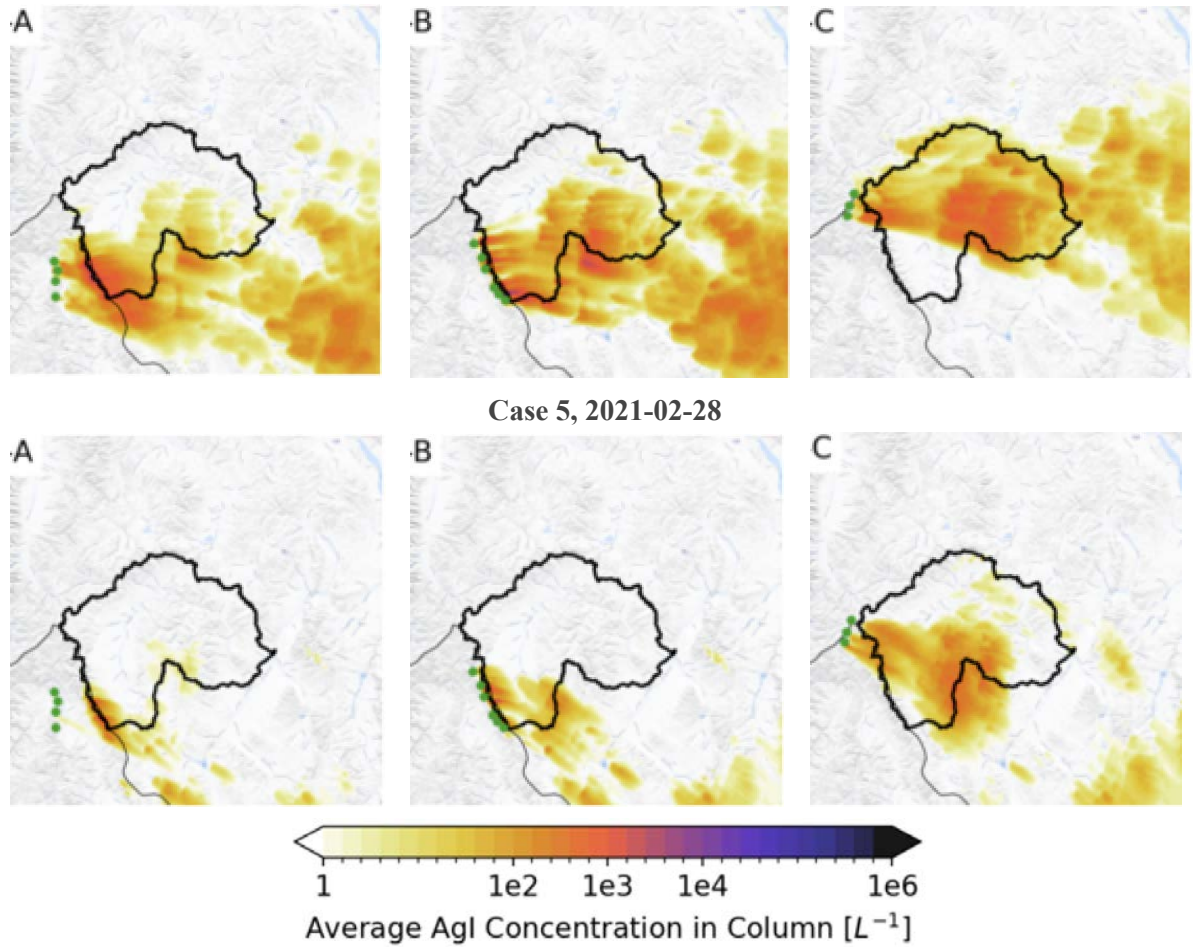


**Figure 5.22.** Spatial AgI dispersion represented by the average AgI concentration during the simulated seeding duration.

The airborne simulation experiments evaluated flight tracks at different orientations (favoring directions perpendicular to the predominant wind), of varying lengths, locations, and altitudes (3750 and 4250 m).

- The greater simulated seeding effect from lower tracks (3750 m) indicate the SLW was generally at a lower elevation for the cases simulated in this region.
- 
- In general, simulations of airborne seeding indicate that it can be highly effective for precipitation enhancement in the region.

**Table 5.14.** Simulated Seeding effect normalized by mass of AgI for the Big Hole Basin and total over the simulation domain. The table rows show the different flight tracks, and the columns show the simulated case studies. Rows with ‘-’ indicate the given flight track was not simulated in that case, given flight tracks are wind direction dependent, which will vary by each case which might be used.

		Agl-Normalized Seeding Effect [AF/kg]				
		3750m	C1	C3	C4	C5
		Track	2018110221	2020011409	2020121912	2021022816
BigHole	SW1	-	885	-	-	-
	SW2	-	195	-	-	-
	SW3	-	360	-	-	-
	NW1	618	-	-	-	437
	NW2	1325	-	-	-	300
	NW3	979	-	-	-	261
	W1	-	351	475	-	-
	W2	-	303	1067	-	-
	W3	-	22	978	-	-
	W4	-	260	100	-	-
	W5	-	127	572	-	-

		Agl-Normalized Seeding Effect [AF/kg]				
		3750m	C1	C3	C4	C5
		Track	2018110221	2020011409	2020121912	2021022816
Domain	SW1	-	1178	-	-	-
	SW2	-	353	-	-	-
	SW3	-	481	-	-	-
	NW1	1180	-	-	-	558
	NW2	1571	-	-	-	447
	NW3	1271	-	-	-	333
	W1	-	570	2060	-	-
	W2	-	336	2463	-	-
	W3	-	254	2146	-	-
	W4	-	640	1977	-	-
	W5	-	269	2580	-	-

Seeding effect by case  
  
 High Low

In Case 1, the airborne seeding simulations indicate a substantially greater seeding potential for airborne seeding than for ground-based seeding. This was likely due to an elevated altitude of SLW in this case, as it had more convective cloud features as well. In addition, the simulated airborne seeding effect for this case with track NW2 was largely obtained over the Big Hole target (84% of the simulated seeding effect accumulated over the Big Hole).

In contrast to Case 1, Case 3 showed ground-based seeding potentially yielding a greater simulated seeding effect than airborne seeding, likely due to the location of SLW near the ground. Ground generator groups A and B showed the largest simulated seeding effect (1520 and 803 AF, respectively), with Beaverhead North being the primary target. Airborne seeding using the SW1 track was the only track to yield a similar simulated seeding effect (885 AF).

For Case 4, both ground and airborne seeding showed potential, supported by ample, widespread SLW and favorable westerly winds. Simulations of seeding with ground generator groups A and C (678 and

1500 AF, respectively), along with airborne tracks W2 and W3 (1067 and 978 AF, respectively), effectively targeted the Beaverhead North and Anaconda West.

Similarly, for Case 5, both ground-based and airborne seeding demonstrated potential; the environment was characterized by smaller, diffuse amounts of SLW combined with NW winds. Ground generator groups D and E (501 and 421 AF, respectively), along with NW1 and NW2 tracks (437 and 300 AF, respectively), targeted the Pioneer Mountains.

In general, based on the climatology analysis where greater SLW is near the surface, ground seeding opportunities are more frequent; nonetheless, when dispersion criteria are considered, ground-based seeding has reduced frequencies in some regions. The effectiveness of ground seeding is highly dependent on wind direction, orientation of ranges, and location of the generator groupings. Airborne seeding can be more versatile and the model simulations have shown it to be effective, oftentimes more so than ground-based seeding; however, the climatology indicates opportunities for airborne seeding are less frequent. Simulations of airborne seeding using the 3750 m altitude show a larger simulated seeding effect than the 4250 m altitude, which matches with results from the climatology analysis, where more SLW is at lower altitudes.

## 5.7. Cost-Benefit Analysis

A cost-benefit analysis was conducted to compare the cost of potential cloud seeding to the potential benefit (i.e. streamflow) that could result from the cloud seeding. The potential benefit of streamflow from cloud seeding was calculated using an estimated change in streamflow relative to a change in precipitation using regressions of historical precipitation and streamflow records from the CONUS404 simulation. This method was similar to that used in other weather-modification feasibility studies (e.g., Wyoming Range, Bighorn Mountains). There are several estimations and assumptions required for this approach, including the magnitude of the seeding effect on precipitation, which includes impact amount and spatial area of impact, and the relationship of winter snowfall to streamflow runoff, all of which contribute to a substantial range of uncertainty in the results. The components of this analysis include:

- Calculation of the 'runoff ratio' to estimate the streamflow relationship to precipitation (snowpack)
- Estimation of the amount of total seasonal snowpack that could be impacted by seeding based upon the fraction of seedable precipitation from the feasibility analysis
- Apply assumptions about the spatial impact area and percentage increase of precipitation from seeding to calculate the estimated amount of precipitation increase to apply to the fraction of seedable precipitation and runoff ratio to estimate potential streamflow impacts
- Comparisons of potential streamflow impacts to cost estimates of operating cloud seeding programs to calculate a cost per acre foot estimate

A first-order estimate of the runoff ratio using precipitation and runoff simulated by the CONUS404 simulation. Model output of runoff includes both surface and sub-surface runoff from the Noah-MP Land Surface Model (LSM). The simulation was not run with a hydrological model, which would give detailed hydrological routing of runoff to water bodies such as streams, rivers, and lakes. Therefore, the current

dataset does not allow for an estimate of runoff amount that distributes to specific rivers/streams. However, the model dataset allows us to examine the spatial distribution of runoff and give insight to the relationship between the distribution of precipitation and runoff. It should be further noted that snow water equivalent (SWE) is substantially underestimated over the full CONUS404 domain (Rasmussen 2023); this bias is not accounted for in this study but could have meaningful impacts on the estimates provided in this section.

[Figure 5.23](#) contains a scatter plot showing the relationship between April–July simulated runoff in elevated terrain in the target region compared to April 1 SWE. Data points are from model grid values within the target basin, excluding points whose average April 1 SWE is negligible. The relationship between these two values indicates how much water stored in the mountain snow ultimately becomes runoff water, with higher values indicating a more efficient transfer of mountain snowpack to downstream water. Using the best-fit line for the simulated runoff and April 1 SWE, the ratio of snowpack increase to streamflow increase is estimated to be 0.74. The results of Super and McPartland (1993) indicated that the ratio of snowpack increase to streamflow increase observed at several locations in Colorado, Utah, and Wyoming varied between 0.6 and 2.1 with a median of 1.05. Detailed hydrological models tend to show ratios much less than 1.0 (e.g., Acharya et al. 2011); thus, the resulting 0.74 from the runoff to SWE best-fit is within reason. The average April 1 SWE within the basin is 240 mm, and the average basin April to July runoff is 1.3 million AF.

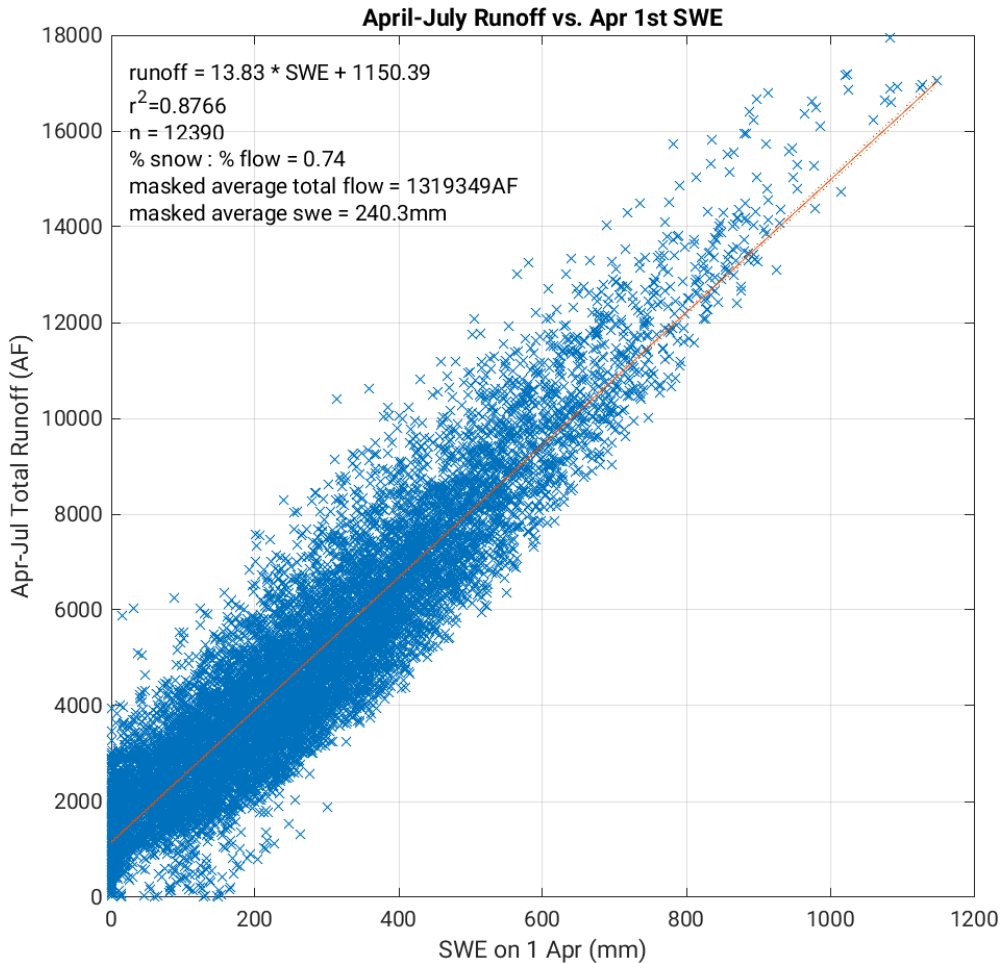


**Figure 5.23.** Scatter plot of simulated total runoff (acre feet) during April through July compared with SWE (mm) on April 1st, excluding points whose 40-year average April 1 SWE is less than 10 mm. The red line shows the best fit.

[Section 4](#) provides seasonal estimates of the frequency of seedable conditions for multiple targets within the Big Hole Basin. For ground-based seeding, the most favorable seedable conditions (with respect to fraction of precipitation falling during seedable periods) occurred with seeding from the Group C generators in Beaverhead North, and precipitation simulated at Saddle Mountain, accounting for roughly 37% of the total winter (November–April) precipitation on average for the 40-year climatology. Across all of the target regions, the median fraction of precipitation falling during ground-based seedable conditions was 30%. Airborne seeding conditions affected 31–42% of the total precipitation on average for the same period across all regions, with a median value of 35%. For the calculations used in estimating the streamflow changes due to cloud seeding, the median values of fraction of seedable precipitation are used.

The spatial coverage of seeding effects varies depending on the storm and seeding conditions. Following the methodology of the Wyoming Weather Modification Pilot Project (WWMPP) and subsequent seeding feasibility studies in Wyoming, a range of 50–80% impact area will be used here. This area only considers the Big Hole Basin and does not include any of the potentially substantial precipitation changes seen in the modeling case studies beyond the southern and eastern basin periphery.

Streamflow change calculations are performed similarly to the technique in the WWMPP report, using an estimated 5–15% range of seeding effects relative to seedable storms. [Figure 5.24](#) shows estimated streamflow increases at various estimated seeding effects relative to seedable storms for ground-based or airborne seeding, where the shaded regions indicate the uncertainty based on areal coverage (50–80%), and key values for ground-based and airborne seeding are summarized in [Table 5.15](#) and [Table 5.16](#), respectively.

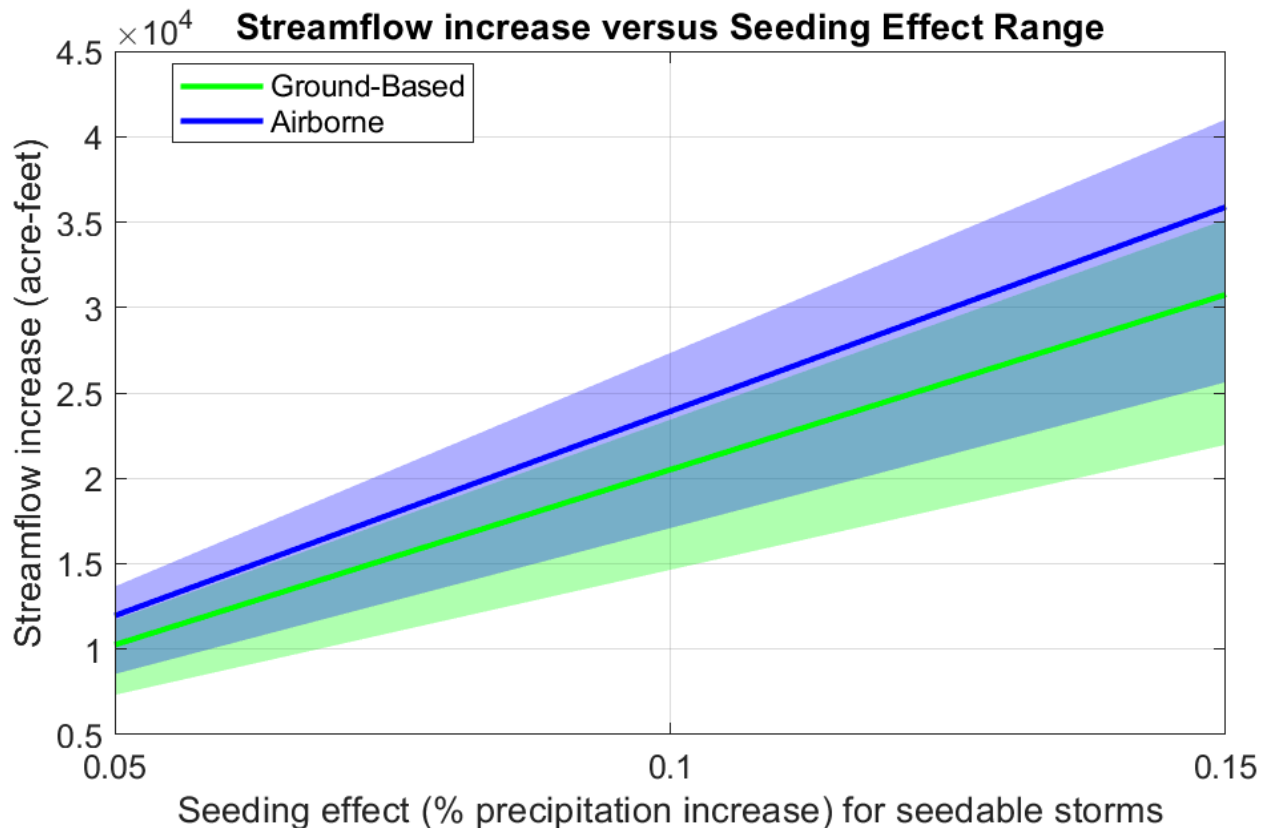


**Figure 5.24.** Estimates of streamflow increases into the study area using 5, 10, and 15% levels of seasonal seeding effects for seedable storms. The streamflow calculations include adjustments to relate the seeding effects to total assessment area precipitation, which requires an estimate of assessment area seeding coverage. The range of streamflow estimates for the various levels of area coverage (50–80%) are denoted by the different color-shaded areas. The 70% area coverage (solid lines within the color-shaded areas) are used for streamflow estimates assumed in the benefit/cost calculations. Ground-based seeding is indicated by green colors, and airborne by blue.

**Table 5.15.** Streamflow increase estimates using various seeding impact parameters for a ground-based seeding program (5, 10, 15% seeding effect and 50–80% seeding impact area). Estimated April–July streamflow increases (AF) are provided using the 70% impact area (shaded row) estimated increases. Seeding impact is calculated as the product of the seed effect (SE; first row), the portion of precipitation occurring during seedable conditions (pcp/total pcp; see Section 4.6), and the ratio of snowpack increase to streamflow increase (%flow:%snow = 0.74; see above).

	Seeding Effect Scenario
--	-------------------------

Seed Effect	5%	10%	15%
Seeding Impact (SE * (pcp/total pcp) * (%flow:%snow))	1.11%	2.22%	3.33%
50% area	0.56%	1.11%	1.66%
70% area	0.78%	1.55%	2.33%
80% area	0.89%	1.78%	2.66%
Apr-Jul Streamflow Increase (AF) @ 1.3 MAF total	10,251.34	20,502.68	30,754.03

**Table 5.16.** Streamflow increase estimates using various seeding impact parameters for an airborne seeding program (5, 10, 15% seeding effect and 50–80% seeding impact area). Estimated April–July streamflow increases (AF) are provided using the 70% impact area (shaded row) estimated increases. Seeding impact is calculated as the product of the seed effect (SE; first row), the portion of precipitation occurring during seedable conditions (pcp/total pcp; see Section 4.6), and the ratio of snowpack increase to streamflow increase (%flow:%snow = 0.74; see above).

Seed Effect	Seeding Effect Scenario		
	5%	10%	15%
Seeding Impact SE * (pcp/total pcp) * (%flow:%snow)	1.29%	2.59%	3.89%
50% area	0.65%	1.30%	1.94%
70% area	0.91%	1.81%	2.72%
80% area	1.04%	2.07%	3.11%
Apr-Jul Streamflow Increase (AF) @ 1.3 MAF total	11,959.90	23,919.80	35,879.70

Cost estimates are generated following recommendations from the modeling results in [Section 5](#). Resource costs are estimated from 2024 operational budgets in surrounding regions. Assuming 10–20 remote generators (~\$150k–\$300k annual) and 1 aircraft (~\$700k annual) and supporting forecasting and operational labor (~\$30k), an approximate annual cost of combined ground-based and airborne seeding operations is \$1.03M. These costs are only for operations and not for initiating a new program (i.e. permit fees, etc). There are several opportunities to greatly reduce this cost. Given that the Beaverhead targets have the greatest frequency of opportunities, a program running only 10 generators and cost sharing with operations in Idaho could reduce the cost of ground-based operations by a substantial amount. Since the Big Hole region is accessible and well-populated, it may be feasible to operate manual generators throughout the basin rather than remotes, reducing the cost of the additional, Montana-only targeting (e.g.,

generator groups I and J). It is important to note that model estimates of seeding impact were conducted assuming a remote generator release rate. It may also be reasonable to share an aircraft with any operations around the Lemhi basin in Idaho; however, further analysis would need to be done to see how frequently each basin would individually benefit from using a shared aircraft.

Estimated costs per AF of streamflow for a ground-based only (assuming 20 generators) and an airborne only program are summarized in [Table 5.17](#). The results of [Section 4](#) indicate minimal overlap between ground-based and airborne seeding opportunities; thus, an additional row considering a combined program is included using the total precipitation falling during airborne or ground-based operations.

**Table 5.17.** Cost per AF estimates using various seeding impact parameters for an airborne or ground-based seeding program (5, 10, 15% seeding effect and 50–80% seeding impact area). Ground-based cost assumes 20 remote generators operated by a single program.

Source	Cost (\$)	Minimum \$/AF (80% area, 15% effect)		Maximum \$/AF (50% area, 5% effect)	
		Effect (AF)	\$/AF	Effect (AF)	\$/AF
Ground	330,000	30754	10.73	10251	32.19
Airborne	730,000	35879	20.35	11959	61.04
Combined	1,030,000	66633	15.46	22210	46.38

## 6. Overall Summary and Recommendations

This report summarizes the results of the feasibility assessment of cloud-seeding potential, as well as the preliminary design that was developed and tested. A fact sheet was also developed, and public meetings were held to present the concepts of cloud seeding and preliminary results of this study to various audiences and stakeholders in the Big Hole Basin and surrounding areas. The public meetings included substantial time for addressing questions and concerns as well.

### Cloud-seeding potential

The potential for cloud seeding was assessed by conducting a climatological analysis of historical data. The historical precipitation data from SNOTEL snow gauge observations, as well as from the CONUS404 simulation, showed that the greatest wintertime precipitation (>800 mm) falls in the Beaverhead Mountains on the western divide of the Big Hole Basin. The Anaconda Range in the north is also a focal point for winter precipitation (>700 mm), while the Pioneer Mountains, in the center of the basin, typically accumulate much less precipitation during the winter (400-600 mm on average).

Given the lack of observations beyond precipitation data from SNOTEL gauges, the rest of the climatological analysis was conducted using the CONUS404 simulation to assess the frequency of opportunities for cloud seeding. Especially of interest, in order to characterize and quantify potential seeding opportunities, is the presence of SLW at appropriate temperatures for AgI to nucleate ice, referred

to as seedable SLW. The key areas that have enhanced frequency of seedable SLW are the same regions where the greatest wintertime precipitation falls. The ground-seeding layer has greater overall frequencies of seedable SLW than the airborne seeding layer, though the locations of seedable conditions are largely the same between the two layers. The less frequent seedable SLW in the airborne layer is in part due to the SLW being more common closer to the ground in these regions than at the aircraft flight altitude.

When considering additional factors that are important for ground-based seeding to be effectively dispersed over the targeted mountain barrier, namely wind direction, wind speed, and stability of the atmosphere, some of the regions with the greatest frequency of seedable SLW in the ground-based layer are reduced due to the limited wind direction sector and/or potential for flow blocking that would inhibit the AgI released to reach the targeted clouds over the Big Hole Basin. The northern Beaverhead Mountains had minimal reduction in seeding opportunities due to dispersion criteria though, and showed just over 20% of the wintertime period being amenable for ground-based seeding. The Anaconda Range also showed a similar frequency of opportunities. . The aircraft layer analysis showed most regions had between 10–12% of the winter having seedable SLW. Airborne seeding is less impacted by wind direction limitations or flow blocking since the aircraft can release the AgI directly in the cloud, and these opportunities are not reduced by other atmospheric conditions like they are for ground-based seeding. However, it is important to note that aircraft have limited flight time, so a single aircraft may not be able to fully target all of the available opportunities. The ability of ground-based seeding to effectively disperse and impact the targeted clouds compared to airborne seeding was evaluated with WRF-WxMod modeling simulations as part of the preliminary design testing.

From the climatology analysis, ground-based seeding in the northern Beaverhead Mountains has the most potential, even more so than aircraft seeding based upon the overall frequency of seeding opportunities. Analysis of a future climate simulation that represents a warming climate indicates that SLW in the region will generally increase, while temperatures generally warm. Therefore, airborne seeding opportunities would increase; however, with warming temperatures especially near the surface, ground-based seeding opportunities may decrease.

### **Preliminary program design**

Based upon the climatological analysis, preliminary designs for both airborne and ground-based cloud seeding programs were developed and tested with WRF-WxMod. These designs included 10 groups of hypothetical ground-based generators and various aircraft flight tracks. The design options were tested using multiple case studies that represent various common weather patterns in the region (based upon the climatological analysis). Each ground-based seeding case study was simulated to test all hypothetical ground-based generator groups combined as well as each group individually.

The simulated seeding effects from hypothetical ground generator groups placed along the westward side of Big Hole Basin (A, B, C, D, E, and F) were shown to be more favorable for achieving simulated precipitation enhancements targeting the Big Hole than hypothetical generator groups farther east. *The simulations for these groups indicate the effects are highly dependent on the wind direction and location of SLW.* For example, Group F is located at the northernmost side of the Big Hole, and so its potential to impact the Big Hole decreases when wind directions are not predominantly from the north or northwest. Groups A and C were the top performing generator groups for targeting the Big Hole and beyond,

although their effects for targeting the Big Hole may be diminished in wind directions with a predominantly northerly component (yet they could impact regions south of the Big Hole in those situations). Even though the eastern generator groups (G, H, I, and J) showed more modest simulated seeding effects in some of the cases, the location of these groups leads to simulated seeding effects downwind beyond the catchment of the Big Hole, so they may be effective overall, but less so for immediately targeting the Big Hole Basin. In summary, Groups A, B, and C are the primary generator groups being recommended, and Groups D, E, and I may be secondary groups depending on the extent of the ground-based seeding program to be deployed. [Figure 6.1](#) provides a map of these final recommendations of ground-based generators for cloud seeding.

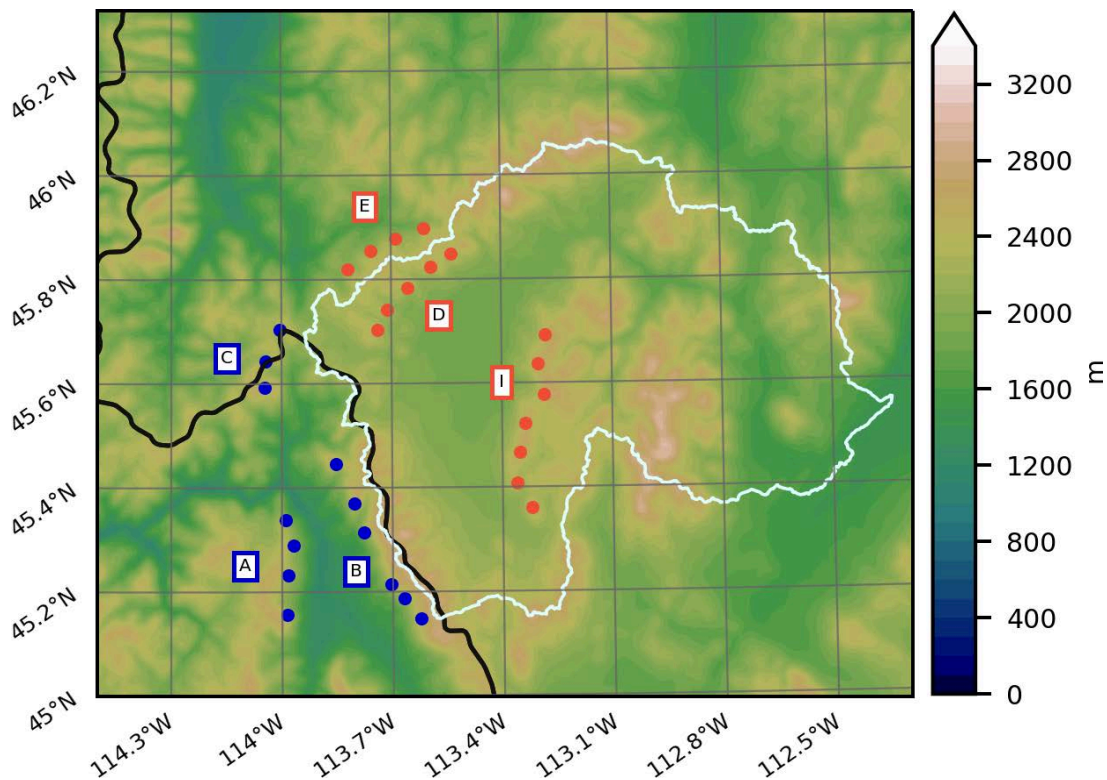


**Figure 6.1.** Recommended generator groups. The primary generator groups being recommended are blue (A, B, and C), and the secondary generator groups are salmon (D, E, I).

The airborne seeding simulation experiments evaluated seeding flight tracks at different orientations (favoring directions perpendicular to the predominant wind of each case), of varying lengths, locations, and altitudes (3750 and 4250 m). The results showed greater simulated seeding effects from lower altitude tracks (3750 m) in all cases. This is an indication that the SLW was generally at a lower altitude for the cases simulated in this region, which was also reflected in the climatology analysis that indicated most SLW was most frequently at lower altitudes. In general, simulations of airborne seeding indicated that it can be highly effective for precipitation enhancement in the region, perhaps more so than for ground-based seeding, given the flight tracks can be versatile to accommodate the SLW and wind conditions for each case. [Figure 6.2](#) provides the final recommendations of airborne cloud-seeding flight

tracks. These should be adjusted for operations based upon wind speed, direction, and the location of SLW based upon the forecast for each case.

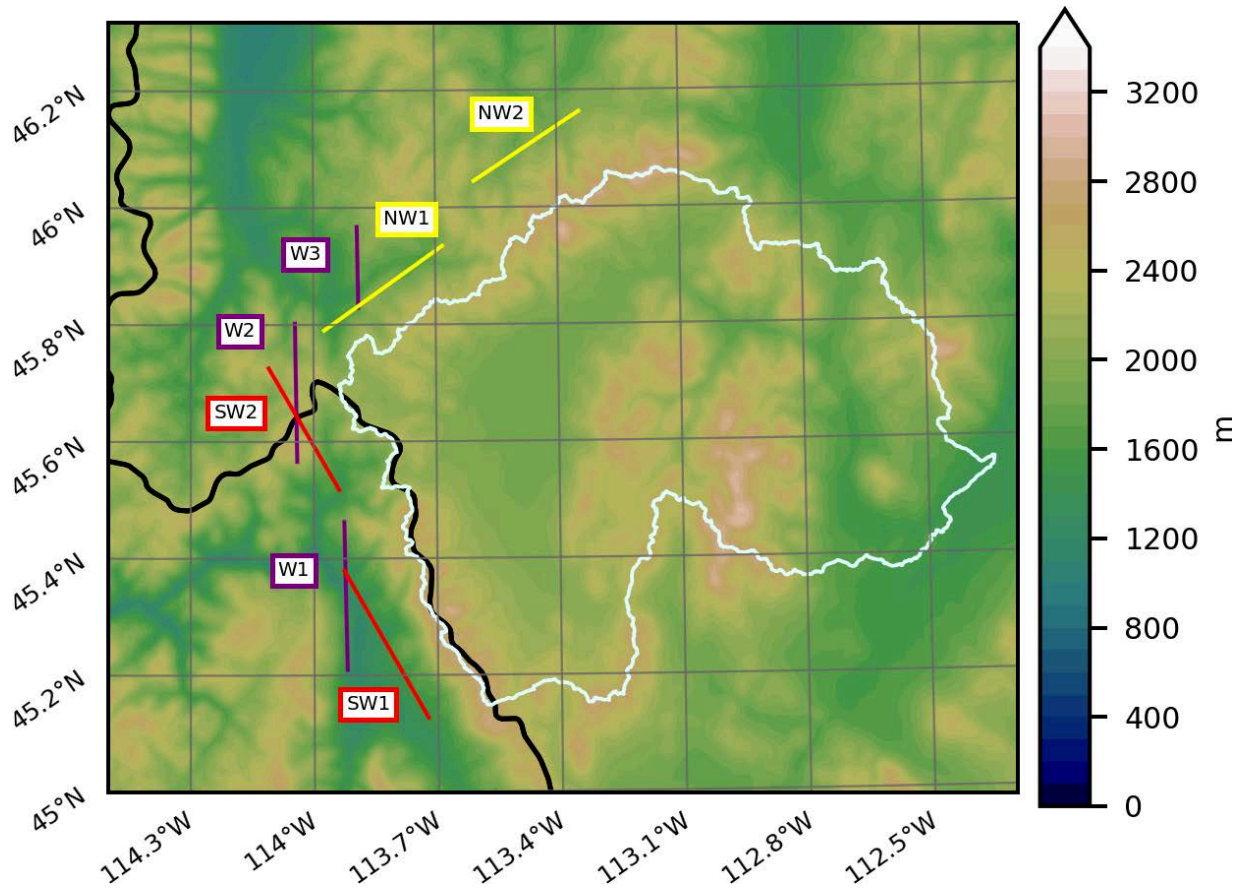


**Figure 6.2.** Recommended airborne cloud-seeding flight tracks; western flight tracks are in purple, southwestern flight tracks are in red, and northwestern flight tracks are in yellow.

### Cost benefit

The potential benefit of streamflow from cloud seeding was calculated using an estimated change in streamflow relative to a change in precipitation using regressions of historical precipitation and streamflow records from the CONUS404 simulation combined with climatological estimates of the fraction of seedable precipitation and estimated ranges of seeding impact areas and magnitudes. These estimates were compared to ballpark costs of cloud seeding operations to calculate a cost per acre foot from potential seeding. This analysis indicated that costs of water produced by seeding could be in the range of approximately \$10 to \$60 per acre foot in this region, depending on the type of seeding and the magnitude of its impact. A program including both ground-based and airborne operations would maximize targeting capability—especially since conditions rarely occur at both heights simultaneously—resulting in a very small increase in cost per AF relative to the less expensive ground-based program alone, but with a non-trivial potential increase in water produced.

In summary, the climatological analysis suggests that ground seeding, at least in some mountain ranges surrounding the Big Hole (namely the Beaverhead Mountains), may have more potential than airborne

seeding due a greater frequency of seeding opportunities in the lowest layer of the atmosphere than at higher altitudes. However, some mountain ranges may be constrained by wind direction to target the Big Hole and/or impacted by flow blocking thereby limiting the potential for ground-based seeding, and making it occur less frequently than airborne seeding. Airborne seeding simulations have shown that airborne seeding is effective in a variety of cases in the region. Airborne seeding generally has greater operational costs than ground seeding, depending on the type and number of ground-based generators. Yet, the versatility and more consistent climatology of airborne seeding opportunities (without potential flow blocking limitations of ground seeding) and the effectiveness of airborne seeding in the WRF-WxMod simulations led to similar cost-benefit estimates for ground and airborne seeding in this region. This indicates that while ground-based seeding may cost less overall, the amount of water potentially produced by ground-based seeding may also be less.

### **Program design and pilot study recommendations**

The following recommendations are made based upon the results of this cloud seeding feasibility and design study. These recommendations can be used to develop a pilot cloud-seeding program in the region.

- Based upon the overall SLW and wind direction frequencies, the Beaverhead Mountains should be a primary focus for seeding, which presents opportunities to share a seeding program with Idaho.
  - Hypothetical ground generators in Groups A-C should be explored, with Group A in particular being most relevant to Idaho interests.
  - Airborne seeding should also be considered, in conjunction with ground seeding for this region as it has versatility to target multiple wind directions and locations in the region and has been shown to be effective. A combined ground and airborne seeding program may provide the most overall opportunities for seeding given the climatology of seeding opportunities for ground and airborne tended to not occur simultaneously.
    - Flight tracks should be focused on the western portion of the region to most effectively target the Big Hole Basin, given flight tracks farther east (in the middle of the Big Hole) tended to have more simulated precipitation enhancement downwind of the Big Hole.
- While less frequent and strongly dependent on the occurrence of northwesterly winds, the Anaconda Range could be a secondary target, utilizing ground generators Groups D-E. However, airborne seeding could target these wind conditions and may be more advantageous than ground seeding in this region.
- The Pioneer Mountains should also be a secondary target; however, they can be targeted by upwind seeding facilities (e.g., Groups A-E generator sites or airborne seeding). A section of possible generators in Group I may also be considered to target this area and may be more feasible and cost effective as manual generator sites, though manual generator release rates were not explicitly tested in this study.
- Ground-based seeding should focus on the November through February months for the most favorable flow and greatest amount of SLW.
- Opportunities to share infrastructure for a cloud seeding program with Idaho should be explored to further boost the cost-benefit by reducing the State of Montana's cost of operations.

It should also be noted that these recommendations are focused on targeting the Big Hole Basin, however the results of this study also indicate that there is the potential for cloud seeding to enhance precipitation in other regions of Montana surrounding the Big Hole. Therefore, even if some of the generator groups or aircraft flight tracks were not recommended for the Big Hole, they may have potential for use to target the surrounding regions.

Based upon these results and recommendations, for a cloud-seeding pilot program, we recommend an initial focus on the Beaverhead Mountains and siting 8-12 generators in the primary generator groups A-C. We recommend a pilot study that would include three winter seasons of seeding, to capture year-to-year variability in seeding opportunities and storm conditions, along with an evaluation component after each year of seeding, so the total project period would roughly span four years. Besides the greatest opportunities for seeding in the Beaverhead Mountains region, there is also an opportunity to partner with the State of Idaho, which could lead to cost sharing and reduced overall program costs for a pilot program. However, a shared infrastructure study to determine how to design a combined program that benefits both states would be a valuable next step before beginning a pilot project shared with Idaho. Aircraft-based seeding could also be deployed in this region for a pilot study and would be most cost efficient if shared with the State of Idaho as well. A low cost addition to the pilot study could include 2-4 manual generators sited on the western slopes of the Pioneer Mountains (Group I), however this aspect would not be amenable to cost sharing with Idaho.

Besides the cloud-seeding facilities (i.e. ground generators and/or seeding aircraft), a pilot program would also need to include forecasters who determine when to seed and who operate the program. Additional instrumentation would be helpful for a pilot study, to help aid forecasters in determining when to seed, as well as to provide data for an evaluation of the pilot program. Recommended instrumentation includes high-resolution precipitation gauges, a measure of the SLW in the clouds from icing rate sensors or a microwave radiometer, and weather balloon launches to assess cloud temperatures, winds, and atmospheric stability. Numerical weather prediction models would also be helpful for forecasting seeding events.

To complete the pilot study, an evaluation would be recommended that includes analysis of any observational data collected, as well as a numerical model-based evaluation study of all seeded events to estimate the impact of seeding on precipitation and/or streamflow. A best practice is for the evaluation to be conducted independent from the entity operating the cloud-seeding program. Numerical modeling tools like WRF-WxMod and WRF-Hydro are valuable for program evaluation. Statistical analyses are another option for program evaluation, however such approaches are not conclusive when sample sizes are small and therefore often require 10+ years to build a statistically-robust sample of cases. In contrast, a numerical modeling evaluation can be conducted on a storm-by-storm or year-by-year basis, and can be constrained by observations collected during the pilot program.

# List of Acronyms

AF: Acre-Feet  
AgI: Silver Iodide  
AGL: Above Ground Level  
ASCII: AgI Seeding Cloud Impact Investigation  
BOR: Bureau of Reclamation  
CAIC: Colorado Avalanche Information Center  
CC: Current Climate  
CESM2: Community Earth System Model 2  
CFAD: Contoured Frequency by Altitude Diagrams  
CWCB: Colorado Water Conservation Board  
CONUS404: 40-year high-resolution (4-km) Weather Research and Forecasting (WRF) model simulation  
DNRC: Department of Natural Resources and Conservation  
ECMWF: European Centre for Medium-Range Weather Forecasts  
ERA5: ECMWF Reanalysis version 5  
HB: House Bill  
HIPLEX: High Plains Cooperative Research Program  
IDWR: Idaho Department of Water Resources  
IPC: Idaho Power Company  
IWC: Ice Water Content  
IWRB: Idaho Water Resources Board  
INP: Ice Nucleating Particle  
IWP: Ice Water Path  
LENS2: Large Ensemble Community Project  
LSM: Land Surface Model  
LWC: Liquid Water Content  
MMF: Miguez-Macho-Fan groundwater scheme  
MSL: Mean Sea Level  
Noah-MP: Noah multi-physics LSM  
NRCS: U.S. Department of Agriculture Natural Resource Conservation Service  
NSF NCAR: National Science Foundation National Center for Atmospheric Research  
NWS: National Weather Service  
OBS: Observations  
PBL: Planetary Boundary Layer  
PGW: pseudo-global warming  
RRTMG: Rapid Radiative Transfer Model for GCMs  
SB: Senate Bill  
SLW: Supercooled Liquid Water  
SLWP: Supercooled Liquid Water Path  
SNOTEL: Snow Telemetry snow gauge network  
SNOWIE: Seeded and Natural Orographic Wintertime clouds: the Idaho Experiment  
UDWR: Utah Division of Water Resources  
UTC: Coordinated Universal Time

WRF: Weather Research and Forecasting  
WWDC: Wyoming Water Development Commission  
WWDO: Wyoming Water Development Office  
WWMPP: Wyoming Weather Modification Pilot Project

## References

- Acharya, A., T. Piechota, H. Steven, and G. Tootle, 2011: Modeled streamflow response under cloud seeding in the North Platte River watershed. *J. Hydrology*, **409**, 305–314.
- Ancell, B. C., A. Bogusz, M. J. Lauridsen, and C. J. Nauert, 2018: Seeding Chaos: The Dire Consequences of Numerical Noise in NWP Perturbation Experiments. *Bull. Amer. Meteor. Soc.*, **99**, 615–628, <https://doi.org/10.1175/BAMS-D-17-0129.1>.
- Barlage, M., F. Chen, R. Rasmussen, Z. Zhang, G. Miguez-Macho, 2021: The importance of scale-dependent groundwater processes in land-atmosphere interactions over the Central United States. *Geophys. Res. Lett.*, **48**(5), doi: 10.1029/2020GL092171.
- Bergeron, T., 1949: The problem of artificial control of rainfall on the globe. I. General effects of ice-nuclei in clouds. *Tellus*, **1**, 32–43.
- Breed, D., R. Rasmussen, C. Weeks, B. Boe, and T. Deshler, 2014: Evaluating Winter Orographic Cloud Seeding: Design of the Wyoming Weather Modification Pilot Project (WWMPP). *J. Appl. Meteor. Climatol.*, **53**, 282–299, <https://doi.org/10.1175/JAMC-D-13-0128.1>.
- Carr, J.T. Jr., 1981: Cooperative Weather Modification Project. *Journal of the Water Resources Planning and Management Division*, **107**, 97-104, doi: 10.1061/JWRDDC.0000209.
- Colorado Department of Natural Resources, 2012: Colorado Weather Modification Rules and Regulations. <https://dnrweblink.state.co.us/CWCB/0/edoc/210673/WeatherModRegs.pdf>
- Coons, R. D., R. C. Gentry, and R. Gunn, 1948: First partial report on the artificial production of precipitation: Stratiform clouds, Ohio. *Bull. Amer. Met. Soc.*, **29**, 266–269.
- DeMott, P. J., 1995: Quantitative descriptions of ice formation mechanisms of silver iodide-type aerosols. *Atmos. Res.*, **38**, 63–99.
- Dennis, A.S., 1983: Augmentation of rainfall from summer cumulus clouds. *Agricultural Water Management*, **7**, 3-14, [https://doi.org/10.1016/0378-3774\(83\)90070-7](https://doi.org/10.1016/0378-3774(83)90070-7).
- Findeisen, W., 1938: Kolloid-meteorologische Vorgänge bei Niederschlagsbildung. – *Meteorol. Z.* **55**, 121–133. (translated and edited by Volken, E., A.M. Giesche, S. Brönnimann. – *Meteorol. Z.* **24** (2015), DOI: 10.1127/metz/2015/0675)
- Friedrich, K., K. Ikeda, S. A. Tessendorf, J. French, Rauber, R.M., B. Geerts, L. Xue, R. M. Rasmussen, D. R. Blestrud, M. L. Kunkel, N. Dawson, and S. Parkinson, 2020: Making snow—Quantifying snowfall from orographic cloud seeding. *Proc. Natl. Acad. Sci.*, doi: 10.1073/pnas.1917204117.
- French, J.R., K. Friedrich, S.A. Tessendorf, R.M. Rauber, B. Geerts, R.M. Rasmussen, L. Xue, M.L. Kunkel, and D.R. Blestrud, 2018: Precipitation formation from orographic cloud seeding. *Proc. Natl. Acad. Sci.*, doi: 10.1073/pnas.1716995115.
- Geerts, Bart, Binod Pokharel, Katja Friedrich, Daniel Breed, Roy Rasmussen, Yang Yang, Qun Miao, Samuel Haimov, Bruce Boe, and Evan Kalina, 2013: The AgI seeding cloud impact investigation (ASCII) campaign 2012: Overview and preliminary results. *J. Wea. Modif.*, **45**, 24-43.
- Geresdi, I., R. Rasmussen, W. Grabowski, and B. Bernstein, 2005: Sensitivity of freezing drizzle formation in stably stratified clouds to ice processes. *Meteor. Atmos. Phys.*, **88**, 91–105, <https://doi.org/10.1007/s00703-003-0048-5>.
- Hallett, J. and Mossop, S. C., 1974: Production of Secondary Ice Particles during the Riming Process. *Nature*, **249**, 26–28. <https://doi.org/10.1038/249026a0>
- Harrold, M. A., S. A. Tessendorf, L. Xue, J. K. Wolff, E. M. Dougherty, D. J. Gochis, B. Geerts, 2024: Evaluating the Precipitation Impacts of Cloud Seeding in the Medicine Bow and Sierra Madre Ranges

- Using WRF-WxMod® within an Ensemble Modeling Framework. *24th Conference on Planned and Inadvertent Weather Modification*, Baltimore, MD, January 28-February 1, 2024.
- Hong, S.-Y., Y. Noh, and J. Dudhia, 2006: A new vertical diffusion package with an explicit treatment of entrainment processes. *Mon. Wea. Rev.*, **134**, 2318–2341, doi:10.1175/MWR3199.1.
- Hoose, C., O. Mohler, 2012: Heterogeneous ice nucleation on atmospheric aerosols: a review of results from laboratory experiments. *Atmos. Chem. Phys.*, **12**, 9817–9854.
- Huggins, A. W., 1995: Mobile microwave radiometer measurements: Spatial characteristics of supercooled cloud water and cloud seeding implications. *J. Appl. Meteor.*, **34**, 432–446.
- Iacono, M. J., J. S. Delamere, E. J. Mlawer, M. W. Shephard, S. A. Clough, and W. D. Collins, 2008: Radiative forcing by long-lived greenhouse gases: Calculations with the AER radiative transfer models. *J. Geophys. Res.*, **113**, D13103, doi:10.1029/2008JD009944.
- Johnson, J. B., and D. Marks, 2004: The detection and correction of snow water equivalent pressure sensor errors. *Hydrological Processes*, **18**, 3513–3525.
- Kraus, E. B., and P. Squires, 1947: Experiments on the simulation of clouds to produce rain. *Nature*, **159**, 489–491.
- Langmuir, I., 1948: The growth of particles in smokes and clouds and the production of snow from supercooled clouds. *Proc. Am. Philos. Soc.*, **92**, 167.
- Mazzetti, T., B. Geerts, and L. Xue, 2023: A Numerical Evaluation of the Impact of Operational Ground-Based Glaciogenic Cloud Seeding on Precipitation over the Wind River Range, Wyoming. *J. Appl. Meteor. Climatol.*, **62**, 489–510, <https://doi.org/10.1175/JAMC-D-22-0132.1>.
- Miguez-Macho, G., Fan Y., Weaver C. P., Walko R., and Robock A., 2007: Incorporating water table dynamics in climate modeling: 2. Formulation, validation, and soil moisture simulation. *J. Geophys. Res.*, **112**, D13108, doi:10.1029/2006JD008112.
- Niu, G.-Y., and Coauthors, 2011: The community Noah land surface model with multiparameterization options (Noah-MP): 1. Model description and evaluation with local-scale measurements. *J. Geophys. Res.*, **116**, D12109, doi: 10.1029/2010JD015139.
- Rasmussen, R., and Coauthors, 2012: How well are we measuring snow? The NOAA/FAA/NCAR Winter Precipitation Test Bed. *Bull. Amer. Meteor. Soc.*, **93**, 811– 829.
- Rasmussen, R. M., Tessendorf, S. A., Xue, L., Weeks, C., Ikeda, K., Landolt, S., Breed, D., Deshler, T., & Lawrence, B., 2018: Evaluation of the Wyoming Weather Modification Pilot Project (WWMPP) Using Two Approaches: Traditional Statistics and Ensemble Modeling. *J. Appl. Meteor. Climatol.*, **57**(11), 2639–2660.
- Rasmussen, R. M., and Coauthors, 2023: CONUS404: The NCAR–USGS 4-km Long-Term Regional Hydroclimate Reanalysis over the CONUS. *Bull. Amer. Meteor. Soc.*, **104**, E1382–E1408, <https://doi.org/10.1175/BAMS-D-21-0326.1>.
- Rauber, R. M., and L. O. Grant, 1986: The characteristics and distribution of cloud water over the mountains of northern Colorado during wintertime storms. Part II: Spatial distribution and microphysical characteristics. *J. Appl. Meteor. Climatol.*, **25**, 489–504.
- Rauber, R. M., and Coauthors, 2019: Wintertime Orographic Cloud Seeding—A Review. *J. Appl. Meteor. Climatol.*, **58**, 2117–2140, <https://doi.org/10.1175/JAMC-D-18-0341.1>.
- Rodgers, K. B., Lee, S.-S., Rosenbloom, N., Timmermann, A., Danabasoglu, G., Deser, C., Edwards, J., Kim, J.-E., Simpson, I. R., Stein, K., Stuecker, M. F., Yamaguchi, R., Bódai, T., Chung, E.-S., Huang, L., Kim, W. M., Lamarque, J.-F., Lombardozzi, D. L., Wieder, W. R., and Yeager, S. G.: Ubiquity of

- human-induced changes in climate variability, *Earth Syst. Dynam.*, **12**, 1393–1411, <https://doi.org/10.5194/esd-12-1393-2021>, 2021.
- Schaefer, V. J., 1946: The production of ice crystals in a cloud of supercooled water droplets. *Science* **104**, 457–459.
- Serreze, M. C., M. P. Clark, R. L. Armstrong, D. A. McGinnis, and R. S. Pulwarty, 1999: Characteristics of the western United States snowpack from snowpack telemetry (SNOTEL) data. *Water Resour. Res.*, **35**, 2145–2160.
- Serreze, M. C., M. P. Clark, and A. Frei, 2001: Characteristics of large snowfall events in the montane western United States as examined using snowpack telemetry (SNOTEL) data. *Water Resour. Res.*, **37**, 675–688.
- Skamarock, W. C., and Coauthors, 2008: A description of the Advanced Research WRF version 3. NCAR Tech. Note NCAR/TN-475+STR, 113 pp., doi:10.5065/D68S4MVH.
- Super, A. D., 1986: Further Exploratory Analysis of the Bridger Range Winter Cloud Seeding Experiment. *J. Appl. Meteor. Climatol.*, **25**, 1926–1933, [https://doi.org/10.1175/1520-0450\(1986\)025<1926:FEAOTB>2.0.CO;2](https://doi.org/10.1175/1520-0450(1986)025<1926:FEAOTB>2.0.CO;2).
- Super, A. B., and J. A. Heimbach, 1983: Evaluation of the Bridger Range Winter Cloud Seeding Experiment Using Control Gages. *J. Appl. Meteor. Climatol.*, **22**, 1989–2011, [https://doi.org/10.1175/1520-0450\(1983\)022<1989:EOTBRW>2.0.CO;2](https://doi.org/10.1175/1520-0450(1983)022<1989:EOTBRW>2.0.CO;2).
- Super, A.B., and J.T. McPartland, 1993: Preliminary estimates of increased runoff from additional high elevation snowfall in the Upper Colorado River Basin. *J. Wea. Modif.*, **25**, 74–81.
- Tessendorf, S.A., J. French, K. Friedrich, B. Geerts, R.M. Rauber, R. M. Rasmussen, L. Xue, K. Ikeda, D. Blestrud, M. Kunkel, S. Parkinson, J. R. Snider, J. Aikins, S. Faber, A. Majewski, C. Grasmick, P. Bergmaier, A. Janiszewski, A. Springer, C. Weeks, D. J. Serke, and R. Bruintjes, 2019: Transformational approach to winter orographic weather modification research: The SNOWIE Project. *Bull. Amer. Meteor. Soc.*, **100**(1), 71–92.
- Thompson, G., Field, P. R., Rasmussen, R. M., & Hall, W. D., 2008: Explicit Forecasts of Winter Precipitation Using an Improved Bulk Microphysics Scheme. Part II: Implementation of a New Snow Parameterization, *Mon. Wea. Rev.*, **136**(12), 5095–5115. <https://doi.org/10.1175/2008MWR2387.1>
- Thompson, G. and T. Eidhammer, 2014: A study of aerosol impacts on clouds and precipitation development in a large winter cyclone. *J. Atmos. Sci.*, **71**, 3636–3658.
- Thompson, G., J. Berner, M. Frediani, J. A. Otkin, and S. M. Griffin, 2021: A Stochastic Parameter Perturbation Method to Represent Uncertainty in a Microphysics Scheme. *Mon. Wea. Rev.*, **149**, 1481–1497, <https://doi.org/10.1175/MWR-D-20-0077.1>.
- Vonnegut, B., 1947: The nucleation of ice formation by silver iodide. *J. Appl. Phys.*, **18**, 593–595.
- Xue, L., A. Hashimoto, M. Murakami, R. Rasmussen, S. Tessendorf, D. Breed, S. Parkinson, P. Holbrook, and D. Blestrud, 2013a: Implementation of a Silver Iodide Cloud Seeding Parameterization in WRF: Part 1: Model Description and Idealized 2D Sensitivity Tests. *J. Appl. Meteor. Climatol.*, **52**, 1433–1457.
- Xue, L., S. Tessendorf, E. Nelson, R. Rasmussen, D. Breed, S. Parkinson, P. Holbrook, and D. Blestrud, 2013b: Implementation of a Silver Iodide Cloud Seeding Parameterization in WRF: Part 2: 3D Simulations of Actual Seeding Events and Sensitivity Tests. *J. Appl. Meteor. Climatol.*, **52**, 1458–1476.
- Xue, L., X. Chu, R. Rasmussen, D. Breed, B. Boe, and B. Geerts, 2014: The dispersion of silver iodide particles from ground-based generators over complex terrain. Part 2: WRF large-eddy simulations

- versus observations. *J. Appl. Meteor. Climatol.*, **53**, 1342–1361, <https://doi.org/10.1175/JAMC-D-13-0241.1>.
- Xue, L., X. Chu, R. Rasmussen, D. Breed, and B. Geerts, 2016: A case study of radar observations and WRF LES simulations of the impact of ground-based glaciogenic seeding on orographic clouds and precipitation. Part II: AgI dispersion and seeding signals simulated by WRF. *J. Appl. Meteor. Climatol.*, **55**, 445–464, <https://doi.org/10.1175/JAMC-D-15-0115.1>.
- Xue, L., and Coauthors, 2017: WRF large-eddy simulations of chemical tracer deposition and seeding effect over complex terrain from ground- and aircraft-based AgI generators. *Atmos. Res.*, **190**, 89–103, <https://doi.org/10.1016/j.atmosres.2017.02.013>.
- Xue, L., and others, 2022: Comparison between observed and simulated AgI seeding impacts in a well-observed case from the SNOWIE field program. *J. Appl. Meteor. Climatol.*, **61**, 345–367. <https://doi.org/10.1175/JAMC-D-21-0103.1>.
- Xue, L., Rasmussen, R.M., Chen, F., Liu, C., Ikeda, K., Prein, A., Kim, J., Schneider, T., Dai, A., Gochis, D., Dugger, A., Zhang, Y., Jaye, A., Dudhia, J., He, C., Harrold, M., Chen, S., Newman, A., Dougherty, E., Abolafia-Rozenzweig, R., Lybarger, N., Viger, R., Rasmussen, K., and Miguez-Macho, G., 2024: CONUS404 PGW: Four-kilometer long-term regional hydroclimate reanalysis perturbed with pseudo-global warming (PGW) conditions over the conterminous United States. *U.S. Geological Survey data release*, <https://doi.org/10.5066/P9HH85UU>.
- Yang, D., B. E. Goodison, J. R. Metcalfe, V. S. Golubev, R. Bates, T. Pangburn, and C. L. Hanson, 1998: Accuracy of NWS 8" standard nonrecording precipitation gauge: results and application of WMO intercomparison. *J. Atmos. Oceanic Technol.*, **15**, 54–68.

# Appendix A: Investigating Sensitivities to Simulated Precipitation

When the 2 Nov. 2018 case was originally scoped, two potential seeding windows were identified. The first seeding window was identified as being early on 2 Nov. 2018, and the second seeding window was identified as being early on 3 Nov. 2018. For the experiment design, the two seeding windows were included in one, longer simulation. The first seeding window did not produce a significant simulated seeding effect, and it was ultimately decided to resimulate the event, focusing only on the second seeding window. However, in the process of analyzing the results, it was noticed that the precipitation differences of the seeded and control run over the full simulation had some areas of noisier differences; these areas typically were outside of the main area of positive simulated seeding effect. To better understand how numerical noise in gridpoint models can propagate, two additional types of experimental simulations were performed.

Ancell et al. (2018) demonstrated that small, artificial perturbations can rapidly propagate through a model grid in time and space, introducing difficulty distinguishing between real atmospheric processes and perturbation-related artifacts, which can have obvious impacts on interpretation of results and predictability, especially in this case of simulating impacts of cloud seeding relative to a control (no seeding) simulation. To investigate the sensitivity of simulations to small perturbations, the first experiment included adding random noise to the water vapor mixing ratio in the initial conditions (based on methodology in Thompson et al. 2021). A noise field with random samples from a normal distribution was created, and then the water vapor mixing ratio field in the initial conditions was perturbed between -1% and 1% of the original field using the generated noise field. Using the newly generated initial conditions, a control run (i.e., no seeding) was performed. [Figure A.1](#) shows the differences between the original control simulation and the simulation with perturbed initial conditions. While most grid points have small differences between the two control simulations, there are more coherent areas that exceed 2 standard deviations, indicating that by simply adding noise to the initial conditions, sensitivities to precipitation are noted. These larger sensitivities are often seen over higher terrain.

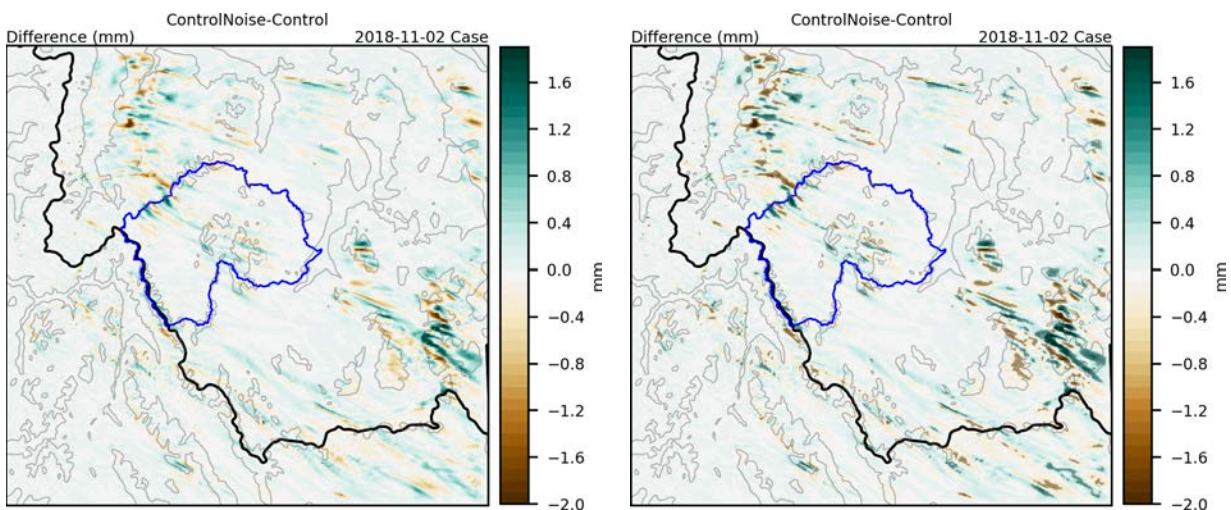


**Figure A.1.** Runtime precipitation differences (mm) of the original control simulation from the simulation with perturbed water vapor mixing ratio in the initial conditions (left). Green (brown) hues indicate the perturbed simulation has greater (less) precipitation than the original control simulation. The precipitation differences were calculated over the length of the entire simulation (0200 UTC 2 Nov. 2018 – 0900 UTC 3 Nov. 2018). Precipitation differences that exceed  $\pm 2$  standard deviations are shaded (right).

The second experiment focused on performing a simulation with the same initial and boundary conditions as well as model configuration, but on a different HPC system. For this experiment, the additional simulation was performed on Montana Tech’s HPC platform, Oredigger. WRF-WxMod was compiled on Oredigger with Intel, which is what was used for the original control simulation on NSF NCAR HPC, Derecho; however, other external library and compiler-related dependencies differed slightly from Derecho. [Figure A.2](#) shows the differences between the original control simulation and the simulation performed on Oredigger. Even with the same initial and boundary conditions and model configuration options, by changing the compute platform, small differences in the precipitation field are introduced, and they grow with time by the end of the full simulation. Similar to the first experiment with perturbations, larger differences are noted over areas of higher terrain.

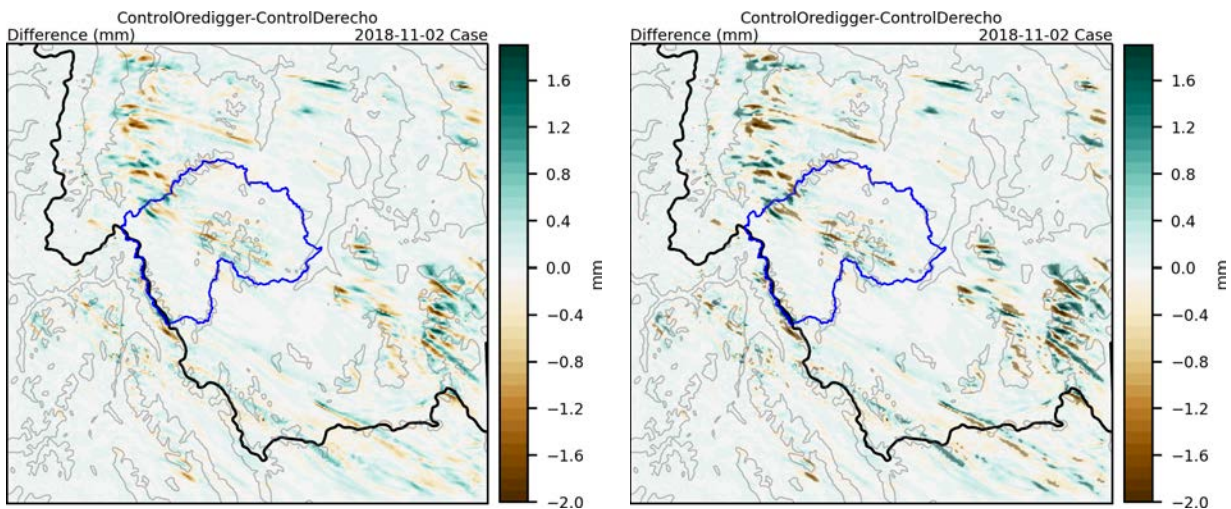


**Figure A.2.** Runtime precipitation differences (mm) of the original control simulation performed on Derecho from the simulation performed on Oredigger (left). Green (brown) hues indicate the simulation on Oredigger has greater (less) precipitation than the original control simulation on Derecho. The precipitation differences were calculated over the length of the entire simulation (0200 UTC 2 Nov. 2018 – 0900 UTC 3 Nov. 2018). Precipitation differences that exceed  $\pm 2$  standard deviations are shaded (right).

While these additional experiments focused on control simulations with no seeding, the key findings can be extended when interpreting results from seeding simulations. In some simulations (e.g., ground-based seeding in Case 1) where minimal impact from seeding is noted over the Big Hole Basin, signals that are small or noisy need cautious interpretation. Numerical instabilities are often small compared to the physical impacts from seeding. Therefore, in areas where the seeding effect is minimal and difficult to

discern, it is possible that a sum of precipitation differences over an area may result in small, net negative values due to numerical noise.

## Appendix B: Case 2 (14 December 2019)

For Case 2, the WRF-WxMod simulation began at 0900 UTC on 14 Dec. 2019. Simulated ground-based seeding commenced at 1200 UTC on 14 Dec. 2019 and lasted 3.5 h, ending at 1530 UTC. The simulation ended 3 h later at 1830 UTC.

Key environmental conditions at various times throughout the simulation period are shown in [Figure B.1](#). At 1200 UTC on 14 Dec. 2020, winds at 700 hPa (left column) were northwest over the northwest portion of the Big Hole Basin, while a more northerly flow was generally dominant over the eastern and southern portions. As the simulation progressed, wind direction shifted slightly, becoming more from the NNW. IWP was generally small over the Big Hole Basin, with the greatest values at 1530 UTC, but never exceeding 0.2 mm in the basin. SLWP was present in the northern and western portions of the basin at 1200 UTC, becoming slightly more widespread by 1345 UTC. At 1530 UTC, the greatest SLWP shifted south but generally had small values over the basin.

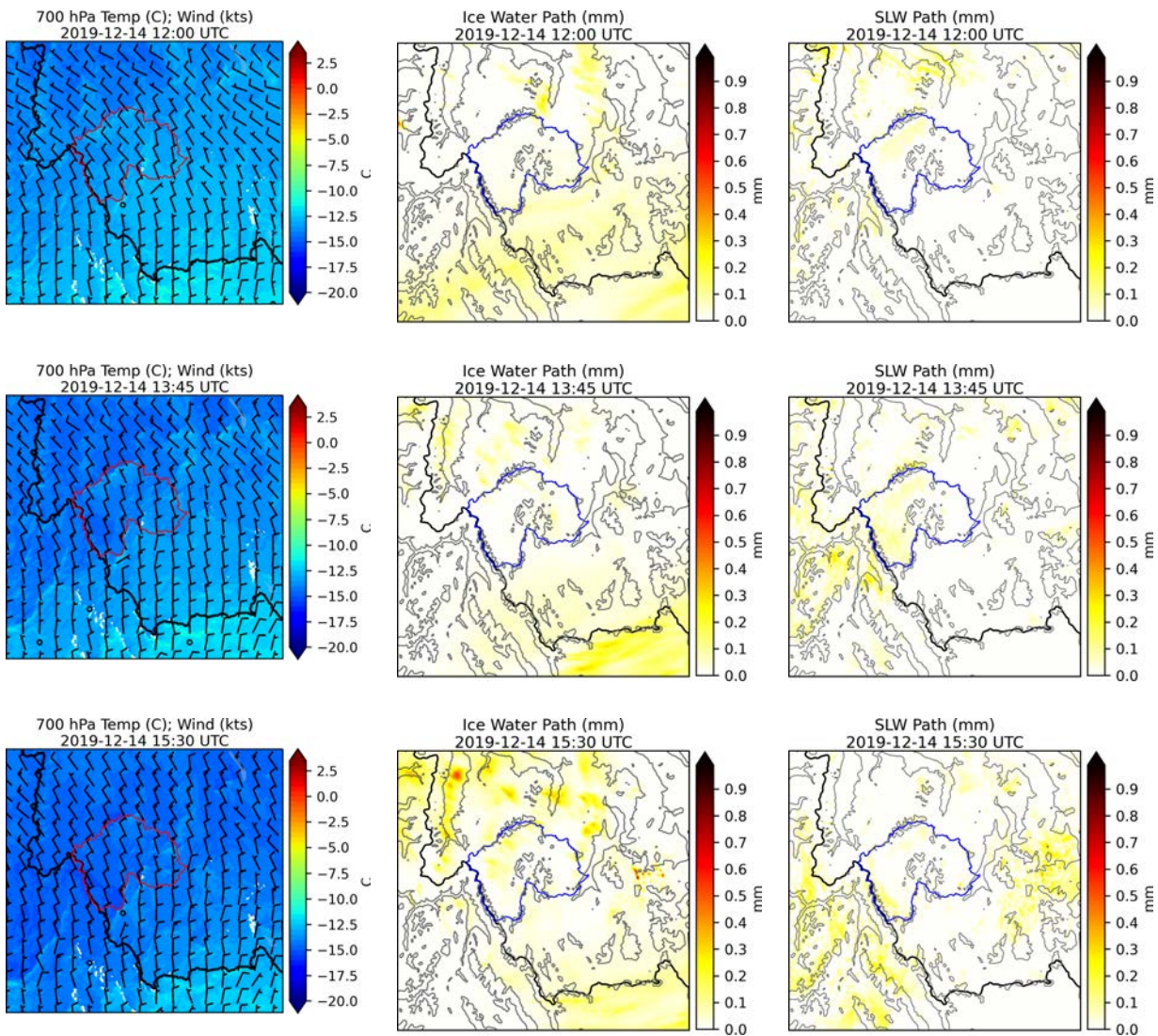


**Figure B.1.** Temperature ( $^{\circ}\text{C}$ ) and wind barbs (knots) at 700 hPa (left column), IWP (mm; middle column), and SLWP (mm; right column) at 1200 UTC on 14 Dec. 2019 (top row), 1345 UTC on 14 Dec. 2019 (middle row), and 1530 UTC on 14 Dec. 2019 (bottom row) from the control simulation.

The total control precipitation from the control simulation for Case 2 is shown in [Figure B.2](#). Overall, the area of maximum precipitation is in the NW portion of the computational domain, outside of the Big Hole Basin. The Anaconda Range has areas of local maxima of precipitation in excess of 5 mm, but most of the Big Hole Basin has  $<2$  mm of accumulated precipitation over the full simulation.

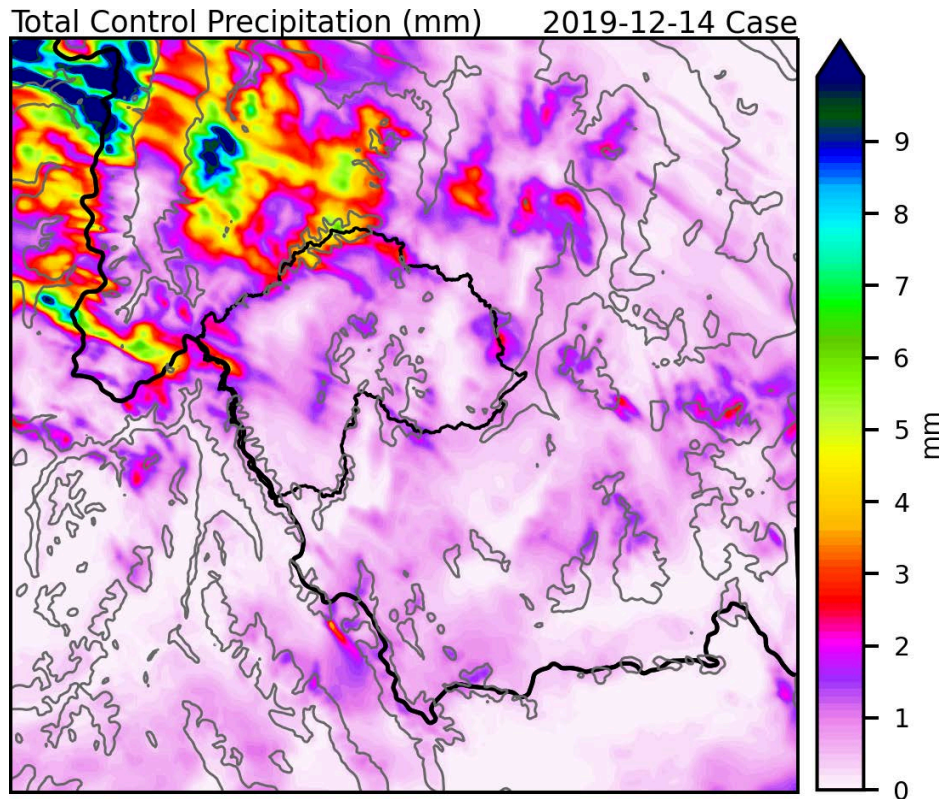
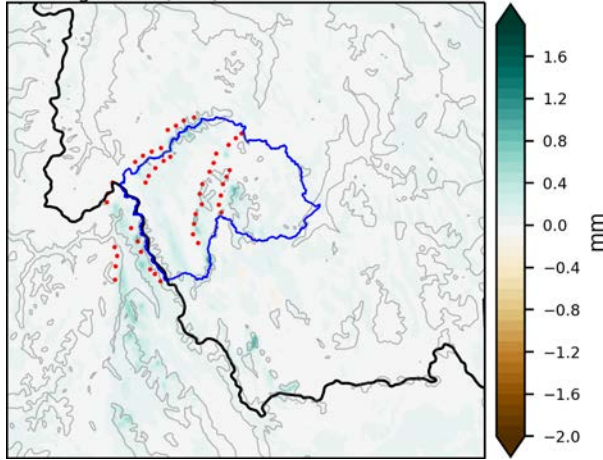


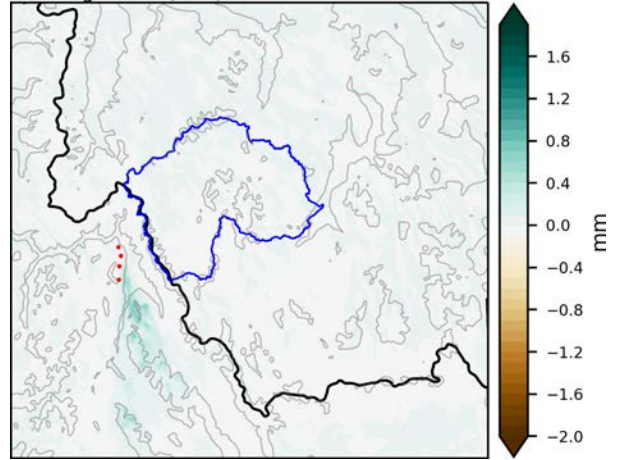
**Figure B.2.** Total control precipitation (mm) for the 14 Dec. 2019 case (0900 UTC 14 Dec. - 0600 UTC 15 Dec. 2019).

The simulated seeding effects for the 14 Dec. 2019 case for all generators and each individual generator are shown in [Figure B.3](#). Overall, the simulated seeding effect for all individual generator groups was small – both over the Big Hole Basin and across the entire domain (see [Table B.1](#)). This was likely driven by the primarily NNW flow, presence of diffuse areas of IWP and minimal SLWP over the Big Hole Basin. Due to the wind direction, generator groups D, I and J had the largest, but still modest, simulated seeding effects over the Big Hole Basin (81 AF, 48 AF, and 51 AF, respectively). Generator groups A and B had the largest positive simulated seeding effects over the full domain (262 AF and 124 AF, respectively), but the enhanced precipitation primarily fell in Idaho, due to the wind direction and location of generators.

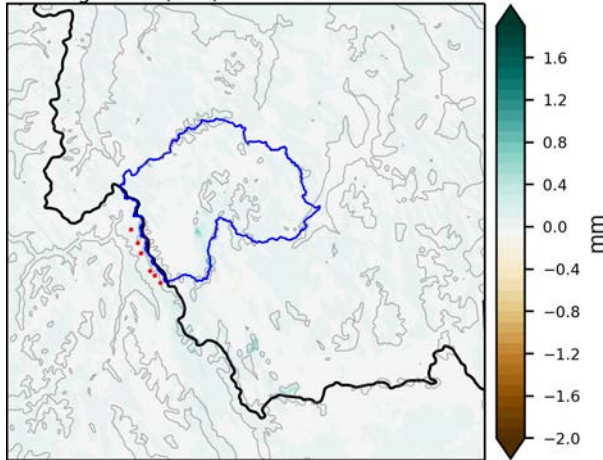
ALL-CTRL  
Seeding Effect (mm) 2019-12-14 Case



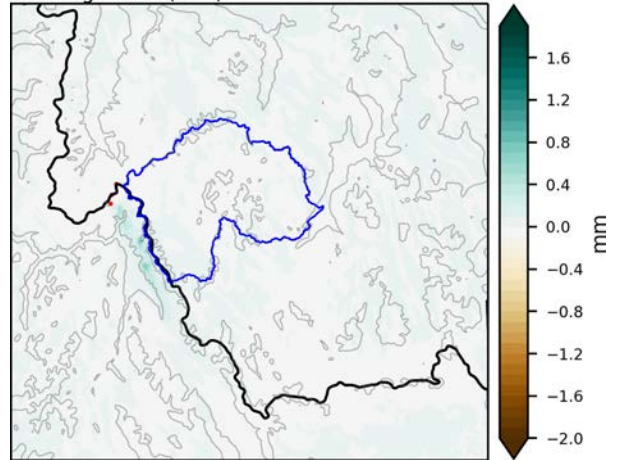
A-CTRL  
Seeding Effect (mm) 2019-12-14 Case



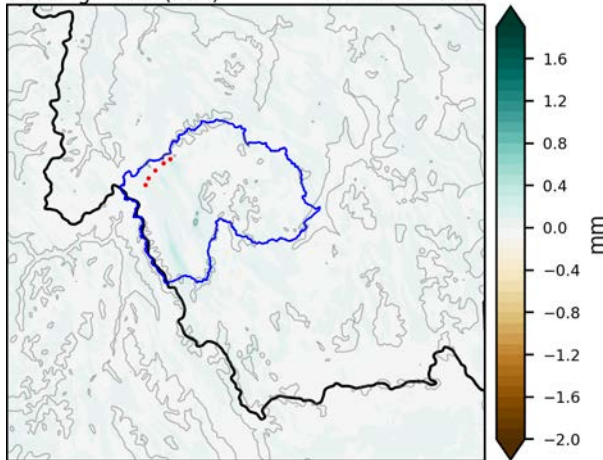
B-CTRL  
Seeding Effect (mm) 2019-12-14 Case



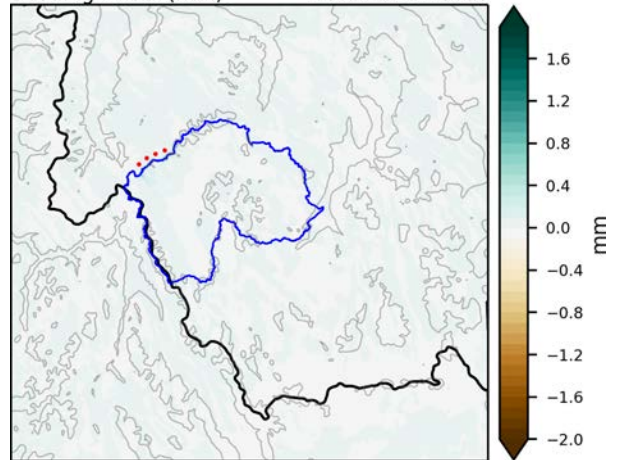
C-CTRL  
Seeding Effect (mm) 2019-12-14 Case



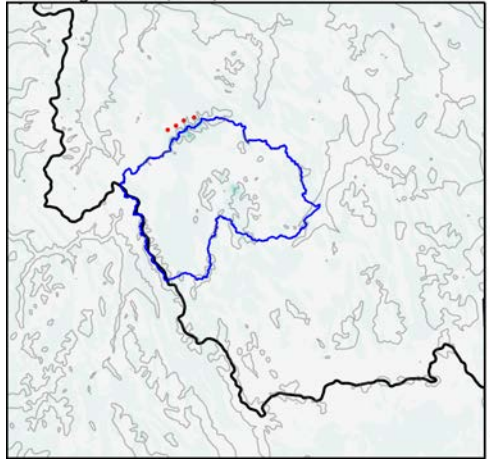
D-CTRL  
Seeding Effect (mm) 2019-12-14 Case



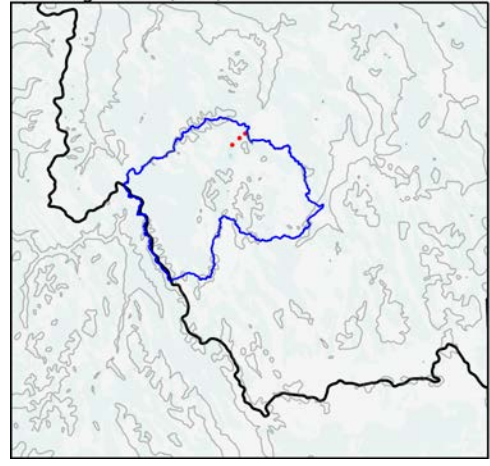
E-CTRL  
Seeding Effect (mm) 2019-12-14 Case



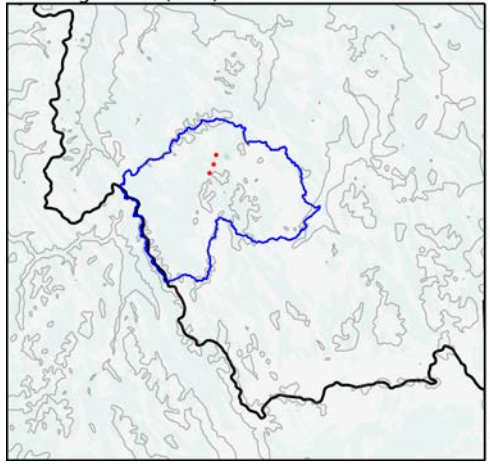
F-CTRL  
Seeding Effect (mm) 2019-12-14 Case



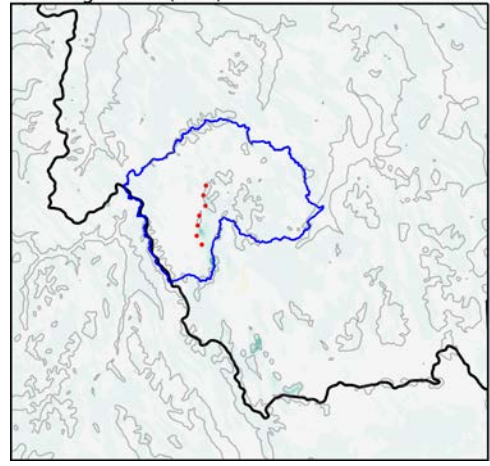
G-CTRL  
Seeding Effect (mm) 2019-12-14 Case



H-CTRL  
Seeding Effect (mm) 2019-12-14 Case



I-CTRL  
Seeding Effect (mm) 2019-12-14 Case



J-CTRL  
Seeding Effect (mm) 2019-12-14 Case

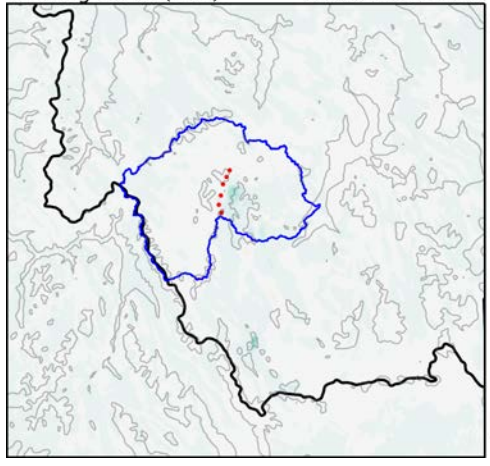


**Figure B.3.** Simulated seeding effect from all generator groups (A-J) and each individual generator group for the 14 Dec. 2019 case study. Green hues indicate an increase in simulated precipitation due to seeding; brown hues indicate a decrease in simulated precipitation due to seeding.

**Table B.1.** Simulated seeding effect for individual ground-based generator groups A-J and all generators from groups A-J combined ('All') in Case 2.

		Simulated Seeding Effect for 2019-12-14 [AF]										
		gA	gB	gC	gD	gE	gF	gG	gH	gI	gJ	All
Big Hole		-6	41	5	81	28	36	7	7	48	51	166
Domain		262	124	95	54	28	35	7	5	89	53	492